UNIVERSITEIT VAN PRETORIA
UNIVERSITY OF PRETORIA
YUNIBESITHI YA PRETORIA

Electrical characterization of process- and radiation-induced defects in 4H-SiC

by

Ezekiel Omotoso

UNIVERSITEIT VAN PRETORIA
UNIVERSITY OF PRETORIA
YUNIBESITHI YA PRETORIA

Submitted in partial fulfilment of the requirements of the degree

Doctor of Philosophy (PhD) in Physics

in the Faculty of Natural and Agricultural Science at the University of Pretoria

Promoter: Prof. Walter E. Meyer

Co-promoter: Prof. F. Danie Auret

November 2015

© University of Pretoria

Declaration of originality

I, Ezekiel Omotoso, declare that the thesis which I hereby submit for the degree Doctor of Philosophy (PhD) in Physics at the University of Pretoria is my own work and has not previously been submitted by me for a degree at this or any other tertiary institution.

SIGNATURE:

DATE: 04/02/2016

© University of Pretoria

UNIVERSITEIT VAN PRETORIA
UNIVERSITY OF PRETORIA
YUNIBESITHI YA PRETORIA

Electrical characterization of process- and radiation-induced defects in 4H-SiC

by

Ezekiel Omotoso

E-mail: ezekiel.omotoso@up.ac.za

Submitted in partial fulfilment of the requirements for the degree **DOCTOR OF PHILOSOPHY (PhD) IN PHYSICS** in the Faculty of Natural and Agricultural Sciences, University of Pretoria

Promoter: Prof. Walter E. Meyer

Co-supervisor: Prof. F. Danie Auret

Abstract

Devices for operation in aerospace, manufacturing industries, defence and radiation-harsh environments need to be manufactured from materials that are resistant to the frequent damage caused by irradiation and high-temperature environments. Silicon carbide (SiC) is a wide-bandgap semiconductor material that promises to provide solutions to these problems based on its capability to operate under extreme conditions of temperature and radiation. These conditions introduce defects in the materials. Such defects play an important role in determining the properties of devices, albeit beneficial or detrimental. Therefore it is very important to characterize the defects present in as-grown material as well as defects introduced during processing and irradiation.

In this research, resistive evaporation (RE) as well as electron-beam deposition was employed for the fabrication of ohmic and Schottky barrier contacts on nitrogen-doped, *n*-type 4H-SiC substrate. The quality of the Schottky barrier diodes (SBDs) deposited was confirmed by current-voltage (*I-V*) and capacitance-voltage (*C-V*) measurements. Deep level transient spectroscopy (DLTS) and high-resolution Laplace DLTS were successfully used to characterize the electrically active defects present in the 4H-SiC SBDs before and after bombarding them with high-energy electrons and alpha-particles as well as after exposing the sample to electron beam deposition conditions.

© University of Pretoria

I-V and *C-V* measurements showed that the SBDs deposited by RE were of good quality with an ideality factor close to unity, a low series resistance and low reverse leakage current. After irradiation, the electrical properties deviated significantly based on the irradiation types and fluences. Thermionic emission dominated at high temperatures close to room temperature, while other current transport mechanisms became dominant at lower temperatures. The ideality factor increased and Schottky barrier heights decreased with decreasing temperature, which has been attributed to barrier inhomogeneities at the metal–4H-SiC interface. Irradiation by high-energy particles had no effect on mean barrier height, but influenced the modified Richardson constant of the devices.

Results obtained from the DLTS and LDLTS measurements revealed the presence of four electrically active deep levels in the as-grown 4H-SiC, and the presence of two and three extra defects after bombardment with alpha-particle and high-energy electron (HEE) irradiation, respectively. The irradiation by both alpha-particle and HEE caused an increase in concentration of electrically active defects attributed to nitrogen impurities as well as the Z_1/Z_2 intrinsic defect attributed to the carbon vacancy. However, the structure of two of the defects observed with energies E_C – 0.22 and E_C – 0.76 eV were unknown.

Electron-beam deposition as well as exposure to electron-beam deposition conditions introduced two additional electrically active defects in 4H-SiC These two defects were close to the metal-semiconductor junction, but the process did not cause any noticeable increase in the concentration of defects previously observed in the as-grown 4H-SiC SBDs deposited by resistive evaporation technique. These electrically active defects with energies E_C – 0.42 and E_C – ~0.70 eV were probably caused by the product of elastic collisions between 10 keV electrons and residual vacuum gases which were ionized around the filament and accelerated by the electric field towards the substrate.

© University of Pretoria

Dedication

To my dear wife

Kehinde Oluwaseun

and

my daughters

Rhoda Oluwaferanmi and Phebe Oluwafikunayomi

© University of Pretoria

Acknowledgements

For the success of this study, I cannot fully thank the people who made it possible

- My promoter, Professor Walter. E. Meyer and Co-promoter, Professor F. Danie Auret for support, guidance and discussions throughout this study.
- Obafemi Awolowo University Ile-Ife, Nigeria for granting me study leave
- Prof. M. Diale, Mr M. J. Legodi and Dr. J. Nel for the discussion and support during the course of this work.
- Alexander Paradzah for the helpful discussions throughout the study.
- Johan Van Rensburg for helping with the temperature dependent *I-V* and *C-V* set-up and DLTS troubleshooting.
- Dr. S. M. M. Coelho for the help with electron-beam deposition of contacts and exposure of the samples.
- I would also like to extend many thanks to the following members of the Electronic material and Thin Films Group whose contribution is appreciated; Dr M. Schmidt, E. Igumbor, P. Ngoepe, S.M.M. Tuhuma, H. Danga, F. J. Nambala, A. Mayimele, K. Maabong, K. Ostavar and Dr C. Zander.
- I want to thank the Head of the Physics Department, Prof. C. Theron for affording me an opportunity to do part time work in the department.
- Fellow senior students in the Physics department, Dr. A. Bello, Dr. D. Y. Momodu, O. Odutemewo, T. T. Thabette, J. Madito and H. Elnour for their encouragement.
- I would like to thank my mother, mother-in-law, brother and sister for their love and constant prayers which kept me standing in the midst of struggling.
- Last but not the least, this section will not be completed if I failed to mention those who prayed and stood for me when I was not there to play my roles as a husband and as a father. I sincerely appreciate God's will, Rhoda and Phebe for their love and understanding.

Above everything else, I bless the Lord; God of heaven and earth, who has never left me for a second.

© University of Pretoria

Table of contents

Declaration of originality ii
Dedication v
Acknowledgements vi
Table of contents vii
List of figures xi
List of tables xii
Chapter 1 1
Introduction 1
1.1 Motivation 1
1.2 Aims and objectives 3
1.3 Thesis layout 3
1.4 References 5
Chapter 2 7
Theoretical aspects 7
2.1 Introduction 7
2.2 SiC crystal structure 8
2.3 Properties and applications of SiC 10
2.4 SiC growth techniques 11
2.4.1 Physical vapour transport 11
2.4.2 High temperature chemical vapour deposition 12
2.4.3 Chemical vapour deposition 12
2.5 Metal-Semiconductor interface 12
2.5.1 Introduction 12
2.5.2 Schottky contacts 13
2.5.3 The depletion region 15

© University of Pretoria

2.5.4 Current transport mechanisms 20
2.5.5 Schottky barrier height 26
2.5.6 The Richardson constant 31
2.5.7 Ohmic contacts 34
2.6 Defects in semiconductors 36
2.6.1 Introduction 36
2.6.2 Point defects 37
2.7 Defect characterization 42
2.7.1 Introduction 42
2.7.2 Shallow level defects and deep-level defects 42
2.7.3 Emission and capture of carriers by trapping centres 43
2.7.4 Deep-level transient spectroscopy 47
2.8 References 54
Chapter 3 63
Experimental techniques 63
3.1 Introduction 63
3.2 Sample preparation 63
3.2.1 SiC cleaning and etching 63
3.2.2 Ohmic contact fabrication 64
3.2.3 Schottky barrier diode fabrication 64
3.3 Introduction of defects 66
3.3.1 Alpha particles from Americium-241 (Am-241) 66
3.3.2 High-energy electrons from Strontium-90 (Sr-90) 67
3.3.3 Electron-beam deposition and exposure 68
3.4 Annealing procedure 69
3.5 Electrical characterization 69
3.5.1 Room temperature *I-V* and *C-V* measurements 70

© University of Pretoria

3.5.2 Temperature dependent *I-V* and *C-V* measurements 70

3.5.2 Deep-level transient spectroscopy and high-resolution Laplace DLTS........71

3.6 References 74

Chapter 4 76

Results and discussion 76

4.1 Introduction..76

4.2 Defects in as-grown *n*-type 4H-SiC 76

4.2.1 Current-voltage (I-V) and capacitance-voltage (C-V) characteristics 77

4.2.2 Deep-level transient spectroscopy (DLTS) measurements............................79

4.2.3 Concluding remarks..80

4.3 Irradiation induced defects in 4H-SiC 80

4.3.1 High-energy electron (HEE) irradiation 80

4.3.2 Alpha-particle irradiation induced defects in 4H-SiC.......................................81

4.3.3 Concluding remarks..81

4.4 Electron-beam deposition and exposure 82

4.4.1 Electron-beam (e-beam) deposition 82

4.4.2 Electron-beam exposure..82

4.4.3 Concluding remarks..86

4.5 Defect annealing...87

4.5.1 Concluding remarks..87

4.6 Temperature dependent *I-V* and *C-V* measurements on 4H-SiC SBDs 88

4.6.1 Concluding remarks..89

PAPER I: Effects of 5.4 MeV alpha-particle irradiation on the electrical properties of nickel Schottky diodes on 4H-SiC..90

PAPER II: The influence of high energy electron irradiation on the Schottky barrier height and the Richardson constant of Ni/4H-SiC Schottky diodes 96

© University of Pretoria

PAPER III: Response of Ni/4H-SiC Schottky barrier diodes to alpha-particle irradiation at different fluences 104

PAPER IV: Electrical characterization of deep levels created by bombarding nitrogen-doped 4H-SiC with alpha-particle irradiation 110

PAPER V: Electrical characterization of defects introduced during electron beam deposition of W Schottky barrier diodes on *n*-type 4H-SiC 116

PAPER VI: Electrical characterization of defects introduced in *n*-type N-doped 4H-SiC during electron beam exposure 129

PAPER VII: Electrical characterization of 5.4 MeV alpha-particle irradiated 4H-SiC with low doping density 137

4.7 References 143

Chapter 5 145

Conclusions 145

5.1 Further research 147

Appendix A 148

List of publications and conferences attended 148

A.1 List of Publications 148

A.2 List of national and international conferences attended and contributed 149

Appendix B 152

Deep level defects analysed in 4H-SiC 152

IBMM 2014 in Belgium 154

IBA 2015 in Croatia 155

SAIP 2015 in South Africa 156

ICDS 2015 in Finland 157

GADEST 2015 in Germany 158

© University of Pretoria

List of figures

Figure 2.1: The tetragonal bonding of a (i) silicon atom with the four nearest carbon 9

Figure 2.2: Stacking sequence of the 2H-, 3C-, 4H- and 6H-SiC polytypes. 9

Figure 2.3: The formation of a Schottky contact 15

Figure 2.4: Graphs of the ρ(x), E(x) and V(x) 18

Figure 2.5: Graph of $1/C^2$ as a function of voltage V as measured for a SBD. 20

Figure 2.6: Basic current mechanisms across a forward biased barrier. 21

Figure 2.7: Energy band diagram of Schottky barrier potential. 27

Figure 2.8: A semi-logarithmic forward and reverse I-V plots of Ni/n-type 4H-SiC.......... 28

Figure 2.9: C-V characteristic obtained from a Ni/n-type 4H-SiC device............................ 29

Figure 2.10: The plot of ln (I_S/T^2) versus $1/T$ obtained from a Ni/n-type 4H-SiC 30

Figure 2.11: The plot of ln $(I_S/T^2) - q^2\sigma_{S0}{}^2/2K^2T^2$ versus $1000/T$. 34

Figure 2.12: Electron energy diagrams between a metal and n-type semiconductor 36

Figure 2.13: The schematic diagram of point defects in semiconductor............................... 38

Figure 2.14: The schematic diagram of different carrier transitions 45

Figure 2.15: The variation of the depletion region width and trap occupation 48

Figure 2.16: Filling (top) and subsequent emission (bottom) of electrons. 50

Figure 2.17: The change in the shape of a DLTS transient. 52

Figure 2.18: DLTS spectra obtained from a measured Ni/4H-SiC SBD 52

Figure 3.1: Schematic diagram of the resistive deposition system 65

Figure 3.2: Schematic diagram for electron-beam evaporation system. 66

Figure 3.3: Schematic diagram of the samples before (a) and during (b) irradiation 67

Figure 3.4: Energy distribution of electrons emitted by a Sr-90 radionuclide. 68

Figure 3.5: A block diagram of the I-V and C-V station 71

Figure 3.6: Schematic diagram of the DLTS and Laplace DLTS set-up 73

Figure 4.1: The forward semi-logarithmic I-V characteristics. 78

Figure 4.2: $1/C^2$as a function of voltage characteristics of as-grown Ni/4H-SiC. 78

Figure 4.3: DLTS spectrum obtained from as-grown Ni/4H-SiC SBD 79

Figure 4.4: A forward semi-logarithmic I-V characteristics of Ni/4H-Si. 84

Figure 4.5: $1/C^2$ as a function of voltage for Ni/4H-SiC Schottky contacts........................... 85

Figure 4.6: Conventional DLTS spectra of Ni/4H-SiC 86

© University of Pretoria

UNIVERSITEIT VAN PRETORIA
UNIVERSITY OF PRETORIA
YUNIBESITHI YA PRETORIA

List of tables

Table 2.1: Comparison of properties of common SiC polytypes.. 11
Table 4.1: Some electrical parameters of an as-grown Ni/4H-SiC SBDs........................78
Table 4.2: SBDs parameters obtained from I-V and C-V measurements...........................83
Table B.1: Deep levels defects observed and characterized in 4H-SiC..........................153

© University of Pretoria

Chapter 1

Introduction

In 1824 the existence of the silicon-carbon chemical bond was suggested and synthesized first by J. J. Berzelius [1]. Berzelius discovered this outstanding semiconductor material when he was trying to synthesize diamonds. E. G. Acheson discovered a commercial process of manufacturing large quantities of silicon carbide (SiC) which was patented in 1893 [2], and named this new material, consisting of dark SiC crystals, *carborundum* [3]. Naturally occurring SiC is very rare and was first discovered by Henri Moissan in 1905, who found small hexagonal platelets in a meteorite [4]. This mineral is named Moissanite, and this has become the name of commercial gemstones made from SiC. Because of SiC's extraordinary abrasive properties, the material was marketed mainly for cutting and grinding purposes; though the quality of the SiC was low in hardness when compared to diamond. Various growth methods have been employed in synthesizing SiC in large and high-quality crystals. In 1950s, research in solid-state electronic devices started and SiC was one of the semiconductors investigated. A technique to grow high-quality single crystal SiC was developed by Lely in 1955, but the production of large-area single crystal was prone to defects [5]. Since then, many techniques have been implemented to grow high-quality SiC. Among the growth techniques are physical vapour transport and chemical vapour deposition.

1.1 Motivation

The challenge that still has to be addressed in the production of semiconductor material is how to grow defect-free semiconductor crystals. Introduction of defects in the semiconductor lattice may occur during processing steps including semiconductor growth, particle irradiation, plasma etching and metallization. The presence of defects influences the substrate's properties and thereby modifies the performance of the devices fabricated on the substrate. These defects may have a detrimental effect on the performance of semiconductor devices such as in solar-cell applications, where they act as efficient recombination centres and affect the carrier lifetime [6]. On the other hand,

© University of Pretoria

these defects may also enhance the performance of semiconductor devices such as fast-switching power devices [7, 8].

Wide bandgap semiconductors such as SiC, zinc oxide (ZnO) and gallium nitride (GaN) have received attention as outstanding device materials that are capable of operating at high-voltage, frequency and temperature. Wide bandgap semiconductors, which allow high-power electrical devices to be built are relatively cheap and more energy-efficient compared to conventional semiconductor materials. Among all the wide bandgap semiconductors, GaN provides better high frequency and high-voltage performance, but lack of good quality bulk substrates needed for power devices and lower thermal conductivity are a disadvantage. SiC overcomes both these shortcomings. Consequently, SiC is often seen as the best wide bandgap semiconductor for high- voltage devices. High quality SiC power devices grown on good quality substrates with high thermal conductivity have been manufactured and sold commercially [9]. SiC has displayed the capability to operate under extreme conditions of temperature and radiation [10, 11]. SiC-based electronics can be used in low-noise capacity and optoelectronic operation. In addition, the advantages of SiC devices in the area of cost cannot be overemphasized. The cost has dropped over the decades and the outstanding performance has proven itself superior to Si and GaAs devices. SiC is a key material for next-generation photonics, and has the ability to outperform current Si power devices [12, 13]. Among the SiC polytypes, 4H-SiC is the most promising polytype for vertical type high-voltage devices due to its higher bulk mobility and smaller anisotropy [14].

Furthermore, it is worth considering that the understanding of how defects affect the performance of devices is the basis for fabricating improved 4H-SiC devices. Although many impressive findings have been reported, characterization of defects induced by processing and irradiation of 4H-SiC Schottky barrier-diodes (SBDs) is still a very active field of study and many aspects of defects in SiC are not yet well understood.

Defects in semiconductors have been characterized by different techniques, such as positron annihilation spectroscopy, admittance spectroscopy, cathodoluminescence, photoluminescence, Hall effect, Rutherford backscattering spectroscopy, X-ray diffraction, scanning electron microscopy and deep-level transient spectroscopy. In this study, deep-level transient spectroscopy was employed.

© University of Pretoria

Deep-level transient spectroscopy (DLTS) is a powerful electrical technique that provides details about the *signature* (the activation energy and capture cross-section) of an electrically active defect with one or more levels in the bandgap of a semiconductor. DLTS can characterize defects using different kinds of space-charge based devices such as Schottky barrier diodes, p-n junctions and metal oxide semiconductor structures [15, 16]. The invention of high-resolution Laplace DLTS increased the utility of this technique significantly. Laplace DLTS makes separation of the closely spaced energy levels that appear as single broad defect in conventional DLTS possible [17, 18].

1.2 Aims and objectives

The aims and objectives of this research are as follows:

- To fabricate high quality ohmic and Schottky contacts on 4H-SiC by employing the best cleaning methods and optimizing the metal deposition technique.
- To characterize the electrically active defects present in Schottky barrier diodes manufactured on as-grown 4H-SiC.
- To fabricate contact systems for operation at extreme temperature and in radiation harsh environments, such as aerospace, nuclear and satellite applications.
- To investigate the radiation response of 4H-SiC devices at different fluences.
- To determine the effect of irradiating *n*-type 4H-SiC devices at high fluence and investigate the annealing of the induced electrically active defects.
- To ascertain if process induces defects in SiC, a wide bandgap and radiation hard material.

1.3 Thesis layout

This thesis is divided into five (5) chapters:

Chapter 1 is an introduction that contains the motivations, aims and objectives as well as the outline of the thesis.

© University of Pretoria

Chapter 2 presents the theoretical background of semiconductors with special reference to SiC, on which this study is based. The chapter briefly describes Schottky contacts, defects in 4H-SiC and characterization of defects by convectional DLTS and high-resolution Laplace DLTS.

Chapter 3 describes the experimental techniques employed to fabricate Schottky and ohmic contacts. The introduction of deep-level defects by high-energy particles and electron-beam deposition will also be discussed.

Chapter 4 presents and discusses the results obtained during the course of this study. Most of the results have been published in peer reviewed journals. The results are summarised in a number of sections, with references to the full papers for detail. The relevant papers are included at the end of Chapter 4.

Chapter 5 summarizes the conclusions drawn from the study and proposes further research to be performed.

© University of Pretoria

1.4 References

1. Berzelius, J.J., *Studies on the fluor spar acid and its remarkable connections.* Annals of Physics, 1824. **77**(6): p. 169-230.

2. Acheson, E.G. 1893, U.S. patent no. 492767.

3. Acheson, E.G., *Carborundum: Its history, manufacture and uses.* Journal of the Franklin Institute, 1893. **136**(4): p. 279-289.

4. Moissan, H., *Micrographic study of the canon diablo meteorite.* Comptes Rendus, 1905. **140**: p. 405-506.

5. Lely, J.A., *Preparation of single crystals of silicon carbide and mastery of nature and amount of built- associations.* Berischte the German Ceramic Society, 1955. **32**: p. 229-231.

6. Schmidt, J. and K. Bothe, *Structure and transformation of the metastable boron- and oxygen-related defect center in crystalline silicon.* Physical Review B, 2004. **69**(2): p. 024107.

7. Tamaso, H., et al., *Development of Fast-Switching SiC Transistor.* Sei Technical Review-English Edition, 2008. **66**: p. 43-49.

8. Sawko, D. and J. Bartko, *Production of fast switching power thyristors by proton irradiation.* Nuclear Science, IEEE Transactions on, 1983. **30**(2): p. 1756-1758.

9. Millan, J., et al., *A Survey of Wide Bandgap Power Semiconductor Devices.* Power Electronics, IEEE Transactions on, 2014. **29**(5): p. 2155-2163.

10. Siad, M., M. Abdesslam, and A.C. Chami, *Role of carbon in the formation of ohmic contact in Ni/4HSiC and Ni/Ti/4HSiC.* Applied Surface Science, 2012. **258**(18): p. 6819-6822.

11. Madar, R., *Materials science: Silicon carbide in contention.* Nature, 2004. **430**(7003): p. 974-975.

12. Yamada, S., et al., *Silicon carbide-based photonic crystal nanocavities for ultra-broadband operation from infrared to visible wavelengths.* Applied Physics Letters, 2011. **99**(20): p. 2011021-2011023.

13. Palmour, J.W. *Silicon carbide power device development for industrial markets*. in *Electron Devices Meeting (IEDM), 2014 IEEE International*. 2014. IEEE.

14. Danno, K. and T. Kimoto, *Investigation of deep levels in n-type 4H-SiC epilayers irradiated with low-energy electrons.* Journal of Applied Physics, 2006. **100**(11): p. 113728.

15. Auret, F.D. and P.N. Deenapanray, *Deep level transient spectroscopy of defects in high-energy light-particle irradiated Si.* Critical Reviews in Solid State and Materials Sciences, 2004. **29**(1): p. 1-44.

© University of Pretoria

16. Khan, A., et al. *DLTS: A Promising Technique for the Identification of the Recombination and Compensator Centers in Solar Cell Materials*. in *Photovoltaic Energy Conversion, Conference Record of the 2006 IEEE 4th World Conference on*. 2006.

17. Dobaczewski, L., A. Peaker, and K.B. Nielsen, *Laplace-transform deep-level spectroscopy: The technique and its applications to the study of point defects in semiconductors.* Journal of Applied Physics, 2004. **96**(9): p. 4689-4728.

18. Dobaczewski, L., et al., *Laplace transform deep-level transient spectroscopic studies of defects in semiconductors.* Journal of Applied Physics, 1994. **76**(1): p. 194-198.

© University of Pretoria

Chapter 2

Theoretical aspects

2.1 Introduction

Theoretical aspects of semiconductor, with particular reference to SiC, are presented in this chapter.

Section 2.2 briefly presents the crystal structure of SiC as a binary semiconductor with chemical formula of SiC. This section also describes SiC as an indirect wide bandgap semiconductor that varies from 2.36 to 3.26 eV at room temperature, depending on the polytypes.

Properties and applications as well as crystal growth techniques of SiC are presented in Sections 2.3 and 2.4. The application of SiC for high temperature, high frequency, high saturation carrier velocity, high mechanical strength and high power device applications are due to its high critical field for breakdown, high thermal conductivity and large bandgap properties.

In Section 2.5, the importance and the influence of Schottky contacts in the fabrication of semiconductor devices is briefly described. It is also clearly stated in this section that the reliability, the performance and the stability of devices depend on the contacts or interface properties for their optimum operations.

The classification of states into shallow and deep-level defects according to their positions within the energy bandgap of SiC is briefly introduced in Section 2.6. The roles and the common types of point defects in SiC are also emphasized.

Section 2.7 briefly describes the characterization of defects by the standard DLTS and high-resolution Laplace DLTS. Advantage of Laplace DLTS over the conventional DLTS in separating traps or states with similar emission rates is also described.

© University of Pretoria

2.2 SiC crystal structure

A crystal structure is formed when atoms are uniquely arranged in a crystal. In the case of SiC structure, an atom of carbon is tetrahedrally bonded to four neighbouring atoms of silicon that are placed in the corner and vice-versa as shown in Figure 2.1. The bond between silicon and carbon is very strong because of the short bond length and hybridization of sp^3. The bond between them is nearly covalent with ~12% ionic bonding. There are about ~250 crystalline forms of SiC, however, only a small number of these are frequently observed [1]. The frequently observed structures are all close-packed structures and show a 1-dimensional polymorphism called *polytypism* [2, 3]. The term polytypism is a special case of polymorphism that takes place when two polymorphs differ only in the stacking of identical, 2-dimensional sheets or layers [4]. The orientation sequences by which layers of tetrahedral are arranged are the only differences among the polytypes. The differences of the same chemical compound are identical in two but differ in the third dimensions. Therefore, they can be observed as layers arranged in a definite sequence [2, 5]. The most common SiC polytypes are grouped into four: the cubic (3C-SiC), the hexagonal (4H-SiC and 6H-SiC), the rhombohedral (15R-SiC) and Tetragonal (T). The different crystalline polytypes can be described by allocating a number corresponding to the number of layers in the unit cell followed by the crystal symmetry. For instance, in 4H-SiC and 6H-SiC, four and six different layers are repeated in the material and the structure is hexagonal. Figure 2.2 shows the stacking sequence of the 2H-, 3C-, 4H- and 6H-SiC polytypes.

The α- and the β-SiC are the most common polymorphs. The α-SiC occurred at temperature above 1700°C, and has a crystal structure of hexagonal. It is mainly 2H-, 4H-, and 6H-SiC which has Wurtzite structure. The 2H-SiC is purely hexagonal, while 4H-SiC is 50% of hexagonal (and 50% cubic) and 6H-SiC is 33% hexagonal (and 67% cubic) [2, 6, 7].

The β-SiC formed at temperature below 1700°C, and has the zinc-blende crystal structure. The cubic 3C polytype is mainly referred to as β-SiC with structure similar to diamond. Also, the β-SiC is 100% cubic. The bonding between Si and C atoms in neighbouring bilayer plane is of cubic (zinc blend) or hexagonal (wurtzite) in nature.

For more details about crystallography of SiC, the readers should consult *ref.* [8].

© University of Pretoria

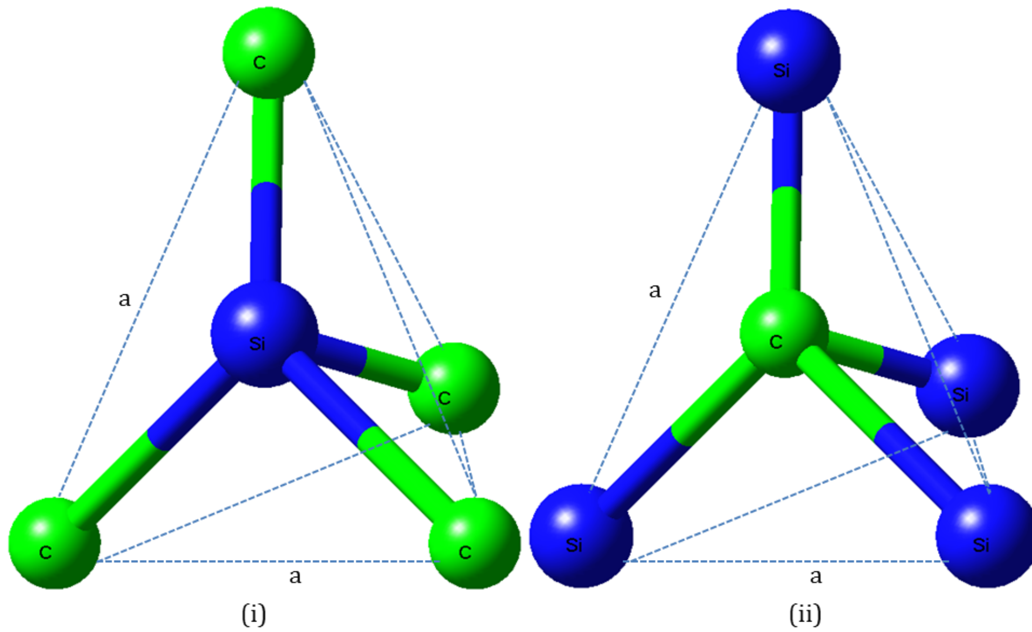

Figure 2.1: The tetragonal bonding of a (i) silicon atom with the four nearest carbon neighbours, and (ii) carbon atom with the four nearest silicon neighbours. The distances a and C-Si are approximately 3.08 and 1.89 Å, respectively.

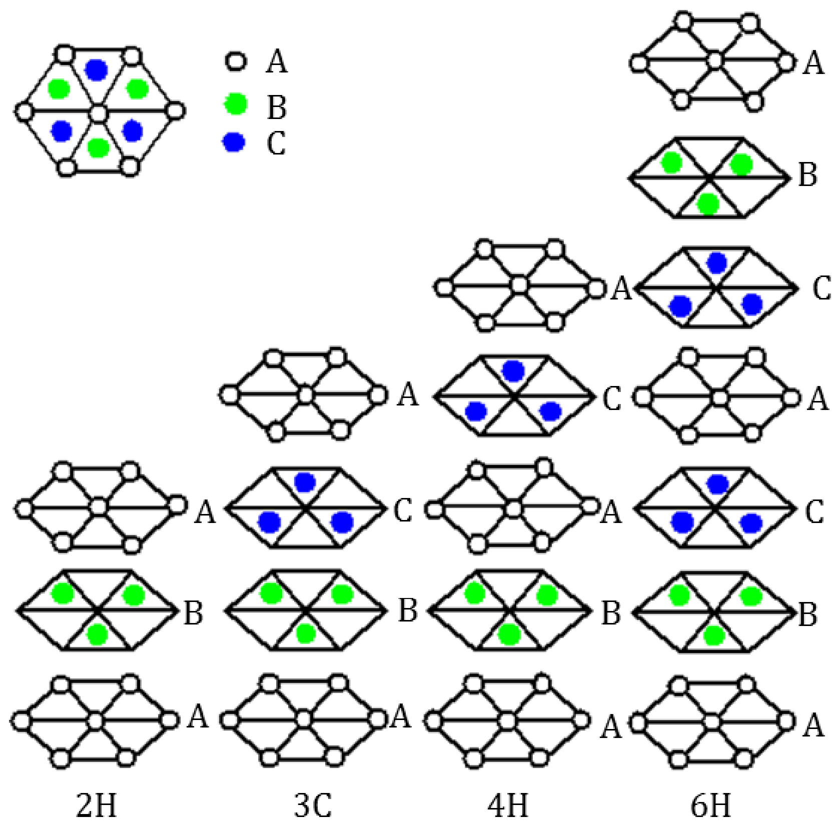

Figure 2.2: Stacking sequence of the 2H-, 3C-, 4H- and 6H-SiC polytypes [9].

© University of Pretoria

2.3 Properties and applications of SiC

SiC is an indirect wide bandgap semiconductor material that is notable due to its high saturation carrier velocity, high mechanical strength, high electrical breakdown field and high thermal conductivity compared to conventional semiconductor materials such as Ge, Si and GaAs [10-12]. The physical properties of SiC polytypes are compared to conventional semiconductor materials in Table 2.1.

The bandgap of SiC is approximately three times that of Si. Depending on the polytypes, its bandgap varies from 2.36 to 3.26 eV, as shown in Table 2.1. The wide bandgap means that electron is not easily thermally excited from the valence band to the conduction band. The number of electrons in the conduction band or the number of holes in valence band of an intrinsic semiconductor (a semiconductor without impurities or defects) is called the intrinsic carrier concentration. The number of electrons or holes present depends on the band gap and the temperature of the material. SiC has a very low intrinsic carrier concentration at ambient conditions compared to Si. This makes it possible to control conduction through the doping of impurities at higher temperatures. Its larger bandgap and low intrinsic carrier concentration, makes SiC an appropriate material for high temperature devices. This would include devices operating in harsh environments (e.g. automotive and aerospace applications) as well as high power devices that generate large amount of heat. SiC can withstand thermal temperature ~1000°C compare to Si that can deteriorate at temperature ~250°C [13]. Also, the wide bandgap makes SiC suitable for the emission and detection of short wavelength light.

SiC has a very high dielectric breakdown field strength that is ten times that of Si. Therefore devices made from SiC can perform without breakdown at larger power densities, again making the material ideal for high power applications.

© University of Pretoria

Table 2.1: Comparison of properties of common SiC polytypes with various conventional semiconductors [10].

	E_g (eV)	n_i (cm^{-3})	E_b ($MVcm^{-1}$)	μ_e ($cm^2V^{-1}s^{-1}$)	μ_h ($cm^2V^{-1}s^{-1}$)	v_s (cms^{-1})	κ ($Wcm^{-1}K^{-1}$)
4H-SiC	3.26	$\approx 10^{-7}$	2.0-3.0	720	120	2.0×10^7	3-5
6H-SiC	3.02	$\approx 10^{-5}$	2.5	370	80	2.0×10^7	3-5
3C-SiC	2.36	≈10	>1.5	900	40	2.0×10^7	3-5
Si	1.12	10^{10}	0.6	1350	480	1.0×10^7	1.5
GaAs	1.42	2×10^6	0.6	8500	400	2.0×10^7	0.5
GaN	3.40	10^{-10}	2-3	1000	30	2.5×10^7	1.3

NOTE: *Energy bandgap, E_g; intrinsic carrier concentration, n_i; breakdown voltage, E_b; electron mobility, μ_e; hole mobility, μ_h ; saturation electron velocity, v_s; and thermal conductivity, κ.*

2.4 SiC growth techniques

Naturally, SiC occurs as the rare mineral moissanite. Industrially, SiC is available as a bulk crystal as well as an epitaxial crystal. Because of the high melting point of stoichiometric SiC (> 3200°C) [14], the common methods of growing bulk semiconductor crystals such as Czochralski, liquid-encapsulated Czochralski, Bridgman, and gradient freeze, cannot be used for the manufacture of SiC, however, the physical vapour transport process known as a modified Lely, and high temperature chemical vapour deposition may be used.

2.4.1 Physical vapour transport

This method allows a large variation in crystal quality, for uses ranging from abrasives to semiconductor wafers for electronic components. According to this method, solid SiC (referred to as the source) is placed at the bottom of a furnace, which is either evaculated or filled with argon or helium. The source is heated to high temperature (1600° ≤ t ≤ 2700°C) until vaporisation takes place. The vapour rises and migrates to cooler, upper portions of the furnace, where it comes into contact with a monocrystalline seed of SiC and is deposited thereby increasing the size of the crystal. The Acheson process, the Lely process, and the modified Lely process are techniques

© University of Pretoria

considered versions of physical vapour transport method. More details on this section could be found in *refs* [14, 15].

2.4.2 High temperature chemical vapour deposition

This is an alternative method of growing bulk SiC crystals. This method uses gas phase precursors instead of SiC powder in physical vapour transport method. The source materials are constantly served into the reactor. This method is free from problems associated with the use of closed systems (such as a lack of the source powder during productions). The production of high quality bulk SiC crystal is possible using this method, and that makes it a better substitute to physical vapour transport [16].

In addition, the uses of two sources, SiH_4 for the Si source and CH_4 or C_3H_8, for the C source are possible with this crystal growth method [16]. It is advantageous over the physical vapour transport because the stoichiometry of the deposits can be easily controlled. More details on this section could be found in *refs* [14, 16, 17]

2.4.3 Chemical vapour deposition

This method is used for growing thin crystalline layers right from the gas phase [18]. With this method, a mixture of source gases for Si (Silane is the common Si source) and C (a hydrocarbon is used for C), and a carrier gas (high purity H_2) is injected into the growth chamber with substrate at temperatures greater than 1300˚C. The high purity H_2 as a carrier gas is also acts as a co-reactant. Multi-source (conventional Si and C) and single-source precursors have been successfully used and reproducible chemical vapour deposition epitaxial films have been produced. The single-source precursor can be grown at temperature lower than 1100˚C. This process is used to manufacture high quality, high-performance, solid materials. More details on this section could be found in *refs*. [14, 19].

2.5 Metal-Semiconductor interface

2.5.1 Introduction

A metal-semiconductor (M-S) interface is a junction in which metal is in contact with semiconductor material. This junction can be rectifying (Schottky barrier) or non-rectifying (ohmic contact) [20]. Schottky contacts can be used in device applications such as rectifiers, mixers, microwave receiver detectors and field effect transistors [21,

© University of Pretoria

22]. The Schottky contacts can also be used to form a space charge region that can be used to investigate the semiconductor energy bandgap and measure the properties of the deep-level defects present at and below the M-S interface. The reliability, the performance and the stability of devices is highly dependent on the interface properties. The quality of the M-S junction is determined by the difference between the Fermi energies of the metal and semiconductor, the processing of the semiconductor before fabrication of the contact and the techniques used in the fabrication of devices [21, 23, 24].

This section is very important and too broad to be discussed in detail in this thesis. More details can be found in *refs* [21, 25].

2.5.2 Schottky contacts

Schottky contacts are metal-semiconductor contacts that can rectify signal device in forward bias and not allowing current to flow in reverse bias. The mechanism according to which a Schottky diode is formed for an ideal case (i.e. without surface effects, interface states and other anomalies) was described by Schottky [26], the barrier height between a metal (say Ni) and an *n*-type semiconductor (say 4H-SiC) is equal to difference between the work function of metal and the electron affinity of semiconductor [27-29], which can be written as Equation 2.1

$$\phi_b = \phi_m - \chi \qquad 2.1$$

As a typical example for Ni/*n*-type 4H-SiC, the barrier height, ϕ_b = 2.05 eV, the work function of Ni, ϕ_m = 5.15 eV, and the electron affinity of *n*-type 4H-SiC of orientation (0001), χ = 3.1 eV [30]. The principle of Schottky contact according to Schottky-Mott theory is shown schematically in Figure 2.3. In Figure 2.3a shows the metal and semiconductor isolated and electrically neutral with the $\phi_m > \phi_s$. In Figure 2.3b, the metal is brought into thermodynamic contact with the semiconductor by means of a thin wire, electrons flow from semiconductor to metal due to the difference in work function. The flow of electrons from the semiconductor to the metal takes place until the thermal equilibrium occurs. At equilibrium, the Fermi level of the metal coincides with the Fermi level of semiconductor as shown in Figure 2.3b. Due to the redistribution of electrons, there is an accumulation of negative surface charges around the metal side

© University of Pretoria

that is compensated by the positive charges in the semiconductor in the vicinity of the surface. Consequently, an electric field exists within the gap between the metal and the semiconductor. As stated by Rhoderick [25], the negative charge on metal's surface consists of extra electrons confined within the Thomas-Fermi screening distance of approximately 0.5 Å. In *n*-type semiconductor, the positive charge will be provided by electrons withdrawing from the surface and leave uncompensated positive donor ions in an area depleted of electrons. Due to the fact that the concentration of electrons in the metal is much greater than the concentration of donors, the uncompensated donors occupy a layer of appreciable depth w. There is a change in potential due to the charge distribution in the depletion region and thereby results in band bending upward in the semiconductor as shown in Figure 2.3b. The difference between the electrostatic potentials at the surface of the metal and semiconductor is given by Equation 2.2

$$V_i = \delta E_i \tag{2.2}$$

where V_i is the difference in electrostatic potentials, δ is their separation between metal and semiconductor and E_i is the electric field in the gap. As the gap between the metal and the semiconductor is decreased, the electric field remains finite (Figure 2.3c), and V_i tends to zero as the gap vanishes. Figure 2.3d shows an ideal M-S contact in which the barrier as a result of vacuum disappears wholly, and the only barrier seen by electrons, is due to band bending in the semiconductor.

As seen in Figure 2.3d, the height of barrier relative to the conduction band's position in the neutral region of the semiconductor is referred to as the diffusion potential (built-in potential or voltage), represented by V_{bi}. The built-in voltage can be expressed as Equation 2.3

$$V_{bi} = \phi_b - \xi \tag{2.3}$$

where ξ is the energy difference between the Fermi level and the conduction band (referred to as Fermi or chemical potential of semiconductor). For charge neutrality according *ref*. [21], the chemical potential is given as

$$\xi = kT \ln \frac{N_c}{N_d} \tag{2.4}$$

© University of Pretoria

where N_c is the density of states in the conduction band of the semiconductor and N_d is the doping density.

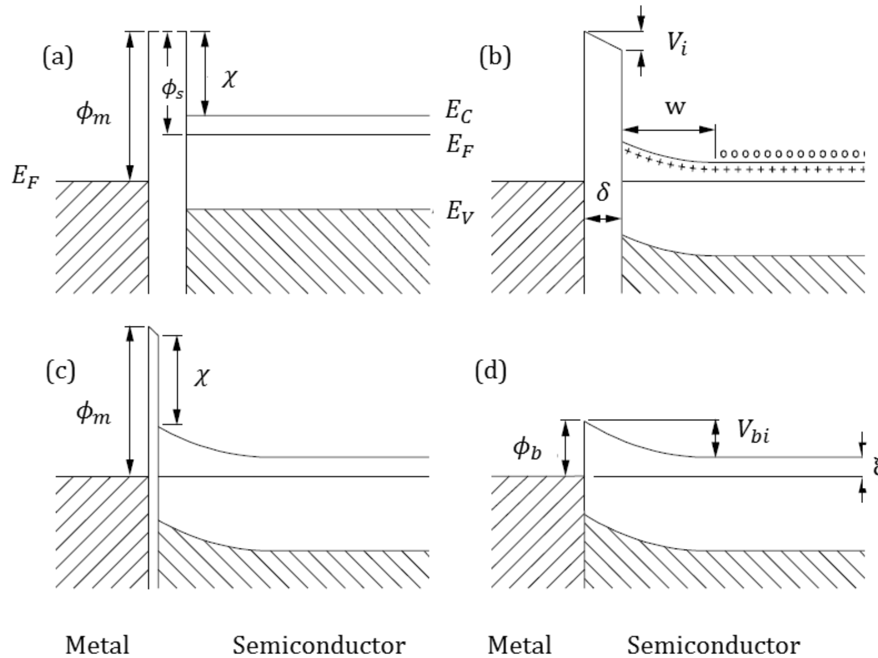

Figure 2.3: The formation of a Schottky contact (a) between a metal and semiconductor in their isolated states, (b) electrically connected, (c) separated by a narrow gap, and (d) in a perfect contact. Redrawn from ref [25].

In reality, Figure 2.3d is not achievable in the fabrication of Schottky contacts by vacuum deposition. A thin insulating oxide layer of about 10 – 20 Å thick usually forms on the surface of semiconductor. This insulating layer is frequently referred to as an interfacial layer. A practical Schottky contact is represented by Figure 2.3c. The barrier presented to the electrons by the interfacial oxide layer is very thin so that electrons can tunnel effortlessly and cause the case not to be distinguishable from the ideal one. In addition, the potential drop V_i is too small that Equation 2.1 still remains reasonable approximation.

2.5.3 The depletion region

Bringing a metal into close contact with a semiconductor during the formation of a Schottky diode, the conduction band and the valence bands of the semiconductor at the

© University of Pretoria

surface are brought into a definite energy relationship with the metal's Fermi level [21]. This causes charge carriers to flow between the metal and the semiconductor until the Fermi level on both sides of the junction is equal. In the metal, all charges accumulate close to the interface, however in the semiconductor the charge is provided by ionized donors or acceptors, which have a much lower concentration than electrons in the metal. The result is that a region devoid of charge carriers, called the depletion region is formed next to the interface.

Mathematically, the electric field, potential and carrier concentration in the depletion region may be calculated by Poisson equation in the semiconductor (4H-SiC). The boundary conditions are obtained from the barrier height at the interface, and taking the electric field in the bulk of the semiconductor to be zero.

Taking $x = 0$ at the interface, the boundary conditions can be written as

$V(0) = V_{bi}$ and $E(\infty) = 0$

where V is the potential, V_{bi} is the built-in potential and E is the electric field.

The solution to Poisson's one-dimension equation can be written as

$$\frac{d^2V}{dx^2} = -\frac{\rho(x)}{\varepsilon_s} \quad 2.5$$

where $\rho(x)$ is the charge density at a depth, x, and ε_s is the permittivity of the semiconductor.

In general, the charge density at a depth x should include contributions from the valence and the conduction band, ionized donors and acceptors, and deep-levels in the bandgap. This leads to a complicated equation which can be solved numerically. The abrupt or depletion region approximation is used to simplify the complicated equation. According to this approximation, the semiconductor is divided into two regions:

(i) depletion region, directly below the metal which contains only ionized dopants and no free carriers, and
(ii) the bulk semiconductor, which is electrically neutral and in which there is no electric field (i.e. electric field is zero).

© University of Pretoria

Now, for contacts on n-type 4H-SiC semiconductor, under the abrupt approximation that the total charge density, $\rho(x)$ in the depletion region where there is no electron in the conduction band is given by [21, 31]

$$\rho(x) = \begin{cases} qN_d & x \leq w \\ 0 & x > w \end{cases} \quad 2.6$$

where N_d is the density of dopants at a depth x from the interface, respectively, q is the electron charge and w is the depletion width.

By integrating Equation 2.5 and applying the boundary conditions, the electric field and electrostatic potential in the semiconductor are given below

$$E(x) = -\frac{qN_d}{\varepsilon_s}(w - x) \quad 2.7$$

and

$$V(x) = -V_{bi} + \frac{qN_d}{\varepsilon_s}(wx - \frac{x^2}{2}) \quad 2.8$$

ρ(x), E(x) and V(x) for a Schottky barrier can be graphically represented as shown in Figure 2.4.

Solving the Equation 2.5 by integrating it twice and applying the boundary conditions, the depletion width is

$$w = \sqrt{\frac{2\varepsilon_s}{qN_d}V_{bi}}. \quad 2.9$$

When an external bias V is applied to the contact, the depletion width is given as

$$w = \sqrt{\frac{2\varepsilon_s}{qN_d}\left(V_{bi} - V - \frac{kT}{q}\right)}, \quad 2.10$$

where kT/q arises from the contribution of the majority carrier distribution tail, k is the Boltzmann constant and T is the temperature in Kelvin. From Equation 2.10, the

© University of Pretoria

depletion width varies as the square root of the applied voltage V and as the reciprocal of the square root of the semiconductor's dopant density.

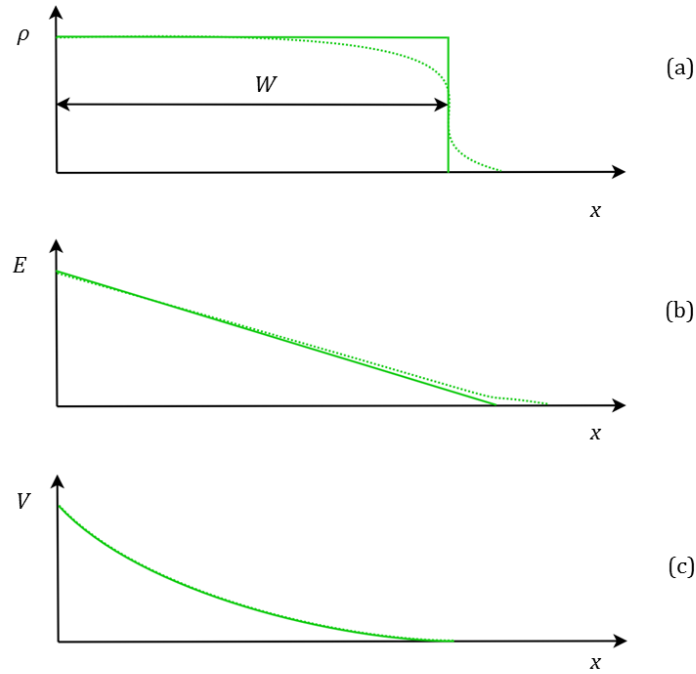

Figure 2.4: Graphs of the charge density ρ(x), electric field E(x), and electrostatic potential V(x) in the Schottky barrier diode's depletion region. The results according to depletion approximation and the effects of non-zero Debye length are represented by solid line and dashed line, respectively. [32]

The space charge Q_s per unit area of the semiconductor and the depletion layer capacitance C per unit area are given by Equations 2.11 and 2.12, respectively [21, 27]

$$Q_s(V) = qN_d w = \sqrt{2\varepsilon_s q N_d \left(V_{bi} - V - \frac{kT}{q}\right)} \qquad 2.11$$

and

$$C = \frac{|\partial Q_s|}{\partial V} = \sqrt{\frac{\varepsilon_s q N_d}{2(V_{bi} - V - kT/q)}} = \frac{\varepsilon_s}{w} \qquad 2.12$$

The Equation 2.12 can be written in the form below;

© University of Pretoria

$$\frac{1}{C^2} = \frac{2(V_{bi} - V - kT/q)}{\varepsilon_s q N_d} \quad 2.13$$

from which it follows that

$$N_d = \frac{2}{q\varepsilon_s}\left[-\frac{1}{d(^1/_{C^2})/dV}\right] \quad 2.14$$

A plot of $1/C^2$ versus V yields a straight line and the doping density, N_d can be calculated from the slope $(-2/(q\varepsilon_s N_d))$ if N_d is constant throughout the depletion region, otherwise the doping profile can be calculated from Equation 2.14 by using the differential capacitance technique [27].

By using voltage axis intercept, the Schottky barrier height ϕ_b is given by

$$\phi_b = V_{bi} + \xi + \frac{kT}{q} - \Delta\phi \quad 2.15$$

where V_{bi} is the voltage axis intercept (known as built-in voltage or potential) and $\Delta\phi$ is the image force barrier lowering and is given as

$$\Delta\phi = \left(\frac{qE_m}{4\pi\varepsilon_s}\right)^{1/2} \quad 2.16$$

where E_m is the maximum electric field, given by

$$E_m = \left(\frac{2qN_dV_{bi}}{\varepsilon_s}\right)^{1/2} \quad 2.17$$

Figure 2.5 shows a measured graph of $1/C^2$ versus V.

© University of Pretoria

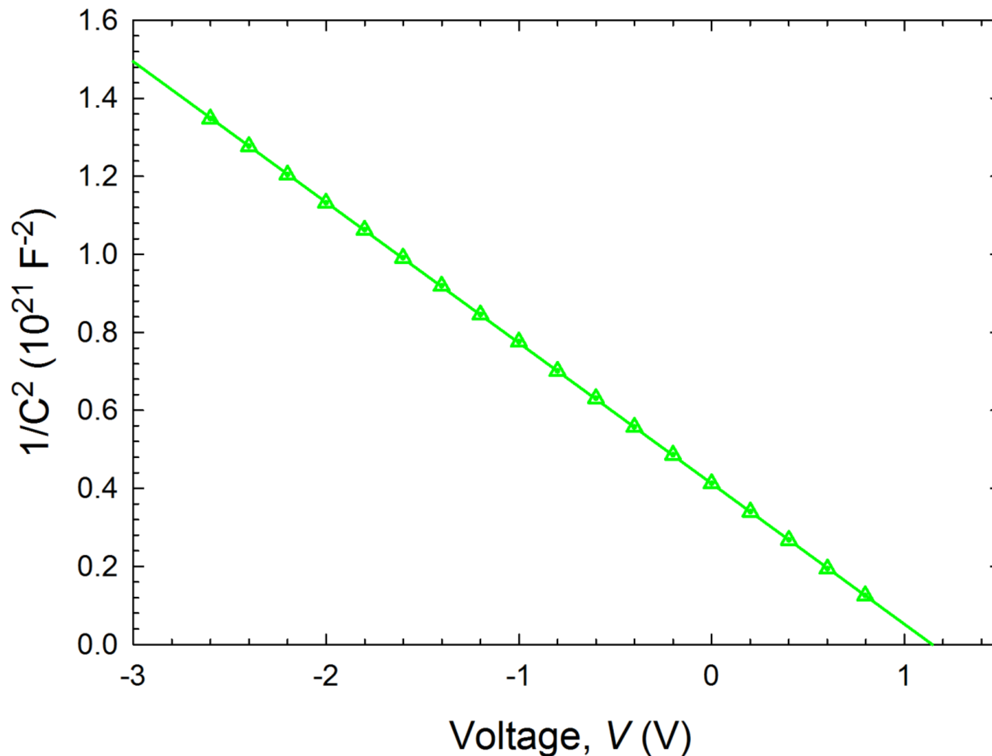

Figure 2.5: Graph of $1/C^2$ as a function of voltage V as measured for a SBD of Ni/4H-SiC at room temperature (300 K).

2.5.4 Current transport mechanisms

This section is extracted from *refs.*[21, 25, 33] and details can be read in the texts.

In metal-semiconductor junctions, majority carriers are primarily responsible for the current transport, unlike *p-n* junctions, where minority carriers are responsible for the flow of current. These majority carriers can either be electrons (for *n*-type semiconductors) or holes (for *p*-type semiconductors) [21]. There are four main processes by which carrier transport can occur in Schottky barriers in forward biased direction [21]. These mechanisms or processes are

(i) thermionic emission (TE) over the Schottky potential barrier from semiconductor into the metal,

(ii) quantum-mechanical tunnelling through the barrier, which is important for highly doped semiconductors and accountable for most ohmic contacts,

(iii) carrier recombination and generation in the depletion region, and

© University of Pretoria

(iv) hole injection from the metal to the semiconductor (recombination in the neutral).

These transport mechanisms are illustrated schematically in Figure 2.6.

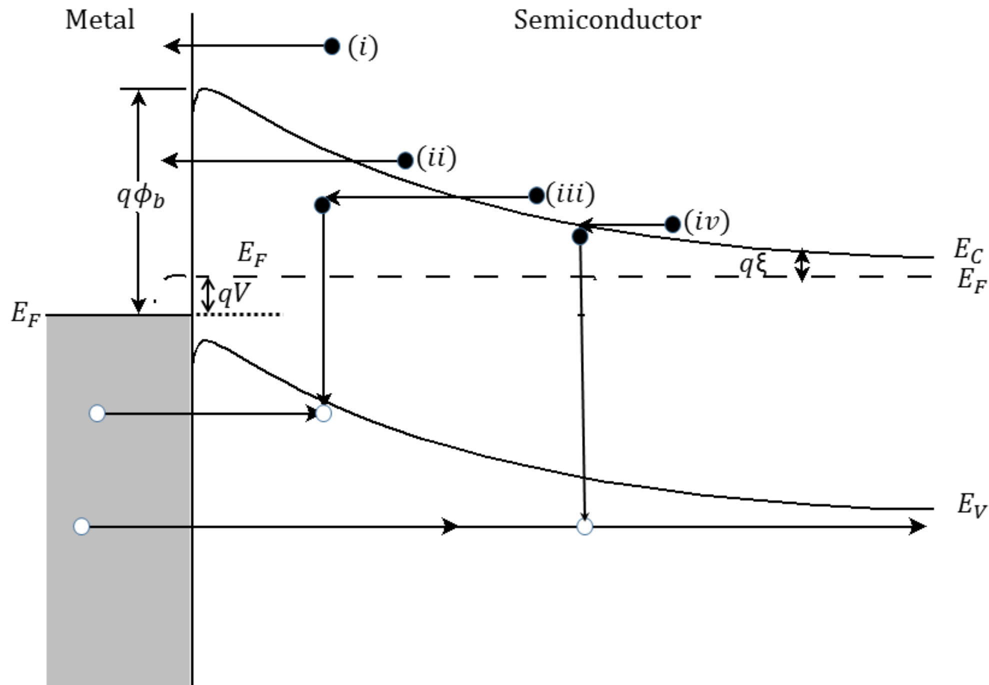

Figure 2.6: Basic current mechanisms across a forward biased barrier, redrawn from ref. [21, 25, 27].

2.5.4.1 Thermionic emission

Thermionic emission is dominant for Schottky barrier diodes on lightly doped semiconductors, and operates at moderate temperatures [21]. The TE theory was derived by Bethe [34], and assumes that

(i) the Schottky barrier height is much greater than characteristic energy (i.e. $q\emptyset_{bn} \gg kT$);

(ii) thermal equilibrium is established at the plane that determines emission, and

(iii) this thermal equilibrium is not affected by the existence of the net current flow, therefore the two current fluxes can superimpose (i.e. from metal to semiconductor, and vice-versa, each with a different quasi Fermi level [21].

It can be deduced from these assumptions that the flow of current from semiconductor to metal is solely dependent on the Schottky barrier height and independent on the

© University of Pretoria

shape of barrier profile. Therefore, the shape of the barrier profile can be ignored. The current density from semiconductor to metal (denoted as $J_{S\to M}$), which is determined by the number of electrons that have sufficient energy to overcome the barrier, is given by

$$J_{S\to M} = \int_{E_{Fn}+e\Phi_{bn}}^{\infty} ev_x dn \quad 2.18$$

where v_x is the component of the carrier velocity in the direction of current flow, and $E_{Fn} + e\Phi_{bn}$ is the minimum energy necessary for TE into metal. To consider the electron density in an incremental energy range, we have Equation 2.19

$$dn = N(E)F(E)dE$$
$$\approx \frac{4\pi(2m^*)^{3/2}}{h^3}\sqrt{E - E_c}\exp\left(-\frac{E - E_c + qV_n}{kT}\right)dE \quad 2.19$$

where $N(E)$ is the density of states, $F(E)$ is the distribution function, m^* is the effective mass of semiconductor, qV_n is (E_C – E_F) and E is the electrons' energy. Let postulate that all the energy associated with electrons in the conduction band is kinetic energy, and is given as

$$E = E_C + \frac{1}{2}m^*v^2 \quad 2.20$$

From Equation 2.20, $dE = m^*vdv$, and Equation 2.19 can be written as [21, 27]

$$dn \approx 2\left(\frac{m^*}{h}\right)^3 \exp\left(-\frac{e\Phi_n}{kT}\right)\exp\left(-\frac{m^*v^2}{2kT}\right)(4\pi v^2 dv) \quad 2.21$$

This equation gives the number of electron per unit volume with speeds between v and $v + dv$ that are distributed in all directions and h is the Planck's constant. Resolving the velocity into components along the axes in such a way that x-axis parallel to the direction of transport, we have

$$v^2 = {v_x}^2 + {v_y}^2 + {v_z}^2 \quad 2.22$$

© University of Pretoria

Using the transformation $4\pi v^2 dv = dv_x dv_y dv_z$, we obtain current density from Equations 2.18, 2.21 and 2.22

$$J_{S\rightarrow M} = \frac{4\pi q m^* k^2}{h^3} T^2 \exp\left(-\frac{qV_n}{kT}\right) \exp\left(-\frac{m^* {v_{ox}}^2}{2kT}\right) \quad 2.23$$

where v_{ox} is the minimum velocity required in the x-direction to overcome the barrier and is given by

$$\frac{1}{2} m^* v_{ox}^2 = q(V_{bi} - V) \quad 2.24$$

where V_{bi} is the built-potential at zero bias. Let substitute Equations 2.24 into 2.23, we have

$$\begin{aligned} J_{S\rightarrow M} &= \frac{4\pi q m^* k^2}{h^3} T^2 \exp\left(-\frac{q(V_n + V_{bi})}{kT}\right) \exp\left(-\frac{qV}{kT}\right) \\ &= A^* T^2 \exp\left(-\frac{q\phi_b}{kT}\right) \exp\left(\frac{qV}{kT}\right) \end{aligned} \quad 2.25$$

where ϕ_b is the Schottky barrier height and is equal to the sum of V_n and V_{bi}, and A^* is the effective Richardson constant for thermionic emission, which is given as

$$A^* = \frac{4\pi q m^* k^2}{h^3} \quad 2.26$$

Since the barrier height for electrons moving from the metal into the semiconductor remains constant, the current flowing from the metal is not affected by the applied voltage [21]. At thermal equilibrium and 0 V bias, the current through the diode has to be zero, therefore the current flowing from the metal to the semiconductor should be equal to the current flowing from the semiconductor to the metal. Therefore, independent of bias, it follows that

$$J_{M\rightarrow S} = A^* T^2 \exp\left(-\frac{q\phi_b}{kT}\right) \quad 2.27$$

The resultant current density is therefore

© University of Pretoria

$$J_n = \left[A^* T^2 \exp\left(-\frac{q\phi_b}{kT}\right)\right]\left[\exp\left(\frac{qV}{kT}\right) - 1\right] \quad 2.28$$

and can also be written as

$$J_n = J_s\left[\exp\left(\frac{qV}{kT}\right) - 1\right] \quad 2.29$$

where J_s is the saturation current density of thermionic emission and is given by

$$J_s = \left[A^* T^2 \exp\left(-\frac{q\phi_b}{kT}\right)\right] \quad 2.30$$

Equation 2.29 gives the current density of an ideal diode. This equation can be re-written for the non-ideal case, in which series resistance and ideality factor will be included. The expression now becomes

$$J_n = J_s \exp\left(\frac{qV - IR_S}{nkT}\right)\left[1 - \exp\left(\frac{qV - IR_S}{kT}\right)\right] \quad 2.31$$

The ideality factor n is calculated from the gradient of the linear region of the semi-logarithmic *I-V* plot, and is given as

$$n = \frac{q}{kT}\frac{dV}{d(\ln I)} \quad 2.32$$

The series resistance is obtained from the deviation of the semi-logarithmic *I-V* plot from linearity at high currents [33], is given as

$$R_S = \frac{\Delta V}{I} \quad 2.33$$

2.5.4.2 Generation-recombination (G-R) current

This mechanism is due to the generation and recombination of carriers within the space charge region, and is usually observed at low temperature [25]. The recombination in the depletion region normally takes place via localized (defect) states. The most effective G-R centres are those with energies lying near the centre of the bandgap [25].

© University of Pretoria

The theory describing such a recombination centre is the same for both Schottky diodes and *p-n* junctions [35, 36]. The current density under forward bias is given by

$$J_r = J_{r0} \exp\left(\frac{qV}{2kT}\right)\left[1 - \exp\left(-\frac{qV}{kT}\right)\right] \quad 2.34$$

where $J_{r0} = qn_i w/2\tau_r$, and n_i is the intrinsic electron concentration, that is proportional to $\exp(-qE_g/2kT)$, where w is the depletion width and τ_r is the lifetime of carriers within the depletion region. This equation is derived by assuming that the energy levels of the centres coincide with intrinsic Fermi-level, that the capture cross sections for holes and electrons are the same and that the centres are distributed uniformly through the depletion region [25]. Recombination occurs in two processes (i.e. direct and indirect recombination) [37].

(i) *Direct recombination process:* In this process, an electron falls from the conduction band and then recombines directly with a hole in the valence band. This is also referred to as band to band recombination. It is common as radiative transitions in direct bandgap semiconductors. The conservation of energy for this process is ensured since electrons and holes recombining are located close to the semiconductor's band edge.

(ii) *Indirect recombination process:* In this case, an electron falls into a trap where it can recombine to a hole later. It can also be referred to as trap-assisted recombination. Since generation or recombination processes require conservation of energy and momentum, this event requires a lattice defect that will allow the conservation of momentum. This lattice defect is generally impurity atom with an energy state deeper in the bandgap. When electrons undergo transitions from the conduction band to the valence band, they collapse into the trap until the trap is filled up such that the acceptance of electrons is no more possible. Once this occurs, the electron that occupies the trap can in a second step fall into the valence band, therefore completing the recombination process. It can be deduced from the aforementioned that recombination can be determined by deep states and not intrinsic or doping dependent property.

© University of Pretoria

2.5.4.3 Quantum-mechanical tunnelling

This is the dominant transport mechanism in a Schottky diode on a highly doped semiconductor at low temperatures [21]. This takes place when electrons don't have sufficient energy for thermionic emission to take place, and the depletion region is narrow enough to allow quantum mechanical tunnelling through the barrier. According to *ref.* [25], the thermionic emission process is modified into the field and thermionic field emission when carriers tunnel in highly doped semiconductor at low temperatures.

(i) *Field emission:* This occurs when the current flow in the forward bias is as a result of tunneling of electrons with energies close to the Fermi level in the semiconductor.

(ii) *Thermionic field emission:* This occurs when the temperature is raised such that electrons are excited to higher energies where the barrier is adequately thin for tunneling to take place [25, 27, 33]. Although the number of excited electrons reduces very rapidly with increasing energy, there is maximum contribution to the current from electrons which have energy well above the bottom of conduction band.

Details discussions about quantum-mechanical tunnelling can be read in *refs.* [21, 27, 38, 39].

2.5.5 Schottky barrier height

The material used for illustration in this section is *n*-type 4H-SiC. Figure 2.7 shows the band diagram of a SBD on an *n*-type 4H-SiC substrate. In the ideal case, the barrier height of ϕ_{b0} occurs when the Schottky diode is strongly forward biased. Usually, the image force barrier lowering, interface states and some other factors are responsible for the difference between the actual barrier height of ϕ_b and the ideal barrier height.

© University of Pretoria

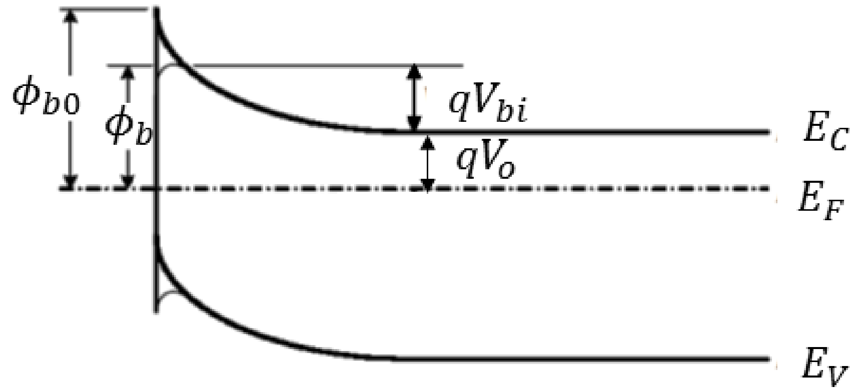

Figure 2.7: Energy band diagram of Schottky barrier potential showing lowering of the barrier due to image charges in the metal.

2.5.5.1 Current-Voltage (I-V) characteristics

This is a common technique to determine the quality of Schottky contacts in the semiconductor industry and laboratories. The technique involves measuring the forward and the reverse current through the device under different bias conditions. From these measurements, the Schottky barrier height, ideality factor and series resistance can be determined which in their turn indicate the quality of the diodes.

Neglecting the series and shunt resistance, thermionic emission predicts the *I-V* characteristics of a Schottky barrier diode to be [33]

$$I = AA^*T^2 \exp\left(-\frac{q\phi_b}{kT}\right)\left[\exp\left(\frac{qV}{nkT}\right) - 1\right] = I_s\left[\exp\left(\frac{qV}{nkT}\right) - 1\right] \quad 2.35$$

where I_s is the saturation current, A is the area of diode, $A^* = 146\ Acm^{-2}K^{-2}$ is the Richardson constant for n-type 4H-SiC, ϕ_b is the effective barrier height, V is the applied voltage, and n is the ideality factor. Figure 2.8 shows experimental results where the logarithm of the current was plotted versus voltage. The Schottky barrier height and the ideality factor can be calculated from the plot.

© University of Pretoria

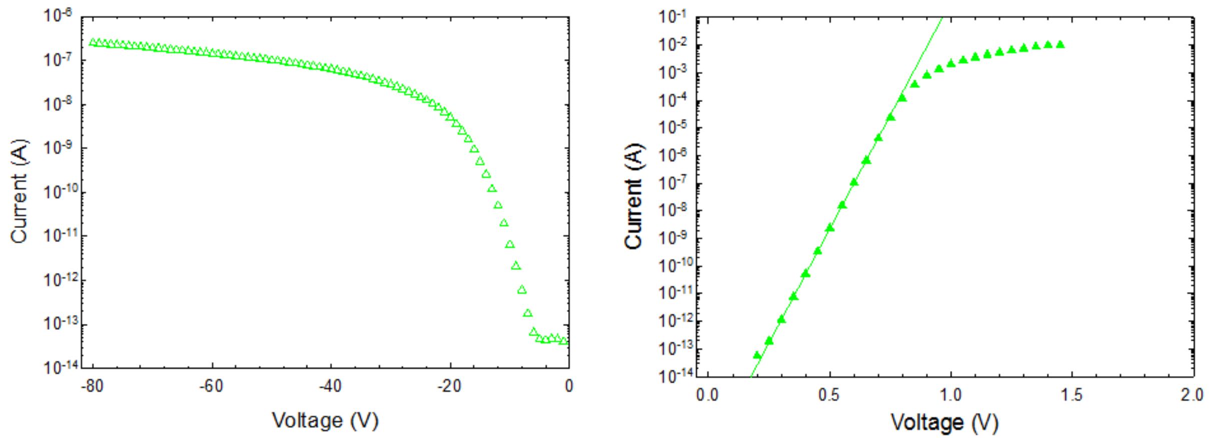

Figure 2.8: A semi-logarithmic forward and reverse I-V plots of Ni/n-type 4H-SiC device obtained at room temperature. The parameters n, I_s and ϕ_b were determined to be 1.04, 15.5×10^{-18} A and 1.25 eV, respectively [40]

The ideality factor obtained from the slope of the linear region of the plot according to Equation 2.36

$$n = \frac{q}{2.3kT\left[{d(\ln I)}/{dV}\right]} = \frac{q}{2.3kT \times s} \qquad 2.36$$

where s is the slope obtained from the straight line. The saturation current I_s can be calculated from the intercept of the plot (i.e. $\ln I$ axis at $V = 0$) as

$$I_s = AA^*T^2\exp(-\frac{q\phi_b}{kT}) \qquad 2.37$$

The Schottky barrier height can be determined from Equation 2.38 as

$$\phi_b = \frac{kT}{q}\ln(\frac{AA^*}{I_s}) \qquad 2.38$$

It follows that the barrier height ϕ_b depends on the value of the Richardson constant A^*. Therefore any uncertainty in the value of A^* translates to an inaccuracy in the barrier height [33].

© University of Pretoria

2.5.5.2 Capacitance-Voltage (C-V) characteristics

C-V measurements rely on the change of the width of the space charge region of a reverse-biased Schottky diode and provide an understanding of the dopant and defect distribution beneath the contact, an important parameter for the semiconductor industry. The capacitance of a 4H-SiC diode was measured and plotted as a function of voltage in Figure 2.9

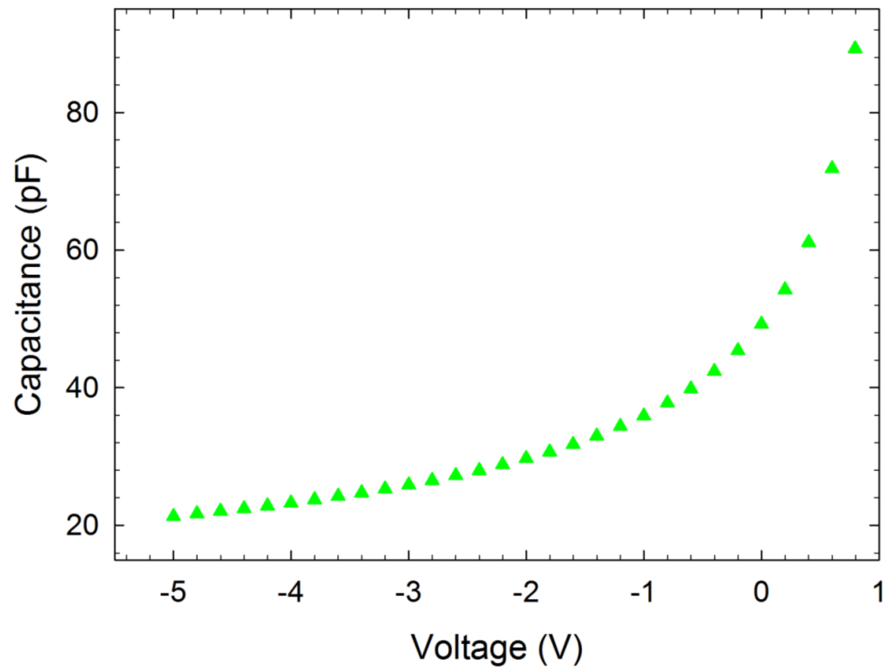

Figure 2.9: C-V characteristic obtained from a Ni/n-type 4H-SiC device at room temperature.

The *C-V* barrier height and doping density profile of the diode may be obtained as described in Section 2.5.3.

2.5.5.3 Current-Temperature (I-T)

For $V \gg {}^{kT}/_{q}$, Equation 2.35 becomes

$$\ln\left(\frac{I}{T^2}\right) \approx \ln(AA^*) - \frac{q}{kT}\left(\phi_b - \frac{V}{n}\right) \qquad 2.39$$

© University of Pretoria

A plot of $\ln(I/T^2)$ versus $1/T$ for a fixed bias voltage $V = V_1$ is known as a Richardson plot. If the ideality factor n is known independently, the slope $-q(\phi_b - V_1/n)/k$ and intercept $\ln(AA^*)$ of this plot may be used to determine the Schottky barrier height ϕ_b and the Richardson constant A^*, respectively. The Richardson constant A^* is often prone to error due to the extrapolation over a long distance.

As mentioned earlier, at the intercept of the extrapolated $\ln I$ vs V characteristics of a diode, $I = I_s$ and $V = 0$. If the *I*-*V* characteristics of a diode is measured as a function of temperature, it follows by substitution into Equation 2.39, that

$$\ln\frac{I_s}{T^2} = \ln(AA^*) - \frac{q\phi_b}{kT} \qquad 2.40$$

Figure 2.10 shows the plot of $\ln(I_s/T^2)$ versus $1/T$. The Schottky barrier height ϕ_b is now obtained from the slope equal to $-q\phi_b/kT$. The ideal behaviour of a diode and deviation of n-type 4H-SiC was obtained and explained by *refs.* [40, 41].

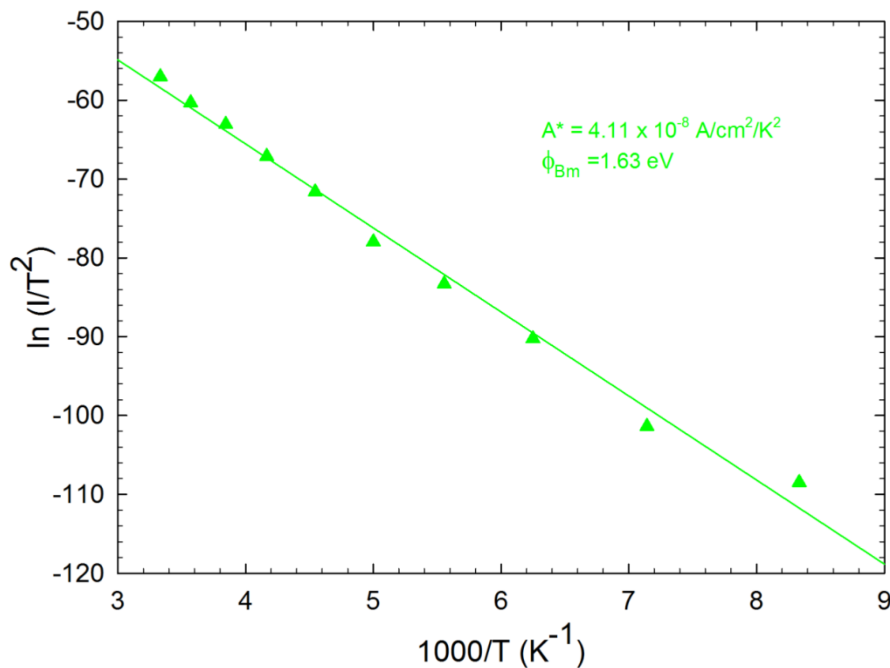

Figure 2.10: The plot of $\ln(I_s/T^2)$ versus $1/T$ obtained from a Ni/n-type 4H-SiC device before irradiation.

© University of Pretoria

2.5.6 The Richardson constant

Assuming pure thermionic emission (i.e. absence of series resistance), the determination of barrier height in M-S contacts is dependent on the saturation current I_s and the Richardson constant A^* (Equation 2.37). There is always an inaccuracy in the value of the barrier height due to uncertainty in the value of the Richardson constant [33]. Theoretically, the Richardson constant is dependent on the effective mass of the electron, m^* which is in turn depends on the temperature. It has been reported by Constantinescu and Nan showed that the variation of m^* with temperature is found to be a few per cent and is mostly determined by the temperature variation of the bandgap [42].

Experimentally, the Richardson constant may be determined as described in Section 2.5.5.1. The intercept of the extrapolated linear plot of $\ln I_s/T^2$ versus $1/T$ of Figure 2.10 were used to determine the Richardson constant. That is

$$A^* = \frac{\exp c_y}{A} \qquad 2.41$$

where c_y is an intercept at y-axis and A is the area of the diode.

Many researchers have reported different values of the Richardson constant over different temperature ranges [43-45]. The A^* is not only depends on the effective mass of the electron, but also depends on the quality of the contact (in turn depends on the cleaning of the surface during preparation), metal thickness and method of metal deposition (such as thermal/resistive evaporation, sputter deposition and electron beam deposition method) [46]. Also, as suggested by *ref.* [25], the value of the A^* can be affected by an oxide layer formed between the metal and the semiconductor during the deposition of the contact. The aforementioned effects influence the saturation current leading to the modification of the barrier, and therefore affect the value of the Richardson constant [47]. Another effect causing deviation of the Richardson constant from the theoretical value is contact barrier inhomogeneity [43].

2.5.6.1 Barrier height inhomogeneities

The effect of barrier height inhomogeneity was investigated by assuming that the barrier height varies across the area of the interface [48, 49]. The different barrier

© University of Pretoria

heights are attributed to the formation of an interface (oxide) layer between the metal and the semiconductor. The current flowing through the Schottky barrier diode will flow preferentially through the lower barriers in the potential distribution because of these potential instabilities at the interface [50, 51]. Corrections for the inhomogeneities have been reported in the literature [43, 50, 51]. Assuming a Gaussian distribution of the Schottky barrier height with a mean value of $\bar{\phi}_b$ and the standard deviation σ_s, the proportion of the diode with a barrier height $\bar{\phi}_b$ is given by [51-53]

$$P(\phi_b) = \frac{1}{\sigma_s\sqrt{2\pi}} \exp\left(-\frac{(\phi_b - \bar{\phi}_b)^2}{2\sigma_s^2}\right) \qquad 2.42$$

where $1/\sigma_s\sqrt{2\pi}$ is the normalization constant of the Gaussian barrier height distribution. The total current, $I(V)$ flowing across a diode is given by [43]

$$I(V) = \int_{-\infty}^{+\infty} I(\phi_b, V)P(\phi_b)d\phi \qquad 2.43$$

where $I(\phi_b, V)$ is the current at bias V for a barrier height based on the ideal thermionic emission diffusion.

After integrating Equation 2.43 and substitution, the $I(V)$ becomes

$$I(V) = A^*AT^2 \exp\left(-\frac{q\phi_{ap}}{kT}\right) \exp\left(\frac{qV}{n_{ap}}\right)\left[1 - \exp\left(-\frac{qV}{kT}\right)\right] \qquad 2.44$$

with

$$I_s = A^*AT^2 \exp\left(-\frac{q\phi_{ap}}{kT}\right) \qquad 2.45$$

where I_s is the saturation current, ϕ_{ap} and n_{ap} are the apparent barrier height and apparent ideality factor at bias equal to zero, respectively, and given by

$$\phi_{ap} = \bar{\phi}_{b0(T=0)} - \frac{q\sigma_{s0}^2}{2kT} \qquad 2.46$$

and

© University of Pretoria

$$\left(\frac{1}{n_{ap}} - 1\right) = \rho_2 - \frac{q\rho_3}{2kT} \qquad 2.47$$

Assuming $\bar{\phi}_b$ and σ_s are linearly bias-dependent on Gaussian parameters, such that mean value of the Schottky barrier height, $\bar{\phi}_b = \bar{\phi}_{b0} + \rho_2 V$, and the standard deviation, $\sigma_s = \sigma_s + \rho_3 V$, where ρ_2 and ρ_3 are voltage coefficients that may depend on temperature that quantify the voltage deformation of the Schottky barrier height distribution [54-56]. Since the temperature dependence of σ_s is small, it has little or no effect, therefore it can be neglected [57]. It is apparent that the decrease of zero-bias barrier height is caused by the existence of the Gaussian distribution and the extent of its influence is determined by its standard deviation. The effect becomes very significant at low temperature [43, 50].

It may be noted that, at low temperatures, tunnelling becomes significant. and it is expected that enhanced tunnelling through the low barrier regions may further influence the measured Schottky barrier height [58].

By fitting the experimental results to Equation 2.45, this gives ϕ_{ap} and n_{ap} which should obey Equations 2.46 and 2.47. Therefore, the plot of ϕ_{ap} against $1000/T$ should give a linear plot, where $\bar{\phi}_{b0}$ and σ_{s0} can be determined from the intercept and slope, respectively. In addition, a fit for the different values of the apparent ideality factor as a function of temperature, which should obey Equation 2.47, should be straight line and the voltage coefficients, ρ_2 and ρ_3 can be determined as the intercept and gradient, respectively. The standard deviation is a measure of the barrier homogeneity [50]. A lower value of σ_{s0}, corresponds to a more homogeneous Schottky barrier and better diode rectifying performance.

The Richardson constant can be modified to take barrier height inhomogeneities into account by combining Equations 2.45 and 2.46

$$\ln\left(\frac{I_s}{T^2}\right) - \left(\frac{q^2\sigma_{s0}^2}{2k^2T^2}\right) = \ln AA^{**} - \frac{q\bar{\phi}_{ap}}{kT} \qquad 2.48$$

© University of Pretoria

where A^{**} is the modified Richardson constant. A plot of $\ln(I_s/T^2) - (q^2\sigma_{s0}^2/2k^2T^2)$ against $1000/T$ should give a straight line with slope giving the mean barrier height and the intercept gives the modified Richardson constant, as shown in Figure 2.18.

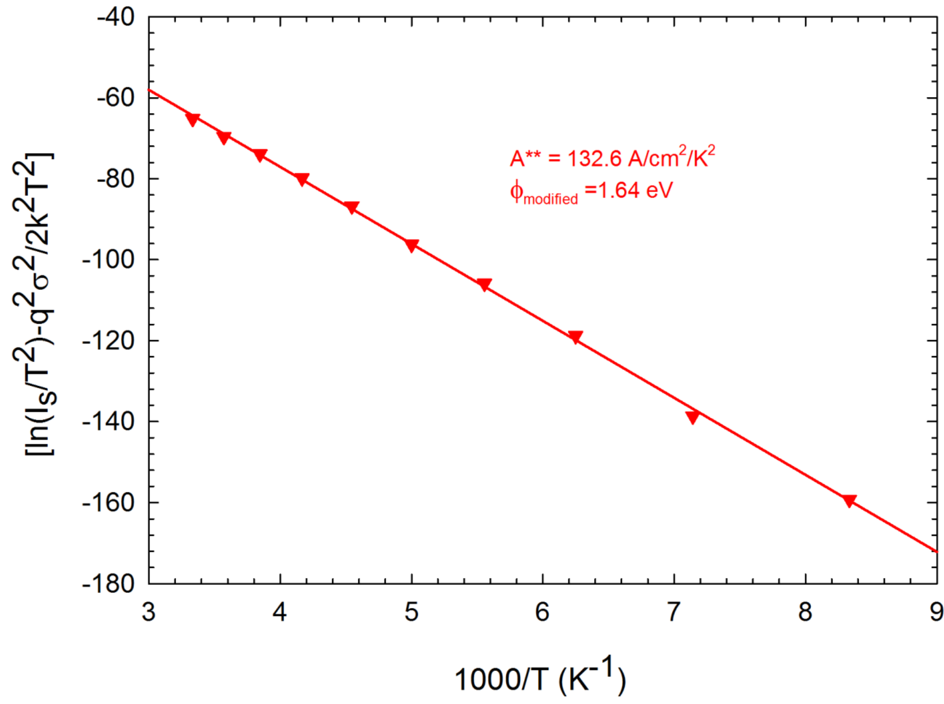

Figure 2.11: The plot of $\ln(I_s/T^2) - (q^2\sigma_{s0}^2/2k^2T^2)$ versus $1000/T$ obtained from a Ni/n-type 4H-SiC device before irradiation.

2.5.7 Ohmic contacts

An ohmic contact is a non-rectifying junction. It is defined as a metal-semiconductor contact that has an insignificant junction resistance compared to the total resistance of the semiconductor device [21]. For an ideal ohmic contact, charge carriers can freely flow in both directions across the metal-semiconductor junction with low or no resistance. The specific junction or contact resistance can be defined as the reciprocal of the current density with respect to voltage. The contact resistance, R_C can be expressed by Equation 2.49 when evaluated at zero volts applied bias

$$R_C = \left(\frac{\partial J}{\partial V}\right)_{V=0}^{-1} \quad 2.49$$

where J is the current density of M-S contact that depends on

© University of Pretoria

(i) the applied voltage,

(ii) the barrier height, and

(iii) the doping density [33].

In order to achieve an ohmic contact to *n*- and *p*-type semiconductor, the following approaches can be used:

(i) The metal work function ϕ_m can be chosen to be below that of semiconductor ($\phi_m < \phi_s$) in *n*-type semiconductor as shown in Figure 2.12a and b, and vice-versa for *p*-type, for an ideal ohmic contact. A low resistance contact to a semiconductor will be obtained if the barrier height is relatively small compared to kT. In this case, carriers can easily flow across the barrier in both directions with little or no resistance Figure 2.12c [21, 59]. Equation 2.50 mathematically relates the contact resistance to the barrier height

$$R_C = \frac{k}{qA^*T}\exp\left(\frac{q\phi_b}{kT}\right) \quad 2.50$$

(ii) If a metal does not exist with low enough work function to produce low barrier height; the tunnel contact is an alternative Figure 2.12d. The contacts should have a high enough doping in the semiconductor so that the layer separating the metal from the semiconductor interface is very thin. According to Sze, the recommended doping density required for the contact is at least 10^{19} cm^{-3} [21].

The two cases are illustrated schematically in Figure 2.12.

© University of Pretoria

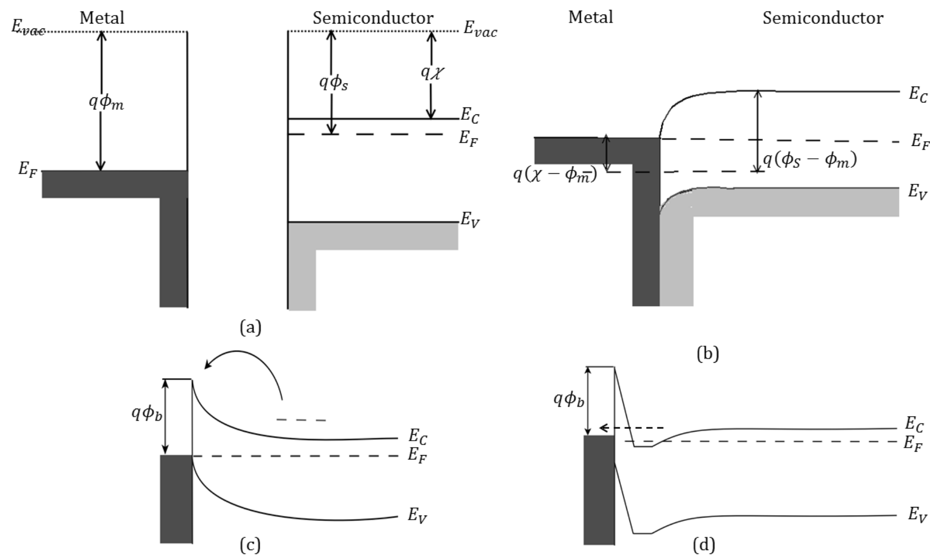

Figure 2.12: Electron energy diagrams between a metal and n-type semiconductor with ($\phi_m < \phi_s$), (a) materials neutral and isolated from each other, (b) thermal equilibrium situation of ideal ohmic contact formation is made, redrawn after ref. [37]. (c) Ohmic contact formation by low Schottky barrier height, and (d) ohmic contact formation by high doping contacts, redrawn after [21].

2.6 Defects in semiconductors

2.6.1 Introduction

A perfect crystal can be defined as a regular arrangement of atoms at particular crystal lattice sites. It contains no point, line, volume or planar imperfections. Even in the most ideal situations, a perfect crystal is impossible to attain. This is due to many reasons including growth methods, subsequent cooling and device processing. Imperfections in semiconductors generally occur as a result of impurities or thermal excitation at finite temperature above 0 K [60]. These imperfections, which may be in different dimensions, are called defects. Defects can be introduced intentionally e.g. by impurity doping into semiconductor to enhance the conductivity of the devices or irradiation to reduce carrier lifetime and increase switching speeds.

Many defects induce electronic states in the bandgaps of semiconductor materials. These states can be classified as shallow and deep-levels. The classification of levels as deep or shallow depends on their location with respect to valence or conduction band

© University of Pretoria

edge. The defects are classified as shallow level defects if their states are located near the valence band for acceptors and near the conduction band for the donors. Deep-level defects have levels found deeper in the bandgap, usually deeper than the dopant levels. Depending on their electron and hole capture cross section, these deep-levels can act as recombination centres or traps. Defects can either be beneficial or detrimental to device operations, depending on their applications. Defects can also be categorised into point and extended defects. In this section, the discussion will be more focus on point defects in SiC.

2.6.2 Point defects

Point defects are zero dimensional defects. They are isolated atoms in confined areas of a host crystal. Figure 2.13 shows the schematic diagram of point defects in a semiconductor such as SiC. Common point defects include:

i) ***Vacancy***: An atom missing from its original lattice position. The vacancy in SiC can either be silicon vacancy, V_{Si} (there is no atom on a silicon lattice site) or carbon vacancy, V_C (there is no atom on a carbon lattice site).

ii) ***Interstitial***: An atom that inhabits a position different from its normal site. Interstitials can be classified as self-interstitials (i.e. if the atom is the same as one of the species of the host lattice), or an interstitial impurity (i.e. if the interstitial atom is different species from the host atoms). In SiC, a self-interstitial can either be silicon, Si_i or carbon, C_i. Often, an interstitial may occupy different lattice sites, e.g. in SiC cubic and hexagonal sites are possible.

iii) ***Frenkel pair***: A self-interstitial atom is located close to a vacancy.

iv) ***Antisite***: In compound semiconductors, an atom of one sub-lattice is positioned in a lattice site of the other element. E.g. in SiC, when Si takes the lattice position of C (a silicon antisite, C_{Si}) or C is on a Si lattice point (a silicon antisite, Si_C).

v) ***Substitutional impurity***: A foreign atom that occupies a lattice site e.g. a nitrogen atom on a C site (N_C).

In addition, combinations of defects may occur, e.g. a vacancy next to a dopant atom. This section is writing after *refs*. [61, 62]. Point defects can also be classified as intrinsic and extrinsic lattice defects.

© University of Pretoria

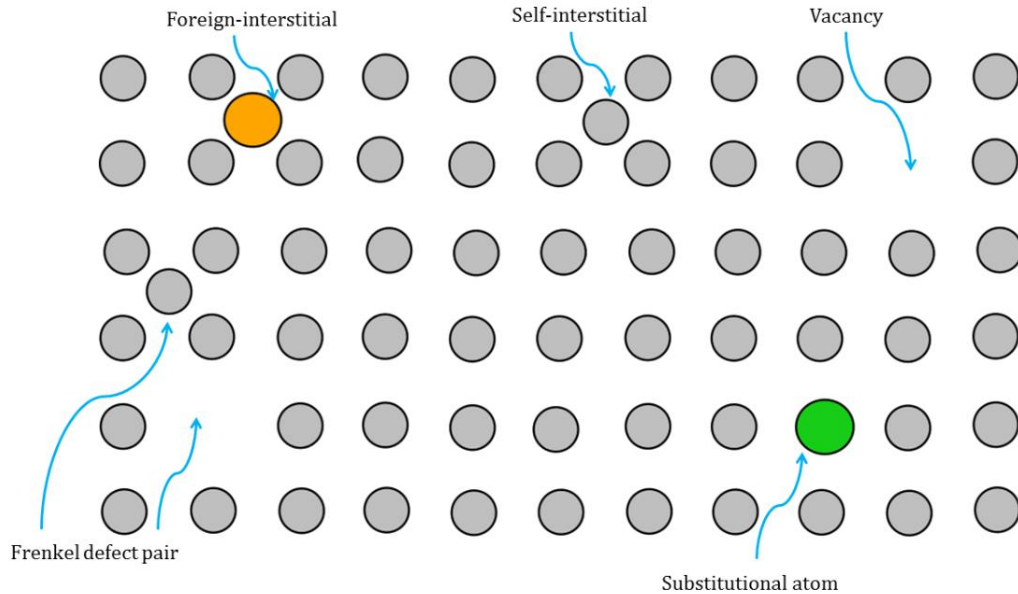

Figure 2.13: The schematic diagram of point defects in semiconductor [63].

2.6.2.1 Intrinsic point defects

Defects that occur as a result of re-arrangement of the host atoms in the lattice site are called intrinsic lattice defects. Intrinsic defects are vacancies, interstitials and antisites. Their properties are dependent on the site. Defects have different energy levels in the bandgap when occupying either cubic (*k*) or hexagonal (*h*) sites. These differences can be observed by optical and electron paramagnetic resonance (EPR) techniques [64] as well as DLTS. The discussion in this sub-section will mainly focus on the well-known defect known as the Z_1/Z_2 in 4H-SiC.

The Z_1/Z_2 has been widely studied and is present in both the as-grown and irradiated *n*-type 4H-SiC [65, 66]. The defect is known for its unusual thermal stability (1700 °C) [67] and has two closely spaced electrical levels. For 6H-SiC polytypes, it was reported that defects E_1 and E_2 have properties similar to Z_1/Z_2 [68-70]. The deep-levels for 4H-SiC and 6H-SiC show negative-*U* behaviour, i.e. they have inverted donor (0/+) and acceptor (−/0) levels [66, 71]. The reported energy levels associated with donor and acceptor levels of Z_1/Z_2 for 4H-SiC range from E_C – 390 to E_C – 460 meV and E_C – 620 to E_C – 710 meV, respectively. In 6H-SiC, the E_1 and E_2 also range from deep-levels from E_C – 190 to E_C – 290 meV and E_C – 380 to E_C – 440 meV [70]. Although it has been confirmed that these defects have intrinsic nature [72], the structure of these defects has long been debated. Researchers have suggested that the Z_1/Z_2 defect is a silicon vacancy [73], a

© University of Pretoria

carbon vacancy [74], a complex of nitrogen with the carbon interstitial [75], a silicon antisite-silicon vacancy complex [76] or a silicon carbon antisite pair [76]. Asghar *et al* carried out a study on 4H-SiC before and after alpha-particle irradiation and suggested that the of Z_1/Z_2 centres involved silicon and carbon vacancies [77]. Hemmingsson *et al* studied the dependence of the deep-level defects in electron irradiated 4H-SiC on the energy of the electrons. He concluded that the structure of the defects could be linked to the Si vacancy since C is lighter than Si and can therefore be displaced by lower energy electrons [66]. After years of argument, the SiC community recently concluded that the Z_1/Z_2 traps are due to the C vacancy [78].

2.6.2.2 Extrinsic point defects

Defects that arise in semiconductors through the presence of foreign atoms such as doping impurities are called extrinsic defects. These defects can alter the electrical conductivity of semiconductor materials. They can be classified further into solutes (if the foreign atom intentionally added during growth by diffusion or ion implantation after growth) and impurities (if added in error or unintentionally during the growth of crystal). The foreign atom may either occupy a lattice site, and be called a substitutional solute, or fill an interstitial position and be called an interstitial solute. The position preferred by a specific solute is determined by the size of the foreign atoms. Since nitrogen, carbon and hydrogen are small in size, they occupy interstitial sites.

(a) Acceptors in SiC

To obtain *p*-type conductivity in SiC, the SiC is doped with group III atoms, commonly boron, aluminium and gallium. Group III elements have one less valence electron than group IV atoms (such as Si and C), therefore one electron is needed to complete the bond, and the defect behaves as an acceptor.

Aluminium is the most preferable *p*-type dopant in SiC because of the group III elements, it has the highest solubility ($\sim 10^{21}$ cm^{-3}) and forms the shallowest acceptor levels [79-81]. The ionization energy of Al decreases from 270 to 100 meV as the concentration increases from 10^{18} to 10^{21} cm^{-3} [80]. Also, the ionization energy of Al in 4H-SiC has been described to be $E_v + 240\, meV$, which does not depend on its concentration up to 5×10^{20} cm^{-3}, provided the degree of compensation of the epitaxial layers, k is less than 1%.

© University of Pretoria

The boron impurity in SiC is also of interest because of its high solubility (~10^{20} cm^{-3}), and rapid diffusion [82]. It has been reported that B has a shallow acceptor impurity in 4H-SiC with ionization energy of $E_v + 350\ meV$ as obtained from Hall measurements.

(b) Donors in SiC

Undoped SiC has *n*-type conductivity [82]. For additional doping group V and VI atoms are donors that contribute extra electrons to the valence band of the semiconductor. The most common dopant of SiC is nitrogen, because of its fairly high solubility (≈10^{21} cm^{-3}) and lowest ionization energy compared to all impurity donors in SiC such as oxygen, phosphorus, indium and arsenic [83, 84].

The N atoms appear to substitute C atoms in the SiC lattice and act as a shallow donors [85, 86]. Nitrogen atoms also occupy non-equivalent lattice positions: cubic (c) and hexagonal (h) lattice site [82]. This influences the energy position of deep-levels related to N atoms [87, 88]. The energy levels associated with N donor are estimated to be 45-65 meV and 90-100 meV below the conduction band for hexagonal and cubic sites, respectively [40, 89-91].

Phosphorus forms shallow levels in SiC with an ionisation energy of 53.9 meV and has a lower solubility compared to N [84]. It has been reported by Capano *et al* that P causes two related energy levels at 53 meV and 93 meV below the conduction band in 4H-SiC after implantation and which are associated with hexagonal and cubic lattice sites [92].

(c) Transition metal impurities in SiC

Due to their incomplete *d*-orbitals, transition metal impurities affect the properties of semiconductors strongly even at low concentrations. The transition metal impurities form electrically active deep-level defects within the bandgap of semiconductors which can capture electrons. The most common transition metal impurities in SiC are titanium, vanadium, chromium and iron [93, 94]. SiC is mostly contaminated with these impurities during high-temperature growth such as the Lely-process [95]. This is mainly due to transition metal contaminants in the graphite parts of the reactor. Consequently, the SiC powder used for SiC crystal growth always contains minute amounts of transition metals. Generally, transition metal defects are detrimental to SiC devices [96].

© University of Pretoria

Titanium impurities have a large effect on the electrical properties of SiC. The existence of centres associated with the presence of Ti impurity has been demonstrated in 4H-SiC by Dalibor *et al* and Maier *et al* using electron spin resonance [97-99]. Two deep-levels related to Ti have been observed in *n*-type 4H-SiC using DLTS [98]. The two energy levels are attributed to attribute ionized titanium acceptors that reside at hexagonal and cubic Si lattice positions and have DLTS ionization energy of E_C – 0.12 eV and E_C – 0.16 eV, respectively. Similar values were obtained by Achtziger *et al al* [100], but within experimental significant error. The structure of these defects was confirmed by electron spin resonance (ESR) and optically detected magnetic resonance (ODMR) [97, 101]. According to the Langer-Heinrich (L-H) rule, the position of the energy levels of transition metals in isovalent semiconducting materials remains constant. For example, the position of Ti levels in SiC does not change with the parameters of the polytypes. Also, the detectability of these centres by different methods depends on the magnitude of the bandgap of individual polytypes. The ground state of Ti observed for 4H-SiC from DLTS will be different for 6H-SiC because of its narrower bandgap [82].

Hobgood *et al* and Mitchel *et al* have reported that doping SiC with vanadium leads to the formation of semi-insulating layers of SiC [94, 102]. Their findings led to the study of properties of vanadium in SiC by many researchers. From the literature, it has been reported that vanadium has amphoteric characteristics in SiC, which leads to creation of acceptor and donor levels [97, 103, 104]. The DLTS results from Dalibor *et al* revealed that vanadium introduce an acceptor-like defect at E_C – 0.88 to 0.97 eV in 4H-SiC polytype [105]. Achtziger *et al* also reported the same results for the energy position of V in *n*-type 4H-SiC [100]. The energy position reported for V in 6H-SiC is E_C – 0.60 to E_C – 0.75 eV [105].

A chromium impurity is another common impurity in SiC. The level associated with Cr in SiC has not been yet been established. Three deep-levels, 0.15, 0.18 and 0.74 eV below the conduction band, have been reported by Achtziger *et al* after the implantation of ^{51}Cr in 4H-SiC also containing stable vanadium. The deep-level defect at E_C – 0.74 eV vanished shortly after implantation [106]. The other two defects disappeared at a rate consistent with the decay of ^{51}Cr [100] and are therefore believed to relate to a chromium in non-equivalent cubic and hexagonal lattice positions [105].

© University of Pretoria

2.7 Defect characterization

2.7.1 Introduction

The electrical characteristics of semiconductors can be affected by even low levels of defect concentrations. Defects in semiconductors can be detrimental or beneficial to the operation of devices. For instance, defects are beneficial to devices in enhancing their operation by increasing the switching speeds by acting as recombination centres [107], but reduce the minority carrier lifetime in photovoltaic applications [108], which is detrimental to the device. Therefore, it is important to have a reliable and accurate technique to characterize the electrical properties of defects in semiconductors.

DLTS is a powerful technique for characterizing electrically active defects in 4H-SiC, and will be described briefly in this section.

2.7.2 Shallow level defects and deep-level defects

Metals, semiconductors and insulators are different from one another by the energy gap between the conduction and valence bands. This gap is the energy region that is free of electronic levels. Defects and dopants add states within the bandgap and thereby modify the semiconductor's electrical conductivity. Electrically active defects have levels in the band gap that can capture or emit charge carriers to the valence and conduction bands. The behaviour of these defects is influenced by the position of the states in the band gap [109]. Electrically active defects can be classified into shallow and deep-level defects.

2.7.2.1 Shallow level defects

Shallow level defects have energy levels within a few tens of milli-electron volts from the semiconductor band edges (i.e. either the conduction band or the valence band) [109]. The shallow defects can be described using the effective mass approximation according to which the potential due to the defect is approximated by a coulomb potential leading to extended wave functions. Experimentally shallow level defects are often characterized by Hall effect measurements. For more details about this section, see *refs*. [27, 110].

© University of Pretoria

2.7.2.2 Deep-level defects

Deep-level defects are defects with highly localised wave functions. Their binding energies cannot be determined by the effective mass approximation [109]. Other techniques such as Green's functions and density functional theory are used to determine the energy levels of deep-level defects [110]. Generally, these levels lie deeper in the semiconductor's bandgap, however in some cases electronic levels are close to the band edges [27]. Despite these states lying close to the band edges, these defects are classified as shallow levels due to their localised wave functions. Therefore, deep-level defects can be broadly defined as any levels that cannot be classified as shallow level defects [110].

2.7.3 Emission and capture of carriers by trapping centres

Deep-level defects that influences the electrical properties of a semiconductor can be described as an electron trap, a hole trap, a recombination centre or a generation centre, based on the nature of the interactions with charge carriers that are transferred between the defect and the conduction and valence bands. A hole trap is a deep-level defect that is full of electrons, and capable of having a trapped electron recombining with a hole [111]. Whereas, an electron trap is a defect level that has deficit of electrons, capable of capturing the electron from the conduction band. In neutral semiconductor, an electron trap is a defect for which the electron capture rate from the conduction band is much greater than the hole capture rate from the valence band (i.e. $c_n \gg c_p$). For a hole trap, the reverse is the case ($c_p \gg c_n$). In contrast with the previous cases, a recombination centre has c_n almost equal to c_p [33, 107]. Figure 2.14 shows the four possible processes that can take place when deep-level interacts with the conduction and valence band. The four processes are represented by (1) to (4):

(1) Here the deep-level defect captures an electron from the conduction band. The process is characterised by electron capture rate c_n.

(2) After electron capture, the deep-level defect can either emit the electron back to the conduction band (called electron emission e_n)

(3) or it can capture a hole from the valence band (hole capture rate, c_p)

© University of Pretoria

(4) After hole capture, the hole can be emitted to the valence band (or (1) may occur).

From Figure 2.14, a recombination event is the combination processes (1) and (3), and a generation event is (2) and (4). A defect where these processes occur is called a generation-recombination centre. The detail description can be found in *ref.* [33].

The kinetics of charge transfer between deep-level defects and the conduction or valence band is extensively discussed in *refs.*[33, 35, 36]. The capture cross section σ_n and the electron capture rate c_n are related according to Equation 2.51 [107]

$$c_n = \sigma_n \langle v_n \rangle n \tag{2.51}$$

where n is the electron concentration in the conduction band and $\langle v_\mathrm{n} \rangle$ is the average thermal velocity of free electrons, which is given by

$$v_n = \sqrt{\frac{3kT}{m_e^*}} \tag{2.52}$$

where k is the Boltzmann constant, T is the temperature in Kelvin and m_e^* is the effective mass of the electron.

A similar expression applicable to the hole capture rate c_p in terms of the hole capture cross section σ_p and the thermal velocity of holes in the valence band v_p.

By applying the principle of detailed balance and considering carrier concentrations at thermal equilibrium, the thermal emission rate of electron deep-level defect to the conduction band as a function of temperature $e_\mathrm{n}(T)$ can be derived [107, 112, 113].

$$e_n(T) = \frac{g_0}{g_1} \sigma_n \langle v_n \rangle N_C exp\left(-\frac{E_C - E_T}{kT}\right) \tag{2.53}$$

where g_0/g_1 is the degeneracy between empty and filled energy levels, $E_C - E_T$ is the activation energy of the deep-level defect and N_C is the effective density of states in the conduction band

© University of Pretoria

$$N_c = 2M_C \left(\frac{2\pi m_e^* kT}{h^2}\right)^{\frac{3}{2}} \quad 2.54$$

where M_C and h represent the number of conduction band minima and Planck's constant, respectively.

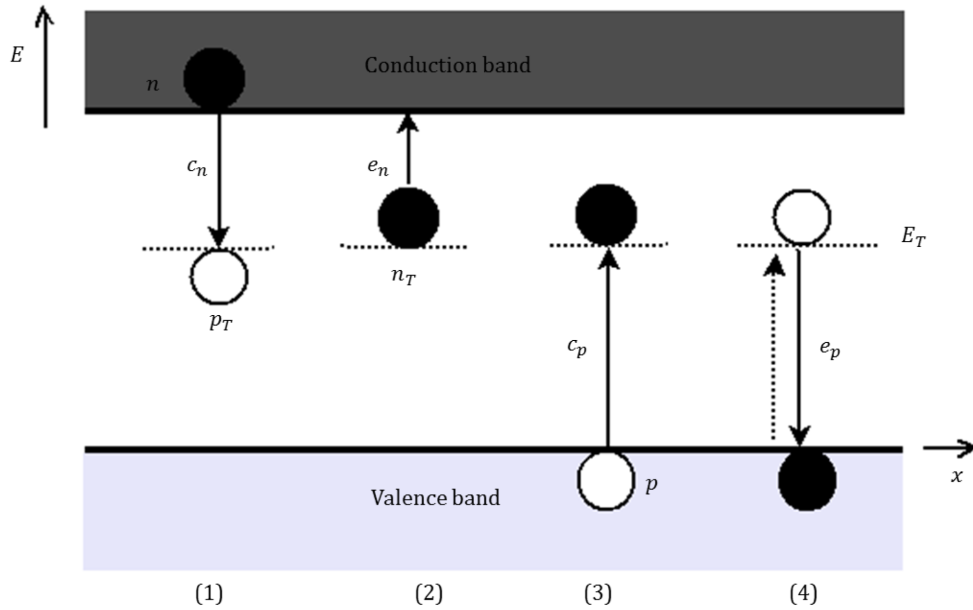

Figure 2.14: The schematic diagram of different carrier transitions between deep-levels and the energy bands. (1) electron capture, (2) electron emission, (3) hole capture, and (4) hole emission. (Redrawn from ref. [33]).

From Equation 2.54, the product of quantities N_C and $\langle v_n \rangle$ has a T^2 dependency. If e_n is measured as a function of temperature, an Arrhenius plot of $\ln(e_n/T^2)$ as a function of $1/T$ gives a straight line from which the apparent capture cross section of the defect, σ_{na}, can be calculated from the intercept ($T^{-1} = 0$) and the activation energy of electron emission from the deep-level defect, $E_C - E_T$, is determined from the slope. The capture cross section determined is an apparent capture cross section. The true capture cross section is determined by measuring capture rates directly and may be temperature dependent [114].

If capture cross section is temperature dependent due to a capture barrier, the capture cross section at temperature T [33, 107, 114]

© University of Pretoria

$$\sigma_n = \sigma_\infty \exp\left[-\frac{\Delta E_\sigma}{kT}\right] \qquad 2.55$$

where σ_∞ is the capture cross section as the temperature tends to infinity and ΔE_σ is the thermal activation energy of the capture process, which is also called the capture barrier. The likely cause of temperature dependence of the capture cross section for many deep-level defects may be as a result of multiphonon emission due to lattice relaxation [111, 115]. The temperature dependence of the true electron capture cross section can be calculated from the plot of $\ln \sigma(T)$ as a function of $1/T$, where the ΔE_σ can be determined from the slope and σ_∞ can be obtained after extrapolation to $T = \infty$.

The activation energy of a deep-level defect whose capture cross section is dependent on temperature is given by

$$\Delta E_a = (E_C - E_T) + \Delta E_\sigma \qquad 2.56$$

From Equation 2.56, the thermal emission rate of electrons can now be re-written as

$$e_n(T) = \frac{g_0}{g_1}\sigma_n\langle v_n\rangle N_C \exp\left(-\frac{(E_C - E_T) + \Delta E_\sigma}{kT}\right). \qquad 2.57$$

The parameter, ΔE_n, is the energy required to excite an electron from the trap level to the conduction band, which is called the Gibbs free energy, given by [116]

$$\Delta E_n = \Delta H_n - T\Delta S_n \qquad 2.58$$

where ΔH is the change in enthalpy, ΔS is the change in entropy and the temperature is T. Re-writing Equation 2.57 and substituting into Equation 2.58, it follows that

$$e_n(T) = \frac{g_0}{g_1}\sigma_n\langle v_n\rangle N_C \exp\left(\frac{\Delta S}{k}\right) \exp\left(-\frac{\Delta H_n}{kT}\right) \qquad 2.59$$

Therefore, the slope of an Arrhenius plot gives the activation enthalpy of the deep-level defect, and not the free energy. The free energy can be calculated from optical measurements [107].

© University of Pretoria

The apparent capture cross section and the activation energy are referred to as the defects "signature". One of the techniques that can be used to determine the signature of a defect from thermal activation of charge carriers is DLTS. This technique will be considered briefly in the following Section.

2.7.4 Deep-level transient spectroscopy

DLTS is a powerful technique that can be used to investigate and characterize the electrically deep-level defects in the space charge region (depletion region) of a semiconductor. This technique was invented by D. V. Lang in 1974 [111], and involves probing the depletion region of a Schottky barrier diode, a *p*-*n* junction, MIS or MOS device structure. DLTS plots a graph, usually a series of peaks, showing the emission of carriers from defects as a function of temperature. The peak's sign indicates whether the deep-level trap is due to minority- or majority-carriers, and the peak's position is determined by the rate window of the instrument and the temperature dependent thermal emission of the corresponding deep-level trap [111]. This technique is fast, sensitive and not difficult to analyse [111]. This powerful tool can be used to determine the *signature* (the activation energy and the capture cross-section) and concentration of deep-level traps.

According to Equation 2.10, the depletion width of the depletion region of a Schottky barrier diode or *p*-*n* junction varies with the applied bias voltage. The depletion width decreases if a forward bias is applied ($V > 0$), and vice-versa. According to Equation 2.12, the relationship between the capacitance of a reverse-biased Schottky diode and the depletion width of the space charge region depends on the charge in the space charge region. This charge is due to the ionized deep-level defects and the dopants [107, 117, 118]. The capacitance from Equation 2.12 is inversely proportional to the depletion width.

Figure 2.15 depicts a SBD on an *n*-type semiconductor with a low concentration of deep-level defects that introduces a deep trap with energy E_T. At equilibrium, the defect level below the Fermi level is filled with electrons, but empty when above the Fermi level, which is in agreement with a step-function approximation of the Fermi distribution function. The shaded circles represent filled traps and the un-shaded circles represent

© University of Pretoria

empty traps in Figure 2.15. The DLTS measurement involves a cyclical process which can be broken into 4 stages.

Stage (a): Applying a steady-state reverse bias voltage, V_a, as shown in Figure 2.15 (a), leads to an increase in the depletion width, which affects the occupation of defects in the space charge region. An increase in the depletion width causes a decrease in capacitance.

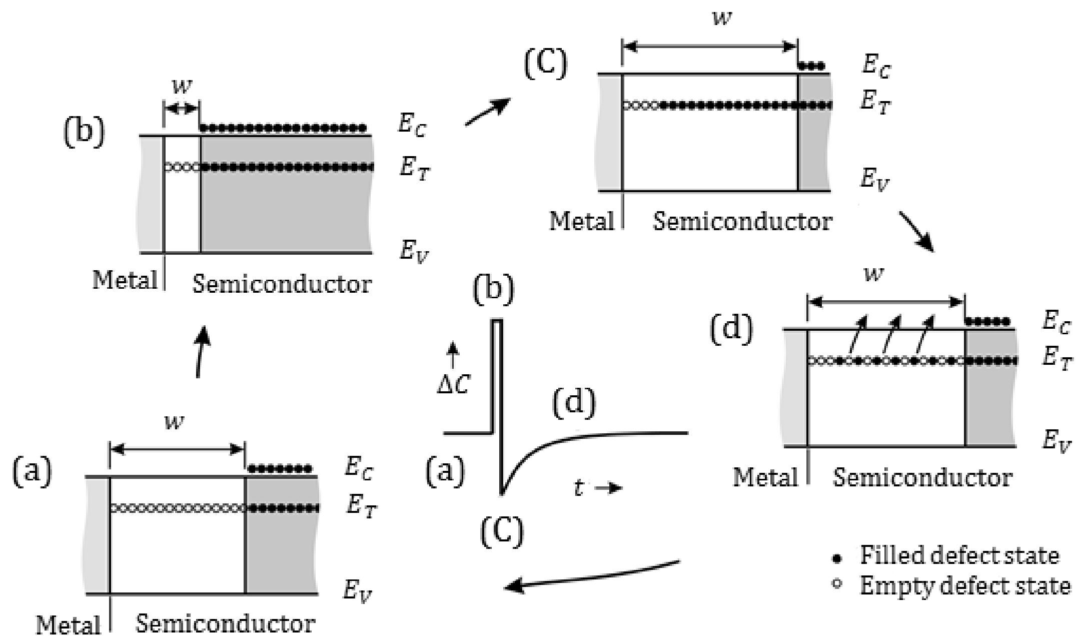

Figure 2.15: The variation of the depletion region width and trap occupation of an electron trap in an n-type semiconductor due to voltage bias and filling pulse during a DLTS measurement.[107].

Stage (b): Reducing the applied reverse bias by applying a majority carrier filling pulse, decreases the depletion width, causing an increase in the capacitance and allows electrons to be trapped by deep-levels. The pulse width at the stage (b) is assumed to be long enough to allow some of the empty levels to be filled.

Stage (c): Removing the applied filling pulse immediately leads to restoration of quiescent reverse bias. Since the electrons remain trapped in the deep-levels, the charge density in the depletion region is decreased compared to that in stage (a), this leads to a widening of the depletion region and a decrease in the capacitance.

© University of Pretoria

Stage (d): At this stage, the filled deep-levels above the Fermi level in the depletion region begin to emit trapped electrons with a characteristic rate into the conduction band. The emitted carriers are removed immediately by the electric field in the depletion region [119]. This increases the charge density in the depletion region and causes the depletion width to decrease and the capacitance to increase. This change in capacitance is usually seen as an exponential decay.

As discussed earlier from *ref.* [107], the emission rate for the electron can be determined experimentally from the time dependence of the capacitance transient. The density of the occupied traps, $N(t)$ at time t after removing the filling pulse is given in Equation 2.60

$$N(t) = N_T \exp(-e_n t) \tag{2.60}$$

where e_n is the thermal emission rate and N_T is the concentration of traps filled by the filling pulse. If $N_\mathrm{T} \ll N_\mathrm{D}$, the depletion width will not change significantly during the emission of carriers, therefore an exponential decay may be used to describe the emission of carriers from the depletion region. The junction capacitance, $C(t)$, of the Schottky diode is given by Equation 2.61

$$C(t) = C_0 - \Delta C_0 \exp(-e_n t) \tag{2.61}$$

where C_0 is the capacitance at quiescent reverse bias voltage and ΔC_0 is the change in capacitance immediately after filling pulse was removed.

The trap concentration, N_T, can be calculated from the change in capacitance by applying Equation 2.12

$$N_\mathrm{T} \approx 2N_\mathrm{D}\frac{\Delta C}{C} \tag{2.62}$$

For the above derivation it has been assumed that the defect level is full in the bulk and empty in the depletion region. Figure 2.16 shows a more realistic model, where the deep-level defect intersects the Fermi level at a distance λ shallower than the depletion region edge, since the deep-level defect is much deeper in the bandgap than the dopant

© University of Pretoria

level. Assuming constant dopant concentration, the region λ is independent of the depletion width and given by

$$\lambda = \sqrt{\frac{2\varepsilon(E_F - E_T)}{qN_D}} \quad 2.63$$

where ε is the dielectric constant of the semiconductor, q is the electron charge, E_F is the Fermi level and $E_T$is the trap level. The DLTS measurement can only probe the region up to a distance λ before the depletion region edge. This condition should be

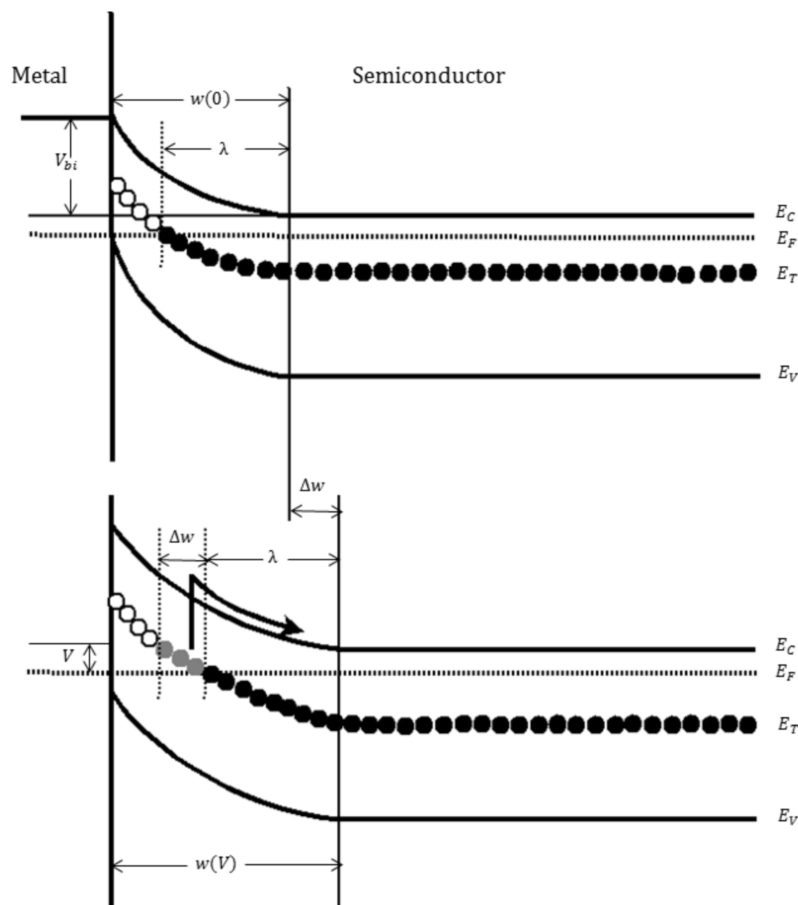

Figure 2.16: Filling (top) and subsequent emission (bottom) of electrons from a deep-level in the depletion region, assuming a constant Fermi level. In the top sketch, the filling of the defect during the filling pulse is shown. Note that because of band bending and the depth of the defect level, the deep-level is filled to a depth λ shallower than the depletion region edge. The depletion region changes by an amount Δw when the filling pulse is removed and the quiescent reverse bias is applied. (redrawn from ref [32].).

© University of Pretoria

taken into consideration when using DLTS to determine the depth profile of deep-level defects or the electric field experienced by the deep-level defect. *Refs* [107, 111, 120] provide more details about DLTS depth profiling.

2.7.3.1 Convectional DLTS

It is important to understand how the DLTS transient signals are converted to a DLTS quasi-spectrum as a function of temperature [121]. According to the method described by *Lang,* the capacitance transient can be measured at two fixed instants (t_1 and t_2) after the filling pulse, and the signal $C(t_1)$–$C(t_2)$ is plotted as a function of temperature (see Figure 2.17) [111, 114]. The emission process from individual deep-level defects is very slow at low temperatures and increases as the temperature increases. Therefore, the capacitance difference is small at low temperature, which corresponds to slow transients as well as at high temperature, which corresponds to fast transients. As shown in Figure 2.17, the peak in the spectrum corresponds to a time constant (τ_{max}) defined by the selected times, t_1 and t_2, is given by:

$$\tau_{max} = \frac{t_1 - t_2}{\ln\left(\frac{t_1}{t_2}\right)} \qquad 2.64$$

where $\tau_{max} = e_{max}$ is the emission rate window.

Since the emission rate is highly dependent on temperature, a thermal scan shows the presence of different traps at a particular temperature when the corresponding emission rates coincide with the rate window. Thermal scanning at different rate windows gives output that can be used to plot an Arrhenius plot and obtain the DLTS signature of a defect, which helps to identify DLTS peaks as well as the temperature at which they occur (see Figure 2.18).

2.7.3.2 Laplace DLTS

The outputs of early DLTS system that made use of double boxcar were prone to low signal-to-noise ratio transient. This double boxcar in standard DLTS was later replaced by lock-in amplifiers which led to reduction in noise, but the time constant resolution was still poor for the study of fine structure. The conventional DLTS technique inherently produces broad and it is not easy to separate different traps that have closely spaced emission rates.

© University of Pretoria

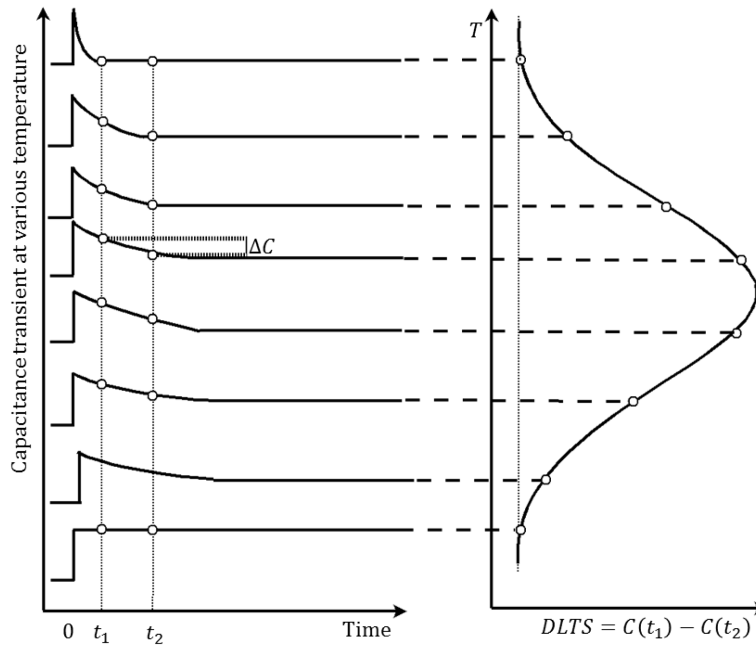

Figure 2.17: The change in the shape of a DLTS transient with increasing temperature from bottom to top (left) and the DLTS signal obtained from the transients plotted versus sample temperature (right). Redrawn from ref. [111].

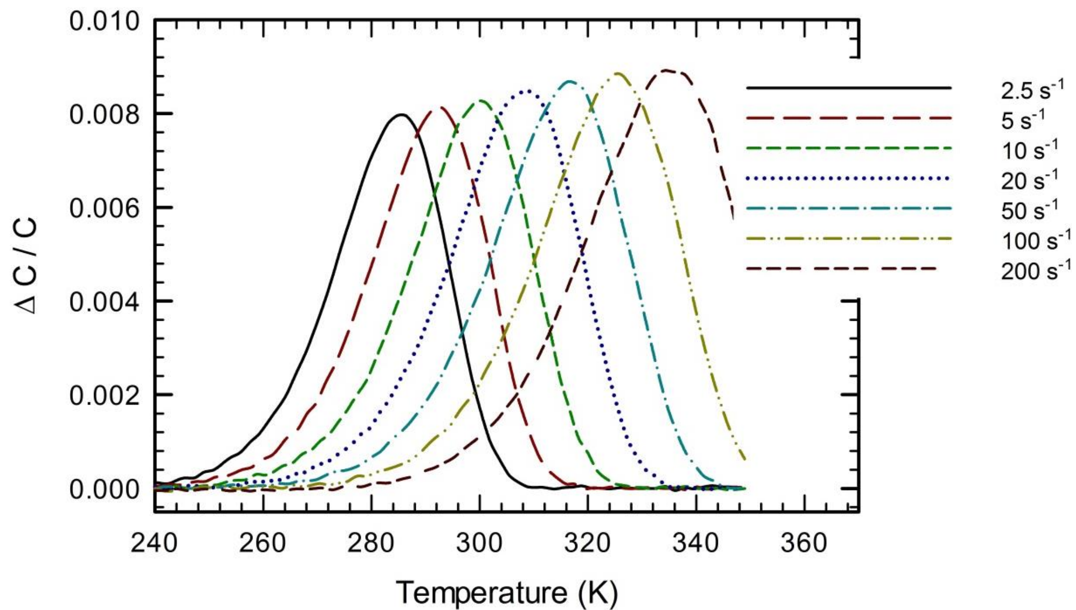

Figure 2.18: DLTS spectra obtained from a measured Ni/4H-SiC SBD from 240 to 350 K. The spectra were obtained using reverse bias of –5 V, pulse width of –1 V and at rate windows 2.5 to 200 s^{-1} [90].

© University of Pretoria

In summary, the standard DLTS discovered in 1974 by *Lang* has a poor time constant resolution and cannot separate two or more defects with closely spaced emission rates. Because of these shortcomings in standard DLTS, there is a need for a more powerful technique that will yield output with good time constant resolution and that can separate the closely spaced defects. In 1994, these shortcomings were overcome by high-resolution version of DLTS which was developed by Dobaczewski *et al* [119, 122]. The technique relies on digital signal processing of the output of the analog capacitance meter which is averaged over many transients in order to minimize the noise level. In contrast with traditional DLTS, this is done at fixed temperature.

To quantitatively describe the multi-exponential nature of the capacitance transients due to a number of defect levels, assuming that the transient is composed of a spectrum of emission rates and is given by [116, 123]

$$f(t) = \int_0^{\infty} F(s)e^{-st}ds \quad 2.65$$

where $F(s)$ is the spectral density function. The Laplace transform of the true spectral function $F(s)$ represents the mathematical expression for the capacitance transient as given in Equation 2.65. To determine an actual spectrum of the emission rates in the transient, an algorithm that calculates an inverse Laplace transform of the function $f(t)$ is required. This produces a spectrum of delta-like peaks for multiple, mono-exponential transients or broad spectrum with no fine structure for a continuous distribution [33].

Laplace DLTS produces intensity versus emission rate graph. The area beneath each delta-like peak is directly proportional to the concentration of the corresponding trap. Compared to conventional DLTS technique, Laplace DLTS gives an order of magnitude better energy resolution and has a good signal-to-noise ratio [33].

In conclusion, Laplace DLTS is the best technique so far that can separate traps or states with similar emission rates.

© University of Pretoria

UNIVERSITEIT VAN PRETORIA
UNIVERSITY OF PRETORIA
YUNIBESITHI YA PRETORIA

2.8 References

1. Cheung, R., *Silicon Carbide Microelectromechanical Systems for Harsh Environments*. 2006: Imperial College Press.

2. Morkoç, H., et al., *Large-band-gap SiC, III-V nitride, and II-VI ZnSe-based semiconductor device technologies.* Journal of Applied Physics, 1994. **76**(3): p. 1363-1398.

3. Laref, A. and S. Laref, *Opto-Electronic Study of SiC Polytypes: Simulation with Semi-Empirical Tight-Binding Approach*. 2011: INTECH Open Access Publisher.

4. Bokij, G., et al., *Nomenclature of polytype structures. Report of the International Union of Crystallography Ad hoc Committee on the nomenclature of disordered, modulated and polytype structures.* Acta Crystallographica Section A: Foundations of Crystallography, 1984. **40**(4): p. 399-404.

5. Rashed, A., *"Properties and characteristics of Silicon Carbide."*. a website publication (www. poco. com), POCO Graphite Inc.: 300 old Greenwood Rd., Decatur, TX 76234.

6. Bechstedt, F., et al., *Polytypism and properties of silicon carbide.* Physica Status Solidi (B), 1997. **202**(1): p. 35-62.

7. Vasileska, D., S. Goodnick, and G. Klimeck, *Computational Electronics: Semiclassical and Quantum Transport Modeling*. 2010, CRC Press, June.

8. Powell, J., P. Pirouz, and W. Choyke, *Growth and characterization of silicon carbide polytypes for electronic applications*. 1993, Bristol, United Kingdom, Institute of Physics Publishing. p. 257-293.

9. Kordina, O., *Growth and characterization of silicon carbide power device material.* 1994.

10. Trew, R.J., *Experimental and Simulated Results of SiC Microwave Power MESFETs.* Physica Status Solidi (A), 1997. **162**(1): p. 409-419.

11. Lee, S.K., *Processing and characterization of silicon carbide (6H-SiC and 4H-SiC) contacts for high power and high temperature device applications.* 2002.

12. Hyung-Seok, L., et al., *High-Current-Gain SiC BJTs With Regrown Extrinsic Base and Etched JTE.* Electron Devices, IEEE Transactions on, 2008. **55**(8): p. 1894-1898.

13. Kumar, A. and M. Aspalli, *SIC: An Advanced semiconductor materials for power devices.*

14. Byrappa, K. and T. Ohachi, *Crystal growth technology*. 2003: Elsevier.

15. Willardson, R.K. and E.R. Weber, *SiC materials and devices*. Vol. 52. 1998: Academic Press.

© University of Pretoria

16. Ellison, A., et al., *High temperature CVD growth of SiC.* Materials Science and Engineering: B, 1999. **61**: p. 113-120.

17. Nam, D.-H., et al., *High-Temperature Chemical Vapor Deposition for SiC Single Crystal Bulk Growth Using Tetramethylsilane as a Precursor.* Crystal Growth & Design, 2014. **14**(11): p. 5569-5574.

18. Matsunami, H. and T. Kimoto, *Step-controlled epitaxial growth of SiC: High quality homoepitaxy.* Materials Science and Engineering: R: Reports, 1997. **20**(3): p. 125-166.

19. Choi, B.J. and D.R. Kim, *Growth of silicon carbide by chemical vapour deposition.* Journal of Materials Science Letters, 1991. **10**(14): p. 860-862.

20. Dasgupta, N. and A. Dasgupta, *Semiconductor Devices: Modelling and Technology*. 2004: PHI Learning Pvt. Ltd.

21. Sze, S.M. and K.K. Ng, *Physics of semiconductor devices*. 2006: John Wiley & Sons.

22. Li, S.S., *Semiconductor physical electronics*. 2012: Springer Science & Business Media.

23. Tung, R.T., *Recent advances in Schottky barrier concepts.* Materials Science and Engineering: R: Reports, 2001. **35**(1): p. 1-138.

24. Mönch, W., *Semiconductor surfaces and interfaces*. Vol. 26. 2013: Springer Science & Business Media.

25. Rhoderick, E. and R. Williams, *Metal-Semiconductor Contacts (2nd edn.) Clarendon*. 1988, Oxford Science, Oxford.

26. Schottky, W., *Semiconductor theory of barrier and peak rectifier.* Zeitschrift für Physik, 1939. **113**(5-6): p. 367-414.

27. Grundmann, M., *The physics of semiconductors.* Springer-Verlag, Heidelberg, 2010.

28. Mott, N. *Note on the contact between a metal and an insulator or semi-conductor*. in *Mathematical Proceedings of the Cambridge Philosophical Society*. 1938. Cambridge Univ Press.

29. Lepselter, M., J. Andrews, and B. Schwartz, *Ohmic contacts to semiconductors.* Electrochemical Society, Princeton, NJ, 1969: p. 159.

30. Zhao, J.H., K. Sheng, and R.C. Lebron-Velilla, *Silicon carbide schottky barrier diode.* International Journal of High Speed Electronics and Systems, 2005. **15**(04): p. 821-866.

31. Schmidt, M., *Space Charge Spectroscopy applied to Defect Studies in Ion-Implanted Zinc Oxide Thin Films.* 2011.

© University of Pretoria

32. Meyer, W.E., *Digital DLTS studies on radiation induced defects in Si, GaAs and GaN*. 2007, University of Pretoria.

33. Schroder, D.K., *Semiconductor Material and Device Characterization.* A John Willey & Sons, inc., 2006. 3rd Edition.

34. Bethe, H.A., *Theory of the boundary layer of crystal rectifiers*. 1942: Radiation Laboratory, Massachusetts Institute of Technology.

35. Shockley, W. and W.T. Read, *Statistics of the Recombinations of Holes and Electrons.* Physical Review, 1952. **87**(5): p. 835-842.

36. Hall, R.N., *Electron-Hole Recombination in Germanium.* Physical Review, 1952. **87**(2): p. 387-387.

37. Streetman, B.G. and S. Banerjee, *Solid state electronic devices*. Vol. 4. 2000: Prentice Hall New Jersey.

38. Padovani, F. and R. Stratton, *Field and thermionic-field emission in Schottky barriers.* Solid-State Electronics, 1966. **9**(7): p. 695-707.

39. Crowell, C.R. and V.L. Rideout, *Normalized thermionic-field (T-F) emission in metal-semiconductor (Schottky) barriers.* Solid-State Electronics, 1969. **12**(2): p. 89-105.

40. Omotoso, E., et al., *Effects of 5.4 MeV alpha-particle irradiation on the electrical properties of nickel Schottky diodes on 4H–SiC.* Nuclear Instruments and Methods in Physics Research Section B: Beam Interactions with Materials and Atoms, 2015: p. 5.

41. Omotoso, E., et al., *The influence of high energy electron irradiation on the Schottky barrier height and the Richardson constant of Ni/4H-SiC Schottky diodes.* Materials Science in Semiconductor Processing, 2015. **39**: p. 112-118.

42. Constantinescu, C. and S. Nan, *Faraday effect investigation on concentration and temperature dependence of effective electron mass in n-type GaAs.* Physica Status Solidi (A), 1973. **18**(1): p. 277-282.

43. Dökme, İ., Ş. Altindal, and M.M. Bülbül, *The barrier height inhomogeneity in Al/p-Si Schottky barrier diodes with native insulator layer.* Applied Surface Science, 2006. **252**(22): p. 7749-7754.

44. Emre, G.r., et al., *High-temperature Schottky diode characteristics of bulk ZnO.* Journal of Physics: Condensed Matter, 2007. **19**(19): p. 196206.

45. Ouennoughi, Z., S. Toumi, and R. Weiss, *Study of barrier inhomogeneities using I–V–T characteristics of Mo/4H–SiC Schottky diode.* Physica B: Condensed Matter, 2015. **456**: p. 176-181.

© University of Pretoria

46. Tōyama, N., *Variation in the effective Richardson constant of a metal-silicon contact due to metal-film thickness.* Journal of Applied Physics, 1988. **63**(8): p. 2720-2724.

47. Mtangi, W., *Electrical characterization of ZnO and metal ZnO contacts*. 2009, University of Pretoria.

48. Altındal, Ş., et al., *The role of interface states and series resistance on the I–V and C–V characteristics in Al/SnO2/p-Si Schottky diodes.* Solid-State Electronics, 2003. **47**(10): p. 1847-1854.

49. Schmitsdorf, R.F., T.U. Kampen, and W. Mönch, *Correlation between barrier height and interface structure of AgSi(111) Schottky diodes.* Surface Science, 1995. **324**(2–3): p. 249-256.

50. Karadeniz, S., et al., *Temperature-dependent barrier characteristics of Ag/p-SnS Schottky barrier diodes.* Semiconductor Science and Technology, 2004. **19**(9): p. 1098.

51. Tuğluoğlu, N., et al., *Temperature-dependent barrier characteristics of Ag/p-SnSe Schottky diodes based on I – V – T measurements.* Semiconductor Science and Technology, 2004. **19**(9): p. 1092.

52. Werner, J.H. and H.H. Güttler, *Barrier inhomogeneities at Schottky contacts.* Journal of Applied Physics, 1991. **69**(3): p. 1522-1533.

53. Song, Y.P., et al., *On the difference in apparent barrier height as obtained from capacitance-voltage and current-voltage-temperature measurements on Al/p-InP Schottky barriers.* Solid-State Electronics, 1986. **29**(6): p. 633-638.

54. Gümüş, A., A. Türüt, and N. Yalcin, *Temperature dependent barrier characteristics of CrNiCo alloy Schottky contacts on n-type molecular-beam epitaxy GaAs.* Journal of Applied Physics, 2002. **91**(1): p. 245-250.

55. Acar, S., et al., *Gaussian distribution of inhomogeneous barrier height in Ag/p-Si (1 0 0) Schottky barrier diodes.* Applied Surface Science, 2004. **233**(1–4): p. 373-381.

56. Gümüş, A., A. Türüt, and N. Yalçin, *Temperature dependent barrier characteristics of CrNiCo alloy Schottky contacts on n-type molecular-beam epitaxy GaAs.* Journal of Applied Physics, 2002. **91**(1): p. 245-250.

57. Hudait, M.K., P. Venkateswarlu, and S.B. Krupanidhi, *Electrical transport characteristics of Au/n-GaAs Schottky diodes on n-Ge at low temperatures.* Solid-State Electronics, 2001. **45**(1): p. 133-141.

58. Mtangi, W., et al., *Analysis of temperature dependent measurements on Pd/ZnO Schottky barrier diodes and the determination of the Richardson constant.* Physica B: Condensed Matter, 2009. **404**(8–11): p. 1092-1096.

© University of Pretoria

59. Li, S., *Metal–Semiconductor Contacts*, in *Semiconductor Physical Electronics*, S. Li, Editor. 2006, Springer New York. p. 284-333.

60. Neamen, D.A., *Semiconductor physics and devices*. 2003: McGraw-Hill Higher Education.

61. Beyer, F.C., *Deep levels in SiC.* 2011.

62. Zolnai, Z., *Irradiation-induced crystal defects in silicon carbide*. 2005, Ph. D. Thesis.

63. Nyamhere, C., *Characterization of process and radiation induced defects in Si and Ge using conventional deep level transient spectroscopy (DLTS) and Laplace-DLTS*. 2009, University of Pretoria.

64. Isoya, J., et al. *EPR Identification of Defects and Impurities in SiC: To be decisive*. in *Materials Science Forum*. 2009. Trans Tech Publ.

65. Dalibor, T., et al., *Radiation-induced defect centers in 4H silicon carbide.* Diamond and Related Materials, 1997. **6**(10): p. 1333-1337.

66. Hemmingsson, C., et al., *Deep level defects in electron-irradiated 4H SiC epitaxial layers.* Journal of Applied Physics, 1997. **81**(9): p. 6155-6159.

67. Storasta, L., et al., *Pseudodonor nature of the D[sub I] defect in 4H-SiC.* Applied Physics Letters, 2001. **78**(1): p. 46.

68. Aboelfotoh, M.O. and J.P. Doyle, *Defect energy levels in electron-irradiated and deuterium-implanted 6H silicon carbide.* Physical Review B, 1999. **59**(16): p. 10823-10829.

69. Gong, M., et al., *Electron-irradiation-induced deep levels in n-type 6H–SiC.* Journal of Applied Physics, 1999. **85**(11): p. 7604-7608.

70. Hemmingsson, C.G., N.T. Son, and E. Janzén, *Observation of negative-U centers in 6H silicon carbide.* Applied Physics Letters, 1999. **74**(6): p. 839-841.

71. Anderson, P.W., *Model for the Electronic Structure of Amorphous Semiconductors.* Physical Review Letters, 1975. **34**(15): p. 953-955.

72. Doyle, J., et al., *Electrically active point defects in n-type 4H–SiC.* Journal of Applied Physics, 1998. **84**(3): p. 1354-1357.

73. Storasta, L., et al., *Deep levels created by low energy electron irradiation in 4H-SiC.* Journal of Applied Physics, 2004. **96**(9): p. 4909-4915.

74. Toru, H. and K. Tsunenobu, *Elimination of the Major Deep Levels in n- and p-Type 4H-SiC by Two-Step Thermal Treatment.* Applied Physics Express, 2009. **2**(9): p. 091101.

© University of Pretoria

75. Pintilie, I., et al., *Formation of the Z1,2 deep-level defects in 4H-SiC epitaxial layers: Evidence for nitrogen participation.* Applied Physics Letters, 2002. **81**(25): p. 4841-4843.

76. Zhang, J., et al., *Electrically active defects in n-type 4H–silicon carbide grown in a vertical hot-wall reactor.* Journal of Applied Physics, 2003. **93**(8): p. 4708.

77. Asghar, M., et al., *Properties of dominant electron trap center in n-type SiC epilayers by means of deep level transient spectroscopy.* Journal of Applied Physics, 2007. **101**(7): p. 073706.

78. Son, N.T., et al., *Negative-U System of Carbon Vacancy in 4H-SiC.* Physical Review Letters, 2012. **109**(18): p. 187603.

79. Van Daal, H.J., W.F. Knippenberg, and J.D. Wasscher, *On the electronic conduction of α-SiC crystals between 300 and 1500°K.* Journal of Physics and Chemistry of Solids, 1963. **24**(1): p. 109-127.

80. Lamakina, G., *Yu. A Vodakov, EN Mokhov, VG Oding and GF Kholuyanov," Compared investigation of the electrical properties of the three silicon carbide polytypes.* Soviet Physics Solid State, 1970. **12**: p. 2356-2360.

81. Mokhov, E., et al., *Doping of the silicon carbide by group III A elements during growth of the crystal from vapor phase.* Inorganic Materials, 1984. **20**: p. 1383-1386.

82. Lebedev, A.A., *Deep level centers in silicon carbide: A review.* Semiconductors, 1999. **33**(2): p. 107-130.

83. T. Dalibor, et al., *Oxygen in silicon carbide: shallow donors and deep acceptors* Materials Science and Engineering: B, 1999.

84. Zetterling, C.M., *Process Technology for Silicon Carbide Devices*. 2002: INSPEC.

85. Harris, G.L., *Properties of silicon carbide*. 1995: INSPEC, London.

86. Schneider, J. and K. Maier, *Point defects in silicon carbide.* Physica B: Condensed Matter, 1993. **185**(1): p. 199-206.

87. Woodbury, H. and G. Ludwig, *Electron spin resonance studies in SiC.* Physical Review, 1961. **124**(4): p. 1083.

88. Ikeda, M., H. Matsunami, and T. Tanaka, *Site effect on the impurity levels in 4 H, 6 H, and 1 5 R SiC.* Physical Review B, 1980. **22**(6): p. 2842.

89. Kimoto, T., et al., *Nitrogen donors and deep levels in high-quality 4H–SiC epilayers grown by chemical vapor deposition.* Applied Physics Letters, 1995. **67**(19): p. 2833-2835.

90. Paradzah, A.T., *Electrical Characterisation of particle irradiated 4H-SiC*. 2014, University of Pretoria.

© University of Pretoria

91. Chen, C.Q., et al., *Photothermal ionization spectroscopy of shallow nitrogen donor states in 4H–SiC.* Journal of Applied Physics, 2000. **87**(8): p. 3800-3805.

92. Capano, M.A., et al., *Ionization energies and electron mobilities in phosphorus- and nitrogen-implanted 4H-silicon carbide.* Journal of Applied Physics, 2000. **87**(12): p. 8773.

93. Schulz, D., et al., *Impurity incorporation during sublimation growth of 6H bulk SiC.* Journal of Crystal Growth, 1999. **198–199, Part 2**: p. 1024-1027.

94. Hobgood, H.M., et al., *Semi-insulating 6H–SiC grown by physical vapor transport.* Applied Physics Letters, 1995. **66**(11): p. 1364-1366.

95. Glasow, P.A., *Amorphous and Crystalline Silicon Carbide.* Springer, 1989. **34.**

96. Weber, E., *Transition metals in silicon.* Applied Physics A, 1983. **30**(1): p. 1-22.

97. Maier, K., H.D. Müller, and J. Schneider. *Transition metals in silicon carbide (SiC): vanadium and titanium*. in *Materials Science Forum*. 1992. Trans Tech Publ.

98. Dalibor, T. and G. Pensl, *Electrical properties of the titanium acceptor in silicon carbide.* Physical Review B, 1997. **55**(22): p. 13618

99. Dalibor, T., et al., *Deep defect centers in silicon carbide monitored with deep level transient spectroscopy.* Physica Status Solidi (A), 1997. **162**(1): p. 199-225.

100. Achtziger, N. and W. Witthuhn, *Band gap states of Ti, V, and Cr in 4H–silicon carbide.* Applied Physics Letters, 1997. **71** (1): p. 110.

101. Lee, K., et al., *Optically detected magnetic resonance study of SiC: Ti.* Physical Review B, 1985. **32**(4): p. 2273.

102. Mitchel, W., et al. *Hobgood, RC Glass, G. Augustine, RH Hopkins*. in *Inst. Phys. Conf. Ser*. 1996.

103. Maier, K., et al., *Electron spin resonance studies of transition metal deep level impurities in SiC.* Materials Science & Engineering. B, Solid-State Materials for Advanced Technology, 1992. **11**(1-4): p. 27-30.

104. Schneider, J., et al., *Infrared spectra and electron spin resonance of vanadium deep level impurities in silicon carbide.* Applied Physics Letters, 1990. **56**(12): p. 1184-1186.

105. Dalibor, T., et al., *Deep Defect Centers in Silicon Carbide Monitored with Deep Level Transient Spectroscopy.* physica status solidi, 1997. **162**(1): p. 199.

106. Achtziger, N. and W. Witthuhn, *Band gap states of Ti, V, and Cr in 4H silicon carbide.* Applied Physics Letters, 1997. **71**(1): p. 110-112.

© University of Pretoria

107. Auret, F.D. and P.N. Deenapanray, *Deep level transient spectroscopy of defects in high-energy light-particle irradiated Si.* Critical Reviews in Solid State and Materials Sciences, 2004. **29**(1): p. 1-44.

108. Green, M., *Solar Cells Prentice-Hall Inc.* Englewood Cliffs, NJ, USA, 1982: p. 97.

109. Queisser, H.J. and E.E. Haller, *Defects in semiconductors: some fatal, some vital.* Science, 1998. **281**(5379): p. 945-950.

110. Peter, Y. and M. Cardona, *Fundamentals of semiconductors: physics and materials properties*. 2010: Springer Science & Business Media.

111. Lang, D.V., *Deep-level transient spectroscopy: A new method to characterize traps in semiconductors.* Journal of Applied Physics, 1974. **45**(7): p. 3023.

112. Garcia, A.A. and M.A. Barranca, *Computerized DLTS system to characterize deep levels in semiconductors.* Revista mexicana de física, 2001. **48**(6): p. 539.

113. P Blood and J.W. Orton, *The electrical characterisation of semiconductors.* Reports on Progress in Physics, 1978. **41**(2): p. 157.

114. Miller, G., D. Lang, and L. Kimerling, *Capacitance transient spectroscopy.* Annual Review of Materials Science, 1977. **7**(1): p. 377-448.

115. Henry, C. and D. Lang, *Nonradiative capture and recombination by multiphonon emission in GaAs and GaP.* Physical Review B, 1977. **15**(2): p. 989-1016.

116. Schroder, D.K., *Semiconductor Material & Device Characterization*. 2006: John Wiley and Sons.

117. Kimerling, L., *Influence of deep traps on the measurement of free-carrier distributions in semiconductors by junction capacitance techniques.* Journal of Applied Physics, 1974. **45**(4): p. 1839-1845.

118. Shiau, J.J., A.L. Fahrenbruch, and R.H. Bube, *Interpretation of capacitance versus voltage measurements in the presence of a high density of deep levels.* Journal of Applied Physics, 1986. **59**(8): p. 2879-2884.

119. Dobaczewski, L., et al., *Laplace transform deep-level transient spectroscopic studies of defects in semiconductors.* Journal of Applied Physics, 1994. **76**(1): p. 194-198.

120. Zohta, Y. and M.O. Watanabe, *On the determination of the spatial distribution of deep centers in semiconducting thin films from capacitance transient spectroscopy.* Journal of Applied Physics, 1982. **53**(3): p. 1809-1811.

121. Claeys, C. and E. Simoen, *Radiation effects in advanced semiconductor materials and devices*. Vol. 57. 2013: Springer Science & Business Media.

© University of Pretoria

122. Dobaczewski, L., A. Peaker, and K.B. Nielsen, *Laplace-transform deep-level spectroscopy: The technique and its applications to the study of point defects in semiconductors.* Journal of Applied Physics, 2004. **96**(9): p. 4689-4728.

123. L. Dobaczewski, A. R. Peaker, and K.B. Nielsen, *Laplace-transform deep-level spectroscopy: The technique and its applications to the study of point defects in semiconductors.* Journal of Applied Physics. 96, 2004. **96**(9): p. 4689.

© University of Pretoria

Chapter 3

Experimental techniques

3.1 Introduction

This chapter describes all the procedures and instrumentation used in this study. Section 3.2 describes the sample preparation procedures such as cleaning, etching, ohmic and Schottky diode fabrication. Some methods by which deep-level defects could be introduced into devices and the annealing set-up are outlined in Sections 3.3 and 3.4, respectively. Also, Section 3.5 outlines the Schottky barrier diodes and defect characterization by current-voltage, capacitance-voltage, DLTS and high-resolution Laplace DLTS.

3.2 Sample preparation

The samples used for this study were cut from homoepitaxially grown, nitrogen-doped, *n*-type 4H-SiC wafers supplied by Cree Research Inc. The epilayer was grown by chemical vapour deposition (CVD) on the Si-face of the SiC substrate, which had a net doping density of 1×10^{18} cm^{-3} and resistivity of approximately 0.020 Ω-cm. Epilayers with fixed doping densities in the range of 4.0×10^{14} to 1.9×10^{16} cm^{-3} were grown on separate substrate wafers.

3.2.1 SiC cleaning and etching

Prior to the fabrication of ohmic and Schottky contacts on the samples, cleaning and etching were carried out. Chemical cleaning and etching of samples play major roles in the performance and the efficiency of microelectronic devices [1]. The cleaning and etching of SiC was carried out in the following steps:

(i) Degreasing: the samples were degreased by boiling for 5 minutes each in trichloroethylene, acetone and methanol, followed by rinsing in de-ionized (DI) water. This was carried out so as to remove the dirt and dust particles.

(ii) Etching: the samples were etched in 40% hydrofluoric acid for 30 seconds, so as to the get rid the native oxide layer that might present.

© University of Pretoria

(iii) The samples were rinsed in DI water, and followed by blow drying with nitrogen gas before thermal fabrication of the ohmic contact.

3.2.2 Ohmic contact fabrication

Figure 3.1 shows a schematic diagram of a resistive evaporation system. The resistive evaporation system is used to evaporate metals that have a melting point below 1600 °C. The whole system was under vacuum, and the sample was mounted about 0.3 m above the crucible. Current was passed through the crucible which heats the metal (e.g. Ni) to be evaporated to its melting point (e.g. 1445 °C in the case of Ni). The molten metal evaporated and deposited onto the sample. The deposition rate was controlled by adjusting the current and monitored by a crystal monitor.

Immediately after the cleaning and etching, the samples were loaded into the resistive evaporation system, which was pumped down to a pressure of $\sim 10^{-6}$ mbar. The nickel ohmic contacts with the thickness of 3000 Å were deposited at rate in the range of 0.4 to 1.0 $Å.s^{-1}$ onto the highly doped (1×10^{18} cm^{-3}) back surface of the samples. Thereafter, the ohmic contacts were annealed in a tube furnace under the flowing argon at 950 °C for 10 minutes to form nickel silicides [2]. The annealing after evaporation of the ohmic contacts helps to improve the contacts by reducing the barrier height, hence lowering the resistivity [3]. The argon ambient was chosen for the annealing to prevent the oxidation of the nickel, and thereby reduced the interfacial layer between the SiC and the nickel.

3.2.3 Schottky barrier diode fabrication

Prior to the fabrication of Schottky contacts, the samples with annealed ohmic contacts were cleaned again by the cleaning procedure described in Section 3.2.1, but the samples were rinsed in an ultrasonic bath for 3 minutes in each chemical. The Schottky contacts used in this study were either fabricated by resistive evaporation or electron beam deposition techniques.

The schematic diagram of the electron beam deposition is shown Figure 3.2. During electron beam deposition, a beam of electrons emitted from a hot filament was focussed on the metal to be evaporated, which is placed in a crucible. These electrons were accelerated by a high voltage and bent toward the metal by a magnetic field. The rate of metal deposition onto the samples depends on the current supplied to the filament and

© University of Pretoria

the melting point of the metal. This technique can deposit metal with either low or high melting point, but its disadvantage is in the introduction of defect(s) into the fabricated devices.

Ni contacts of thickness of 1000 Å were deposited through a metal contact mask with holes of diameter ~0.6 mm onto the epitaxially grown side of the samples. The resistive evaporation technique was employed mainly because it does not introduce defects in measurable quantities.

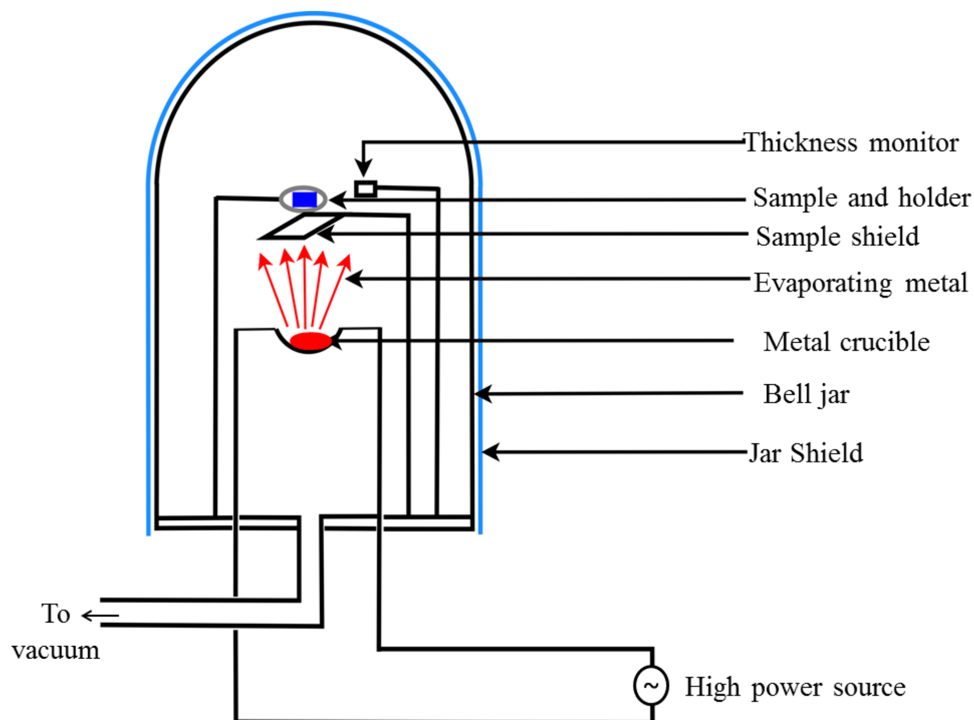

Figure 3.1: Schematic diagram of the resistive deposition system that was used for ohmic and Schottky contact fabrication [4].

© University of Pretoria

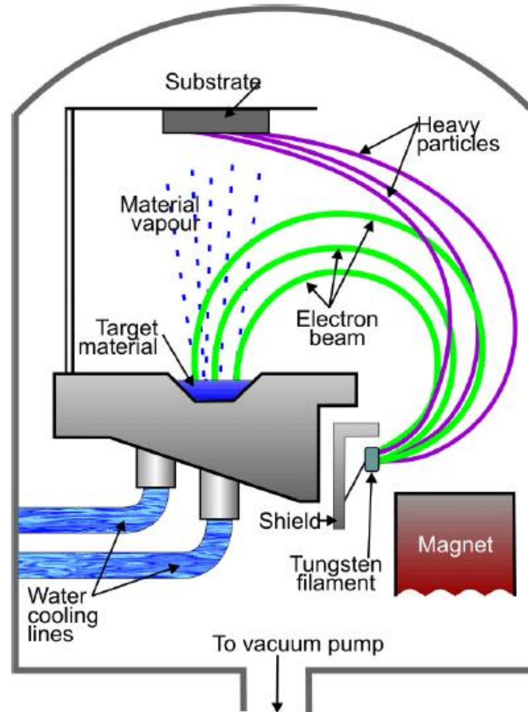

Figure 3.2: Schematic diagram for electron-beam evaporation system[5].

3.3 Introduction of defects

Defects can be introduced into the devices in many ways. In this study, an americium-241 source, a strontium-90 source and an electron beam deposition system (with and without actual deposition of material) were used.

3.3.1 Alpha particles from Americium-241 (Am-241)

Some of the samples used were irradiated with alpha-particle with energy of 5.4 MeV from an Am-241 radionuclide source. An Am-241 radionuclide foil was placed on top of the Schottky barrier diodes in such a way that the emitted alpha-particles were directed towards the diodes as shown in Figure 3.3b. The fluence rate of the alpha-particle source used was 7.1×10^{6} $cm^{-2}.s^{-1}$. The irradiation was performed at room temperature (~300 K).

© University of Pretoria

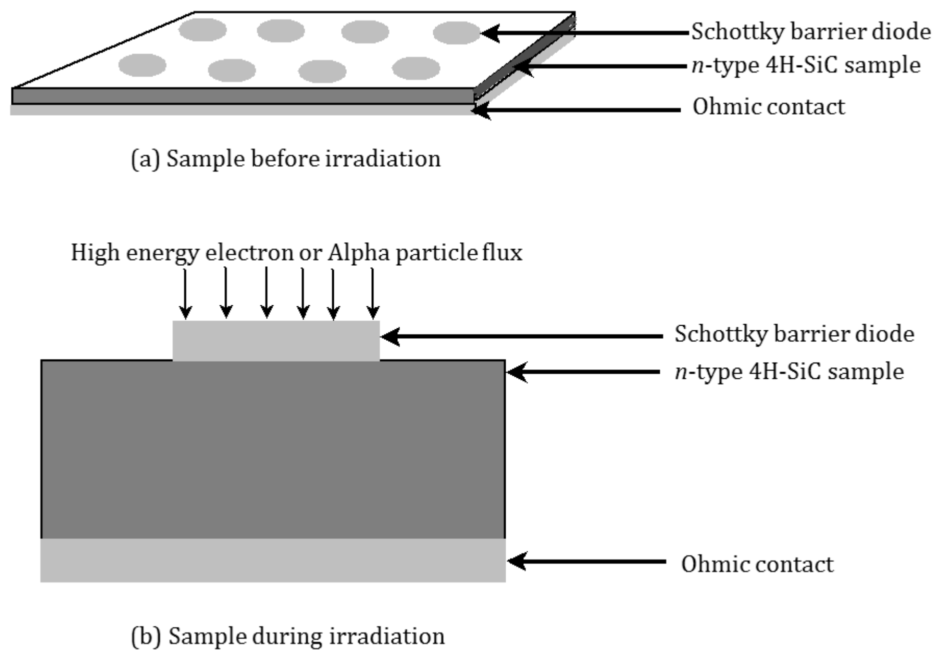

Figure 3.3: Schematic diagram of the samples before (a) and during (b) irradiation with high-energy particles.

3.3.2 High-energy electrons from Strontium-90 (Sr-90)

The strontium radionuclide source was used to bombard some of the samples used in this research. The Sr electron source used was disc-shaped with a diameter of 8.4 mm and an activity of 20 mCi. The Sr-90 radionuclide (half-life of 28.5 years) decays first to yttrium (half-life of 64.1 hours) with the emission of a 0.5 MeV electron. The yttrium then decays by the emission of a 2.27 MeV electron to zirconium. The energy distribution of the electrons emitted from the Sr-90 source is shown in Figure 3.4. From this figure, it is clear that ~70% of the total number of emitted electrons have energies above 0.25 MeV, the threshold energy for electrons to produce defects by elastic collisions [6]. The samples were placed ~1 mm below the surface of the radioactive disc during the irradiation in order to ensure that the particle flux reaching the sample at this position is the same as the flux that leaves the source's surface. The total electron flux emitted was determined from the activity of the Sr-90 source. Because the half-life of strontium is much longer than that of yttrium, each Sr-90 decay results in the emission of two electrons. This total fluence is equal to the area below the curve (Sr + Y) in Figure 3.4. The irradiation was done at room temperature (~300 K) at a flux of 7×10^{9} electrons-$cm^{-2}.s^{-1}$.

© University of Pretoria

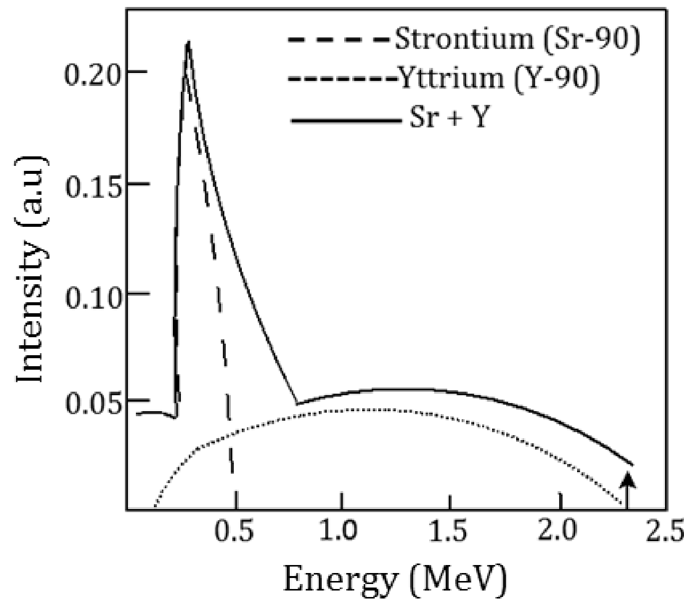

Figure 3.4: Energy distribution of electrons emitted by a Sr-90 radionuclide. The strontium and yttrium contribution has been displaced by an amount indicated by the arrow, for clarification [6].

3.3.3 Electron-beam deposition and exposure

Metallization is a very important processing step in microelectronics and photovoltaic industries. Electron-beam deposition (EBD) is one of the popular techniques for fabrication of ohmic and Schottky barrier contacts, as described in Section 3.23. Auret *et al* [7] and Coelho *et al* [8] have reported that metallization procedures such as EBD and sputtering deposition, induce defects at and close to the metal-semiconductor junction of Si and Ge [9]. These defects influence the performance of the devices and alter the contacts' Schottky barrier heights [10].

Tungsten Schottky contacts were fabricated onto 4H-SiC using electron beam deposition. After cleaning, the samples were quickly transferred into the vacuum chamber which was pumped down to pressure of ~10^{-6} mbar. The samples were first shielded from the source until W in the crucible had melted and started evaporating. The W SBDs fabricated were 0.6 mm in diameter and 400 Å in thickness and evaporated at a rate of ~0.2 Å.s^{-1}. The electron beam deposition of W was achieved using a 10 kV source (MDC model e-Vap 10CVS) at ~240 mA, with samples placed 0.50 m away from the crucible. The relatively high beam current was required due to the high melting

© University of Pretoria

point of W (3422 K). Upon heating, the vacuum dropped to ~1.2×10^{-5} mbar and was maintained at this pressure during the deposition.

For electron beam exposure (EBE), i.e. exposure to electron beam deposition conditions without any actual deposition taking place, SBDs were fabricated in two stages: nickel Schottky contacts of thickness 100 Å were first deposited by resistive evaporation before the samples were quickly transferred to the electron beam deposition chamber. EBE of the samples was achieved also by using the same system described earlier (see also Auret *et al* [7] and Coelho *et al* [8]). The samples were exposed to EBE conditions for 50 minutes by heating tungsten in a crucible using a beam current of 100 mA [8]. This current was not enough to evaporate tungsten, but would have been sufficient to evaporate most other metals. During the entire procedure, the vacuum in the deposition chamber was reduced to 10^{-4} mbar by leaking in forming gas H15 (N_2:H_2 of 85%:15% by volume) [8]. Hereafter, the samples were removed and returned quickly to the resistive deposition chamber where additional Ni was deposited resulting in thickness of 1000 Å Schottky diodes at ~5×10^{-6} mbar by means of resistive evaporation, a process known not to introduce defects measurable by DLTS [8].

3.4 Annealing procedure

As mentioned in Section 3.2.2, the annealing of ohmic contacts prior to fabrication of Schottky barrier diodes was carried out in quartz tube heated by Lindberg Hevi-Duty furnace. In some cases, the SBDs were also annealed before or after irradiation to know which defects anneal out or are introduced during the process.

The furnace used in this study has a minimum and maximum temperature of 200 and 1200 °C, respectively. The quartz tube was connected via a regulator to a cylinder containing the relevant gas. The temperature was monitored by a thermocouple placed in the tube at the same position as the sample and fine adjustments to the temperature were made by adjusting the position of the sample along the quartz tube.

3.5 Electrical characterization

Electrical characterization was carried out immediately after metallization. Current-voltage (*I*-*V*) and capacitance-voltage (*C*-*V*) measurements were performed before and

© University of Pretoria

after irradiation. Also, DLTS and Laplace DLTS were used to characterize the electrically active defects in the semiconductor before and after irradiation or annealing [11-13].

3.5.1 Room temperature current-voltage and capacitance-voltage measurements

The *I-V* measurements were made using an HP 4140 B pA Meter/DC Voltage Source that has ability to measure current with a sensitivity as low as 10^{-14} A. The *C-V* measurements were performed using an HP 4192A LF Impedance Analyzer using a frequency of 1 MHz over a bias voltage ranging from −12 V to 1 V. During measurements, the sample was mounted in a light tight metal enclosure to eliminate light and electrical noise. Figure 3.5 shows the schematic diagram of *I-V* and *C-V* measurements.

The ideality factor, Schottky barrier height (for *I-V* and *C-V*), series resistance, net donor concentration, built-in voltage and reverse leakage current were deduced from the *I-V* and *C-V* measurements so as to determine the quality of the SBDs and the dominant current transport mechanism. The results obtained determined whether the SBDs are suitable for DLTS measurement or not. For SBDs to be suitable for DLTS measurement:

(i) The Schottky barrier height should be high (greater than 1 eV).
(ii) The ideality factor should be close to 1 (less than 2.0).
(iii) The leakage current and series resistance should be low (less than 1×10^{-6} A and 100 Ω, respectively).
(iv) The dissipation factor should be low (less than 0.1).

These measurements were used to monitor the properties of SBDs after DLTS measurements, since SBDs tend to degrade during DLTS measurements due to mechanical stress and vibrations.

3.5.2 Temperature dependent *I-V* and *C-V* measurements

Room temperature *I-V* and *C-V* measurements were performed to confirm that the SBDs were of good quality before proceeding to temperature dependent measurements.

The sample was placed under vacuum in a closed cycle helium cryostat and cooled down to 40 K. The *I-V* and *C-V* measurements were carried out in the temperature range

© University of Pretoria

of 40 – 300 K under control of a program written in Labview™. The same parameters mentioned earlier were extracted at each measurement temperature.

The temperature dependent *I-V* and *C-V* measurements were repeated after irradiating the SBDs with alpha-particle and high-energy electron of fluence 5.1×10^{10} and 6.0×10^{14} cm^{-2}, respectively.

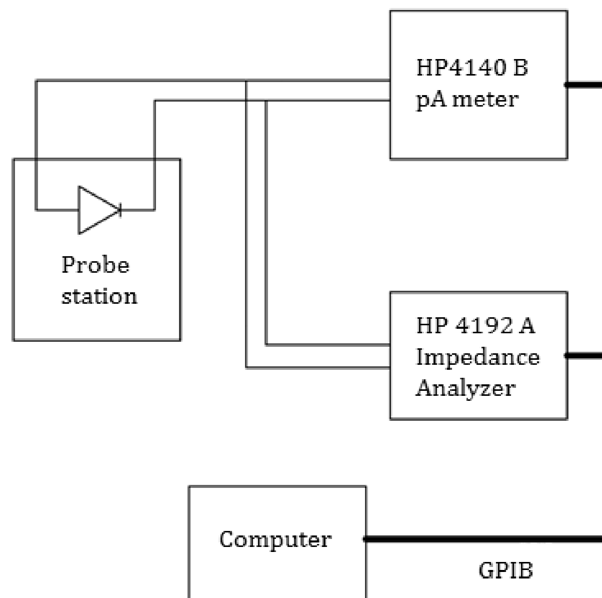

Figure 3.5: A block diagram of the I-V and C-V station for determining the electrical properties of SBDs [14].

3.5.2 Deep-level transient spectroscopy and high-resolution Laplace DLTS

Conventional- and high-resolution Laplace DLTS measurements were performed by the same system, as shown schematically in Figure 3.6. This system was used to characterize deep-level defects present in the as-grown and irradiated samples in this study. The set-up is made up of the following instrumentation (details can be read in *ref.* [15]):

(1) A closed cycle helium cryostat, on which the sample is mounted. The temperature was measured close to the sample using a GaAs diode and controlled by a Lakeshore 332 temperature controller driving a heater in the tip

© University of Pretoria

of the cryostat. Using this system, a temperature range of 20 – 380 K could be achieved.

(2) A Boonton 7200 capacitance meter with 100 mV, 1 MHz test signal is used to monitor the change in capacitance due to thermal emission after the excitation from the pulse generator. A capacitor decade box was connected to the "diff" terminals of the capacitance meter to offset the capacitance of the diode, thus allowing a more sensitive scale to be used.

(3) A dedicated Laplace DLTS card manufactured by UMIST with an internal pulse generator and analogue to digital converter was used to perform the measurements. The desired quiescent reverse bias voltage and pulses [13] are applied by the Laplace DLTS card via the "DC Bias" input of the capacitance meter. The card is also used to record current-temperature and capacitance-temperature measurements.

(4) An HP 33120A 15 MHz arbitrary waveform generator replaced the built in pulse generator when shorter filling pulses were required. This pulse generator was triggered from the pulse generator on the Laplace DLTS card and provided pulses with rounded rising edges to avoid overshoot due to the inductors in the input filter of the capacitance meter [15].

(5) A national instruments GPIB interface card was used to control the temperature controller, capacitance meter and HP 33120A arbitrary waveform generator.

In order to reduce noise, the sample was electrically insulated from earth by mounting it on a circular sapphire disk soldered to the top of the cold finger of the cryostat. Thin indium foil, placed between the sapphire and the sample, provided thermal contact. The indium foil also acted as an electrical contact to the ohmic contact of the sample. Probes made from beryllium-copper wire connected the Schottky barrier diode and on the indium foil to the rest of the circuit.

All measurement parameters for both conventional and Laplace DLTS were set programmatically. This includes measurement temperature, bias conditions, and capacitance transient acquisition conditions. For conventional, temperature scanned DLTS, the capacitance transients measured by the capacitance meter were captured by the Laplace card and analysed using software-based boxcar averagers. Different rate windows (for multi-rate window scans) or two rate windows (for trap view scans) can

© University of Pretoria

be used to produce the DLTS spectra. Throughout the measurements in this study, the samples were kept in dark and a good vacuum was maintained.

For Laplace DLTS mode, the sample was kept at fixed temperature and multiple capacitance transients were recorded and averaged by the Laplace DLTS card to improve the signal to noise ratio. Hereafter a numerical inverse Laplace transform was used to analyse the exponential decay and provide an emission rate spectrum. Three different software routines; CONTIN, FTIKREG and FLOG [13], were available, but only CONTIN was used for measurements in this study.

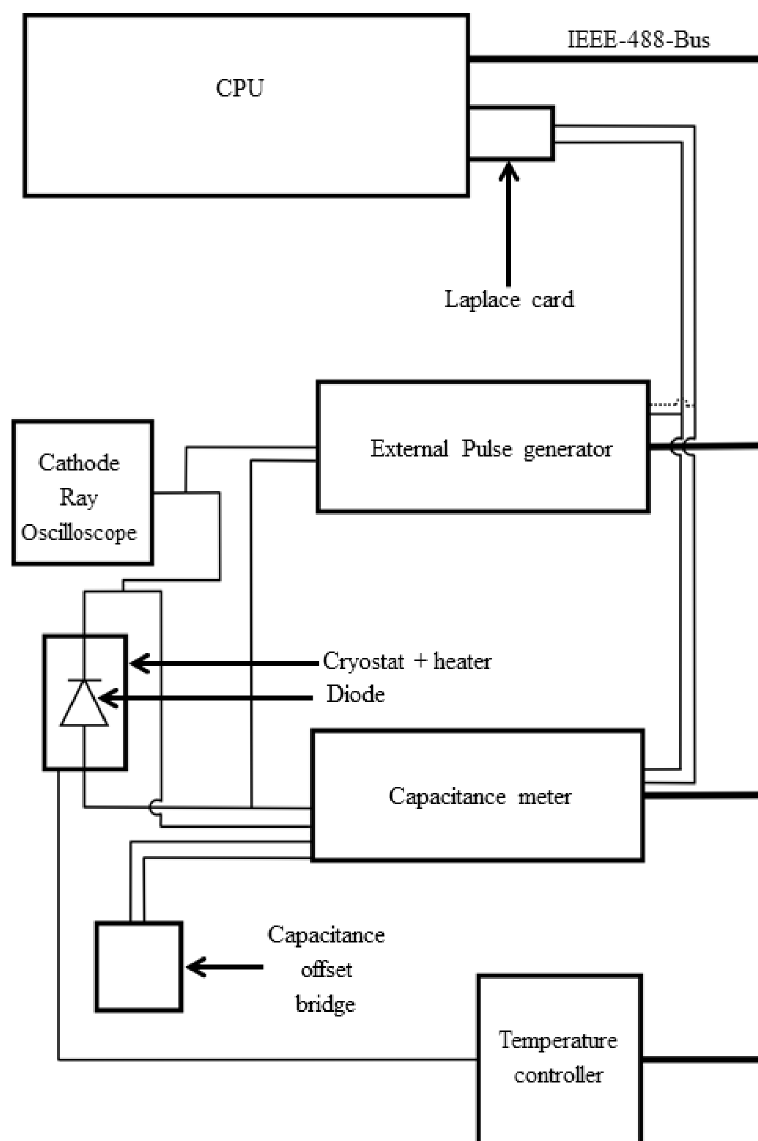

Figure 3.6: Schematic diagram of the DLTS and Laplace DLTS set-up used in this study [4].

© University of Pretoria

3.6 References

1. Williams, R.E., *Gallium arsenide processing techniques*. 1984: Artech House.

2. Marinova, T., et al., *Nickel based ohmic contacts on SiC.* Materials Science and Engineering: B, 1997. **46**(1–3): p. 223-226.

3. Bredell, L.J., et al., *Electrical characterization of argon-ion sputtered n-GaAs.* Applied Surface Science, 1991. **50**(1–4): p. 466-469.

4. Paradzah, A.T., *Electrical Characterisation of particle irradiated 4H-SiC*. 2014, University of Pretoria.

5. Nyamhere, C., *Characterization of process and radiation induced defects in Si and Ge using conventional deep level transient spectroscopy (DLTS) and Laplace-DLTS*. 2009, University of Pretoria.

6. Auret, F., et al., *Electrical characterization of defects introduced in n-GaAs by alpha and beta irradiation from radionuclides.* Applied Physics A, 1993. **56**(6): p. 547-553.

7. Auret, F.D., et al., *Electrical characterization of defects introduced in n-Si during electron beam deposition of Pt.* Physica Status Solidi (A), 2012. **209**(10): p. 1926-1933.

8. Coelho, S.M.M., et al., *Electrical characterization of defects introduced in n-Ge during electron beam deposition or exposure.* Journal of Applied Physics, 2013. **114**(17): p. 1737081-1737088.

9. Auret, F.D. and P.M. Mooney, *Deep levels introduced during electron-beam deposition of metals on n-type silicon.* Journal of Applied Physics, 1984. **55**(4): p. 988-993.

10. Myburg, G. and F. Auret, *Influence of the electron beam evaporation rate of Pt and the semiconductor carrier density on the characteristics of Pt/n-GaAs Schottky contacts.* Journal of Applied Physics, 1992. **71**(12): p. 6172-6176.

11. Lang, D.V., *Deep-level transient spectroscopy: A new method to characterize traps in semiconductors.* Journal of Applied Physics, 1974. **45**(7): p. 3023.

12. Dobaczewski, L., et al., *Laplace transform deep-level transient spectroscopic studies of defects in semiconductors.* Journal of Applied Physics, 1994. **76**(1): p. 194-198.

13. Dobaczewski, L., A. Peaker, and K.B. Nielsen, *Laplace-transform deep-level spectroscopy: The technique and its applications to the study of point defects in semiconductors.* Journal of Applied Physics, 2004. **96**(9): p. 4689-4728.

14. Mtangi, W., *Electrical characterization of process, annealing and irradiation induced defects in ZnO*. 2012, University of Pretoria.

© University of Pretoria

15. Meyer, W.E., *Digital DLTS studies on radiation induced defects in Si, GaAs and GaN*. 2007, University of Pretoria.

© University of Pretoria

Chapter 4

Results and discussion

4.1 Introduction

This chapter contains the results that have been published in various journals as well as manuscript to be submitted for publication. An article may be relevant to one or more sections or sub-sections in this chapter.

The results and discussion chapter is divided into six major sections. Section 4.2 briefly describes the investigation of defects observed in as-grown *n*-type 4H-SiC and their assignment to specific structures.

The deep-level defects induced into 4H-SiC after irradiation with high-energy particles, such as high-energy electron and alpha-particle irradiation, were reported in Section 4.3. Also in Section 4.3, the effect of irradiation on the electrical properties of devices explained in detail.

Section 4.4 reports on metallization induced defects in *n*-type 4H-SiC and compare them to defects in as-grown and high-energy particle irradiated material.

The annealing of radiation induced defects in Ni/4H-SiC SBDs is reported in Section 4.5.

Lastly, Section 4.6 presents temperature dependent current-voltage (*I*-*V*) and capacitance-voltage (*C*-*V*) measurements of Ni/4H-SiC SBDs.

4.2 Defects in as-grown *n*-type 4H-SiC

To carry out a meaningful and accurate study in characterizing the defects introduced intentionally by radionuclides or metallization, such as electron beam deposition or exposure, it is imperative to have knowledge of the defects present in the material prior to irradiation of the material. This study investigates the defects present in the material before irradiation and will serve as a baseline for the study of radiation- and process-induced defects.

© University of Pretoria

The study in this section was carried out on nitrogen-doped, *n*-type 4H-SiC of different doping densities (~4×10^{14} to 1.9×10^{16} cm^{-3}) grown by chemical vapour deposition. However, the report will focus on the material with doping density of 7.1×10^{15} cm^{-3}. The sample was characterized by current-voltage (*I-V*), capacitance-voltage (*C-V*) and deep-level transient spectroscopy (DLTS) after resistively depositing Ni for both ohmic and Schottky contacts. The thickness of the Ni ohmic contact and the Schottky barrier diodes was 3000 and 1000 Å, respectively, and the fabrication was done according to the experimental procedure described in Section 3.2.

4.2.1 Current-voltage (I-V) and capacitance-voltage (C-V) characteristics

The quality of the contacts was confirmed by *I-V* and *C-V* measurements at room temperature (300 °C). These properties were quantified in terms of ideality factor (n), Schottky barrier height ($\phi_{I-V,}\phi_{C-V}$), saturation current (I_s), series resistance (R_s), net donor concentration (N_d) and built-in voltage (V_{bi}).

Figure 4.1 shows the forward semi-logarithmic *I-V* characteristics of a Schottky barrier diode on as-grown 4H-SiC. A linear forward *I-V* relationship was obtained and fitted using the thermionic emission model to determine the electrical parameters, which are tabulated in Table 4.1. The ideality factor obtained was close to one, which shows that the thermionic emission process was the dominant current transport mechanism in the Schottky barrier diodes. The Schottky barrier height for *I-V* characteristics, 1.25 eV, was slightly lower than predicted value by the Schottky model (2.05 eV) [1], which indicates the presence of interface states.

A plot of $1/C^2$ versus V for as-grown 4H-SiC SBD is shown in Figure 4.2. The most linear part was fitted with a straight line and extrapolated to the axis, and N_d, ϕ_{C-V} and V_{bi} were determined as tabulated in Table 4.1.

The values of Schottky barrier heights determined from *I-V* and *C-V* measurements did not agree. This is in confirmation with what has been reported earlier by *refs*. [2-4]. This discrepancy may be attributed to inhomogeneous doping, deep impurity levels, surface inhomogeneity, interfacial layer and state and image force lowering [5].

© University of Pretoria

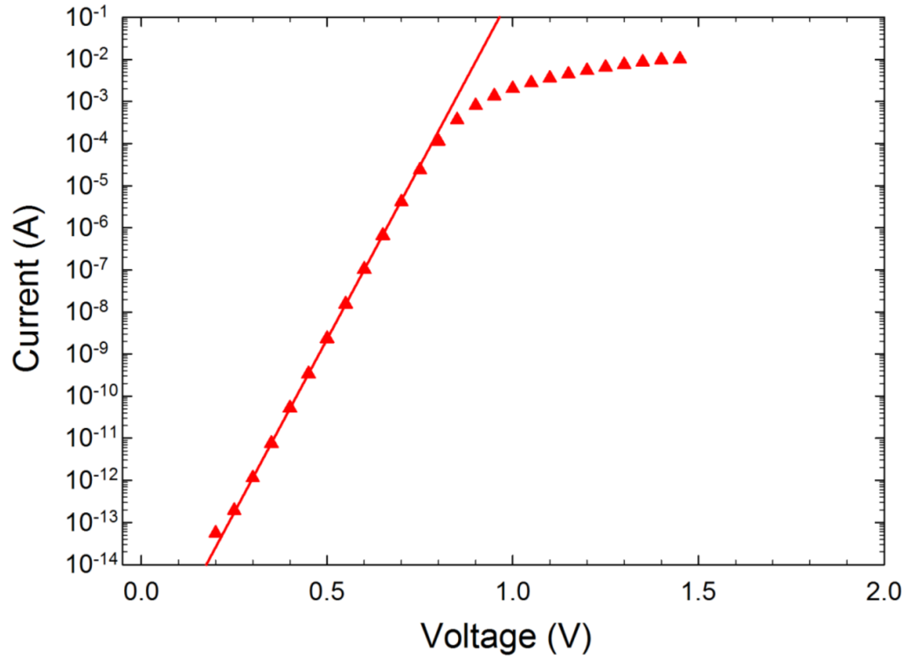

Figure 4.1: The forward semi-logarithmic I-V characteristics of an as-grown Ni/4H-SiC Schottky diode measured at room temperature (300 K).

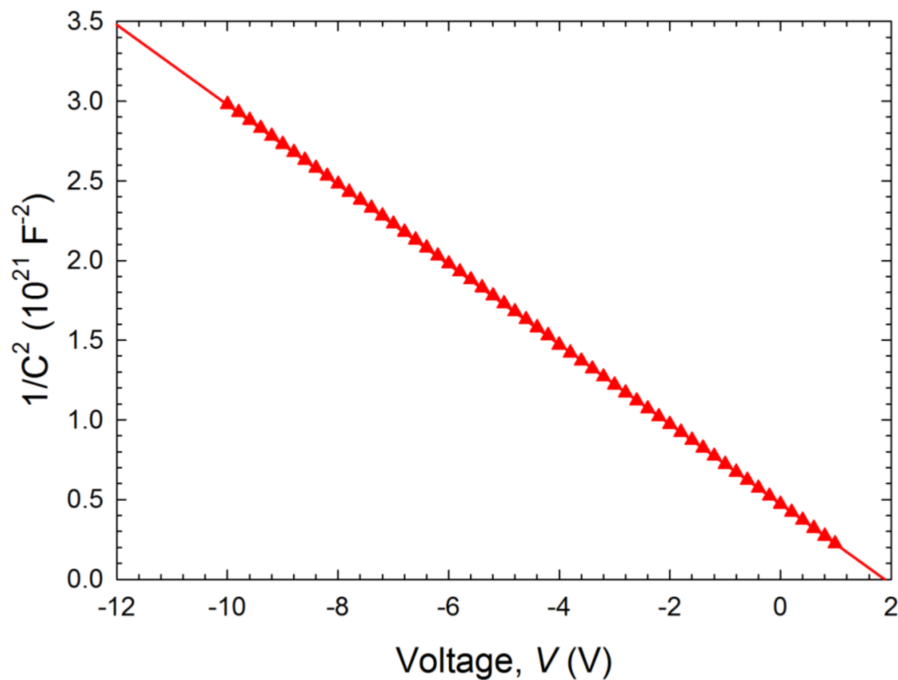

Figure 4.2: $1/C^2$ as a function of voltage characteristics of as-grown Ni/4H-SiC measured at room temperature (300 K).

Table 4.1: Some electrical parameters of an as-grown Ni/4H-SiC Schottky barrier diode.

n	I_s (A)	R_s (Ω)	N_d (cm^{-3})	V_{bi} (V)	ϕ_{I-V} (eV)	ϕ_{C-V} (eV)

© University of Pretoria

1.04	~2×10^{-17}	48	7.8×10^{15}	1.07	1.25	1.36

4.2.2 Deep-level transient spectroscopy (DLTS) measurements

The device used in this section was fabricated by resistive deposition of Ni for both ohmic and Schottky contacts on 4H-SiC sample. This technique does not introduce defects in measurable quantity to the devices. After the electrical characterization by *I-V* and *C-V* measurements, the results obtained indicated that the diodes were of excellent quality, therefore DLTS measurements can be used with confidence to characterize the deep-level defects present in the devices.

Figure 4.3 shows the DLTS spectrum of the as-grown Ni/4H-SiC diode. The spectrum revealed the presence of four electrically active defects which have been labelled $E_{0.09}$, $E_{0.11}$, $E_{0.16}$ and $E_{0.65}$. The signature and attribute of the defects obtained in as-grown Ni/4H-SiC were described in detail in Papers I and VII. It should be noted that the energy and capture cross-section of the same defect may differ between different papers in this chapter; however, the differences were within experimental error.

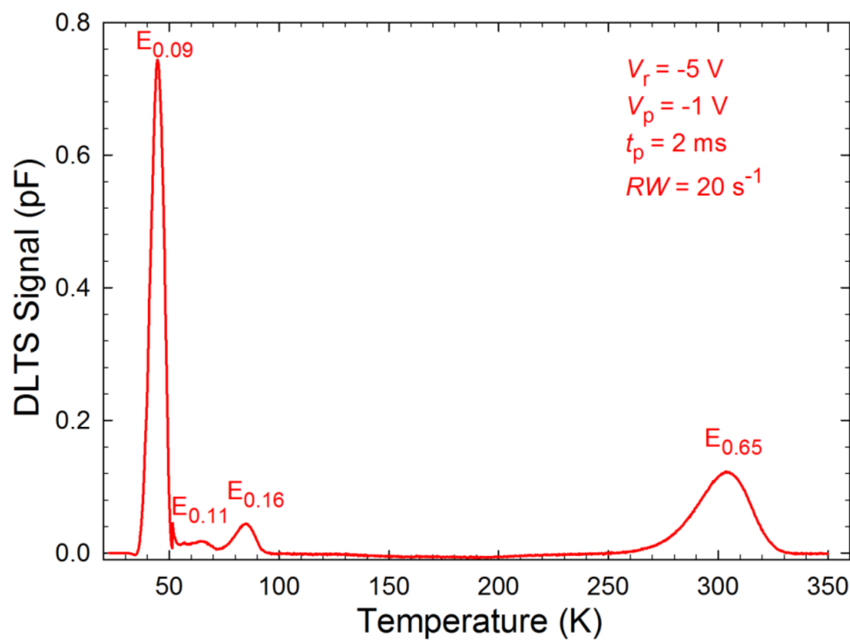

Figure 4.3: DLTS spectrum obtained from as-grown Ni/4H-SiC SBD. The spectrum in the temperature range 52-350 K is scaled up by factor of 10.

© University of Pretoria

4.2.3 Concluding remarks

In this section, the electrically active defects present in the material prior to the intentionally introduction of defects have described.

Resistive evaporation was used successfully for the fabrication of Ni ohmic and Schottky contacts on nitrogen-doped, *n*-type 4H-SiC. The diodes fabricated by this technique were of good quality with ideality factor very close to one (1.04). In as-grown devices, four electrically active defects with energies 0.06 - 0.10 eV, 0.11 - 0.12 eV, 0.16 - 0.18 eV and 0.65 - 0.70 eV were present in all the samples used in this study. These four defects were also observed after electron-beam deposition.

4.3 Irradiation induced defects in 4H-SiC

This section contains results relating to defects introduced in nitrogen-doped, *n*-type 4H-SiC after bombardment with high-energy particles, viz. high-energy electron and alpha-particle irradiation, as well as the changes in electrical properties of the devices after the irradiation. Irradiation by high-energy electrons was performed by using a ^{90}Sr radionuclide source, and the alpha-particle irradiation was carried out by an ^{241}Am radionuclide source.

4.3.1 High-energy electron (HEE) irradiation

A ^{90}Sr radionuclide source was used to intentionally introduce electrically active defects into *n*-type 4H-SiC after Ni ohmic and Schottky contacts had been deposited by means of resistive evaporation. Seven major electron defects (labelled $E_{0.10}$, $E_{0.12}$, $E_{0.16}$, $E_{0.22}$, $E_{0.40}$, $E_{0.65}$ and $E_{0.71}$) were detected by DLTS after bombardment with HEE irradiation. According to their DLTS signatures, three of these defects ($E_{0.22}$, $E_{0.40}$, and $E_{0.71}$) were related to HEE irradiation while the other four defects ($E_{0.10}$, $E_{0.12}$, $E_{0.16}$ and $E_{0.65}$) corresponded to previously observed defects in as-grown Ni/4H-SiC SBDs, as described in Section 4.2. Of the defects in the as-grown material, the concentration of defect attributed to nitrogen impurities ($E_{0.10}$) increased significantly and the defect labelled $E_{0.65}$ attributed to carbon vacancy increased by ~18% in concentration after irradiation. Therefore, it was concluded that these defects were also introduced by electron irradiation. In Paper II, the influence of HEE irradiation on *I-V* and *C-V* properties of M-S devices has been reported. The carrier removal rate of HEE irradiation was also

© University of Pretoria

calculated to be 1.67 cm^{-1}, which was ~4670 times lower than what has been reported after 5.4 MeV alpha-particles on the devices fabricated on the same material.

A detailed about the influence of HEE irradiation on electrical properties of Ni/4H-SiC device is presented in Paper II.

4.3.2 Alpha-particle irradiation induced defects in 4H-SiC

After alpha-particle irradiation of *n*-type Ni/4H-SiC SBDs, six electron defects were observed by DLTS measurements in the temperature range 22 - 350 K. Two of these electrically active defects ($E_{0.39}$ and $E_{0.62}$) were introduced during bombardment, and the remaining four defects were related to defects observed before irradiation. In Paper I, defect labelled $E_{0.09}$ that was attributed to nitrogen impurities occupy the cubic site in 4H-SiC, significantly increased in concentration and transformed to $E_{0.06}$ defect that occupy the hexagonal site after alpha-particle irradiation. In addition, the defect labelled $E_{0.65}$ with energy 0.65 eV before irradiation increased by ~9% in concentration and had energy 0.67 eV after alpha-particle irradiation.

The behaviour of the devices after irradiation was investigated at different fluences and reported in this study. An unexpected result was that an increase in fluence resulted in a decrease in leakage current which was attributed to a reduction in the electric field within the depletion region due to the removal of carriers. In addition, the carrier removal rate of 4H-SiC was calculated to be 6480 cm^{-1}, after alpha-particle irradiation from fluences that ranged from 2.6×10^{10} – 9.2×10^{11} cm^{-2}, which is much less than that of carrier removal rate of Si, 4×10^{5} cm^{-1} [6]. This supported radiation hardness of SiC. Moreover, at higher fluence the devices were still of good quality. It was also observed that two of the shallow defects present in the as-grown material disappeared after irradiation even at low fluence (4.1×10^{11} cm^{-2}). The defects reappeared after annealing in flowing argon at 300 °C for 20 minutes.

Detailed discussions of these results are presented in Papers I, III, IV and VII.

4.3.3 Concluding remarks

Electrically active defects introduced during the irradiation by high-energy particles have been reported. The high-energy electron irradiation introduced three electron defects with lower carrier removal rate compared to the alpha-particle irradiation. HEE

© University of Pretoria

irradiation also influenced two of the electrically active defects observed in the as-grown. Two electron deep-level defects were introduced by alpha-particle irradiation with MeV energy from a ^{241}Am radionuclide source. Two of the defects observed ($E_{0.09}$ and $E_{0.65}$) in the as-grown material also increased significantly in concentration after irradiation. From the results obtained, it was deduced that, due to its radiation hardness, SiC promises to provide solutions to radiation damage of devices in aerospace, manufacturing industries, defence and radiation harsh environments.

4.4 Electron-beam deposition and exposure

It has been reported that metallization, such as electron beam deposition and sputtering deposition, do introduced electrically active defects in measurable quantities at and close to the metal-semiconductor junction in conventional semiconductors such as Si, Ge and GaAs [7-11]. These defects influence the performance of Schottky contacts on these materials. In this section, the research question is: Are process induced defects possible in wide bandgap and radiation hard materials such as SiC?

4.4.1 Electron-beam (e-beam) deposition

The e-beam deposition technique was used to deposit high melting point metals, such as Pt, W, Ir and Ru. In this section, defects induced by e-beam deposition will be compared to alpha and electron irradiation induced defects discussed in the previous sections. Understanding the nature of the process induced defects in SiC will help to develop procedures to control the defects based on their harmful or beneficial properties.

The Paper V gives the details of process induced defects in W/4H-SiC Schottky barrier diodes and their electronic properties.

4.4.2 Electron-beam exposure

The term 'electron beam exposure' refers to the procedure when a sample is exposed to electron beam conditions without actual metal deposition. This technique was introduced with the aim of providing an answer to the question stated in Section 4.4. The electronic properties of defects induced by electron beam exposure during the manufacture of Ni/4H-SiC diodes by resistive evaporation of were reported. The defects induced in this process were compared to defects in as-grown Ni/4H-SiC diodes and

© University of Pretoria

diodes bombardment with alpha-particles and high-energy electrons from an ^{241}Am and a ^{90}Sr source, respectively.

The experimental procedure used for this section has been described in Chapter 3 of this thesis. Paper VI gives the details of the procedure before characterization of the electrically active defects induced during the process.

Since the *I-V* and *C-V* characteristics of these samples were not presented in the Paper VI, they will be discussed below.

Figure 4.4 shows the plots of forward semi-logarithmic *I-V* characteristics of Ni/4H-SiC SBDs for as-grown, after bombardment with alpha-particle and high-energy electron irradiation and electron-beam exposure conditions. These *I-V* characteristics were analysed by fitting a pure thermionic emission model to the linear region of the curves as shown in Figure 4.4. From the results obtained, the ideality factor obtained for the as-grown diodes was close to one. The ideality factor increased after irradiation with electrons, irradiation with alpha particles and exposure to electron beam conditions, in this sequence. Thermionic emission was the dominant current transport mechanism in all cases with only slight deviations induced as a result of defects caused by the irradiation and exposure process. This deviation is probably due to interface states. At higher voltages, the curves show that series resistance dominated. The effect was greater for alpha-particle irradiated sample and least for the e-beam exposed sample, as shown in Table 4.2.

Table 4.2: SBDs parameters obtained from I-V and C-V measurements on Ni/4H-SiC Schottky contacts as-grown, and after alpha-particle and high-energy electron irradiation and electron-beam exposure.

Samples	n	I_s ($\times10^{-18}$ A)	R_s (Ω)	N_d ($\times10^{15}$ cm^{-3})	$\phi_{I\text{-}V}$ (eV)	$\phi_{C\text{-}V}$ (eV)
As-grown	1.04	16	48	7.2	1.24	1.26
α-particle irradiation	1.07	3	70	6.7	1.29	1.36
HEE irradiation	1.13	0.1	60	7.3	1.38	1.60
E-beam exposure	1.26	66	13	7.7	1.21	1.38

© University of Pretoria

The plots of $1/C^2$ as a function of reverse voltage are shown in Figure 4.5. The linearity of the plots indicated the formation of Schottky diodes [12].

It can be deduced from the results of I-V and C-V measurements that e-beam exposure, without metal deposition, resulted in degradation of Schottky contacts.

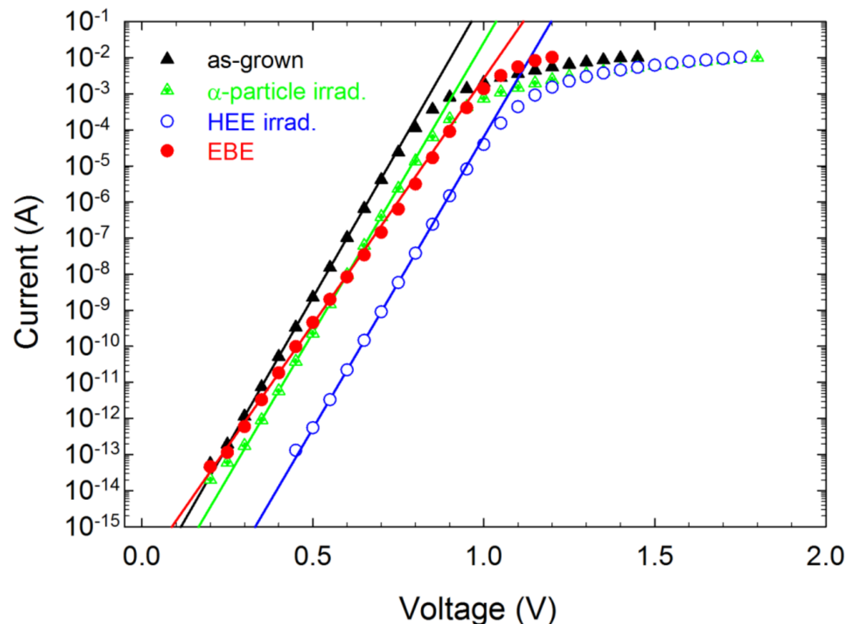

Figure 4.4: A forward semi-logarithmic I-V characteristics of Ni/4H-SiC Schottky contacts for as-grown, alpha-particle and HEE irradiated and electron beam exposed sample, measured at 300 K.

Figure 4.6 shows the DLTS spectra obtained for as-grown, alpha-particle and high-energy electron irradiated and electron beam exposed Ni/4H-SiC SBDs. All the samples revealed the presence of four electrically active defects with energies varying slightly for different processes, but within experimental error. The properties of these defects are reported in Papers I, II, III and VII. Alpha-particle irradiation introduced two defects labelled $E_{0.39}$ and $E_{0.70}$, and HEE irradiation introduced three defects labelled $E_{0.22}$, $E_{0.40}$ and $E_{0.70}$. The electrically active defects have been assigned and described in this study and in Paper VI. The defect labelled $E_{0.22}$ has not been observed before. E-beam exposure induced two defects in Ni/4H-SiC SBD, $E_{0.42}$ and $E_{0.71}$, which have similar attributes to the defects introduced by high-energy particles, but in lower concentration. Furthermore, it is worth noting that it was concluded in the silicon

© University of Pretoria

carbide community that the electron trap with energy that varies from 0.61 to 0.71 eV below the conduction band minimum, (popularly known as Z_1/Z_2) has intrinsic nature and has been linked to the carbon vacancy [13].

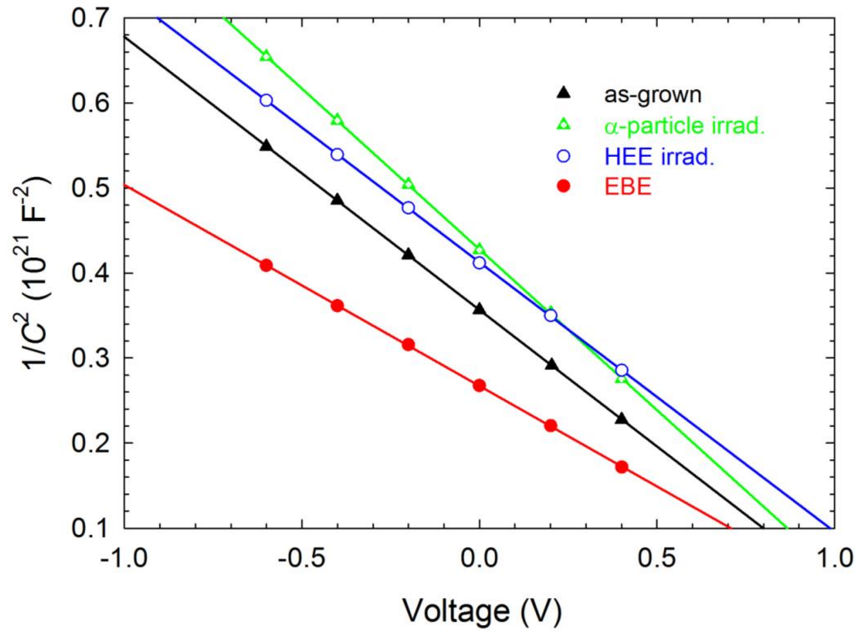

Figure 4.5: $1/C^2$ as a function of voltage for Ni/4H-SiC Schottky contacts for as-grown, alpha-particle and HEE irradiated and e-beam exposure, measured at 300 K.

© University of Pretoria

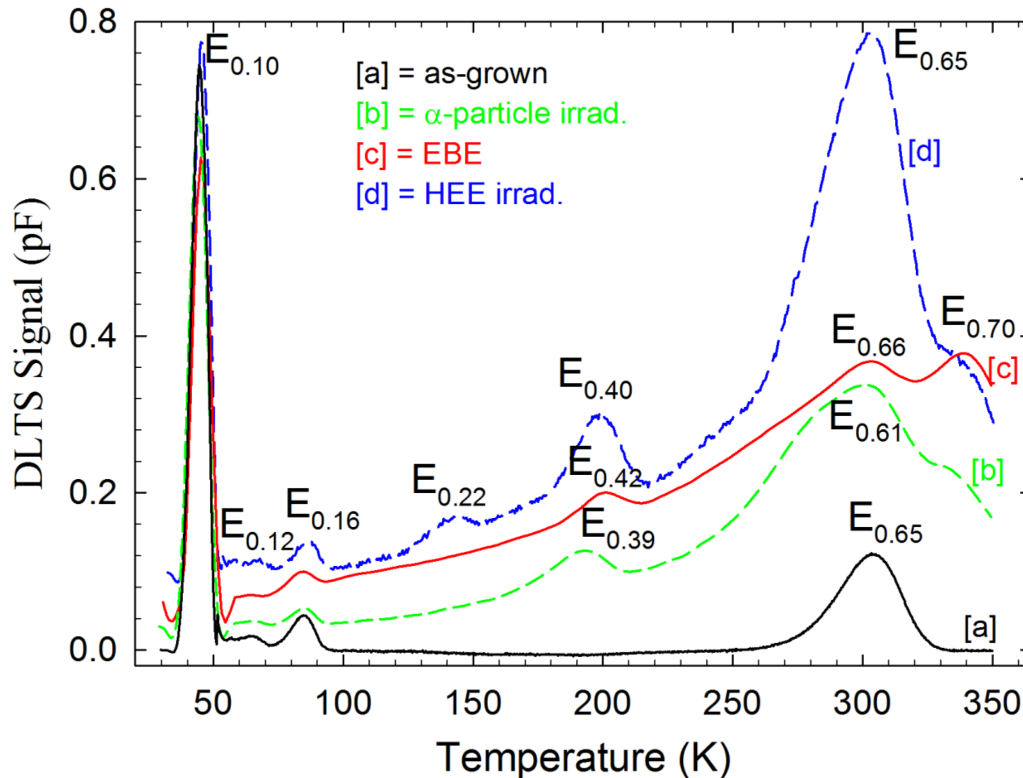

Figure 4.6: Conventional DLTS spectra of Ni/4H-SiC for as-grown, alpha-particle and HEE irradiated and e-beam exposed samples.

4.4.3 Concluding remarks

The results obtained have provided the answer to the question posed at the beginning of Section 4.4. It was demonstrated that electron beam deposition and exposure introduce defects in Ni/4H-SiC SBDs. Some of these defects are similar to those introduced by high-energy particle irradiation. The source of these electrically active defects is possibly due to the residual vacuum gases which were ionized around the filament and accelerated by the electric and magnetic field towards the 4H-SiC substrate. Due to the mass of the residual ions, their speed is much less than that of the electrons. In addition, their mass is also much greater than that of the electrons, so these ions are not deflected significantly by the magnetic field. Due to their heavier mass, these ions are able to induce damage when they collide with the sample. Other possible mechanisms have also been considered by Coelho *et al* [11]. Also, the exposure of samples to electron beam, without metal deposition, could be another mechanism of introducing defects $E_{0.42}$ and $E_{0.70/0.71}$ without high-energy particle irradiation.

© University of Pretoria

4.5 Defect annealing

Annealing at a specific temperature for a specific period may reduce the concentration or completely remove some defects introduced intentionally by irradiation or by processing. Furthermore, defect reactions during annealing in which some defect levels are removed and new levels appear may help in assigning the defect levels to specific structures. Also, annealing may modify a defect with no observable deep-levels to a new defect that is observable using DLTS.

This paragraph highlights some salient points about the annealing of defects as observed and reported in Paper IV of this study. The dominance of series resistance observed in the *I-V* characteristics of Ni/4H-SiC SBDs after bombardment with 5.4 MeV alpha-particles with fluence of 8.9×10^{11} cm^{-3} was reduced after annealing at 300 °C for 20 minutes. Also, the ideality factor of Schottky barrier diodes improved after annealing (i.e. from 1.77 to 1.15). In addition to our observation, annealing of severely irradiated samples for 20 minutes at 300 °C led to re-appearance of some shallow defects (labelled $E_{0.11/0.12}$ and $E_{0.16/0.17}$). It was observed in the un-irradiated and irradiated silicon carbide device. Details are discussed in Paper IV.

Paper VII described annealing studies done to determine the thermal dynamics of both the as-grown and the irradiation induced defects in low doping density 4H-SiC. The SBDs were annealed after irradiation at temperatures ranging from 100 °C to 600 °C in steps of 100 °C under flowing argon gas. We observed that annealing of irradiated SBDs at 200 °C led to the recovery of net donor concentration, and no noticeable recovery was observed when the annealing extended to 600 °C. Also, three defects with energies of 0.42, 0.62 and 0.76 eV below the conduction band were clearly and distinctly appeared after the annealing at 200 °C. However, the levels annealed out at 400 °C. Details are in Paper VII.

4.5.1 Concluding remarks

Annealing of irradiated samples at 300 °C improved the electrical properties of Ni/4H-SiC devices after severe radiation damage. Also, the irradiation induced defects in low doping density SiC were annealed out at temperatures below 600 °C.

© University of Pretoria

4.6 Temperature dependent *I-V* and *C-V* measurements on 4H-SiC Schottky barrier diodes

The interest of this section lies in the applications of wide bandgap materials (e.g. SiC) in low and high temperature environments (such as satellites and power electronics) as well as radiation fields. The in-depth study of electrical characteristics of silicon carbide devices at different temperatures and radiation conditions is technologically paramount for radiation sensing applications as well as manufacturing processes and high temperature and high power applications. Also, this study investigated the extent to which the performance and reliability of an M-S (say nickel-4H-SiC) device is affected by the quality of the junction between the nickel and the 4H-SiC. The barrier height of an M-S device is determined by the interface states as well as the difference between the energy levels of the majority carriers on either side junction [14].

In this section, *I-V* and *C-V* measurements were carried out at temperatures ranging from 40 to 300 K for as-grown, alpha-particle irradiated (fluence 5.1×10^{10} cm^{-2}) and high-energy electron irradiated (fluence 6.0×10^{14} cm^{-2}) samples.

The samples used for this study were first characterized at room temperature (300 K). The electrical properties were extracted from a semi-logarithmic plot of the forward *I-V* and the $1/C^2$-V plots obtained as shown in Papers I and II, and tabulated in Table 4.2. These values were estimated according to the equations derived in Chapter 2 of this study. From these results, conclusions could be drawn that the devices were of good quality for the temperature dependent measurements, even though there was degradation of the SBDs due to the irradiation by alpha-particle and high-energy electron of the devices.

In order to understand the ideal diode behaviour of the SBDs, analysis of experimental *I-V* characteristics was performed using the thermionic emission model as described in Chapter 2. The typical forward *I-V* characteristics of the Ni/4H-SiC SBDs as quoted in Papers I and II indicate very strong temperature dependence at lower temperatures. The characteristics deviated from ideality at lower temperatures (below 120 K) for as-grown and irradiated devices. Below 120 K, there was a gradual deviation from

© University of Pretoria

thermionic emission theory. These deviations were due to the presence of inhomogeneity at the interface.

The C-V characteristics as reported in Paper II showed that the Schottky barrier diodes fabricated were of good quality for both the as-grown and irradiated devices. In the temperature range 80-300 K, the C-V characteristics for both devices changed only slowly with decreasing temperature, however the changes occurred much faster at temperatures below 80 K. It was also deduced from the study that the net donor concentrations decreased with irradiation and temperature which is due to defects introduced by irradiation.

4.6.1 Concluding remarks

The ideality factor as well as Schottky barrier height of Ni/4H-SiC devices had strong temperature dependence at lower temperature. The deviation of the Richardson constants from theoretical value may be as result of barrier inhomogeneity at the metal-semiconductor interface and some other factors such as crystal defects and potential fluctuation and the deviation has been described by a modified Richardson plot. In addition, the unreasonable large Schottky barrier heights obtained from C-V measurements at lower temperatures was because of the carrier freeze out that influenced the electric field, thereby affecting the depletion capacitance and the value of the built-in voltage on the voltage intercept. Furthermore, irradiation by alpha-particle and high-energy electron did not influence the mean barrier height, but influenced the modified Richardson constant.

© University of Pretoria

PAPER I: Effects of 5.4 MeV alpha-particle irradiation on the electrical properties of nickel Schottky diodes on 4H-SiC

E. Omotoso, W. E. Meyer, F. D. Auret, A. T. Paradzah, M. Diale, S. M. M. Coelho, P. J. Janse van Rensburg, and P. N. M. Ngoepe

Nuclear Instruments and Methods in Physics Research Section B: Beam Interactions with Materials and Atoms 365A (2015):264-268.
doi:10.1016/j.nimb.2015.07.019

© University of Pretoria

UNIVERSITEIT VAN PRETORIA
UNIVERSITY OF PRETORIA
YUNIBESITHI YA PRETORIA

Nuclear Instruments and Methods in Physics Research B 365 (2015) 264–268

Contents lists available at ScienceDirect

Nuclear Instruments and Methods in Physics Research B

journal homepage: www.elsevier.com/locate/nimb

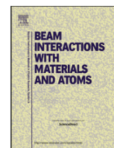

Effects of 5.4 MeV alpha-particle irradiation on the electrical properties of nickel Schottky diodes on 4H–SiC

E. Omotoso [a,b,*], W.E. Meyer [a], F.D. Auret [a], A.T. Paradzah [a], M. Diale [a], S.M.M. Coelho [a], P.J. Janse van Rensburg [a], P.N.M. Ngoepe [a]

[a] Department of Physics, University of Pretoria, Private Bag X20, Hatfield 0028, South Africa
[b] Department of Physics, Obafemi Awolowo University, Ile-Ife 220005, Nigeria

ARTICLE INFO

Article history:
Received 16 September 2014
Received in revised form 16 March 2015
Accepted 8 July 2015
Available online 25 July 2015

Keywords:
Irradiation
DLTS
4H–SiC
Defects
Alpha-particles

ABSTRACT

Current–voltage, capacitance–voltage and conventional deep level transient spectroscopy at temperature ranges from 40 to 300 K have been employed to study the influence of alpha-particle irradiation from an ^{241}Am source on Ni/4H–SiC Schottky contacts. The nickel Schottky barrier diodes were resistively evaporated on n-type 4H–SiC samples of doping density of 7.1×10^{15} cm ^{3}. It was observed that radiation damage caused an increase in ideality factors of the samples from 1.04 to 1.07, an increase in Schottky barrier height from 1.25 to 1.31 eV, an increase in series resistance from 48 to 270 Ω but a decrease in saturation current density from 55 to 9×10 ^{12} A m ^{2} from *I–V* plots at 300 K. The free carrier concentration of the sample decreased slightly after irradiation. Conventional DLTS showed peaks due to four deep levels for as-grown and five deep levels after irradiation. The Richardson constant, as determined from a modified Richardson plot assuming a Gaussian distribution of barrier heights for the as-grown and irradiated samples were 133 and 151 A cm ^{2} K ^{2}, respectively. These values are similar to literature values.
© 2015 Elsevier B.V. All rights reserved.

1. Introduction

SiC is a promising semiconductor with a wide band-gap of 3.26 eV [1]. Because of its wide band-gap, SiC is a suitable substrate for developing devices that are capable of operating at high temperature as well as in harsh radiation fields [2,3]. The electrical and thermal properties of SiC make it suitable devices in the electronics operating at high power, high temperature and high frequency [4]. Irradiation is used to introduce defects in semiconductors in order to investigate the defects' properties by means of deep-level transient spectroscopy (DLTS) on Schottky diodes. Effects of radiation and temperature on semiconductors are technologically important for radiation to sensing applications as well as manufacturing processes and high temperature and high power applications [5].

It has been reported by many researchers that some wide band-gap semiconductors such as SiC and GaN are radiation hard which make them suitable for use in harsh radiation environments [3]. Effects of electron, proton, fast electron and fast neutron irradiation on SiC have been investigated by different researchers [3,6–8]. To the best of our knowledge, the effect of alpha-particles irradiation on Ni/4H–SiC has not been reported.

In this work, the change in electrical properties of Ni/4H–SiC due to alpha-particle irradiation has been investigated by means of current–voltage (*I–V*), capacitance–voltage (*C–V*) and DLTS measurements. The major aim was to determine the effect of 5.4 MeV alpha-particles irradiation on the electrical properties and diode performance of n-type 4H–SiC.

2. Experimental procedure

The Schottky diodes were fabricated on the Si face of chips cut from an n-type (nitrogen doped) 4H–SiC wafer, double polished with resistivity of 0.02 Ω-cm and doping density of 7.1×10^{15} cm^{-3}, supplied by CREE Res. Inc. Samples were degreased by boiling for 5 min each in trichloroethylene, acetone and methanol, followed by a 1 min rinse in de-ionised water. They were etched in 40% hydrogen fluoride for 30 s, then rinsed in de-ionised water and followed by blowing dry with nitrogen gas prior to thermal evaporation of the nickel ohmic contact on the back surface of the samples. The ohmic contact with a thickness of 3000 Å was deposited at a rate of 0.4 Å s^{-1}. The samples were annealed in a tube furnace under flowing argon gas at 950 °C for 10 min to form nickel silicides [9]. Hereafter, the

* Corresponding author at: Department of Physics, University of Pretoria, Private Bag X20, Hatfield 0028, South Africa.

http://dx.doi.org/10.1016/j.nimb.2015.07.019
0168-583X/© 2015 Elsevier B.V. All rights reserved.

© University of Pretoria

UNIVERSITEIT VAN PRETORIA
UNIVERSITY OF PRETORIA
YUNIBESITHI YA PRETORIA

samples were cleaned in an ultrasonic bath for 3 min each in trichloroethylene, acetone and methanol, followed by a 1 min rinse in de-ionised H_2O. They were also blown dry with nitrogen gas before the fabrication of nickel Schottky diodes. The nickel Schottky contacts were deposited through a metal contact mask and had an area of 2.4×10^{-3} cm^2 and a thickness of 1000 Å deposited at a rate of 0.2 Å s^{-1} under a vacuum of approximately 1×10^{-5} Torr.

The current–voltage (*I–V*) and capacitance–voltage (*C–V*) measurements of the sample were carried out at room temperature to test the qualities of the contacts. The *I–V* and *C–V* measurements were carried out by HP 4140 B pA meter/DC voltage source and HP 4192 A LF Impedance Analyzer, respectively. DLTS was used to characterise the defects present in the sample before and after alpha-particles irradiation.

The sample was irradiated with alpha-particle by placing an ^{241}Am source on top of the Schottky diodes. The irradiation was carried out at room temperature and lasted for 2 h. The sample received the fluence of 5.1×10^{10} alpha-particles-cm^{-2} from the foil fluence rate of 7.1×10^6 alpha-particles-cm^{-2}-s^{-1}. The characterisation of the sample was repeated.

3. Results and discussion

3.1. I–V characteristics at room temperature

Fig. 1 shows the forward semi-logarithmic *I–V* characteristics of the Schottky barrier diode measured at 300 K before and after irradiation. The effect of irradiation on the Ni/4H–SiC diode can be quantified in terms of the ideality factor (*n*), Schottky barrier height (SBH), saturation current (I_s) and series resistance (R_s) obtained from the plot. Measurements on the Schottky contacts were taken before and after the samples were irradiated. Table 1 compares the properties of the sample before and after irradiation at 300 K. The SBH of the contacts were determined from the *I–V* characteristics analysed by using the thermionic emission model [10,11]. The I_s was derived from the straight line intercept of ln*I–V* plot at *V* = 0

$$I_s = AA^* \exp\left(-\frac{\phi_{I-V}}{kT}\right) \quad (1)$$

where *A* is the effective diode area, A^* is the effective Richardson constant, ϕ_{I-V} is the effective SBH at zero bias, *k* is the Boltzmann constant and *T* is absolute temperature in Kelvin. From the Eq. (1), SBH, ϕ_{I-V} is given as:

Table 1
Comparison of some electrical parameters of Ni/4H–SiC before and after alpha-particle irradiation estimated from *I–V* and *C–V* characteristics at 300 K.

Samples	n	I_s (A)	R_s (Ω)	V_{bi} (V)	N_t (cm^{-3})	ϕ_{I-V} (eV)	ϕ_{C-V} (eV)
As-grown	1.04	15.5×10^{-18}	48	1.07	7.8×10^{15}	1.25	1.36
Irradiated	1.07	2.6×10^{-18}	270	1.23	7.4×10^{15}	1.31	1.52

$$\phi_{I-V} = \frac{kT}{q} \ln\left(\frac{AA^*T^2}{I_s}\right) \quad (2)$$

and *n* is given as:

$$n = \frac{q}{kT}\left(\frac{dV}{d(\ln I)}\right) \quad (3)$$

which is unity for an ideal diode (i.e. current flows entirely due to thermionic emission). But, *n* is always greater than one, which describes the deviation of the experimental ln*I–V* data from the ideal thermionic model. From Table 1, *n*, ϕ_{I-V} and R_s increases with radiation, but I_s decreases with radiation.

3.2. C–V characteristics at room temperature

Fig. 2 shows the plot of C^{-2} (pF^{-2}) as a function of voltage, *V* (V) before and after alpha-particle irradiation measured at 1 MHz frequency with the sample at room temperature. The capacitance increased with decreasing reverse voltage for both, but the capacitance after irradiation was lower. This is as a result of defects introduced into the sample during the irradiation process which traps electrons [12,13]. The *C–V* parameters are tabulated in Table 1. The zero-bias barrier heights for both samples were determined from Eq. (4).

$$\phi_{C-V} = V_{bi} + \frac{kT}{q} \ln\frac{N_c}{N_d} \quad (4)$$

From Fig. 2, the free carrier concentration of the sample before and after radiation was determined from the slope of the plots. The free carrier removal rate, η can be obtained from Eq. (5) below:

$$\eta = \frac{\Delta(N_D - N_A)}{\varphi} \quad (5)$$

where $\Delta(N_D - N_A)$ is the change in free carrier concentration before and after irradiation, φ is the fluence to which the sample was bombarded [14]. At room temperature (300 K), a fluence of 5.1×10^{10}

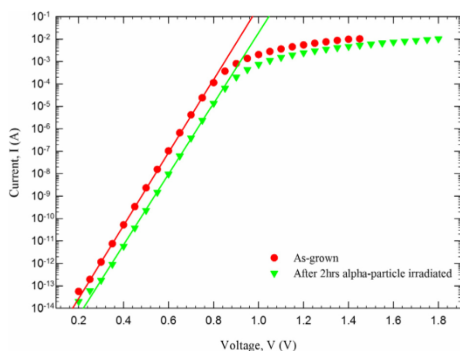

Fig. 1. Forward *I–V* characteristics of Ni/4H–SiC Schottky diodes before and after irradiation measured at 300 K.

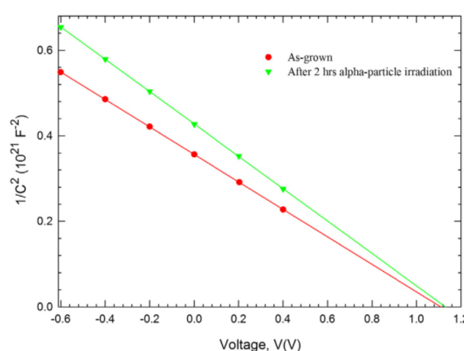

Fig. 2. $1/C^2$ as a function of voltage characteristics of Ni/4H–SiC before and after 5.4 MeV alpha-particles irradiation at 300 K.

© University of Pretoria

UNIVERSITEIT VAN PRETORIA
UNIVERSITY OF PRETORIA
YUNIBESITHI YA PRETORIA

alpha-particles-cm^{-2} resulted in a change in carrier concentration from 7.8×10^{15} to 7.4×10^{15} leading to a carrier removal rate of 7.8×10^{3} cm^{-1}.

Comparing the SBH for I–V and C–V measurements, it was observed experimentally that the SBH's do not agree. The SBH increased after irradiation for both I–V and C–V, but greater for C–V measurements. This is in confirmation with what has been reported in literature [15,16]. The causes for a difference in this parameters are deep impurity level, surface inhomogeneity, quantum mechanical tunnelling, interfacial layer and states, image force lowering, and edge leakage currents [17].

3.3. I–V characteristics at temperature range 40–300 K

Fig. 3 shows the semi-logarithmic forward bias I–V characteristics for both as-grown and irradiated Ni/4H–SiC Schottky barrier diodes measured from temperature ranges 40–300 K in other to determine the effect of temperature on the electrical properties of the samples.

Fig. 4 shows a gradual change in the ideality factor and the SBH before and after irradiation for SBD from temperature above 120 K. It can also be deduced from the plot that there is sporadic deviation of electrical behaviours of SBD from thermionic emission theory at lower temperature (below 120 K). The ideality factor and the SBH of the Ni/4H–SiC have strong reciprocal temperature dependence at lower temperatures. There was no noticeable change in the ideality factors and SBH at temperature 120 K and above, for before and after irradiation.

3.4. The Richardson and the modified Richardson plots

The Richardson's plots of $\ln(I_s/T^2)$ as a function of $1/T$ are shown in Figs. 5 and 6 for SBD before and after irradiation. We can re-write Eq. (1) as shown below;

$$\ln(I_s/T^2) = \ln AA^* - q/k\phi_{BO} \cdot 1/T \qquad (6)$$

The linear part of temperature range 120–300 K of the plots show in the graph. The Richardson constants before and after irradiation were estimated from the intercept of the plot to be 4.1×10^{-8} and 1.2×10^{-11} A cm^{-2} K^{-2}, respectively. The values are extremely small compared to the theoretical value of effective Richardson constant of 146 A cm^{-2} K^{-2} [18,19], which indicate that the active area is smaller than the device area. The mean barrier heights for both were deduced from the slope of the plot to be 1.63 and 0.72 eV. It

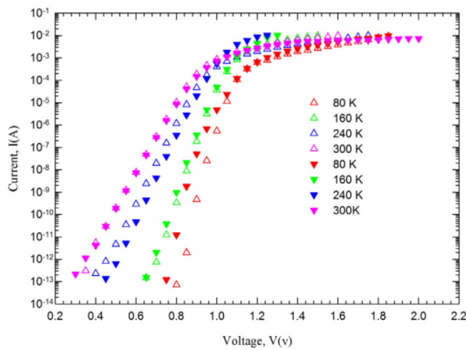

Fig. 3. The current versus voltage characteristics of Ni/4H–SiC before and after irradiation measured at temperature range 40–300 K. The solid symbols represent after irradiation.

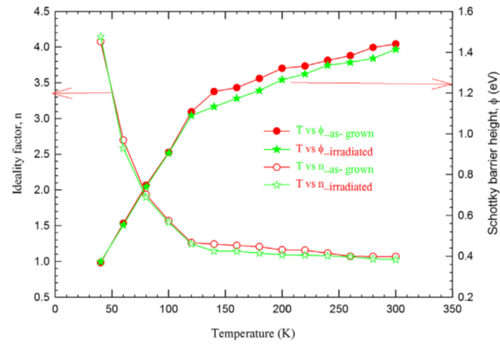

Fig. 4. Ideality factors and Schottky barrier heights as function of temperature before and after irradiation, measured at temperatures range 40–300 K.

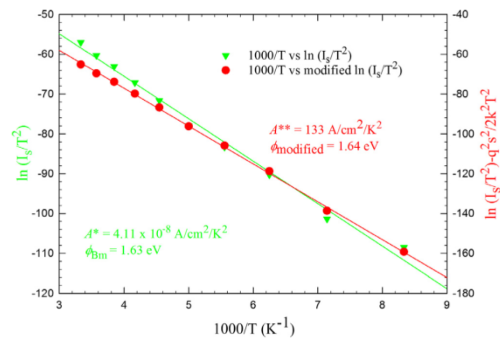

Fig. 5. The Richardson plot and the modified Richardson for as-grown Ni/4H–SiC.

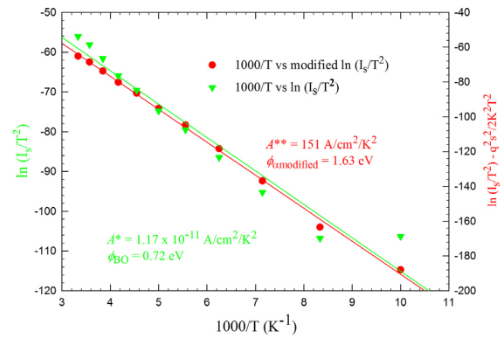

Fig. 6. The Richardson plot and the modified Richardson for Ni/4H–SiC after 2 h irradiation.

has been reported earlier by many researchers that the deviation of the Richardson constants from theoretical value may be as result of effect of the barrier inhomogeneity at the metal–semiconductor (MS) interface and some other factors such as crystal defects, potential fluctuation, etc [20]. Since the deviation cannot be explained by thermionic emission diffusion model, the Gaussian distribution model of barrier height can be used.

© University of Pretoria

UNIVERSITEIT VAN PRETORIA
UNIVERSITY OF PRETORIA
YUNIBESITHI YA PRETORIA

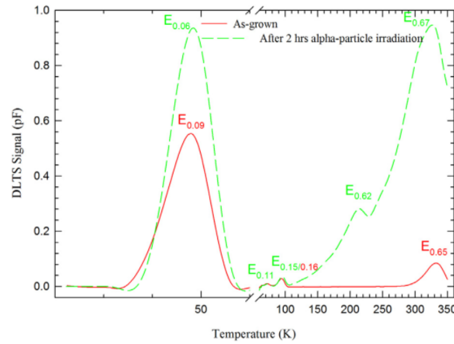

Fig. 7. DLTS spectra for the Ni/4H–SiC before and after alpha-particles irradiation. The temperature range 60–350 K scaled up by factor of 10.

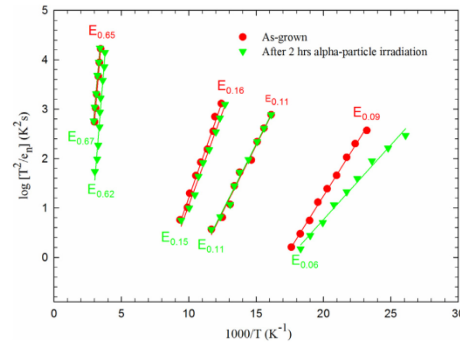

Fig. 8. The Arrhenius plots for the DLTS of as-grown and after irradiation Ni/4H–SiC.

The Gaussian distribution model has been used to correct the deviation that cannot be explained with thermionic emission diffusion which occurred as a result of barrier height inhomogeneities. The deviation between experimental and theoretical values of the Richardson constants was described by the modified Richardson plot according to the aforementioned model.

Eq. (7) is obtained by combining Eq. (2) with Eq. (6).

$$\ln\left(\frac{I_s}{T^2}\right) - \left(\frac{q^2\sigma^2}{2k^2T^2}\right) = \ln(AA^{**}) - \frac{q\phi_{Bm}}{kT} \quad (7)$$

The standard deviation, σ, (which its square was calculated to be 1.08×10^{-2} and 1.21×10^{-2} for as-grown and after irradiation) plays major role in estimating the modified Richardson constant, A^{**}. Figs. 5 and 6 show the plot of $\ln(I_s/T^2) - (q^2\sigma^2/2k^2T^2)$ as function of $1000/T$. The A^{**} before and after irradiation were determined from the intercept of the straight line to be 133 and 151 A cm^{-2} K^{-2}, respectively. The values were in good agreement with the theoretical value. The mean barrier height before and after irradiation were estimated from the slope of the straight line as 1.64 and 1.63 eV, respectively. There was no significant change in the value of barrier height after irradiation.

3.5. DLTS analysis

Fig. 7 shows the DLTS spectra for the samples before and after alpha-particle irradiation. The measurements were obtained at temperatures range 22–350 K, at a quiescent reverse bias of −5.0 V, filling pulse amplitude of 6.0 V, filling pulse width of 1.0 ms and a rate window of 200 s^{-1}. Fig. 8 shows the Arrhenius plots of each defect. The *signatures* of the defects in term of activation energies, E_n and apparent capture cross sections, σ_n were determined from Fig. 8. The activation energy of each defect was determined from the slope, and the corresponding apparent capture cross section was calculated from the intercept of the Arrhenius plot of $\log(T^2/e_n)$ versus $1/T$ as earlier reported by Auret et al. [21]. The sample revealed the presence of four defects before irradiation, and five defects after alpha-particle irradiation as shown in Table 2. Defects with energy levels labelled as $E_{0.09}$, $E_{0.11}$, $E_{0.16}$ and $E_{0.65}$ were obtained before irradiation, and $E_{0.06}$, $E_{0.11}$, $E_{0.15}$, $E_{0.62}$ and $E_{0.67}$ after irradiation, where 'E' refers to an electron trap and the subscript 0.09 refers to an energy level below the conduction band. The properties and attributes of each defect were tabulated in Table 2. The $E_{0.09}$ has been attributed to nitrogen impurities that occupy cubic site and occupy hexagonal site when the activation enthalpy is approximately 0.06 eV [22,23]. The defects $E_{0.11}$ and $E_{0.16}$ are related to transitional metal (titanium) [24,25]. The $E_{0.11}$ and $E_{0.16/0.15}$ have been reported earlier that the two levels could be a single defect occupying different geometric positions in material [26]. The $E_{0.62}$ was the only defect introduced by alpha-particle irradiation, and was attributed to Z_1/Z_2 [22,27]. It has been previously reported that $E_{0.67/0.65}$ could be a defect complex composed of several energy levels [28,29]. The dominant of these energy levels is Z_1/Z_2 and is possibly a di-carbon or silicon interstitial next to a nitrogen atom or a hydrogen related intrinsic defect [23]. There was a shift in temperature of $E_{0.67}$ from 332 K to 326 K. This was as a result of $E_{0.62}$ defect emanated after irradiation. The peak height of $E_{0.67}$ increases after irradiation as well. The formation of a new defect and the increase in intensity of some of the defects causes changes in I–V and C–V characteristics and the parameters of the Schottky contacts.

4. Conclusions

In conclusion, the Ni/4H–SiC Schottky contacts have been successfully fabricated by resistive evaporation technique. The effects of 5.4 MeV alpha-particles irradiation measured at different

Table 2
Electronic properties of defects detected by DLTS in as-deposited and 5.4 MeV alpha-particles irradiation of Ni/4H–SiC.

As-grown				After alpha-particle irradiation				Attribution
Defect	E_T (eV)	σ_a (cm^2)	T_{peak} (K)	Defect	E_T (eV)	σ_a (cm^2)	T_{peak} (K)	
$E_{0.09}$	E_c–0.09	8×10^{-15}	47	$E_{0.06}$	E_c–0.06	6×10^{-17}	48	N impurity [22]
$E_{0.11}$	E_c–0.11	2×10^{-16}	72	$E_{0.11}$	E_c–0.11	2×10^{-16}	74	Ti impurity [25]
$E_{0.16}$	E_c–0.16	1×10^{-15}	94	$E_{0.15}$	E_c–0.15	9×10^{-16}	95	Ti impurity [24]
–	–	–	–	$E_{0.62}$	E_c–0.62	1×10^{-13}	213	Z_1/Z_2 [22,27]
$E_{0.65}$	E_c–0.65	4×10^{-15}	332	$E_{0.67}$	E_c–0.67	8×10^{-15}	326	Z_1/Z_2 (C/Si vacancy [24,29]

Note: The T_{peak} (K) was taken at rate window of 200 s^{-1}.

© University of Pretoria

UNIVERSITEIT VAN PRETORIA
UNIVERSITY OF PRETORIA
YUNIBESITHI YA PRETORIA

temperatures on Ni/4H–SiC SBD have been investigated using *I–V*, *C–V* and conventional DLTS. The *I–V* and *C–V* measurements at 300 K before and after fluence of 5.1×10^{10} alpha-particles-cm^{-2} irradiation revealed good Schottky contacts. From *I–V* measurements, *n*, *SBH*, R_s increases with irradiation but I_s decreases with irradiation measured at 300 K. *C–V* measurements reveal decreases in free carrier concentration. The *I–V* measurements were also repeated at temperature range 40–300 K. The electrical behaviour of SBD deviated from thermionic emission theory at temperatures below 120 K. The modified Richardson constants before and after alpha-particle irradiation are 133 and 151 A cm^{-2} K^{-2}, respectively, by using Gaussian distribution method. The values of A^{**} were in good agreement with the theoretical value. The electrical properties of Ni/4H–SiC SBDs show little response to 5.4 MeV alpha-particle irradiation with free carrier removal rate of 7.8×10^{3} cm^{-1} which corroborate its uses in radiation harsh environments.

Acknowledgements

This work is based on the research supported in part by the National Research Foundation (NRF) of South African (Grant specific unique reference number (UID) 78838). The Grant holder acknowledges that opinions, findings and conclusions or recommendations expressed in this publication generated by the NRF supported are that of authors and that NRF accepts no liability whatsoever in this regard.

References

[1] L.M. Tolbert, B. Ozpineci, S.K. Islam, M.S. Chinthavali, Power Energy Syst. Proc. 1 (2003) 317–321.
[2] V. Kazukauskas, J.-V. Vaitkus, Opto-Electron. Rev. 12 (2004) 377–382.
[3] J. Grant, W. Cunningham, A. Blue, V. O'Shea, J. Vaitkus, E. Gaubas, M. Rahman, Nucl. Instr. Meth. Phys. Res. Sect., A 546 (2005) 213–217.
[4] M.C. Driver, R.H. Hopkins, C.D. Brandt, D.L. Barrett, A.A. Burk, R.C. Clarke, G.W. Eldridge, H.M. Hobgood, J.P. McHugh, P.G. McMullin, R.R. 0053iergiej, S. Sriram, Gallium Arsenide Integrated Circuit (GaAs IC) Symposium, 1993. Technical Digest 1993, 15th Annual, 1993, pp. 19–21.
[5] A. Akbay, H. Korkut, K. Ejderha, T. Korkut, A. Türüt, J. Radioanal. Nucl. Chem. 289 (2011) 145–148.
[6] K. Çınar, C. Coşkun, Ş. Aydoğan, H. Asıl, E. Gür, Nucl. Instr. Meth. Phys. Res., Sect. B 268 (2010) 616–621.
[7] K. Çınar, C. Coşkun, E. Gür, Ş. Aydoğan, Nucl. Instr. Meth. Phys. Res., Sect. B 267 (2009) 87–90.
[8] J. Benkovska, L. Stuchlikova, D. Buc, L. Čaplovic, Phys. Status Solidi A 209 (2012) 1384–1389.
[9] T. Marinova, A. Kakanakova-Georgieva, V. Krastev, R. Kakanakov, M. Neshev, L. Kassamakova, O. Noblanc, C. Arnodo, S. Cassette, C. Brylinski, B. Pecz, G. Radnoczi, G. Vincze, Mater. Sci. Eng., B 46 (1997) 223–226.
[10] S.M. Sze, K.K. Ng, Physics of Semiconductor Devices, John Wiley & Sons, 2006.
[11] E. Rhoderick, R. Williams, Oxford Science, Oxford, 1988.
[12] S. Ashok, J.M. Borrego, R.J. Gutmann, J. Appl. Phys. 51 (1980) 1076–1084.
[13] F. Roccaforte, S. Libertino, F. Giannazzo, C. Bongiorno, F. La Via, V. Raineri, J. Appl. Phys. 97 (2005).
[14] F. Auret, S. Goodman, M. Hayes, M. Legodi, H. Van Laarhoven, D.C. Look, Appl. Phys. Lett. 79 (2001) 3074–3076.
[15] E. Hökelek, G.Y. Robinson, Appl. Phys. Lett. 40 (1982) 426–428.
[16] C.R. Crowell, V.L. Rideout, Solid-State Electron. 12 (1969) 89–105.
[17] C.R. Crowell, Solid-State Electron. 20 (1977) 171–175.
[18] A. Itoh, T. Kimoto, H. Matsunami, Electron Device Lett., IEEE 16 (1995) 280–282.
[19] F. Roccaforte, F. La Via, A. Baeri, V. Raineri, L. Calcagno, F. Mangano, J. Appl. Phys. 96 (2004) 4313–4318.
[20] İ. Dökme, Ş. Altindal, M.M. Bülbül, Appl. Surf. Sci. 252 (2006) 7749–7754.
[21] F.D. Auret, P.N.K. Deenapanray, Crit. Rev. Solid State Mater. Sci. 29 (2004) 1–44.
[22] T. Kimoto, A. Itoh, H. Matsunami, S. Sridhara, L. Clemen, R. Devaty, W. Choyke, T. Dalibor, C. Peppermüller, G. Pensl, Appl. Phys. Lett. 67 (1995) 2833–2835.
[23] A. Castaldini, A. Cavallini, L. Rigutti, F. Nava, S. Ferrero, F. Giorgis, J. Appl. Phys. 98 (2005) 053706.
[24] T. Dalibor, G. Pensl, H. Matsunami, T. Kimoto, W.J. Choyke, A. Schöner, N. Nordell, Phys. Status Solidi A 162 (1997) 199–225.
[25] A.A. Lebedev, Semiconductors 33 (1999) 107–130.
[26] N. Achtziger, W. Witthuhn, Appl. Phys. Lett. 71 (1997) 110–112.
[27] G. Pensl, W.J. Choyke, Phys. B: Condens. Mat. 185 (1993) 264–283.
[28] T.A.G. Eberlein, R. Jones, P.R. Briddon, Phys. Rev. Lett. 90 (2003) 225502.
[29] I. Pintilie, L. Pintilie, K. Irmscher, B. Thomas, Appl. Phys. Lett. 81 (2002) 4841–4843.

© University of Pretoria

PAPER II: The influence of high energy electron irradiation on the Schottky barrier height and the Richardson constant of Ni/4H-SiC Schottky diodes

E. Omotoso, W. E. Meyer, F. D. Auret, A. T. Paradzah, M. Diale, S. M. M. Coelho, and P. J Janse van Rensburg

Materials Science in Semiconductor Processing 39 (2015): 112-118.
doi:10.1016/j.mssp.2015.04.031

© University of Pretoria

UNIVERSITEIT VAN PRETORIA
UNIVERSITY OF PRETORIA
YUNIBESITHI YA PRETORIA

Materials Science in Semiconductor Processing 39 (2015) 112–118

Contents lists available at ScienceDirect

Materials Science in Semiconductor Processing

journal homepage: www.elsevier.com/locate/mssp

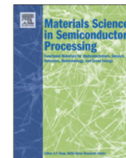

The influence of high energy electron irradiation on the Schottky barrier height and the Richardson constant of Ni/4H-SiC Schottky diodes

E. Omotoso [a,b,*], W.E. Meyer [a], F.D. Auret [a], A.T. Paradzah [a], M. Diale [a], S.M.M. Coelho [a], P.J. Janse van Rensburg [a]

[a] Department of Physics, University of Pretoria, Private Bag X20, Hatfield 0028, South Africa
[b] Departments of Physics, Obafemi Awolowo University, Ile-Ife 220005, Nigeria

ARTICLE INFO

Keywords:
Richardson constant
High energy electron irradiation
Silicon carbide
Schottky barrier height

ABSTRACT

The influence of high energy electron (HEE) irradiation from a Sr-90 radio-nuclide on *n*-type Ni/4H–SiC samples of doping density 7.1×10^{15} cm^{-3} has been investigated over the temperature range 40–300 K. Current–voltage (*I–V*), capacitance–voltage (*C–V*) and deep level transient spectroscopy (DLTS) were used to characterize the devices before and after irradiation at a fluence of 6×10^{14} electrons-cm^{-2}. For both devices, the *I–V* characteristics were well described by thermionic emission (TE) in the temperature range 120–300 K, but deviated from TE theory at temperature below 120 K. The current flowing through the interface at a bias of 2.0 V from pure thermionic emission to thermionic field emission within the depletion region with the free carrier concentrations of the devices decreased from 7.8×10^{15} to 6.8×10^{15} cm^{-3} after HEE irradiation. The modified Richardson constants were determined from the Gaussian distribution of the barrier height across the contact and found to be 133 and 163 A cm^{-2} K^{-2} for as-deposited and irradiated diodes, respectively. Three new defects with energies 0.22, 0.40 and 0.71 eV appeared after HEE irradiation. Richardson constants were significantly less than the theoretical value which was ascribed to a small active device area.

© 2015 Elsevier Ltd. All rights reserved.

1. Introduction

Metal-semiconductor (MS) Schottky barrier diodes (SBDs) are widely used where diodes with low forward voltage drop, junction capacitance and high switching speed are required [1]. This makes them ideal as rectifiers in photovoltaic systems, high-efficiency power supplies and high frequency oscillators [2]. SBDs also have important uses in optoelectronics, high frequency and bipolar integrated circuits applications [3,4]. The reliability of SBDs is influenced significantly by the quality of the MS junction [5]. The performance of the devices can be quantified experimentally study in terms of their ideality factor, Schottky barrier height (SBH), saturation current, series resistance and free carrier concentration. Among these properties of the MS interface, SBH plays a major role in the successful operation of many devices in transporting electrons across the MS junction [6].

Since room temperature (300 K) measurements of *I–V* and *C–V* characteristics alone cannot provide detailed information about the mechanisms responsible for the formation of barrier at the interface of the MS and electrical properties of devices [7], additional insight is gained by characterising the diodes over a wide temperature range (40–300 K). Conclusions may be drawn from the deviation of *I–V–T* characteristics from the

* Corresponding author at: Department of Physics, University of Pretoria, Private Bag X20, Hatfield 0028, South Africa. Tel.: +274842911287.
E-mail address: ezekiel.omotoso@up.ac.za (E. Omotoso).

http://dx.doi.org/10.1016/j.mssp.2015.04.031
1369-8001/© 2015 Elsevier Ltd. All rights reserved.

© University of Pretoria

UNIVERSITEIT VAN PRETORIA
UNIVERSITY OF PRETORIA
YUNIBESITHI YA PRETORIA

ideal thermionic emission current model at lower temperature for many SBDs. The *I–V–T* characteristics of SBDs based on TE theory reveals an abnormal increase in the ideality factor and a decrease in the SBH with decreasing temperature [8–11]. The abnormal behaviour has been attributed to be a function of the atomic structure, and atomic or barrier inhomogeneities at the MS interface, which are caused by defects, multiple phases and grain boundaries. The barrier inhomogeneities in MS SBDs are often modelled as a Gaussian distribution function and used to provide better understanding to experimental *I–V* characteristics [12–15].

SiC is a promising semiconductor with a wide bandgap of 3.26 eV [16]. Because of its wide bandgap and chemical stability, it can be used to produce electronic devices that are capable of operating at high temperature, high frequency and high power semiconductor devices, as well as in harsh radiation fields [17–20]. Effects of radiation and temperature on semiconductors are technologically important for radiation to sensing applications, as well as manufacturing processes and high temperature and high power applications [21]. Deep level transient spectroscopy (DLTS) on SBDs is often used to investigate the properties of defects in semiconductors.

Many researchers have reported that some wide bandgap semiconductors such as SiC, ZnO and GaN are radiation hard which makes them suitable for use in harsh radiation environments [18]. Effects of proton, fast electron and fast neutron irradiation on SiC have been investigated by different researchers [18,22–24]. To the best of our knowledge, the effect of high energy electron (HEE) irradiations at fluence of 6×10^{14} cm^{-2} on Ni/4H–SiC has not been reported.

In this work, we present the effect of HEE irradiations on the electrical characteristics of nickel SBDs fabricated on 4H–SiC SBDs measured over wide temperature range (40–300 K). The major aim of this work is to determine the extent to which the characteristics of nickel on *n*-type 4H–SiC Schottky diodes would be affected by HEE irradiations.

2. Experimental procedure

The samples used for this work were cut from a nitrogen-doped *n*-type 4H–SiC wafer, polished on both sides with the Si face epi ready, resistivity of 0.02 Ω-cm and doping density of 7.1×10^{15} cm^{-3}. The wafers were supplied by CREE Res. Inc. The samples were cut into smaller pieces with dimension of roughly 2×3 mm^2 and degreased by boiling for 5 min each in trichloroethylene, acetone, methanol and followed by 1 min rinse in de-ionized water. They were etched in 40% hydrogen fluoride for 30 s in order to remove the native oxide layer on the samples, then rinsed in de-ionized water, followed by blow drying with nitrogen gas prior to thermally fabrication of nickel ohmic contact on the back surface (1.0×10^{18} cm^{-3} doped side) of the samples.

Resistive evaporation was employed for the fabrication of nickel ohmic and Schottky contacts because it is known to neither introduce defects nor contaminate the samples. The ohmic contact with a thickness of 3000 Å was deposited at a rate of 0.4 Å s^{-1}. For ohmic contact formation, the samples were annealed in a tube furnace under flowing argon gas at 950 °C for 10 min to form nickel silicides [25].

Before deposition of the Schottky contact, the samples were cleaned in an ultrasonic water bath for 3 min each in trichloroethylene, acetone and methanol, followed by 1 min rinsed in de-ionized H_2O after the annealing of the ohmic contact. Nickel Schottky contacts were resistively evaporated through a metal contact mask and had an area of 2.4×10^{-3} cm^2 and a thickness of 1000 Å deposited at a rate of 0.2 Å s^{-1} under a vacuum of approximately 10^{-5} Torr.

The sample was irradiated through the Schottky contacts by HEE from a strontium-90 radioactive source at a fluence rate of 7×10^{9} electrons-cm^{-2} s^{-1}. The irradiation was carried out at room temperature and lasted for 24 h, which resulted in a fluence of 6×10^{14} electrons-cm^{-2}. The energy distribution of electron emitted by strontium-90 radionuclide has been reported by Auret *et al.* [26].The sample was characterized at room temperature and in the dark using *I–V* and *C–V* station, consisting of a HP 4140 B pA metre/DC voltage source and HP 4192 A LF Impedance Analyser, respectively. Hereafter, the sample was placed in a closed cycle helium cryostat and characterised by conventional DLTS, *I–V–T* and *C–V–T* measurements in wide temperature range. This procedure was performed before and after HEE irradiation.

3. Results and discussion

3.1. C–V characteristics

The fabricated devices were subjected to irradiation at room temperature. Both as-deposited and irradiated devices were examined by the *C–V* method at different temperatures. Fig. 1 shows the plot of capacitance as a function of reverse bias voltage. The capacitance decreased with a decrease in temperature. The capacitance increased with decreasing reverse voltage for both, but the capacitance after irradiation was lower, as also be reported [27,28]. The C^{-2} (pF^{-2}) as a function of reverse bias voltage, *V* (V) before and after HEE irradiation measured at 1 MHz with the samples at temperatures range

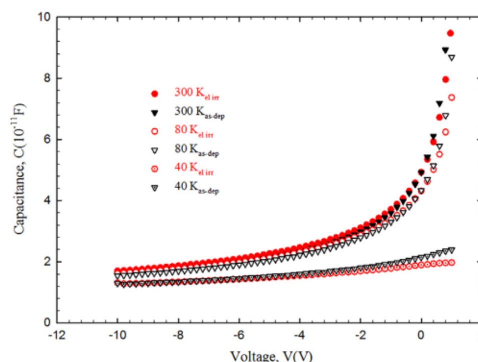

Fig. 1. The *C–V* characteristics of Schottky barrier diodes of Ni/n-4H–SiC before and electron irradiation in temperature range 40–300 K.

© University of Pretoria

UNIVERSITEIT VAN PRETORIA
UNIVERSITY OF PRETORIA
YUNIBESITHI YA PRETORIA

40–300 K are depicted in Fig. 2. The result obtained showed a good SBDs for both devices. There was no abrupt degradation between the as-deposited and irradiated devices at temperature range 80–300 K. The *C–V* characteristics changed more rapidly with temperature, and the difference between the as-deposited and the irradiated diodes became more pronounced below 80 K. The slope of plot C^{-2} versus V is approximately constant for the temperature range 80–300 K for both samples which indicates that all the dopant is ionized due to the presence of the electric field [29]. The plot in Fig. 2 is deduced from Eq. (1) which represents the depletion layer in Schottky diodes. The N_t, V_{bi} and ϕ_{C-V} were determined from the plot and tabulated in Table 1. The free carrier concentrations, N_t decreased with irradiation and temperature which is as a result of the defects introduced from the HEE irradiation into the SiC.

$$\frac{1}{C^2} = \frac{2(V_o - V_{bi})}{q\varepsilon_s A^2 N_t} \tag{1}$$

where q is the charge, ε_s is the permittivity of semiconductor, A is the effective area of the diode, and V_o can be obtained from the intercept of reverse voltage when C^{-2} is equal to zero. The zero-bias barrier heights for both devices were determined from Eq. (2).

$$\phi_{C-V} = V_{bi} + \frac{kT}{q} \ln \frac{N_c}{N_t} \tag{2}$$

From Fig. 2, the free carrier concentrations of the sample were determined from the slope of the plots according to Eq. (1). The free carrier removal rate, η can be obtained

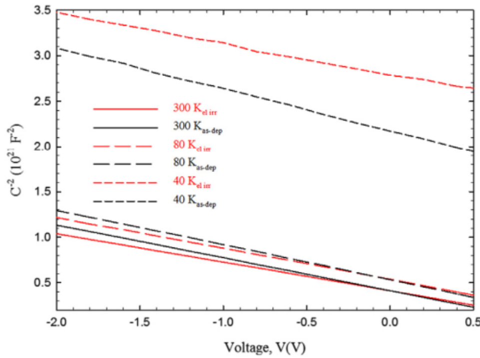

Fig. 2. Graph of C^{-2} as a function of applied voltage characteristic of SBDs of Ni/4H–SiC before and after electron irradiation in temperature range 40–300 K.

from Eq. (3) below

$$\eta = \frac{\Delta(N_D - N_A)}{\varphi} \tag{3}$$

where $\Delta(N_D - N_A)$ is the change in free carrier concentration before and after HEE irradiation, φ is the fluence at which the sample was bombarded [30]. At room temperature (300 K), the change in free carrier concentration from 7.8×10^{15} (before irradiation) to 6.8×10^{15} cm^{-3} (after HEE irradiation) is 1.0×10^{15} cm^{-3} and the fluence received by the sample was 6.0×10^{14} cm^{-2}. The free carrier removal rate was calculated as 1.67 cm^{-1} for irradiation of the sample with energy 546 keV from Sr-90 radionuclide. The value of η calculated here is approximately 4670 times lower than that of SiC bombarded by 5.4 MeV alpha-particles [31]. The HEE irradiation has less impact on the electrical properties of Ni/4 H–SiC than alpha-particle irradiation [31].

3.2. *I–V* characteristics

The forward semi-log *I–V* characteristics of the Ni/4H–SiC SBD measured at temperature range 40–300 K before and after electron irradiation are shown in Fig. 3 in order to know the temperature effects on the deep energy levels. The plots show linearity up to a current of approximately 1×10^{-4} A for as-deposited and irradiated devices except at lower temperatures (80 K below). It can be observed that *I–V* plots show lower current with lower temperature. This is in accord with the equation describing current transport across a SBD by thermionic emission–diffusion theory [32,33].

The effect of irradiation on the Ni/4H–SiC diode as well as temperature can be quantified in terms of the ideality factor (n), Schottky barrier height (ϕ_{I-V}), saturation current (I_s) and series resistance (R_s) obtained from the *I–V* plots. Measurements on the Schottky contacts were taken before and after the devices were irradiated. Table 1 compares the properties of the samples. The effective Richardson constant for both samples were obtained from the Eq. (4). Schottky barrier heights of the contacts were determined from the *I–V* characteristics analysed by using the thermionic emission model [5,32,33].

$$I_s = AA^* \exp\left(-\frac{q\phi_{I-V}}{kT}\right) \tag{4}$$

where A^* is the effective Richardson constant, ϕ_{I-V} is the effective SBH at zero bias, k is the Boltzmann constant and T is absolute temperature in Kelvin.

It could be deduced from Table 1 that the SBH_{I-V} decrease and the ideality factor increase, with decreasing in

Table 1
Comparison of some electrical parameters of Ni/n-type 4H–SiC before and after electron irradiation estimated from *I–V* and *C–V* characteristics at 40 and 300 K.

Samples	n	I_s (A)	R_s (Ω)	V_{bi} (V)	N_t (cm^{-3})	ϕ_{I-V} (eV)	ϕ_{C-V} (eV)
As-deposited(300 K)	1.04	1.5×10^{-20}	48	1.07	7.8×10^{15}	1.44	1.36
As-deposited (40 K)	4.02	2.0×10^{-44}	664	5.03	5.9×10^{15}	0.37	5.06
24h electron irradiation (300 K)	1.13	1.4×10^{-19}	60	1.32	6.8×10^{15}	1.38	1.60
24h electron irradiation (40 K)	4.14	1.4×10^{-45}	1684	7.92	5.2×10^{15}	0.36	7.95

© University of Pretoria

UNIVERSITEIT VAN PRETORIA
UNIVERSITY OF PRETORIA
YUNIBESITHI YA PRETORIA

temperature [33–37]. It was also observed that $SBHs_{I-V}$ decrease and the ideality factors increase after HEE irradiation which corroborated what has earlier reported [23,24], but was in contrast with what was observed by Lin *et al*. [38].

From Eq. (4), ϕ_{I-V} is given as

$$\phi_{I-V} = \frac{kT}{q} \ln\left(\frac{AA^*T^2}{I_s}\right) \quad (5)$$

Comparing the SBH for *I–V* and *C–V* measurements, it was observed experimentally that SBHs' do not agree. The SBH increased after irradiation for both *I–V* and *C–V*, but to greater extent for *C–V* measurements. This is in agreement with what has been reported in literature [39–43]. The causes for a difference in this parameters are deep impurity levels, surface inhomogeneity, quantum mechanical tunnelling, interfacial layer and states, image force lowering, and edge leakage currents [44].

Fig. 4 shows a gradual change in ideality factor and SBH before and after HEE irradiation for SBD from temperatures above 120 K. It can also be deduced from the plot that there was sporadic deviation of electrical behaviours of SBD from thermionic emission theory at lower temperatures (below 120 K). Generation-recombination was dominant at temperatures below 80 K. Ideality factor and SBH of the Ni/4H–SiC had strong reciprocal temperature dependence at lower temperatures. It was also observed earlier for alpha-particle irradiated devices [31]. These deviations are due to the presence of inhomogeneities at the interface (such as surface defects and inhomogeneity in doping concentration) [20,33–37,45–47]. There was little noticeable change in the ideality factors and SBH at temperature 120 K and above, for before and after irradiation.

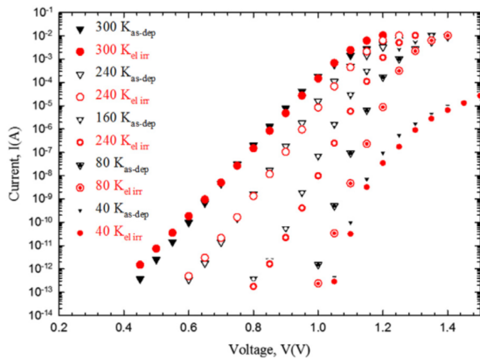

Fig. 3. The current versus voltage characteristics of Ni/4H–SiC before and after irradiation measured in temperature range 40–300 K.

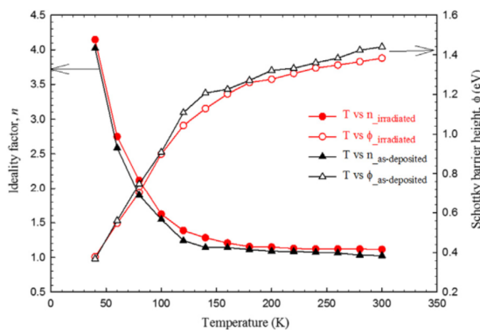

Fig. 4. Ideality factors and Schottky barrier heights as function of temperature before and after irradiation, measured in temperature range 40–300 K.

3.3. The Richardson plot

Fig. 5 shows the Richardson's plot of ln (I_s/T^2) as a function of $1/T$ for as-deposited and HEE irradiated samples. The temperature dependent behaviour of n and SBH predicted an inhomogeneous barrier height and deviation from thermionic emission and diffusion theory as shown in Fig. 4 [20,34,37,47]. Barrier height can be determined in another way by re-writing Eq. (6) as Eq. (9) below

$$\ln\left(I_s/T^2\right) = \ln AA^* - q/k\phi_{I-V}.1/T \quad (6)$$

The diode showed very high dependence of ideality factor on temperature, which led to the distortion of the plot from linearity. The plots were linearized by multiplying *ln* (I_s/T^2) by n as suggested by Schroder [48]. The experimental values of A^* before and after irradiation were estimated from the intercept of the plot to be 4.1×10^{-8} and 2.8×10^{-12} A cm^{-2} K^{-2}, respectively. The values were extremely small compared to the theoretical value of effective Richardson constant of 146 A cm^{-2} K^{-2} [34,36,37,49,50], which indicate that the active area was smaller than the device area [47], and the effect of barrier inhomogeneity [8]. The mean barrier heights for both were deduced from the slope of the insert plot in Fig. 5 to be 1.41 and 1.30 eV. It has been reported earlier by many researchers that the deviation of the Richardson constants from theoretical value may be as a result of the effect of the barrier inhomogeneity at the MS interface and some other factors such as crystal defects and potential

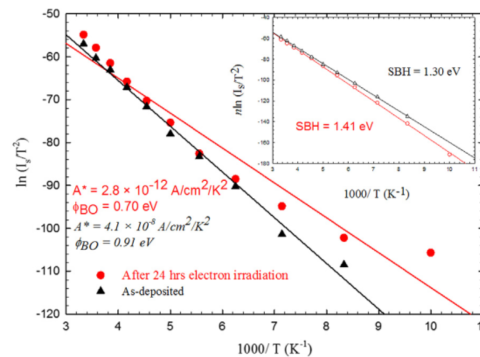

Fig. 5. The Richardson plot, ln(I_s/T^2) versus 1000/*T* for Ni/4H–SiC before and after irradiation in the temperature range 40–300 K. The inset shows the plot of n[ln(I_s/T^2)] versus 1000/*T*.

© University of Pretoria

UNIVERSITEIT VAN PRETORIA
UNIVERSITY OF PRETORIA
YUNIBESITHI YA PRETORIA

fluctuation [8,31,34,47]. Since the deviation cannot be explained by the thermionic emission diffusion model, the Gaussian distribution model of barrier height has been used.

3.4. The modified Richardson plot

The Gaussian distribution model has been used to correct the deviation that cannot be explained with thermionic emission diffusion (TED) which occurred as a result of barrier height inhomogeneities. The abnormal deviation from TE theory has been suggested by some researchers [12,20,33–37,46,47,51] that the distribution barrier heights is a Gaussian distribution $P(\phi_B)$ with mean value of SBH ($\overline{\phi}_B$) and standard deviation as shown in Eq. (7) [10, 13, 32, 52–54].

$$P(\phi_B) = \frac{1}{\sigma_s\sqrt{2\pi}}\exp\left(-\frac{\left(\phi_B-\overline{\phi}_B\right)^2}{2\sigma^2{}_s}\right) \quad (7)$$

where $1/\sigma_s\sqrt{2\pi}$ is the normalisation constant of the Gaussian barrier height distribution. The total current, $I(V)$ across the MS of the SBD containing barrier inhomogeneities that can be expressed in integral form in Eq. (8) [12, 13, 55].

$$I(V) = \int_{-\infty}^{\infty} I(\phi_B, V)P(\phi_B)d\phi_B \quad (8)$$

where $P(\phi_B)$ is the normalised distribution function that gives probability of accuracy of barrier height, and $I(\phi_B, V)$ is the current, at a bias for barrier height based on the ideal TED theory. The expressions for GD of apparent barrier height, ϕ_{ap} at zero bias [10,11,56–59] and apparent ideality factor, n_{ap} [57] are derived from Eq. (4) to be Eqs. (9) and (10) as shown below

$$\phi_{ap} = \overline{\phi}_{BO}(T=0) - \frac{q\sigma^2{}_{so}}{kT} \quad (9)$$

$$\frac{1}{n_{ap}} - 1 = \rho_2 - \frac{q\rho_3}{2kT} \quad (10)$$

where $\overline{\phi}_B(T=0)$ is the mean barrier height at zero bias and was determined from the intercept of Fig. 6 to be 1.64 and 1.63 eV for as-deposited and after HEE irradiation, respectively, and σ_{so} are standard deviation at zero bias (were determined from the slope of Fig. 6 to be 0.113 eV and 0.104 eV) and ρ_2 and ρ_3 are the voltage coefficients which may be temperature dependent [34,36] and they were obtained from the intercept of the insert of Fig. 6 to be -8.9×10^{-2} and -8.0×10^{-3} (for as-deposited), and -6.4×10^{-2} and -5.1×10^{-3} (after HEE irradiation). The results are tabulated in Table 2. It can be assumed from the results obtained that the $\overline{\phi}_B$ and σ_s are linearly bias dependent on the parameters of Gaussian ($\overline{\phi}_B = \overline{\phi}_{BO} + \rho_2 V$ and $\sigma_s = \sigma_{sO} + \rho_3 V$) and quantifying the voltage deformation of Schottky barrier height distribution [10,11,54]. It was observed that the existence of a Gaussian distribution caused a decrease in zero bias barrier height. The extent of deviation was determined by the standard deviation which is generally significant at low temperature.

The deviation between experimental and theoretical values of the Richardson constants was described by a modified Richardson plot. The modified Richardson constant was obtained by combining Eq. (5) with Eq. (6).

$$\ln\left(\frac{I_s}{T^2}\right) - \left(\frac{q^2\sigma^2}{2k^2T^2}\right) = \ln(AA^{**}) - \frac{q\phi_{Bm}}{kT} \quad (11)$$

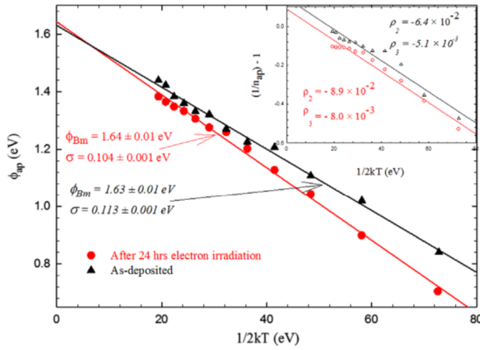

Fig. 6. The zero bias apparent barrier height versus 1/2kT for Ni/4H–SiC before and after irradiation. The insert shows the plot of $(1/n_{ap})-1$ versus 1/2kT.

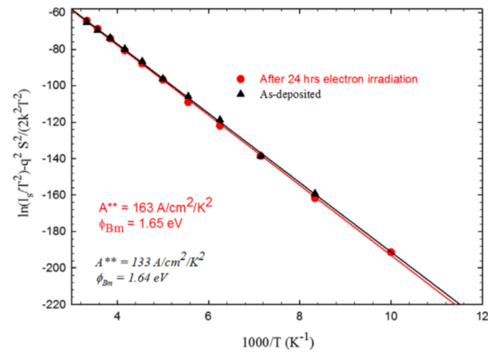

Fig. 7. The modified Richardson plot for Ni/4H-SiC Schottky diode before and after electron irradiation at temperature range 40-300 K.

Table 2
The characteristics of SBDs of 4 H–SiC before and HEE irradiation.

Samples	ρ_2 ($\times10^{-2}$)	ρ_3 ($\times10^{-3}$)	σ_{so} (eV) ±0.001	$\overline{\phi}_{BO}(T=0)$ (eV) ±0.01	$\overline{\phi}_B$(eV) ±0.01	A^* (A cm^{-2} K^{-2})	A^{**} (A cm^{-2} K^{-2})
As-deposited	−6.4	−5.1	0.113	1.63	1.64	4.1×10^{-8}	133
After electron irradiation	−8.9	−8.0	0.104	1.64	1.65	2.8×10^{-12}	163

© University of Pretoria

UNIVERSITEIT VAN PRETORIA
UNIVERSITY OF PRETORIA
YUNIBESITHI YA PRETORIA

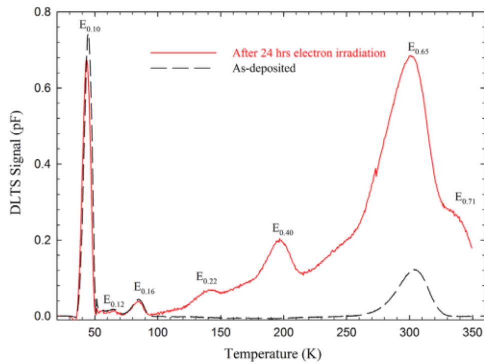

Fig. 8. DLTS spectra for the Ni/4H–SiC before and after electron irradiation. The temperature range 52–350 K scaled up by factor 10.

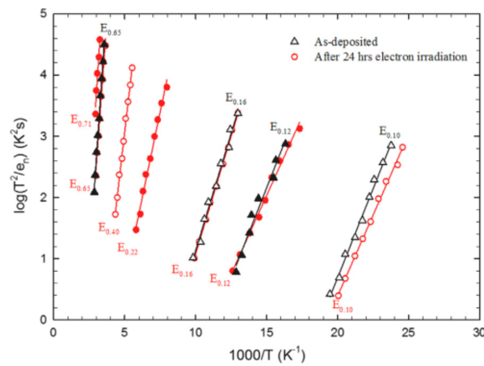

Fig. 9. The Arrhenius plots for the DLTS of as-deposited and after irradiation Ni/4H–SiC.

Fig. 7 shows the plot of $\ln(I_s/T^2) - (q^2\sigma^2/2k^2T^2)$ as function of $1000/T$. The mean $\overline{\phi}_{BO}$ was determined directly from the slope of the plot to be 1.64 ± 0.01 eV and 1.65 ± 0.01 eV for as-deposited and irradiated devices, respectively. The zero mean barrier height obtained was much closer to those obtained from the plot ϕ_{ap} versus 1/2kT in Fig. 6. The modified Richardson constants, A^{**} before and after HEE irradiation was determined from the intercept of the straight line to be 133 and 163 A cm^{-2} K^{-2}, respectively. The values were in good agreement with the theoretical value of 146 A cm^{-2} K^{-2} [49,60], though higher due to spatially inhomogeneous SBHs [20]. The modified Richardson constant obtained was in line with what has been observed during the alpha-particle irradiation [31]. The values of $\overline{\phi}_{BO}$ and A^{**} for as-deposited and irradiated devices showed the extent at which Ni/4H–SiC SBDs could be affected by HEE irradiation at the aforementioned fluence. From these results, we concluded that the HEE irradiation did not influence the mean barrier height, but did influence modified Richardson constant. The same conclusion has been drawn for alpha-particle irradiated 4H–SiC SBDs [31].

3.5. Deep level transient spectroscopy (DLTS)

Fig. 8 shows the DLTS spectra for the samples before and after HEE irradiation. Fig. 9 shows the Arrhenius plots. The measurements were obtained at temperatures range 22–350 K, at a quiescent reverse bias of −5.0 V, filling pulse amplitude of 6.0 V, filling pulse width of 2.0 ms and a rate window of 20 s^{-1}. The sample before irradiation revealed four defects with levels labelled as $E_{0.10}$, $E_{0.12}$, $E_{0.16}$ and $E_{0.65}$ and their corresponding apparent capture cross sections were 3×10^{-11} cm^2, 1×10^{-15} cm^2, 1×10^{-15} cm^2 and 4×10^{-15} cm^2, respectively. The sample after irradiation revealed seven defects with energy levels labelled as $E_{0.10}$, $E_{0.12}$, $E_{0.16}$, $E_{0.22}$, $E_{0.40}$, $E_{0.65}$ and $E_{0.71}$, and their corresponding apparent capture cross sections were 1×10^{-16} cm^2, 4×10^{-12} cm^2, 1×10^{-15} cm^2, 2×10^{-17} cm^2, 3×10^{-15} cm^2 3×10^{-15} cm^2 and 3×10^{-15} cm^2. Some of these defects were confirmed from the literature [61]. Three new defects ($E_{0.22}$, $E_{0.40}$ and $E_{0.71}$) were introduced after the sample was irradiated by HEE. The formation of new defects caused changes in the I–V and C–V characteristics and the parameters of the Schottky barrier diodes.

4. Conclusions

The Ni/4 H–SiC Schottky contacts were successfully fabricated by resistive evaporation. The I–V and C–V measurements at 300 K before and after fluence of 6×10^{14} electrons-cm^{-2} irradiation revealed good Schottky contacts which alone did not provide satisfactory results. From the forward I–V measurements, n, SBH, R_s increased with irradiation but I_s decreased with irradiation measured at 300 K. The reverse currents were significantly constant within the range of our system. C–V measurements revealed a decrease in free carrier concentration. The effects of high energy electron irradiations on Ni/4H–SiC SBD was also investigated using I–V, C–V and DLTS, measured in a wide temperature range 40–300 K. For the temperature range 80–300 K, thermionic emission was the dominant transport mechanism. Generation-recombination proved to be dominant at temperatures below 80 K. The ideality factor and SBH of the devices had strong reciprocal temperature dependence at lower temperature. The modified Richardson constants before and after HEE irradiation were 133 and 163 A cm^{-2} K^{-2}, respectively, by using Gaussian distribution method. The values of A^{**} were in good agreement with the theoretical value. We concluded that HEE irradiation of fluence 6×10^{14} electrons-cm^{-2} did not influence the mean barrier height, but did influence modified Richardson constant. The removal rate of approximately 1.67 cm^{-1} was calculated which corroborate the use of SiC in radiation harsh environments.

Acknowledgements

This work is based on the research supported in part by the National Research Foundation (NRF) of South African (Grant specific unique reference number (UID) 78838). The Grant holder acknowledges that opinions, findings and conclusions or recommendations expressed in this publication

© University of Pretoria

UNIVERSITEIT VAN PRETORIA
UNIVERSITY OF PRETORIA
YUNIBESITHI YA PRETORIA

generated by the NRF supported are that of authors and that NRF accepts no liability whatsoever in this regard.

References

[1] R.L. Van Tuyl, C.A. Liechti, IEEE J. Solid-State Circuits 9 (1974) 269–276.
[2] A. Elasser, M.H. Kheraluwala, M. Ghezzo, R.L. Steigerwald, N.A. Evers, J. Kretchmer, T.P. Chow, IEEE Trans. Ind. Appl. 39 (2003) 915–921.
[3] S. Takayuki, U. Tsuneo, S. Seizo, M. Yoshihiko, Jpn J.Appl. Physics 19 (1980) 459.
[4] A.F. Özdemir, A. Turut, A. Kökçe, Semicond. Sci. Technol. 21 (2006) 298.
[5] E. Rhoderick, R. Williams, Oxford Science, Oxford, 1988.
[6] V. Janardhanam, A. Ashok Kumar, V. Rajagopal Reddy, P. Narasimha Reddy, J. Alloy. Compd. 485 (2009) 467–472.
[7] S. Zeyrek, M.M. Bulbul, S. Altindal, M.C. Baykul, H. Yuzer, Braz. J. Phys. 38 (2008) 591–597.
[8] İ. Dökme, Ş. Altindal, M.M. Bülbül, Appl. Surf. Sci. 252 (2006) 7749–7754.
[9] Ş. Karataş, Ş. Altindal, M. Çakar, Phys. B: Condens. Matter 357 (2005) 386–397.
[10] S. Zhu, R.L. Van Meirhaeghe, C. Detavernier, F. Cardon, G.P. Ru, X.P. Qu, B.Z. Li, Solid-State Electron. 44 (2000) 663–671.
[11] A. Gümüş, A. Türüt, N. Yalçin, J. Appl. Phys. 91 (2002) 245–250.
[12] J.H. Werner, H.H. Güttler, J. Appl. Phys. 69 (1991) 1522–1533.
[13] C. Subhash, Semicond. Sci. Technol. 19 (2004) 82.
[14] Y.P. Song, R.L. Van Meirhaeghe, W.H. Laflère, F. Cardon, Solid State Electron. 29 (1986) 633–638.
[15] P.G. McCafferty, A. Sellai, P. Dawson, H. Elabd, Solid-State Electron. 39 (1996) 583–592.
[16] L.M. Tolbert, B. Ozpineci, S.K. Islam, M.S. Chinthavali, Power and Energy Syst. Proc. 1 (2003) 317–321.
[17] V. Kazukauskas, J.-V. Vaitkus, Opto-Electron. Rev. 12 (2004) 377–382.
[18] J. Grant, W. Cunningham, A. Blue, V. O'Shea, J. Vaitkus, E. Gaubas, M. Rahman, Nucl. Instrum. Methods Phys. Res. A: Accel. Spectrom. Detect. Assoc. Equip. 546 (2005) 213–217.
[19] M.C. Driver, R.H. Hopkins, C.D. Brandt, D.L. Barrett, A.A. Burk, R.C. Clarke, G.W. Eldridge, H.M. Hobgood, J.P. McHugh, P.G. McMullin, R.R. Siergiej, S. Sriram, Gallium Arsenide Integrated Circuit (GaAs IC), in: Proceedings of the 15th Annual Symposium on Technical Digest, 1993, pp. 19–21.
[20] V. Kumar, A.S. Maan, J. Akhtar, J. Vac. Sci. amp; Technol. B 32 (2014) 041203.
[21] A. Akbay, H. Korkut, K. Ejderha, T. Korkut, A. Türüt, J. Radioanal. Nucl. Chem. 289 (2011) 145–148.
[22] K. Çınar, C. Coşkun, Ş. Aydoğan, H. Asıl, E. Gür, Nucl. Instrum. Methods Phys. Res. B: Beam Interact. Mater. Atoms 268 (2010) 616–621.
[23] K. Çınar, C. Coşkun, E. Gür, Ş. Aydoğan, Nucl. Instrum. Methods Phys. Res. B: Beam Interact. Mater. Atoms 267 (2009) 87–90.
[24] J. Benkovska, L. Stuchlikova, D. Buc, L. Čaplovic, Phys. Status Solidi (a) 209 (2012) 1384–1389.
[25] T. Marinova, A. Kakanakova-Georgieva, V. Krastev, R. Kakanakov, M. Neshev, L. Kassamakova, O. Noblanc, C. Arnodo, S. Cassette, C. Brylinski, B. Pecz, G. Radnoczi, G. Vincze, Mater. Sci. Eng.: B 46 (1997) 223–226.
[26] F.D. Auret, S.A. Goodman, G. Myburg, W.O. Barnard, D.T.L. Jones, J. Appl. Phys. 74 (1993) 4339–4342.
[27] S. Ashok, J.M. Borrego, R.J. Gutmann, J. Appl. Phys. 51 (1980) 1076–1084.
[28] F. Roccaforte, S. Libertino, F. Giannazzo, C. Bongiorno, F. La Via, V. Raineri, J. Appl. Phys. 97 (2005).
[29] C. Raynaud, K. Isoird, M. Lazar, C.M. Johnson, N. Wright, J. Appl. Phys. 91 (2002) 9841–9847.
[30] F. Auret, S. Goodman, M. Hayes, M. Legodi, H. Van Laarhoven, D.C. Look, Appl. Phys. Lett. 79 (2001) 3074–3076.
[31] E. Omotoso, W.E. Meyer, F.D. Auret, A.P. Paradzah, M. Diale, S.M.M. Coelho, P.J. Janse Van Rensberg, Nucl. Instr. Meth. Phys. Res. B, submitted for publication, 2015.
[32] S.M. Sze, K.K. Ng, Physics of Semiconductor Devices, John Wiley & Sons, New York, 2006.
[33] M.E. Aydın, N. Yıldırım, A. Türüt, J. Appl. Phys. 102 (2007) 043701.
[34] Z. Ouennoughi, S. Toumi, R. Weiss, Phys. B: Condens. Matter 456 (2015) 176–181.
[35] M. Gülnahar, Superlattices Microstruct. 76 (2014) 394–412.
[36] S. Alialy, Ş. Altındal, E.E. Tanrıkulu, D.E. Yıldız, J. Appl. Phys. 116 (2014) 083709.
[37] S. Shankar Naik, V. Rajagopal Reddy, Superlattices Microstruct. 48 (2010) 330–342.
[38] Z. Lin, Z. Yi-Men, Z. Yu-Ming, H. Chao, M. Yong-Ji, Chin. Phys. B 18 (2009) 1931.
[39] E. Hökelek, G.Y. Robinson, Appl. Phys. Lett. 40 (1982) 426–428.
[40] C.R. Crowell, V.L. Rideout, Solid-State Electron. 12 (1969) 89–105.
[41] M. Soylu, B. Abay, Microelectron. Eng. 86 (2009) 88–95.
[42] M. Soylu, F. Yakuphanoglu, J. Alloy. Compd. 506 (2010) 418–422.
[43] C. Coskun, N. Gedik, E. Balcı, Semicond. Sci. Technol. 21 (2006) 1656.
[44] C.R. Crowell, Solid-State Electron. 20 (1977) 171–175.
[45] R.R. Ciechonski, Device Characteristics of Sublimation Grown 44H–SiCLayers, Linkping Univ., Linkping, 2005.
[46] L. Huang, F. Qin, S. Li, D. Wang, Appl. Phys. Lett. 103 (2013) 033520.
[47] S. Toumi, A. Ferhat-Hamida, L. Boussouar, A. Sellai, Z. Ouennoughi, H. Ryssel, Microelectron. Eng. 86 (2009) 303–309.
[48] D.K. Schroder, A John Willey & Sons, inc., 3rd ed. 2006.
[49] A. Itoh, T. Kimoto, H. Matsunami, Electron Device Lett. IEEE 16 (1995) 280–282.
[50] F. Roccaforte, F. La Via, A. Baeri, V. Raineri, L. Calcagno, F. Mangano, J. Appl. Phys. 96 (2004) 4313–4318.
[51] J.H. Werner, H.H. Güttler, J. Appl. Phys. 73 (1993) 1315–1319.
[52] M.K. Hudait, P. Venkateswarlu, S.B. Krupanidhi, Solid-State Electron. 45 (2001) 133–141.
[53] S. Zhu, R.L. Van Meirhaeghe, C. Detavernier, G.P. Ru, B.Z. Li, F. Cardon, Solid State Commun. 112 (1999) 611–615.
[54] S. Zeyrek, Ş. Altındal, H. Yüzer, M.M. Bülbül, Appl. Surf. Sci. 252 (2006) 2999–3010.
[55] P.M. Gammon, A. Pérez-Tomás, V.A. Shah, O. Vavasour, E. Donchev, J.S. Pang, M. Myronov, C.A. Fisher, M.R. Jennings, D.R. Leadley, P.A. Mawby, J. Appl. Phys. 114 (2013) 223704.
[56] Y.P. Song, R.L. Van Meirhaeghe, W.H. Laflère, F. Cardon, Solid-State Electron. 29 (1986) 633–638.
[57] S. Chand, S. Bala, Appl. Surf. Sci. 252 (2005) 358–363.
[58] E. Özavcı, S. Demirezen, U. Aydemir, Ş. Altındal, Sens. Actuat. A: Phys. 194 (2013) 259–268.
[59] H. Tecimer, S. Aksu, H. Uslu, Y. Atasoy, E. Bacaksız, Ş. Altındal, Sens. Actuat. A: Phys. 185 (2012) 73–81.
[60] F. Roccaforte, C. Bongiorno, F. La Via, V. Raineri, Appl. Phys. Lett. 85 (2004) 6152.
[61] V.V. Kozlovskiĭ, V.V. Emtsev, K.V. Emtsev, N.B. Strokan, A.M. Ivanov, V.N. Lomasov, G.A. Oganesyan, A.A. Lebedev, Semiconductors 42 (2008) 242–247.

© University of Pretoria

PAPER III: Response of Ni/4H-SiC Schottky barrier diodes to alpha-particle irradiation at different fluences

E. Omotoso, W. E. Meyer, F. D. Auret, M. Diale, and P. N. M. Ngoepe

Physica B: Condensed Matter 480 (2015): 196-200
doi:10.1016/j.physb.2015.08.014

© University of Pretoria

UNIVERSITEIT VAN PRETORIA
UNIVERSITY OF PRETORIA
YUNIBESITHI YA PRETORIA

Physica B 480 (2016) 196–200

Contents lists available at ScienceDirect

Physica B

journal homepage: www.elsevier.com/locate/physb

Response of Ni/4H-SiC Schottky barrier diodes to alpha-particle irradiation at different fluences

E. Omotoso [a,b,*], W.E. Meyer [a], F.D. Auret [a], M. Diale [a], P.N.M. Ngoepe [a]

[a] Department of Physics, University of Pretoria, Private Bag X20, Hatfield 0028, South Africa
[b] Departments of Physics, Obafemi Awolowo University, Ile-Ife 220005, Nigeria

A R T I C L E   I N F O

Article history:
Received 15 May 2015
Received in revised form
4 August 2015
Accepted 7 August 2015
Available online 8 August 2015

Keywords:
DLTS
Free carrier removal rate
Carrier concentration
4H-SiC
Alpha-particle irradiation

A B S T R A C T

Irradiation experiments have been carried out on 1.9×10^{16} cm^{-3} nitrogen-doped 4H-SiC at room temperature using 5.4 MeV alpha-particle irradiation over a fluence ranges from 2.6×10^{10} to 9.2×10^{11} cm^{-2}. Current–voltage (*I–V*), capacitance–voltage (*C–V*) and deep level transient spectroscopy (DLTS) measurements have been carried out to study the change in characteristics of the devices and free carrier removal rate due to alpha-particle irradiation, respectively. As radiation fluence increases, the ideality factors increased from 1.20 to 1.85 but the Schottky barrier height (SBH_{I-V}) decreased from 1.47 to 1.34 eV. Free carrier concentration, N_d decreased with increasing fluence from 1.7×10^{16} to 1.1×10^{16} cm^{-2} at approximately 0.70 µm depth. The reduction in N_d shows that defects were induced during the irradiation and have effect on compensating the free carrier. The free carrier removal rate was estimated to be 6480 ± 70 cm^{-1}. Alpha-particle irradiation introduced two electron traps ($E_{0.39}$ and $E_{0.62}$), with activation energies of 0.39 ± 0.03 eV and 0.62 ± 0.08 eV, respectively. The $E_{0.39}$ as attribute related to silicon or carbon vacancy, while the $E_{0.62}$ has the attribute of Z_1/Z_2.

© 2015 Elsevier B.V. All rights reserved.

1. Introduction

Metal-semiconductor (M-S) Schottky barrier diodes (SBDs) are widely used where diodes with low forward voltage drop, low capacitance and high switching speed are required [1]. This makes them ideal as rectifiers in photovoltaic systems and high-efficiency power supplies [2]. SBDs also have important uses in optoelectronics, high frequency and bipolar integrated circuits applications [3,4]. The reliability of SBDs is influenced significantly by the quality of the M-S junction [5]. The performance of the devices can be quantified experimentally in terms of their ideality factor, Schottky barrier height (SBH), saturation current, series resistance and free carrier concentration. Among these properties of the M-S interface, SBH plays a major role in the successful operation of many devices in transporting electrons across the M-S junction [6].

Silicon carbide (SiC) is a promising semiconductor with a wide bandgap of 3.26 eV [7], which has drawn the interest of many researchers due to its excellent properties such as high thermal conductivity, high breakdown field and high saturated drift velocity [8]. These characteristics make SiC a very good semiconductor capable of outperforming silicon in electronic devices for high-power, high-frequency and high-temperature applications [9], and is a key material for the next-generation photonics [10]. SiC is also good candidate for electronic devices used in harsh radiation environments such as in space, accelerator facilities and nuclear power plants [11–13].

In this study, we report the behavior of 4H-SiC SBD prior to and after alpha-particle irradiation at different fluences. In order to use SiC in radiation hard devices, there is need to know the radiation response of SiC. Also, the fluence SiC can withstand before the characteristics of devices fabricated on it degrade and they start to malfunction, needs to be determined. Current–voltage (*I–V*), capacitance–voltage (*C–V*) and deep level transient spectroscopy (DLTS) have been carried out on SBDs to study the change in characteristics of the devices at different fluences.

2. Experimental procedure

The samples used for this work were cut from a nitrogen-doped *n*-type 4H-SiC wafer, double polished with the Si face epi layer. The substrate was doped by 1×10^{18} cm^{-3}, while the epi layer had a resistivity of 0.02 Ω-cm and a doping density of 1.9×10^{16} cm^{-3}. The wafers were supplied by CREE Res. Inc.

The samples were cut into smaller pieces (area of 8 mm^2) and degreased by boiling for 5 min each in trichloroethylene, acetone, methanol and followed by 1 min rinse in de-ionized water. They

* Corresponding author at: Department of Physics, University of Pretoria, Private Bag X20, Hatfield 0028, South Africa.
E-mail address: ezekiel.omotoso@up.ac.za (E. Omotoso).

http://dx.doi.org/10.1016/j.physb.2015.08.014
0921-4526/© 2015 Elsevier B.V. All rights reserved.

© University of Pretoria

UNIVERSITEIT VAN PRETORIA
UNIVERSITY OF PRETORIA
YUNIBESITHI YA PRETORIA

were etched in 40% hydrogen fluoride for 30 seconds in order to remove the native oxide layer on the samples, then rinsed in de-ionized water, followed by blowing dry with nitrogen gas prior to thermally evaporation of nickel ohmic contacts onto the back surfaces (1.0×10^{18} cm^{-3} doped side) of the samples.

Nickel was used for both ohmic and Schottky contacts. Resistive evaporation was employed in both cases as it does not introduce measurable defects. The ohmic contact with a thickness of 2500 Å was deposited at a rate of 0.9 Å s^{-1}. The samples were annealed in a tube furnace under flowing argon gas at 950 °C for 10 min to form nickel silicides [14] in order to minimize contact resistance. The samples were also cleaned in ultrasonic water bath for 3 min each in trichloroethylene, acetone and methanol followed by 1 min rinsed in de-ionized H_2O after the annealing of the ohmic contact. Nickel Schottky contacts were resistively evaporated through a metal contact mask and had an area of 2.4×10^{-3} cm^2. The contacts of thickness 1000 Å were deposited at a rate of 0.5 Å s^{-1} under a vacuum of 3.0×10^{-5} mbar.

Samples were irradiated at room temperature and a fluence rate of 7.1×10^6 cm^{-2} s^{-1} with alpha-particles of energy of 5.4 MeV from a 241-Am radionuclide source. The radioactive foils were placed on top of the SBDs in such a way that the emitted alpha-particles were directed on diodes. The alpha-particle fluence ranged from 2.6×10^{10} to 9.2×10^{11} cm^{-2} (i.e from 1 to 36 h). The same SBD was used throughout the study and the radiation fluence quoted is the cumulative fluence over all radiations. A second SBD was irradiated and measured separately to check for repeatability.

Before in between irradiations, the samples were characterised at room temperature with *I-V* and *C-V* measurements, performed by an HP 4140 B pA meter/DC voltage source and an HP 4192A LF Impedance Analyzer, respectively. Hereafter, the sample was placed in a closed cycle helium cryostat and characterised by conventional DLTS.

3. Results and discussion

3.1. *I–V* and *C–V* characteristics

The devices were tested from *I–V* and *C–V* measurement systems to determine the quality of diodes before in between irradiations. Fig. 1 shows the forward semi-logarithmic *I–V* characteristics of the SBD measured at 300 K for un-irradiated to the radiation fluence of 7.9×10^{11} cm^{-2}. For biases below

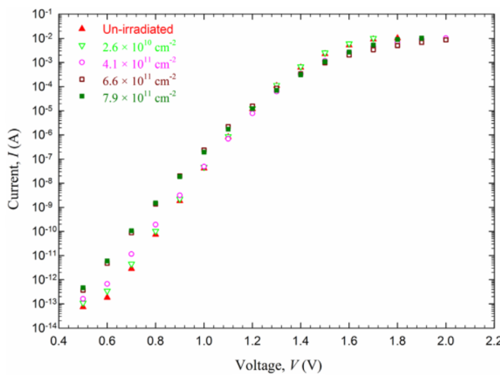

Fig. 1. Forward *I–V* characteristics of 4H-SiC SBD before and after 5.4 MeV alpha-particle irradiation up to fluence 7.9×10^{11} cm^{-2} measured at 300 K.

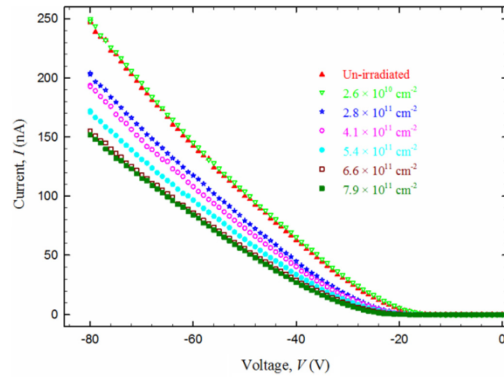

Fig. 2. Semi-logarithmic curves of the reverse leakage current measured up to −80 V as a function reverse voltage measured at fluence ranges from 2.6×10^{10} cm^{-2} to 7.9×10^{11} cm^{-2}.

approximately 1 V, where thermionic emission dominates, a slight increase in forward current was observed as a result of increase in radiation fluence. The ideality factor was 1.20 for the as-deposited sample and increased to 1.85 after 9.2×10^{11} cm^{-2} bombardment. This confirms that the current transport mechanism at low fluence was dominated by thermionic emission. The increase in ideality factor at higher fluences indicates that, in addition to thermionic emission, other transport mechanisms might also contribute. Barrier height inhomogeneiety might also play a role. The Schottky barrier height ($\Phi_{b,\ I-V}$) decreased with increasing irradiation fluence (1.47–1.34) eV and saturation current also increased with fluence from 2.3×10^{-21} to 5.2×10^{-19} A. The fluence dependency of the n, $\Phi_{b,\ I-V}$ and I_s may also connected with the movement (shift) of Fermi level pinning at the surface of SiC, since irradiation-induced defects can creates interface states. The electrical parameters were determined as reported earlier by Omotoso et al. [15,16]. From these characteristics, it shows that 4H-SiC with doping density 1.9×10^{16} cm^{-3} is radiation hard compare to Si [17].

In Fig. 2, the leakage current is less than 1.8×10^{-10} A at reverse voltage (V_r) below 15.0 V for all the *I–V* measurements, starting from as deposited to the fluence of 7.9×10^{11} alpha-particles-cm^{-2}. From Table 1, as the reverse bias increased, an increase in leakage current was observed before and after irradiation. But, contrary to the case in other semiconductors, the leakage current decreased with increase in radiation fluence. This occurs despite a decrease observed in the forward barrier height. A possible explanation would be that the decrease in leakage current is related to the decrease in free carrier density caused by the introduction of compensating defects. This would, in turn, decrease the electric field in the depletion region. Three possible reverse conduction mechanisms were considered: Thermionic emission (with image force barrier lowering), thermionic-field emission

Table 1
Comparison of leakage current and reverse voltage in a Ni/4H-SiC SBD before and after irradiation with alpha-particles.

Reverse voltage (V)	Leakage current (nA)	
	Un-irradiated	At fluence of 7.9×10^{11} cm^{-2}
40	64	27
60	143	85
80	247	153

© University of Pretoria

UNIVERSITEIT VAN PRETORIA
UNIVERSITY OF PRETORIA
YUNIBESITHI YA PRETORIA

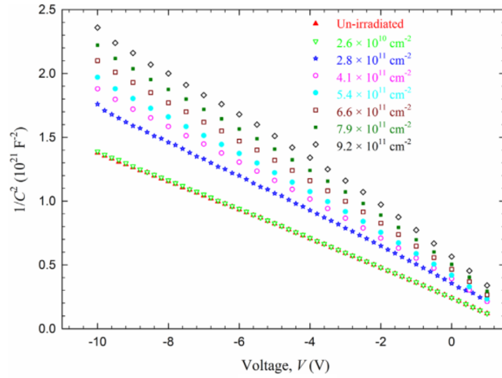

Fig. 3. 1/C2 as a function of voltage characteristics of 4H-SiC SBDs before and after 5.4 MeV alpha-particle irradiation at fluence ranges 2.6×10^{10} cm^{-2} to 9.2×10^{11} cm^{-2}.

(tunneling) and impact ionization. All three mechanisms predict that a reduction in the electric field in the barrier would reduce the reverse current.

The C^{-2} as a function of reverse bias voltage, V before and after step-wise irradiation of the samples at fluences ranges from 2.6×10^{10} to 9.2×10^{11} cm^{-2}, measured at 1 MHz are depicted in Fig. 3. From the C–V measurements, the free carrier concentrations, N_d, and the Schottky barrier heights, $\Phi_{b,\ C\text{-}V}$, were calculated from

$$N_d = \frac{2}{q\varepsilon_s A^2}\frac{d(1/C^2)}{dV} \quad (1)$$

$$\Phi_{b,\ C\text{-}V} = V_{bi} + \frac{kT}{q} + \xi \quad (2)$$

and $x = \varepsilon_s A/C$ is the depletion width of the space charge region, C is the capacitance, V_{bi} is the built-in voltage, k is the Boltzmann constant, T is the temperature, q is the electron charge, ε_s is the permittivity of semiconductor, A is the area of the diode and ξ is the difference between conduction band and the Fermi level.

The capacitance of the sample decreased with increase in radiation fluence. At a reverse bias of −5 V, the capacitance obtained before and after irradiation at fluence 9.2×10^{10} cm^{-2} was 34.9 and 25.6 pF, respectively. The decrease in capacitance of the diodes with irradiation is probably as a result of the semiconductor depletion width increasing due to the introduction of defects with acceptor states in the band gap, reducing the free carrier concentration of the SBD after irradiation. The change in capacitance may also attributed to change in dielectric constant at the interface, however this effect should be negligible as the interfacial layer is very thin. Furthermore, the reduction in free carrier concentration was also observed in the slope of the C^{-2} versus V plot. As shown in Table 2, the SBH for I–V and C–V did not agree. This could be due to the different approach of the measurement techniques. C–V measurement is not a transport technique. This may also be as a result of inhomogeneous Schottky barrier diodes.

From Fig. 3, the free carrier concentrations, $N_d - N_a$ were determined from the slope of the plots C^{-2} versus V. The free carrier concentration of the sample decreases with increase in radiation fluence. The $N_d - N_a$ for the diodes before irradiation and after bombardment with fluence 9.2×10^{10} cm^{-2} were 1.6×10^{16} and 1.1×10^{16} cm^{-3}, respectively. An indication that defects were introduced during the irradiation caused the reduction in the free carrier concentration. It is proposed that these defects are vacancy related. These also have the effect of compensating the free carriers. The change in free carrier concentration of active defect at a depletion width of approximately 0.70 μm from the interface, as function of radiation fluence, is shown in Fig. 4. The free carrier removal rate, η can be obtained from Eq. (3) below:

Table 2
Summary of important parameters before and after bombardment of Ni/4H-SiC SBDs with fluence 9.2×10^{11} cm^{-2} from a 241-Am radionuclide source, calculated from I–V and C–V characteristics. C–V characteristics were determined at depletion width of 0.7 μm.

Sample	n	$\phi_{b,\ I\text{-}V}$ (eV)	$\phi_{b,\ C\text{-}V}$ (eV)	I_s (A)	N_d (cm^{-3})	C (pF) at −5 V
Un-irradiated	1.20	1.47	2.44	2.3×10^{-21}	1.6×10^{16}	34.9
9.2×10^{11} cm^{-2}	1.85	1.34	3.66	5.2×10^{-19}	1.1×10^{16}	25.6

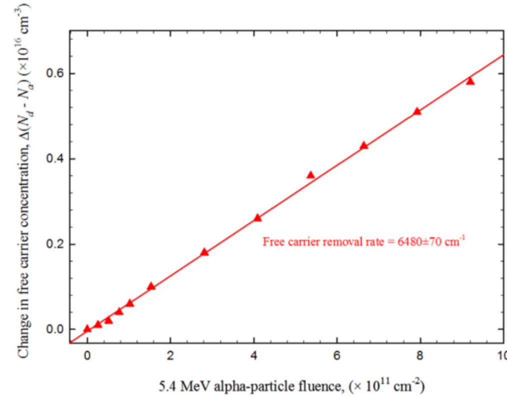

Fig. 4. The change in free carrier concentration of a 4H-SiC SBD after 5.4 MeV alpha-particle irradiation as a function of fluence. The free carrier concentration values were obtained at depth 0.7 μm below the metal-semiconductor interface.

$$\eta = \frac{\Delta(N_d - N_a)}{\varphi} \quad (3)$$

where $\Delta(N_d - N_a)$ is the change in free carrier concentration, φ is the fluence at which the sample was bombarded [18]. The graph of $\Delta(N_d - N_a)$ against the corresponding fluence received by the sample was plotted. The free carrier removal rate was determined to be 6480 ± 70 cm^{-1} from the slope of the plot. This value is two orders of magnitude less than the value for Si reported by Kozlovski et al. who determined a free carrier removal rate of 4×10^{5} cm^{-1} in Si with an initial free carrier concentration of 1×10^{15} cm^{-3} irradiated by 1.7 MeV alpha-particle at a fluence of 2×10^{9} cm^{-2} [19].

From the results of both I–V and C–V characteristics at different fluences, it is apparent that the diodes were of a reasonable electrical quality and were suitable for the analysis of DLTS.

3.2. Deep level transient spectroscopy analysis

Fig. 5 shows the normalized DLTS spectra of the devices before and after step-wise bombardment with 5.4 MeV from a 241-Am radionuclide source with fluence ranges from 2.56×10^{10} to 9.20×10^{11} cm^{-2} at rate window of 200 s^{-1}. The measurements were obtained over the temperature range 22–350 K, at a quiescent reverse bias of −5.0 V, filling pulse of amplitude 6.0 V and width 2.0 ms and at different rate windows (2.5 to 1000 s^{-1}).

© University of Pretoria

UNIVERSITEIT VAN PRETORIA
UNIVERSITY OF PRETORIA
YUNIBESITHI YA PRETORIA

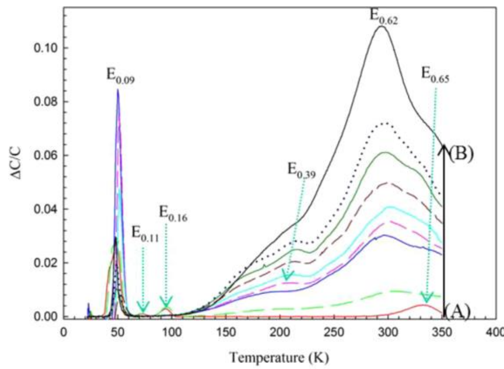

Fig. 5. Normalized DLTS spectra of 4H-SiC before and after irradiation at radiation fluence ranges from 2.6×10^{10} cm^{-2} to 9.2×10^{11} cm^{-2} at rate window of 200 s^{-1}. Line A to B represents from un-irradiated to 2.6×10^{10}, 2.8×10^{11}, 4.1×10^{11}, 5.4×10^{11}, 6.6×10^{11}, 7.9×10^{11}, 9.2×10^{11} cm^{-2} to 1 week after 9.2×10^{11} cm^{-2}, spectra.

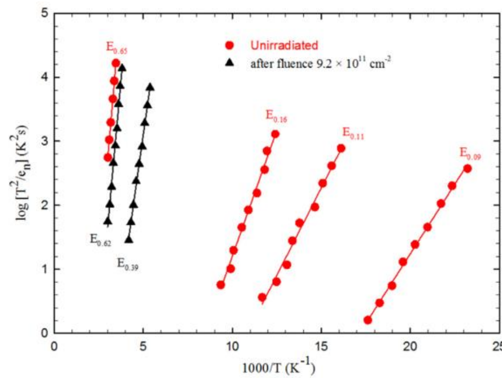

Fig. 6. Arrhenius plots for defects n-type 4H-SiC observed before and after irradiation with 5.4 MeV alpha-particles irradiation at fluence 9.2×10^{11} cm^{-2}.

Fig. 6 shows the Arrhenius plot of the defects observed before and after the step-wise bombardment. The *signatures* of the defects in terms of activation energy E_n and apparent capture cross section, σ_n were determined from Fig. 6. The activation energy of each defect was determined from the slope, and the corresponding apparent capture cross section was calculated from the intercept of the Arrhenius plot of log (T^2/e_n) versus $1/T$ as earlier reported by Auret et al. [20]. Four deep levels labeled $E_{0.09}$, $E_{0.11}$, $E_{0.16}$ and $E_{0.65}$ (where 'E' refers to an electron trap and the subscript 0.09 refers to an energy level below the conduction band), were present before irradiation as previously observed by Omotoso et al. [16]. After the sample was bombarded, it was observed that two defects were introduced by irradiation. One of the defects had a broad peak, probably due to the presence of several states or defects with closely spaced emission rates as observed earlier [21]. The irradiation induced defects were labeled as $E_{0.39}$ and $E_{0.62}$. The electronic properties of the deep levels labeled $E_{0.09}$, $E_{0.11}$, $E_{0.16}$, $E_{0.62}$ and $E_{0.65}$ have been presented by Omotoso et al. [16]. The activation energy and apparent capture cross section of $E_{0.39}$ after fluence 9.2×10^{11} cm^{-2} are 0.39 ± 0.03 and 1.7×10^{-15} cm^2, respectively. As the two emanated defects becoming conspicuous, the intensity of $E_{0.09}$, $E_{0.11}$ and $E_{0.16}$ reduced. The defects, $E_{0.11}$ and $E_{0.16}$ disappeared after irradiation to a fluence of 4.1×10^{11} cm^{-2}. After receiving irradiation to a fluence of 9.2×10^{11} cm^{-2}, the $E_{0.09}$ reduced to 12% of its intensity before irradiation.

Table 3
Electronic properties of defects detected by DLTS in Ni/4H-SiC SBD before and after bombarded with fluence of 9.2×10^{11} alpha-particles-cm^{-2}.

Defect	E_T (eV)	σ_a (cm^2)	T_{peak} (K)	Attribution
$E_{0.09}$	E_c–0.09	8×10^{-15}	51	N impurity [29]
$E_{0.11}$	E_c–0.11	2×10^{-16}	74	Ti impurity [30]
$E_{0.16}$	E_c–0.16	1×10^{-15}	94	Ti impurity [26]
$E_{0.39}$	E_c–0.39	2×10^{-15}	217	V_{Si} [22]
$E_{0.62}$	E_c–0.62	1×10^{-13}	301	Z_1/Z_2 [29, 31]
$E_{0.65}$	E_c–0.65	4×10^{-15}	332	Z_1/Z_2 (C/Si vacancy [26,27])

NOTE: The T_{peak}(K) was taken at rate window of 200 s^{-1}.

Table 3 shows the attributes of each defect. A defect similar to $E_{0.39}$ showing acceptor-like behavior, was reported earlier after electron irradiation by Doyle et al. [22]. From Fig. 4, the decrease in the free carrier concentration indicates an increase in compensation with radiation fluence which suggests the acceptor-like behavior of deep levels introduced into the device. A similar defect level has been attributed to the silicon vacancy [23], carbon vacancy, split interstitial or antisites after low energy electron irradiation [24]. It was observed that defect $E_{0.39}$ disappeared after leaving the sample at room temperature for a week, showing that the defect was not stable at room temperature. The deep level defects $E_{0.62}$ and $E_{0.65}$ have been previously reported to be defects composed of several energy levels commonly referred to as the Z_1/Z_2 [16,25–28].

4. Conclusions

In summary, the effect of alpha-particle irradiation at different fluences resulted in a decrease in leakage current from 64 nA (for un-irradiated) to 27 nA (fluence of 9.2×10^{11} cm^{-2}) at reverse voltage of 40 V. The decrease was attributed to a reduction in the electric field in the depletion region due to a reduction in the space charge density because of compensating acceptors introduced during irradiation. A reduced electric field would explain lower reverse current for a number of current transport mechanisms including thermionic emission with image force barrier lowering, thermionic-field emission (tunneling) and impact ionization. For forward conduction, thermionic emission was dominant at lower fluence, while deviations were observed after irradiation at higher fluence.

The capacitance of diodes decreased with increase in radiation fluence as a result of increase in the depletion width due to reduction in free carrier concentration of the SBD after irradiation.

Our DLTS results revealed the presence of four electron deep levels before irradiation with energy levels labeled $E_{0.09}$, $E_{0.11}$, $E_{0.16}$ and $E_{0.65}$. Alpha-particle irradiation at fluence ranges from 2.56×10^{10} to 9.2×10^{11} cm^{-2} induced two broad electron defects with energies E_c–0.39 and E_c–0.62, respectively. The presence of broad peak indicates presence of several states or defects with close activation energies. The defect $E_{0.39}$ showed an acceptor-like behavior and can be attributed to be a silicon or carbon vacancy. It was observed that defect $E_{0.39}$ disappeared after leaving the sample at room temperature for a week. The deep level defects $E_{0.62}$ and $E_{0.65}$ are widely agreed to be intrinsic in nature and commonly referred to as the Z_1/Z_2 defect.

© University of Pretoria

UNIVERSITEIT VAN PRETORIA
UNIVERSITY OF PRETORIA
YUNIBESITHI YA PRETORIA

Acknowledgment

This work is based on the research supported in part by the National Research Foundation (NRF) of South African (Grant specific unique reference number (UID) 78838). The Grant holder acknowledges that opinions, findings and conclusions or recommendations expressed in this publication generated by the NRF supported are that of authors and that NRF accepts no liability whatsoever in this regard.

References

[1] R.L. Van Tuyl, C.A. Liechti, IEEE J. Solid-State Circuits 9 (1974) 269–276.
[2] A. Elasser, M.H. Kheraluwala, M. Ghezzo, R.L. Steigerwald, N.A. Evers, J. Kretchmer, T.P. Chow, IEEE Trans. Ind. Appl. 39 (2003) 915–921.
[3] S. Takayuki, U. Tsuneo, S. Seizo, M. Yoshihiko, Jpn. J. Appl. Phys. 19 (1980) 459.
[4] A.F. Özdemir, A. Turut, A. Kökçe, Semicond. Sci. Technol. 21 (2006) 298.
[5] E. Rhoderick, R. Williams, Oxford Science, Oxford, 1988.
[6] V. Janardhanam, A. Ashok Kumar, V. Rajagopal Reddy, P. Narasimha Reddy, J. Alloy. Compd. 485 (2009) 467–472.
[7] L.M. Tolbert, B. Ozpineci, S.K. Islam, M.S. Chinthavali, Proc. Power Energy Syst. 1 (2003) 317–321.
[8] M. Siad, M. Abdesslam, A.C. Chami, Appl. Surf. Sci. 258 (2012) 6819–6822.
[9] R. Madar, Nature 430 (2004) 974–975.
[10] S. Yamada, B.-S. Song, T. Asano, S. Noda, Appl. Phys. Lett. 99 (2011) 2011021–2011023.
[11] T. Nishijima, T. Ohshima, K.K. Lee, Nucl. Instrum. Methods Phys. Res. Sect. B: Beam Interact. Mater. Atoms 190 (2002) 329–334.
[12] F. Nava, E. Vittone, P. Vanni, G. Verzellesi, P.G. Fuochi, C. Lanzieri, M. Glaser, Nucl. Instrum. Methods Phys. Res. Sect. A: Accel. Spectrometers Detect. Assoc. Equip. 505 (2003) 645–655.
[13] L. Kin Kiong, T. Ohshima, H. Itoh, IEEE Trans. Nucl. Sci. 50 (2003) 194–200.
[14] T. Marinova, A. Kakanakova-Georgieva, V. Krastev, R. Kakanakov, M. Neshev, L. Kassamakova, O. Noblanc, C. Arnodo, S. Cassette, C. Brylinski, B. Pecz, G. Radnoczi, G. Vincze, Mater. Sci. Eng. B 46 (1997) 223–226.
[15] E. Omotoso, W.E. Meyer, F.D. Auret, A.T. Paradzah, M. Diale, S.M.M. Coelho, P. J. Janse van Rensburg, Mater. Sci. Semicond. Process. 39 (2015) 112–118.
[16] E. Omotoso, W.E. Meyer, F.D. Auret, A.T. Paradzah, M. Diale, S.M.M. Coelho, P. J. Janse van Rensburg, P.N.M. Ngoepe, Nucl. Instrum. Methods Phys. Res. Sect. B: Beam Interact. Mater. Atoms (2015) 5.
[17] A.A. Lebedev, V.V. Kozlovski, Semiconductors 48 (2014) 1293–1295.
[18] F. Auret, S. Goodman, M. Hayes, M. Legodi, H. Van Laarhoven, D.C. Look, Appl. Phys. Lett. 79 (2001) 3074–3076.
[19] V. Kozlovski, V. Abrosimova, Int. J. High Speed Electron. Syst. 15 (2005) 1–253.
[20] F.D. Auret, P.N.K. Deenapanray, Crit. Rev. Solid State Mater. Sci. 29 (2004) 1–44.
[21] Ž. Pastuović, I. Capan, D.D. Cohen, J. Forneris, N. Iwamoto, T. Ohshima, R. Siegele, N. Hoshino, H. Tsuchida, Nucl. Instrum.Methods Phy. Res. Sect. B: Beam Interact. Mater. Atoms 348 (2015) 233–239.
[22] J. Doyle, M.K. Linnarsson, P. Pellegrino, N. Keskitalo, B. Svensson, A. Schoner, N. Nordell, J. Lindstrom, J. Appl. Phys. 84 (1998) 1354–1357.
[23] F. Nava, G. Bertuccio, A. Cavallini, E. Vittone, Meas. Sci. Technol. 19 (2008) 102001.
[24] L. Storasta, J.P. Bergman, E. Janzén, A. Henry, J. Lu, J. Appl. Phys. 96 (2004) 4909–4915.
[25] T.A.G. Eberlein, R. Jones, P.R. Briddon, Phys. Rev. Lett. 90 (2003) 2255021–2255024.
[26] T. Dalibor, G. Pensl, H. Matsunami, T. Kimoto, W.J. Choyke, A. Schöner, N. Nordell, Phys. Status Solidi A 162 (1997) 199–225.
[27] I. Pintilie, L. Pintilie, K. Irmscher, B. Thomas, Appl. Phys. Lett. 81 (2002) 4841–4843.
[28] A.T. Paradzah, F.D. Auret, M.J. Legodi, E. Omotoso, M. Diale, Nucl. Instrum. Methods Phys. Res. Sect. B: Beam Interact. Mater. Atoms 358 (2015) 112–116.
[29] T. Kimoto, A. Itoh, H. Matsunami, S. Sridhara, L. Clemen, R. Devaty, W. Choyke, T. Dalibor, C. Peppermüller, G. Pensl, Appl. Phys. Lett. 67 (1995) 2833–2835.
[30] A.A. Lebedev, Semiconductors 33 (1999) 107–130.
[31] G. Pensl, W.J. Choyke, Phys. B: Condens. Matter 185 (1993) 264–283.

© University of Pretoria

PAPER IV: Electrical characterization of deep levels created by bombarding nitrogen-doped 4H-SiC with alpha-particle irradiation

Ezekiel Omotoso, Walter. E. Meyer, F. Danie. Auret, Alexander. T. Paradzah, and Matshisa J. Legodi

Nuclear Instruments and Methods in Physics Research Section B: Beam Interactions with Materials and Atoms (2015): doi:10.1016/j.nimb.2015.09.084

© University of Pretoria

UNIVERSITEIT VAN PRETORIA
UNIVERSITY OF PRETORIA
YUNIBESITHI YA PRETORIA

ARTICLE IN PRESS

Nuclear Instruments and Methods in Physics Research B xxx (2015) xxx–xxx

Contents lists available at ScienceDirect

Nuclear Instruments and Methods in Physics Research B

journal homepage: www.elsevier.com/locate/nimb

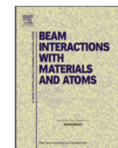

Electrical characterization of deep levels created by bombarding nitrogen-doped 4H-SiC with alpha-particle irradiation

Ezekiel Omotoso [a,b,*], Walter E. Meyer [a], F. Danie Auret [a], Alexander T. Paradzah [a], Matshisa J. Legodi [a]

[a] Department of Physics, University of Pretoria, Private Bag X20, Hatfield 0028, South Africa
[b] Departments of Physics, Obafemi Awolowo University, Ile-Ife 220005, Nigeria

ARTICLE INFO

Article history:
Received 20 June 2015
Received in revised form 28 September 2015
Accepted 28 September 2015
Available online xxxx

Keywords:
DLTS
4H-SiC
Alpha-particle irradiation
Annealing
Schottky barrier diode

ABSTRACT

Deep-level transient spectroscopy (DLTS) and Laplace-DLTS were used to investigate the effect of alpha-particle irradiation on the electrical properties of nitrogen-doped 4H-SiC. The samples were bombarded with alpha-particles at room temperature (300 K) using an americium-241 (^{241}Am) radionuclide source. DLTS revealed the presence of four deep levels in the as-grown samples, $E_{0.09}$, $E_{0.11}$, $E_{0.16}$ and $E_{0.65}$. After irradiation with a fluence of 4.1×10^{10} alpha-particles-cm ^{2}, DLTS measurements indicated the presence of two new deep levels, $E_{0.39}$ and $E_{0.62}$ with energy levels, $E_C - 0.39$ eV and $E_C - 0.62$ eV, with an apparent capture cross sections of $2 \times 10^{\;16}$ and $2 \times 10^{\;14}$ cm^2, respectively. Furthermore, irradiation with fluence of 8.9×10^{10} alpha-particles-cm ^{2} resulted in the disappearance of shallow defects due to a lowering of the Fermi level. These defects re-appeared after annealing at 300 °C for 20 min. Defects, $E_{0.39}$ and $E_{0.42}$ with close emission rates were attributed to silicon or carbon vacancy and could only be separated by using high resolution Laplace-DLTS. The DLTS peaks at $E_C - (0.55–0.70)$ eV (known as Z_1/Z_2) were attributed to an isolated carbon vacancy (V_C).

© 2015 Elsevier B.V. All rights reserved.

1. Introduction

The importance of deep level defects that act as charge carrier traps in semiconductor industry and applications of semiconductor devices cannot be over-emphasized [1,2]. The deep level defects (both hole and electron traps) are formed during the growth of the semiconductor, processing during fabrication of the electronic device (e.g. electron beam and sputtering deposition) and operation in radiation harsh environments. Deep levels can be introduced intentionally into electronic devices and can be beneficiary or detrimental. For detrimental defects, it is important to find methods to remove these defects. Some of the defects anneal out at room or elevated temperatures while some emanate at certain annealing temperature. The signatures of a deep level (i.e. its activation energy in the band gap and apparent capture cross section) can be determined from temperature depended deep level transient spectroscopy (DLTS) and Laplace DLTS measurements on Schottky barrier diodes (SBDs). Effects of radiation and annealing temperature on semiconductors are technologically important for radiation sensing applications as well as manufacturing processes and high temperature and high power applications [3].

SiC is a promising semiconductor with a wide bandgap of 3.26 eV [4]. Because of its wide bandgap, SiC is a suitable substrate for developing devices that are capable of operating at high temperature as well as in harsh radiation fields [5,6], such as space, accelerator facilities and nuclear power plants [7–9]. The electrical and thermal properties of SiC also make it suitable for electronic devices operating at high power, high temperature and high frequency [10]. Furthermore, SiC is a key material for the next generation of photonics [11]. Because of the aforementioned features, SiC is superior to Si in a number of applications.

In this work, the effect of alpha-particle irradiation at high fluences and annealing of 4H-SiC has been investigated by means of current–voltage (*I*–*V*), capacitance–voltage (*C*–*V*), DLTS and Laplace DLTS measurements. The major aim was to determine the effect of irradiating *n*-type 4H-SiC at high fluence and investigate the annealing of these defects.

2. Experimental procedure

The samples used for this work were cut from a nitrogen-doped *n*-type 4H-SiC wafer. The samples were grown on the Si-face of a SiC substrate with a net doping density of 10^{18} cm^{-3} and a resistiv-

* Corresponding author at: Department of Physics, University of Pretoria, Private Bag X20, Hatfield 0028, South Africa. Tel.: +27 4842911287.
E-mail addresses: ezekiel.omotoso@up.ac.za (E. Omotoso), wmeyer@up.ac.za (W. E. Meyer).

http://dx.doi.org/10.1016/j.nimb.2015.09.084
0168-583X/© 2015 Elsevier B.V. All rights reserved.

Please cite this article in press as: E. Omotoso et al., Electrical characterization of deep levels created by bombarding nitrogen-doped 4H-SiC with alpha-particle irradiation, Nucl. Instr. Meth. B (2015), http://dx.doi.org/10.1016/j.nimb.2015.09.084

© University of Pretoria

UNIVERSITEIT VAN PRETORIA
UNIVERSITY OF PRETORIA
YUNIBESITHI YA PRETORIA

ARTICLE IN PRESS

ity of 0.02 Ω-cm. The epilayer had a doping density of 7.1×10^{15} cm^{-2}. The wafers were supplied by CREE Res. Inc.

The samples were cut into smaller pieces and prepared according to the procedure reported by Omotoso et al. [12]. Resistive evaporation was employed for the deposition of ohmic and Schottky contacts since it does not introduce defect(s) in measurable quantity. Nickel was used for both contacts. The ohmic contact with a thickness of 3000 Å was deposited at a rate of 0.9 Å s^{-1} onto the highly doped (10^{18} cm^{-3}) back surface of the samples. The samples were annealed in a tube furnace under flowing argon at 950 °C for 10 min to form nickel silicides [13] in order to obtain low resistivity ohmic contacts. Before deposition of the Schottky contacts, the samples were degreased as previously reported [12]. Directly after cleaning, the samples were inserted into a vacuum chamber where NiAu (20% Au) Schottky contacts were resistively evaporated through a metal contact mask on the Si-face. The diameter and the thickness of the Ni/Au Schottky barrier diodes (SBDs) were 0.57 mm and 1000 Å respectively, and they were deposited at a rate of 0.5 Å s^{-1} under a vacuum of approximately 3×10^{-5} mbar on Si-face.

The samples were irradiated at room temperature with alpha particles of average energy 5.4 MeV by placing the samples on a ^{241}Am radio-nuclide foil. The samples were irradiated for 16 h, measured, and then irradiated for a further 19 h. The fluence rate from this foil was 7.1×10^{6} alpha-particles cm^{-2} s^{-1}. The total fluence received by the SBD after 19 h was 8.9×10^{11} alpha-particles cm^{-2}. The quality of the Schottky barrier diodes was tested by carrying out current–voltage (*I–V*) and capacitance–voltage (*C–V*) measurements in the dark at room temperature. The *I–V* and *C–V* measurements were carried out by an HP 4140 B pA meter/DC voltage source and an HP 4192A LF Impedance Analyzer, respectively. Conventional DLTS as well as Laplace DLTS were used to characterize the defects present in the as-grown and alpha-particle irradiated material, as well as after annealing in argon ambient at 300 °C for 20 min.

3. Results and discussion

3.1. I–V and C–V characteristics at room temperature

I–V and *C–V* measurements were performed to test the suitability of the devices for the study. Fig. 1 shows the semi-logarithmic *I–V* characteristics of the Schottky barrier diodes (SBDs) as grown (i), after bombardment with a fluence of 4.1×10^{11} (ii) and 8.9×10^{11} cm^{-2} (iii), and after annealing at 300 °C for 20 min in

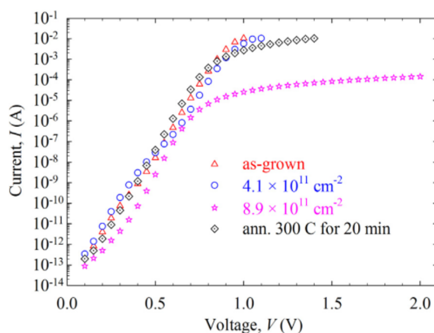

Fig. 1. Forward *I–V* characteristics of 4H-SiC SBD in as-grown (i), irradiated with 5.4 MeV alpha-particles at fluence 4.1×10^{11} (ii), 8.9×10^{11} cm^{-2} (iii), and after annealing at 300 °C for 20 min in flowing argon (iv), measured at 300 K.

flowing argon (iv). The effect of irradiation and annealing on the SBDs can be quantified in terms of the ideality factor (n), Schottky barrier height (ϕ_b), saturation current (I_s) and series resistance (R_s), as obtained from the plots in Fig. 1. The ideality factor obtained in (i) was 1.12 suggesting that thermionic emission is the dominant current transport mechanism. In (ii) and (iii), the ideality factor increased to 1.20 and 1.77, respectively. The increase in ideality factor was attributed to deviation from thermionic emission. This suggests that other current transport mechanisms such as generation recombination could be dominant as well especially at lower voltages. Above 0.7 V, series resistance is dominant in (iii). After the annealing at 300 °C, the dominance of series resistance reduced as shown in the plot represented by (iv). Table 1 compares the properties of the diode at aforementioned conditions. The ϕ_b of the contacts were determined from the *I–V* characteristics analyzed using the thermionic emission model [14,15]. The I_s was derived from the straight line intercept of log*I–V* plot at $V = 0$. The fluence and annealing dependency of n, $\phi_{b,I-V}$ and I_s may connected to the movement (or shift) of Fermi level pinning at the surface of SiC, since irradiation-induced defects can create interface states. Fig. 2 shows the plot of C^{-2} (pF^{-2}) as a function of voltage, V (V) for (i)–(iv) processes as defined earlier, all were measured at a frequency of 1 MHz with the sample at room temperature. The capacitance increased with decrease in reverse voltage for all conditions, but the capacitance of (iii) was the lowest and very distinct from others because of the position of the Fermi level with respect to the conduction band. A decrease in the capacitance after irradiation was attributed to the reduction of net donor concentration at 4H-SiC interface due to the effect of radiation induced defects. The *C–V* characteristics for the different conditions are also tabulated in Table 1.

3.2. Conventional DLTS analysis

Fig. 3 shows the DLTS spectra for SBD under different conditions. The measurements were obtained over a temperature range 30–380 K, at a quiescent reverse bias of −5.0 V, filling pulse amplitude of 6.0 V, filling pulse width of 1.0 ms and at different rate windows (2.5–1000 s^{-1}). The *signatures* of the defects in terms of activation energy, E_n and apparent capture cross section, σ_n were determined from the Arrhenius plot in Fig. 4. The activation energy of each defect was determined from the slope, and the corresponding apparent capture cross section was calculated from the intercept of the Arrhenius plot of log (T^2/e_n) versus $1/T$ as reported by Auret et al. [16]. The attributes of all the electron traps in (i)–(iv) are tabulated in Table 2.

Curve (i) is the spectrum of the as-grown sample and indicates the presence of four electron traps ($E_{0.09}$, $E_{0.11}$, $E_{0.16}$ and $E_{0.65}$) with energies 0.09, 0.11, 0.16 and 0.65 eV below the conduction band. These defects were associated with the growth of 4H-SiC. The Arrhenius plots of the defects present in as-grown 4H-SiC as well as their attributes have been reported by Omotoso et al. [12,17].

Table 1
Comparison of some electrical parameters of 4H-SiC in as-grown (i), irradiated with 5.4 MeV alpha-particles at fluence 4.1×10^{11} (ii) 8.9×10^{11} cm^{-2} (iii), and after annealing at 300 °C for 20 min in flowing argon (iv). The parameters estimated from *I–V* and *C–V* characteristics measured at 300 K.

Process	n	I_s (A)	R_s (Ω)	V_{bi}	N_D (cm^{-3})	$\phi_{b,I-V}$ (eV)	$\phi_{b,C-V}$ (eV)
(i)	1.12	2.1×10^{-14}	12	0.93	7.0×10^{15}	1.06	1.21
(ii)	1.20	1.1×10^{-14}	15	2.38	4.6×10^{15}	1.08	2.68
(iii)	1.77	6.9×10^{-15}	13,000	18.3	2.9×10^{15}	1.09	18.6
(iv)	1.15	1.9×10^{-15}	48	2.96	4.4×10^{15}	1.13	3.25

Please cite this article in press as: E. Omotoso et al., Electrical characterization of deep levels created by bombarding nitrogen-doped 4H-SiC with alpha-particle irradiation, Nucl. Instr. Meth. B (2015), http://dx.doi.org/10.1016/j.nimb.2015.09.084

© University of Pretoria

UNIVERSITEIT VAN PRETORIA
UNIVERSITY OF PRETORIA
YUNIBESITHI YA PRETORIA

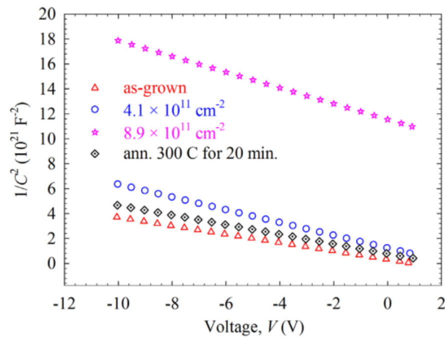

Fig. 2. $1/C^2$ as a function of voltage characteristics of 4H-SiC SBDs in as-grown (i), irradiated with 5.4 MeV alpha-particles at fluence 4.1×10^{11} (ii), 8.9×10^{11} cm^{-2} (iii), and after annealing at 300 °C for 20 min in flowing argon (iv), measured at 300 K.

In curve (ii), the amplitude of the shallow defect labeled $E_{0.09}$ was reduced to 12% of its height in the as-grown material. The defects labeled $E_{0.09}$ and $E_{0.10}$ have identical level, and slightly different energy. The $E_{0.09/0.10}$ has been assigned to nitrogen impurities that occupy the cubic site [18]. The defect labeled $E_{0.39}$ with energy, 0.39 eV below the conduction band emanated after the diode received a fluence of 4.1×10^{11} alpha-particle-cm^{-2} from a ^{241}Am source. The level labeled $E_{0.39}$ has been attributed to silicon vacancy (V_{Si}) [19]. The defect $E_{0.65}$ from as-grown was replaced with two defects with energies 0.62 and 0.67 eV and both displaying broad peaks. From curve (ii), we conclude that ^{241}Am with energy 5.4 MeV introduced new defects into the diode after bombardment with fluence 4.1×10^{11} alpha-particle-cm^{-2}.

Curve (iii) was measured after bombardment of the devices with total fluence of 8.9×10^{11} alpha-particle-cm^{-2}. From curve (iii), the disappearance of shallow defects ($E_{0.09/0.10}$, $E_{0.11/0.12}$ and $E_{0.16/0.17}$) occurred. It was as a result of intense damage that lowered the position of the Fermi level deeper into the bandgap, below the shallow defect levels. The result is that these defects were never filled by the DLTS filling pulse and therefore remain invisible. Also, the two broad defects observed earlier in (ii) remained, displaying activation energies and apparent capture cross sections as 0.55 and 0.67 eV, and 2.4×10^{-15} and 2.9×10^{-15} cm^2, respectively. In addition to those electron traps present in (iii), $E_{0.70}$ with activation energy of 0.70 eV and apparent capture cross section of 1.0×10^{-15} cm^2 appeared above 380 K for rate window plotted, but was only visible at much lower rate windows. We believe that the $E_{0.62}$ and $E_{0.67}$ in curve (ii) are due to the same defect as the $E_{0.55}$ and $E_{0.67}$ in curve (iii). The reason for the difference in the observed peak shapes and position difference between the $E_{0.62}$ and $E_{0.55}$ in the two curves may be explained by the field effect. Since the carrier concentration for curve (iii) is much lower than that for curve (ii), it follows that the defects measured in curve (ii) experience a higher electric field. Due to field enhanced emission, the peaks in curve (ii) are therefore expected to move towards the lower temperature. This seems to be true for the $E_{0.67}$ in curves (ii) and (iii).

Curve (iv) was recorded after annealing the twice irradiated device, in flowing argon at 300 °C for 20 min. The shallow defects re-appeared, the $E_{0.42}$ (which has the same attribute with $E_{0.39}$) became distinct and prominent, and also the two distinct defects in (iii) ($E_{0.55}$ and $E_{0.65}$) reduced to one prominent defect with electron trap label, $E_{0.67}$ and a defect $E_{0.74}$ as a shoulder at the high-temperature end of the $E_{0.65}$. The re-appearance of the low energy defects is consistent with our explanation for their disappearance in curve (iii): after annealing, the free carrier density of the material recovered to approximately the same level as after the first irradiation, therefore, the low energy peaks in curves (ii) and (iv) are expected to be the same.

3.3. Laplace-DLTS analysis

We used Laplace-DLTS to investigate the peaks in the annealed sample in more detail. In Fig. 5, we have shown Laplace DLTS spectra recorded at 200 and 205 K. The spectra indicate the presence of two defects, labeled $E_{0.39}$ and $E_{0.42}$ instead of the single peak observed by conventional DLTS. At 200 and 205 K, the emission rate of $E_{0.42}$ is less than one third of $E_{0.39}$. By monitoring the change of the peak positions over a wide range of temperature, it was deduced that the two small peaks that appeared at lower emission rate of Fig. 5 are artefacts. The two defects are distinctly illustrated in the Arrhenius plots in Fig. 7 and their properties tabulated in Table 2.

The spectra in Fig. 6 were recorded at temperatures 300 and 310 K, and revealed the presence of peaks labeled $E_{0.65}$, $E_{0.70}$ and $E_{0.76}$. The peaks of the deep level defects were clearly separated by Laplace DLTS. The signatures of the three traps in term of acti-

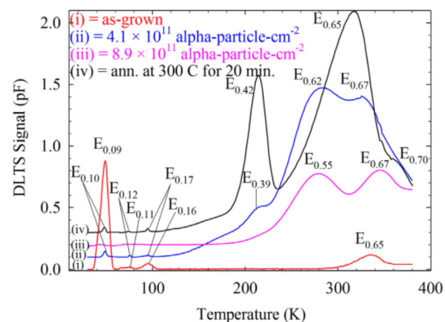

Fig. 3. Conventional DLTS spectra of 4H-SiC showing the present of defects in as-grown (i), irradiated with 5.4 MeV alpha-particles at fluence 4.1×10^{11} (ii), 8.9×10^{11} cm^{-2} (iii), and after annealing at 300 °C for 20 min in flowing argon (iv). In curve (i), the spectrum was scaled up by factor of 5 from 55 to 380 K. The rate window is 200 s^{-1}.

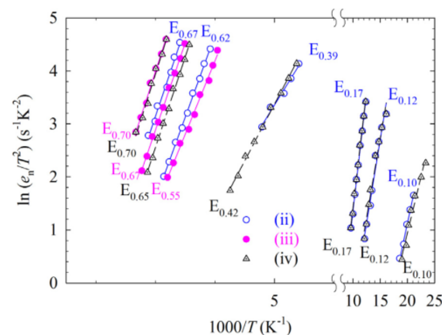

Fig. 4. Arrhenius plots of 4H-SiC SBD for irradiated with 5.4 MeV alpha-particles at fluence 4.1×10^{11} (ii) 8.9×10^{11} cm^{82} (iii), and after annealing at 300 °C for 20 min in flowing argon (iv).

Please cite this article in press as: E. Omotoso et al., Electrical characterization of deep levels created by bombarding nitrogen-doped 4H-SiC with alpha-particle irradiation, Nucl. Instr. Meth. B (2015), http://dx.doi.org/10.1016/j.nimb.2015.09.084

© University of Pretoria

UNIVERSITEIT VAN PRETORIA
UNIVERSITY OF PRETORIA
YUNIBESITHI YA PRETORIA

Table 2
Electronic properties of defects detected in 4H-SiC SBD by DLTS in as-grown (i), irradiated with 5.4 MeV alpha-particles at fluence 4.1×10^{11} (ii) 8.9×10^{11} cm^{-2} (iii), and after annealing at 300 °C for 20 min in flowing argon (iv), and L-DLTS after process after (iv).

Process	Defect label	E_T [eV]	σ_a [cm^2]	Defect ID	Refs.
(i)	$E_{0.09}$	$E_C - 0.09$	8×10^{-15}	N	[18]
	$E_{0.11}$	$E_C - 0.11$	2×10^{-16}	Ti	[25]
	$E_{0.16}$	$E_C - 0.16$	1×10^{-15}	Ti	[20]
	$E_{0.65}$	$E_C - 0.65$	4×10^{-15}	V_C (Z_1/Z_2)	[21,23]
(ii)	$E_{0.10}$	$E_C - 0.10$	8×10^{-14}	N	[18]
	$E_{0.12}$	$E_C - 0.12$	2×10^{-15}	Ti	[25]
	$E_{0.17}$	$E_C - 0.17$	9×10^{-15}	Ti	[20]
	$E_{0.39}$	$E_C - 0.39$	2×10^{-16}	$V_{C/Si}$	[19]
	$E_{0.62}$	$E_C - 0.62$	2×10^{-14}	V_C (Z_1/Z_2)	[21,23]
	$E_{0.67}$	$E_C - 0.67$	2×10^{-15}	V_C (Z_1/Z_2)	[21,23]
(iii)	$E_{0.55}$	$E_C - 0.55$	2×10^{-15}	V_C (Z_1/Z_2)	[20,22]
	$E_{0.67}$	$E_C - 0.65$	3×10^{-15}	V_C (Z_1/Z_2)	[21,23]
	$E_{0.70}$	$E_C - 0.70$	1×10^{-15}	V_C (Z_1/Z_2)	[21,23]
(iv)	$E_{0.10}$	$E_C - 0.10$	9×10^{-15}	N	[18]
	$E_{0.12}$	$E_C - 0.12$	5×10^{-16}	Ti	[25]
	$E_{0.17}$	$E_C - 0.17$	7×10^{-15}	Ti	[20]
	$E_{0.42}$	$E_C - 0.42$	6×10^{-15}	$V_{C/Si}$	[19]
	$E_{0.65}$	$E_C - 0.67$	1×10^{-14}	V_C (Z_1/Z_2)	[21,23]
	$E_{0.70}$	$E_C - 0.70$	2×10^{-15}	V_C (Z_1/Z_2)	[21,23]
L-DLTS	$E_{0.39}$	$E_C - 0.39$	5×10^{-15}	$V_{C/Si}$	[19]
	$E_{0.42}$	$E_C - 0.42$	5×10^{-15}	$V_{C/Si}$	[19]
	$E_{0.65}$	$E_C - 0.65$	8×10^{-15}	V_C (Z_1/Z_2)	[21,23]
	$E_{0.70}$	$E_C - 0.70$	4×10^{-14}	V_C (Z_1/Z_2)	[21,23]
	$E_{0.76}$	$E_C - 0.74$	1×10^{-14}	?	[19,24]

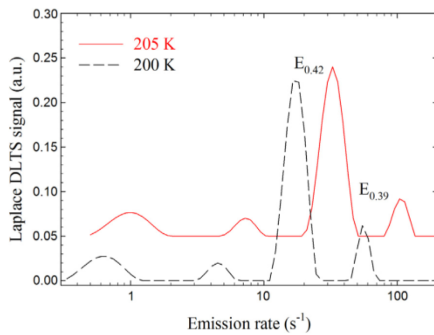

Fig. 5. Laplace-DLTS spectra recorded at different temperatures to show the presence of defects with closely spaced energy levels: (a) 200 K and 205 K.

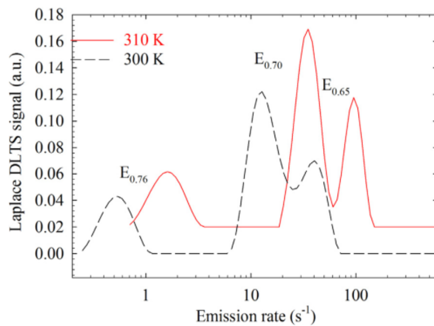

Fig. 6. Laplace-DLTS spectra recorded at different temperatures to show the presence of defects with closely spaced energy levels: (a) 300 K and 310 K, after annealing the irradiated sample, at 300 °C for 20 min in flowing argon.

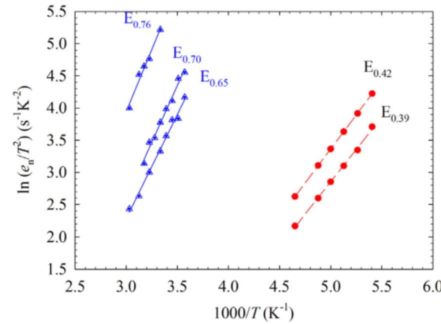

Fig. 7. Arrhenius plots of some of the deep-level defects with closely spaced energy levels, obtained after annealing the irradiated sample, at 300 °C for 20 min in flowing argon.

vation energies were 0.65, 0.70 and 0.76 eV, and the corresponding apparent capture cross sections were 7.7×10^{-15} and 3.6×10^{-14} and 1.2×10^{-14} cm^2, respectively. The Arrhenius plots of the three defects that were successfully split by Laplace DLTS are shown in Fig. 7. The defects $E_{0.65}$ and $E_{0.70}$ are closer to each other, and have been assigned in the literature to be Z_1/Z_2 [20–23]. Son et al. has recently identified the levels as the double acceptor (2–/0) of an isolated carbon vacancy [23]. The defect labeled $E_{0.76}$ obtained at higher temperature side of the measurements. The structure of defect $E_{0.76}$ has not been reported despite its presence after electron and proton irradiation [19,24].

The properties of all the defects present using both conventional and Laplace-DLTS on 4H-SiC are summarized in Table 2.

4. Conclusions

In conclusion, the results obtained from *I–V* and *C–V* characteristics at four different processes (as-grown, irradiation at fluences 4.1×10^{11} and 8.9×10^{11} cm^{-2}, annealing at 300 °C) demonstrated the suitability of Ni/4H-SiC SBDs for the study. The defects introduced in *n*-type 4H-SiC during alpha-particle irradiation from a ^{241}Am radionuclide with energy of 5.4 MeV followed by annealing in flowing argon were characterized by deep level transient spectroscopy (DLTS) and high resolution Laplace-DLTS. Four deep levels with activation energies $E_{0.09}$, $E_{0.11}$, $E_{0.16}$, and $E_{0.65}$ present in as-grown material. The intensity of $E_{0.09}$ reduced to 12% after bombardment with fluences 4.1×10^{11} cm^{-2} and two new defects with trap levels $E_C - 0.39$ and $E_C - 0.62$ were introduced. After the SBD received the fluence 8.9×10^{11} cm^{-2}, the shallow defect labeled ($E_{0.09}$, $E_{0.11}$ and $E_{0.16}$) disappeared. Both the lowering after the first irradiation and the disappearance of the defect may be as a result of intense damage that lowered the position of the Fermi level deeper into the bandgap, thereby not filling this shallow defect during the forward bias pulse. Also, three deep levels with energy level $E_{0.55}$, $E_{0.67}$ and $E_{0.70}$ were observed. Re-appearance of shallow defects occurred after the temperature annealing of irradiated SBD at 300 °C for 20 min in flowing argon. Laplace-DLTS was used to split defect $E_{0.42}$ into $E_{0.39}$ and $E_{0.42}$ with the same or closely attribute related to silicon or carbon vacancy. In addition, Laplace-DLTS revealed the presence of three defects ($E_{0.65}$, $E_{0.70}$ and $E_{0.76}$), with $E_{0.65}$ and $E_{0.70}$ having close emission rates attributed to the Z_1/Z_2, which, according to literature are identified as the double acceptor of an isolated carbon vacancy. The defect labeled $E_{0.76}$ is not yet identified.

Please cite this article in press as: E. Omotoso et al., Electrical characterization of deep levels created by bombarding nitrogen-doped 4H-SiC with alpha-particle irradiation, Nucl. Instr. Meth. B (2015), http://dx.doi.org/10.1016/j.nimb.2015.09.084

© University of Pretoria

UNIVERSITEIT VAN PRETORIA
UNIVERSITY OF PRETORIA
YUNIBESITHI YA PRETORIA

ARTICLE IN PRESS

Acknowledgments

This work is based on the research supported in part by the National Research Foundation (NRF) of South African (Grant specific unique reference number (UID) 78838). The Grant holder acknowledges that opinions, findings and conclusions or recommendations expressed in this publication generated by the NRF supported are that of authors and that NRF accepts no liability whatsoever in this regard.

References

[1] L. Pelaz, L.A. Marquês, M. Aboy, P. López, I. Santos, Eur. Phys. J. B 72 (2009) 323–359.
[2] Ž. Pastuović, I. Capan, D.D. Cohen, J. Forneris, N. Iwamoto, T. Ohshima, R. Siegele, N. Hoshino, H. Tsuchida, Nucl. Instr. Meth. Phys. Res. Sect. B 348 (2015) 233–239.
[3] A. Akbay, H. Korkut, K. Ejderha, T. Korkut, A. Türüt, J. Radioanal. Nucl. Chem. 289 (2011) 145–148.
[4] L.M. Tolbert, B. Ozpineci, S.K. Islam, M.S. Chinthavali, Proc. Power Energy Syst. 1 (2003) 317–321.
[5] V. Kazukauskas, J.-V. Vaitkus, Opto-Electron. Rev. 12 (2004) 377–382.
[6] J. Grant, W. Cunningham, A. Blue, V. O'Shea, J. Vaitkus, E. Gaubas, M. Rahman, Nucl. Instr. Meth. Phys. Res. Sect. A 546 (2005) 213–217.
[7] T. Nishijima, T. Ohshima, K.K. Lee, Nucl. Instr. Meth. Phys. Res. Sect. B 190 (2002) 329–334.
[8] F. Nava, E. Vittone, P. Vanni, G. Verzellesi, P.G. Fuochi, C. Lanzieri, M. Glaser, Nucl. Instr. Meth. Phys. Res. Sect. A 505 (2003) 645–655.
[9] L. Kin Kiong, T. Ohshima, H. Itoh, IEEE Trans. Nucl. Sci. 50 (2003) 194–200.
[10] M.C. Driver, R.H. Hopkins, C.D. Brandt, D.L. Barrett, A.A. Burk, R.C. Clarke, G.W. Eldridge, H.M. Hobgood, J.P. McHugh, P.G. McMullin, R.R. Siergiej, S. Sriram, in: Gallium Arsenide Integrated Circuit (GaAs IC) Symposium, 1993, Technical Digest 1993, 15th Annual, 1993, pp. 19–21.
[11] S. Yamada, B.-S. Song, T. Asano, S. Noda, Appl. Phys. Lett. 99 (1023) (2011) 2011021–2011023.
[12] E. Omotoso, W.E. Meyer, F.D. Auret, A.T. Paradzah, M. Diale, S.M.M. Coelho, P.J. Janse van Rensburg, Mater. Sci. Semicond. Process. 39 (2015) 112–118.
[13] T. Marinova, A. Kakanakova-Georgieva, V. Krastev, R. Kakanakov, M. Neshev, L. Kassamakova, O. Noblanc, C. Arnodo, S. Cassette, C. Brylinski, B. Pecz, G. Radnoczi, G. Vincze, Mater. Sci. Eng. B 46 (1997) 223–226.
[14] S.M. Sze, K.K. Ng, Physics of Semiconductor Devices, John Wiley & Sons, 2006.
[15] E. Rhoderick, R. Williams, Oxford Science, Oxford, 1988.
[16] F.D. Auret, P.N.K. Deenapanray, Crit. Rev. Solid State Mater. Sci. 29 (2004) 1–44.
[17] E. Omotoso, W.E. Meyer, F.D. Auret, A.T. Paradzah, M. Diale, S.M.M. Coelho, P.J. Janse van Rensburg, P.N.M. Ngoepe, Nucl. Instr. Meth. Phys. Res. Sect. B (2015) 5.
[18] T. Kimoto, A. Itoh, H. Matsunami, S. Sridhara, L. Clemen, R. Devaty, W. Choyke, T. Dalibor, C. Peppermüller, G. Pensl, Appl. Phys. Lett. 67 (1995) 2833–2835.
[19] J. Doyle, M.K. Linnarsson, P. Pellegrino, N. Keskitalo, B. Svensson, A. Schoner, N. Nordell, J. Lindstrom, J. Appl. Phys. 84 (1998) 1354–1357.
[20] T. Dalibor, G. Pensl, H. Matsunami, T. Kimoto, W.J. Choyke, A. Schöner, N. Nordell, Phys. Status Solidi A 162 (1997) 199–225.
[21] C. Hemmingsson, N.T. Son, O. Kordina, J.P. Bergman, E. Janzén, J.L. Lindström, S. Savage, N. Nordell, J. Appl. Phys. 81 (1997) 6155–6159.
[22] I. Pintilie, L. Pintilie, K. Irmscher, B. Thomas, Appl. Phys. Lett. 81 (2002) 4841–4843.
[23] N.T. Son, X.T. Trinh, L.S. Løvlie, B.G. Svensson, K. Kawahara, J. Suda, T. Kimoto, T. Umeda, J. Isoya, T. Makino, T. Ohshima, E. Janzén, Phys. Rev. Lett. 109 (2012) 187603.
[24] A. Castaldini, A. Cavallini, L. Rigutti, F. Nava, Appl. Phys. Lett. 85 (2004) 3780–3782.
[25] A.A. Lebedev, Semiconductors 33 (1999) 107–130.

Please cite this article in press as: E. Omotoso et al., Electrical characterization of deep levels created by bombarding nitrogen-doped 4H-SiC with alpha-particle irradiation, Nucl. Instr. Meth. B (2015), http://dx.doi.org/10.1016/j.nimb.2015.09.084

© University of Pretoria

PAPER V: Electrical characterization of defects introduced during electron beam deposition of W Schottky barrier diodes on *n*-type 4H-SiC

Ezekiel Omotoso, Walter Ernst Meyer, Francois Danie Auret, and Sergio Manuel Martins Coelho

In manuscript

© University of Pretoria

UNIVERSITEIT VAN PRETORIA
UNIVERSITY OF PRETORIA
YUNIBESITHI YA PRETORIA

Electrical characterization of defects introduced during electron beam deposition of W Schottky contacts on *n*-type 4H-SiC

E. Omotoso[1,2], W.E. Meyer[1], F.D. Auret[1], S.M.M. Coelho[1], M. Diale[1] and P.N.M. Ngoepe[1]

[1] *Department of Physics, University of Pretoria, Private Bag X20, Hatfield 0028, South Africa*

[2] *Departments of Physics, Obafemi Awolowo University, Ile-Ife, 220005, Nigeria*

Corresponding author e-mail address: ezekiel.omotoso@up.ac.za; wmeyer@up.ac.za

ABSTRACT

We have studied the defects introduced in *n*-type 4H-SiC during electron beam deposition (EBD) of tungsten by deep-level transient spectroscopy (DLTS). The results from current-voltage and capacitance-voltage measurements showed deviations from ideality due to damage, but were still well suited to a DLTS study. We compared the electrical properties of six electrically active defects observed in EBD Schottky barrier diodes with those introduced in resistively evaporated material on the same material, as-grown, as well as after high energy electron irradiation (HEEI). We observed that EBD introduced two electrically active defects with energies E_C – 0.42 and E_C – 0.70 eV in the 4H-SiC at and near the interface with the tungsten. The defects introduced by EBD had properties similar to defect attributed to the silicon or carbon vacancy, introduced during HEEI of 4H-SiC. EBD was also responsible for the increase in concentration of a defect attributed to nitrogen impurities (E_C – 0.10) as well as a defect linked to the carbon vacancy (E_C – 0.67). Annealing at 400 °C in Ar ambient removed these two defects introduced during the EBD.

Keywords: 4H-SiC, defects, DLTS, annealing, electron beam deposition,

1. Introduction

Metal-semiconductor (M-S) Schottky barrier diodes (SBDs) are widely used where diodes with low forward voltage drop, low capacitance and high switching speed are required [1]. The reliability of the SBDs is influenced significantly by the quality of the M-S junction [2]. The performance of devices can be quantified experimentally in terms of their ideality factor, Schottky barrier height, saturation current, series resistance and free carrier concentration. Among these properties of the M-S devices, SBH plays a

© University of Pretoria

major role in the successful operation of many devices in transporting electrons across the M-S junction [3].

Silicon carbide (SiC) is a promising semiconductor with a wide bandgap of 3.26 eV [4]. The excellent properties of SiC such as high thermal conductivity, high breakdown field and high saturated drift velocity have drawn the interest of many researchers [5]. These characteristics make SiC a very good semiconductor capable of outperforming silicon in electronic devices for high-power, high-frequency and high-temperature applications [6]. SiC is a key material for the next-generation photonics [7] and a good candidate for electronic devices use in harsh radiation environments such as in aerospace, accelerator facilities and nuclear power plants [8-10].

In earlier studies, the properties of deep level defects introduced during alpha-particles irradiation, high energy electron irradiation (HEEI) and electron beam exposure have been reported [11-13]. It has been reported that metallization processes, such as electron beam deposition and sputter deposition, do introduced electrically active defects in measurable quantities at and close to M-S junction in conventional semiconductors such as Si, Ge and GaAs [14-17]. The defects introduced influence the performance of devices and may alter the barrier height of metal-semiconductor contacts [18-20]. Deep-level defects responsible for barrier alterations are formed when energetic particles strike the surface of semiconductor and interact with semiconductor creating interface states, while defects deeper in the semiconductor usually lead to levels in the band gap that trap and emit carriers. Defects may either be beneficial for or detrimental to device performance depending on the application. It has been known that the defects introduced during high-energy electron and proton irradiation of silicon increase in switching speed of devices [21]. To the best of our knowledge, no in-depth investigations regarding the deep level defects introduced in *n*-type 4H-SiC during the metallization process has been reported.

In this paper, we report the electronic characteristics of deep level defects introduced in nitrogen-doped, *n*-type 4H-SiC during electron beam deposition (EBD) of W Schottky contacts. The defects introduced by EBD will be compared to the defects introduced after HEE of 4H-SiC.

© University of Pretoria

2. Experimental procedure

The samples used for this study were cut from homoepitaxially grown, N-doped, *n*-type 4H-SiC wafers supplied by Cree Research Inc. The epilayer was grown by chemical vapour deposition on the Si-face of the SiC substrate, which had a net doping density of 1×10^{18} cm^{-3} and resistivity of 0.019 Ω-cm. The epilayer had a doping density of 3.7×10^{14} cm^{-3}.

Before metallization, the samples were degreased by boiling for 5 minutes each in trichloroethylene, acetone and methanol, followed by 1 minute rinse in de-ionized water. They were etched in 40% hydrofluoric acid for 30 seconds in order to remove the native oxide layer on the samples, and then rinsed in de-ionized water followed by blowing dry with nitrogen gas. Directly after cleaning, the samples were inserted into a vacuum chamber where Ni was resistively evaporated on the highly doped back surfaces to form an ohmic contact. The ohmic contact with a thickness of 300 nm was deposited at a rate of ~0.1 $nm.s^{-1}$. The samples were annealed in a in quartz tube heated by a Lindberg Hevi-Duty furnace under flowing argon gas at 950°C for 10 minutes to form nickel silicides [22] in order to reduce contact resistance. The samples were cleaned in an ultrasonic water bath for 3 minutes each in trichloroethylene, acetone and methanol followed by a 1 minute rinse in de-ionized H_2O after the annealing of the ohmic contact [11].

Tungsten contacts, 0.6mm in diameter and 40 nm in thickness, were evaporated in an EBD system through a metal contact mask at a rate of ~0.02 $nm.s^{-1}$. The EBD of tungsten was achieved using a 10 kV source (MDC model e-Vap 10CVS) and a beam current of ~240 mA with samples placed ~50 cm away from the W crucible. A high beam current was required because of the high melting point of W (3422 °C). The vacuum of ~1.2×10^{-5} mbar was maintained during the deposition.

Ni Schottky contacts of thickness 100 nm were resistively evaporated (RE) through a metal contact mask on an identical sample at a deposition rate of 0.05 $nm.s^{-1}$ under a vacuum of 5.0×10^{-5} mbar, which served as a control.

In addition, the control samples were irradiated at room temperature with high energy electron (HEE) irradiation from a ^{90}Sr radioactive source for 24 hours at fluence rate of

© University of Pretoria

7×10^9 $cm^{-2}.s^{-1}$. The ^{90}Sr radionuclide decays with the emission of a 0.5 MeV electron into yttrium which then decays to zirconium with the emission of a 2.3 MeV electron,. The emitted electrons from the electron source have a continuous energy distribution with approximately 70% of the total number of emitted electrons having energy above 250 keV [23].

The electrical properties of devices fabricated by EBD were characterized at room temperature using a current-voltage (*I*-*V*) and capacitance-voltage (*C*-*V*) system comprising an HP 4140 B pA Meter/DC Voltage Source and an HP 4192A LF Impedance Analyzer, respectively. Thereafter, electrically active defects were characterized by deep level transient spectroscopy (DLTS). The SBDs fabricated by EBD were annealed in Ar ambient at the interval of 100 °C for 20 minutes to know the stability of the defects introduced during metallization.

3. Results and discussion

The forward and reverse *I*-*V* characteristics of W Schottky contacts deposited by EBD are shown in Fig. 1. Thermionic emission model was used to analyse the *I*-*V* characteristics of EBD of W/4H-SiC SBD. It was deduced from the *I*-*V* plot that thermionic emission dominated above ~0.55 V, measured at 300 K in the dark. At lower voltages (below 0.55 V), generation-recombination dominated. The effect of a series resistance was observed at the high voltage region of the plot. The electrical parameters that were extracted from *I*-*V* and *C*-*V* characteristics are tabulated in Table 1. From the results, a high value of ideality factor n was observed and was attributed to deviation from thermionic emission theory. The *I*-*V* Schottky barrier height $\phi_{I\text{-}V}$ obtained from the plot was 0.98 eV, which is slightly lower than the predicted value by the Schottky model ($\phi_M - \chi$ = 1.40 eV), which indicates the influence of interface states. From the inset of Fig. 1, the reverse current increased with voltage, but remained below 100 pA up to a reverse voltage of 80 V. It can be deduced from the *I*-*V* measurements that EBD degraded the Schottky contacts.

Fig. 2 shows the plot of C^{-2} as a function of bias voltage, V for EBD of W/4H-SiC SBD. The N_d estimated was greater than the doping density of material. An increasing negative slope of the graph towards the interface is an indication of a decreased net doping density close to the interface. Both these effects indicated the presence of deep level

© University of Pretoria

defects probably emanating from the EBD. The $\phi_{C\text{-}V}$ (1.68eV) obtained was greater the $\phi_{I\text{-}V}$ (0.98 eV) which is probably due to deep impurity levels, but may also be due to surface inhomogeneity, interfacial layer or states, image force barrier lowering and edge leakage current [24].

The *I-V* and *C-V* characteristics of the control SBDs before and after HEE irradiation were not compared to the SBD by EBD because metals have different influence on characteristics of devices.

From the results of both *I-V* and *C-V* characteristics obtained, it is apparent that the rectification quality of the control and EBD Schottky diodes were of a reasonable electrical quality and were suitable for the analysis of DLTS.

Figs. 3 and 4 depict the DLTS spectra of EBD of W/4H-SiC (a), RE deposition of Ni/4H-SiC after HEE irradiation (b), and control RE deposition of Ni/4H-SiC (c). The DLTS spectra in Fig. 3 were obtained over the temperature range 22 – 360 K, at a quiescent reverse bias of −3.0 V, filling pulse of amplitude 0.5 V, width of 2.0 ms and at rate window of 10 s^{-1}. Fig. 4 was obtained with the same conditions except with the quiescent reverse bias of −5.0 V and filling pulse of amplitude 4.0 V. The signatures of the electrically active defects present, namely their activation energy E_n and apparent capture cross section σ_n were determined from Arrhenius plots. The activation energy of each defect was determined from the slope and the corresponding apparent capture cross section was calculated from the intercept of the Arrhenius plot of log (T^2/e_n) versus $1/T$ [25].

The spectra (c) in Figs. 3 and 4 revealed the presence of four electron deep levels labelled $E_{0.10}$, $E_{0.12}$, $E_{0.16}$ and $E_{0.67}$ (where 'E' refers to an electron trap and the subscript 0.10 refers to an energy level below the conduction band in eV) in the as-grown Ni/4H-SiC SBD. These levels were studied previously [11, 12, 26]. The conclusions related to these and other defects are summarised in Table 2.

The spectra (b) revealed the presence of six electrically active electron defects after bombarding the Ni/4H-SiC SBD with high-energy electron. The defects were labelled $E_{0.10}$, $E_{0.12}$, $E_{0.15}$, $E_{0.40}$, $E_{0.63}$ and $E_{0.71}$, following the same naming convention as earlier. From the defect signatures as tabulated in Table 2, two of these defects ($E_{0.42}$ and $E_{0.71}$) were introduced by HEEI while the other four defects ($E_{0.10}$, $E_{0.12}$, $E_{0.15}$, and $E_{0.63}$) were

© University of Pretoria

present in the as-grown diode. The concentration of defects $E_{0.10}$ and $E_{0.63}$ decreased after the HEEI and the activation energy of $E_{0.63}$ reduced from 0.67 eV to 0.63 eV, but still within the experimental error. These defects were attributed to nitrogen impurities and carbon vacancy, respectively. We believe that the decrease in the relatively shallow $E_{0.10}$, which is ascribed to nitrogen impurities [27], is due to a lowering of the Fermi level because of deep levels in the band gap. The decrease in the $E_{0.63}$, which is ascribed to the carbon vacancy, could be due to some of the vacancies being filled by diffusing interstitials. It is noteworthy that despite the changes in DLTS biasing conditions (as revealed in spectra in Figs. 3 and 4), there was no visible changes in the concentration of the defects.

The EBD spectra of W/4H-SiC SBDs for both measurement conditions are labelled (a) in Figs. 3 and 4. From Fig. 3, six electron deep level defects were present in the W/4H-SiC SBD deposited by EBD when measured at a quiescent reverse bias of −3.0 V, filling pulse of amplitude 0.5 V. The defects were also labelled as $E_{0.10}$, $E_{0.12}$, $E_{0.16}$, $E_{0.42}$, $E_{0.67}$ and $E_{0.70}$, with four defects ($E_{0.10}$, $E_{0.12}$, $E_{0.16}$ and $E_{0.67}$) corresponding to defects that have been observed in RE Ni/4H-SiC SBDs. The two defects ($E_{0.42}$ and $E_{0.70}$) were introduced as a result of metallization by EBD. The DLTS spectrum of EBD W/4H-SiC Schottky diodes measured at a quiescent reverse bias of −5.0 V and filling pulse of amplitude 4.0 V (Fig. 4(a)) sampled a broader depth range under the contact, and revealed the presence of five electrically active defects. This included all the defects observed previously except $E_{0.42}$. It is important to point out that defects introduced by EBD were at or close to the W/4H-SiC interface.

By comparing spectra (b) and (c) in Fig. 3, it seems that HEEI reduced the peak height of $E_{0.67}$ slightly and that of $E_{0.10}$ significantly, while increasing the peak height due to $E_{0.42}$. By comparing (a) to the other two spectra, it is clear that $E_{0.42}$ was much less pronounced in (a) than in (b). This can be used to explain the lesser reduction of $E_{0.10}$ in (b) compared to (a), if it is assumed that both processes introduce defects in roughly the same ratios. At first glance, the height of the $E_{0.67}$ seems to be higher in (a) than in (b). However, if the skewed baseline of (a) is taken into account, the peak heights are very similar and no definite conclusions can be drawn. This is also the case for the spectra in Fig. 4. On both (a) and (b) spectra, the $E_{0.70}$ peaks seem to have approximately the same size, it is therefore concluded that $E_{0.70}$ is introduced in relatively greater proportions by

© University of Pretoria

EBD than HEEI. The decrease in the peak heights of $E_{0.42}$ and $E_{0.70}$ in the EBD material with larger reverse bias demonstrates the limited depth range of the EBD defects.

The structure of the electrically active defects introduced after electron beam deposition of W/4H-SiC SBD were identified by comparing them with the defects present after HEEI of Ni/4H-SiC SBD, of which the structures have previously been identified. The attribution of the electrically active defects observed in this study has been tabulated in Table 2.

Finally, the thermal stability of EBD induced defects in W/4H-SiC was investigated. No noticeable changes were observed after annealing at 100 °C for 20 minutes. The concentration of defects labelled $E_{0.42}$ and $E_{0.70}$ started decreasing after the annealing at 200 °C. After the annealing at 400 °C, the two electrically active deep levels associated with EBD were removed completely after approximately 20 minutes.

4. Conclusions

The quality of EBD of W on *n*-type 4H-SiC Schottky barrier contacts for DLTS has been investigated by *I*-*V* and *C*-*V* measurements. The *I*-*V* and *C*-*V* measurements of EBD diodes showed that EBD resulted in the degradation of the device due to the presence of deep levels introduced during the deposition. However these diodes were still suitable for the DLTS study. DLTS of the EBD deposited diodes revealed the presence of six electrically active defects with energies 0.10, 0.12, 0.16, 0.42, 0.67 and 0.70 eV below the conduction band minimum in EBD SBDs. Closely comparing these defects with defects present in the as-grown Ni/4H-SiC SBDs and after bombardment with high energy electron revealed that EBD introduced two electrically active deep level defects ($E_{0.42}$ and $E_{0.70}$) that have the same electronic properties as defects introduced by HEEI. These two electrically active defects with energies, E_C – 0.42 and E_C – 0.70 eV, possibly introduced as a result of the product of elastic collisions between 10 keV electrons and residual vacuum gases which were ionized around the filament and accelerated by the electric field towards the substrate. The two electrically active deep levels were removed after the annealing at 400 °C in Ar.

© University of Pretoria

Acknowledgements

This work is based on the research supported in part by the National Research Foundation (NRF) of South African (Grant specific unique reference number (UID) 78838). The Grant holder acknowledges that opinions, findings and conclusions or recommendations expressed in this publication generated by the NRF supported are that of authors and that NRF accepts no liability whatsoever in this regard.

References

1. Van Tuyl, R.L. and C.A. Liechti, *High-speed integrated logic with GaAs MESFET's.* IEEE Journal of Solid-State Circuits, , 1974. **9**(5): p. 269-276.

2. Rhoderick, E. and R. Williams, *Metal-Semiconductor Contacts (2nd edn.) Clarendon*. 1988, Oxford Science, Oxford.

3. Janardhanam, V., et al., *Study of current-voltage-temperature (I-V-T) and capacitance-voltage-temperature (C-V-T) characteristics of molybdenum Schottky contacts on n-InP (1 0 0).* Journal of Alloys and Compounds, 2009. **485**(1-2): p. 467-472.

4. Tolbert, L.M., et al., *Wide bandgap semiconductors for utility applications.* Power and Energy Systems, Proceedings, 2003. **1**: p. 317-321.

5. Siad, M., M. Abdesslam, and A.C. Chami, *Role of carbon in the formation of ohmic contact in Ni/4HSiC and Ni/Ti/4HSiC.* Applied Surface Science, 2012. **258**(18): p. 6819-6822.

6. Madar, R., *Materials science: Silicon carbide in contention.* Nature, 2004. **430**(7003): p. 974-975.

7. Yamada, S., et al., *Silicon carbide-based photonic crystal nanocavities for ultra-broadband operation from infrared to visible wavelengths.* Applied Physics Letters, 2011. **99**(20): p. 2011021-2011023.

8. Nishijima, T., T. Ohshima, and K.K. Lee, *Investigation of the radiation hardness on semiconductor devices using the ion micro-beam.* Nuclear Instruments and Methods in Physics Research Section B: Beam Interactions with Materials and Atoms, 2002. **190**(1–4): p. 329-334.

9. Nava, F., et al., *Radiation tolerance of epitaxial silicon carbide detectors for electrons, protons and gamma-rays.* Nuclear Instruments and Methods in Physics Research Section A: Accelerators, Spectrometers, Detectors and Associated Equipment, 2003. **505**(3): p. 645-655.

10. Kin Kiong, L., T. Ohshima, and H. Itoh, *Performance of gamma irradiated p-channel 6H-SiC MOSFETs: high total dose.* Nuclear Science, IEEE Transactions on, 2003. **50**(1): p. 194-200.

© University of Pretoria

11. Omotoso, E., et al., *Effects of 5.4 MeV alpha-particle irradiation on the electrical properties of nickel Schottky diodes on 4H–SiC.* Nuclear Instruments and Methods in Physics Research Section B: Beam Interactions with Materials and Atoms, 2015: p. 5.

12. Omotoso, E., et al., *The influence of high energy electron irradiation on the Schottky barrier height and the Richardson constant of Ni/4H-SiC Schottky diodes.* Materials Science in Semiconductor Processing, 2015. **39**(0): p. 112-118.

13. Omotoso, E., et al. *Electrical Characterization of Defects Introduced in n-Type N-Doped 4H-SiC during Electron Beam Exposure*. in *Solid State Phenomena*. 2015. Trans Tech Publ.

14. Auret, F., et al., *Electrical characterization of argon ion sputter-induced defects in GaAs.* South African Journal Science, 1991. **87**(3): p. 127-129.

15. Auret, F.D., et al., *Electrical characterization of defects introduced in n-Si during electron beam deposition of Pt.* Physica Status Solidi (A), 2012. **209**(10): p. 1926-1933.

16. Auret, F.D., et al., *Electrical characterization of defects introduced during electron beam deposition of Pd Schottky contacts on n-type Ge.* Applied Physics Letters, 2006. **88**(24): p. 242110.

17. Coelho, S.M.M., et al., *Electrical characterization of defects introduced in n-Ge during electron beam deposition or exposure.* Journal of Applied Physics, 2013. **114**(17): p. 1737081-1737088.

18. Auret, F.D., O. Paz, and N.A. Bojarczuk, *Characterization of process-induced defects and device properties of ion beam sputter-deposited Mo contacts on Si.* Journal of Applied Physics, 1984. **55**(6): p. 1581-1589.

19. Auret, F.D., et al., *Sputter deposition-induced electron traps in epitaxially grown n-GaN.* Applied Physics Letters, 1999. **74**(15): p. 2173-2175.

20. Myburg, G. and F. Auret, *Influence of the electron beam evaporation rate of Pt and the semiconductor carrier density on the characteristics of Pt/n-GaAs Schottky contacts.* Journal of Applied Physics, 1992. **71**(12): p. 6172-6176.

21. Sawko, D.C. and J. Bartko, *Production of Fast Switching Power Thyristors by Proton Irradiation.* Nuclear Science, IEEE Transactions on, 1983. **30**(2): p. 1756-1758.

22. Marinova, T., et al., *Nickel based ohmic contacts on SiC.* Materials Science and Engineering: B, 1997. **46**(1–3): p. 223-226.

23. Auret, F., et al., *Electrical characterization of defects introduced in n-GaAs by alpha and beta irradiation from radionuclides.* Applied Physics A, 1993. **56**(6): p. 547-553.

24. Crowell, C.R., *The physical significance of the T0 anomalies in Schottky barriers.* Solid-State Electronics, 1977. **20**(3): p. 171-175.

© University of Pretoria

25. Auret, F.D. and P.N.K. Deenapanray, *Deep Level Transient Spectroscopy of Defects in High-Energy Light-Particle Irradiated Si.* Critical Reviews in Solid State and Materials Sciences, 2004. **29**(1): p. 1-44.

26. Paradzah, A.T., et al., *Electrical characterization of 5.4 MeV alpha-particle irradiated 4H-SiC with low doping density.* Nuclear Instruments and Methods in Physics Research Section B: Beam Interactions with Materials and Atoms, 2015. **358**(0): p. 112-116.

27. Kimoto, T., et al., *Nitrogen donors and deep levels in high-quality 4H–SiC epilayers grown by chemical vapor deposition.* Applied Physics Letters, 1995. **67**(19): p. 2833-2835.

28. Lebedev, A.A., *Deep level centers in silicon carbide: A review.* Semiconductors, 1999. **33**(2): p. 107-130.

29. Dalibor, T., et al., *Deep defect centers in silicon carbide monitored with deep level transient spectroscopy.* Physica Status Solidi (A), 1997. **162**(1): p. 199-225.

30. Doyle, J., et al., *Electrically active point defects in n-type 4H–SiC.* Journal of Applied Physics, 1998. **84**(3): p. 1354-1357.

31. Pensl, G. and W.J. Choyke, *Electrical and optical characterization of SiC.* Physica B: Condensed Matter, 1993. **185**(1–4): p. 264-283.

© University of Pretoria

Table

Table 1: Electrical parameters obtained from *I-V* and *C-V* of W/4H-SiC SBD deposited by electron beam.

n	I_S (A)	R_S (Ω)	V_{bi} (V)	N_d (cm^{-3})	ϕ_{I-V} (eV)	ϕ_{C-V} (eV)
2.50	6.2×10^{-13}	158	1.68	5.4×10^{14}	0.98	1.68

Table 3: Electronic properties of defects introduced in *n*-type 4H-SiC during W EBD and HEEI of 4H-SiC SBDs

Process	Defect label	E_T (eV)	σ_a (cm^2)	Defect ID	References
EBD	$E_{0.10}$	$E_c - 0.10$	1.4×10^{-13}	N	[27]
	$E_{0.12}$	$E_c - 0.12$	2.7×10^{-15}	Ti	[28]
	$E_{0.16}$	$E_c - 0.16$	2.9×10^{-15}	Ti	[29]
	$E_{0.42}$	$E_c - 0.42$	6.3×10^{-15}	$V_{C/Si}$	[30]
	$E_{0.67}$	$E_c - 0.67$	9.9×10^{-15}	Z_1/Z_2 (V_C)	[27, 31]
	$E_{0.70}$	$E_c - 0.70$	1.2×10^{-15}	Z_1/Z_2 (V_C)	[27, 31]
HEEI	$E_{0.10}$	$E_c - 0.10$	2.6×10^{-14}	N	[27]
	$E_{0.12}$	$E_c - 0.12$	8.4×10^{-16}	Ti	[28]
	$E_{0.15}$	$E_c - 0.15$	1.2×10^{-15}	Ti	[29]
	$E_{0.40}$	$E_c - 0.40$	3.0×10^{-15}	$V_{C/Si}$	[30]
	$E_{0.63}$	$E_c - 0.63$	3.0×10^{-15}	Z_1/Z_2 (V_C)	[27, 31]
	$E_{0.71}$	$E_c - 0.71$	2.7×10^{-15}	Z_1/Z_2 (V_C)	[27, 31]

Figures

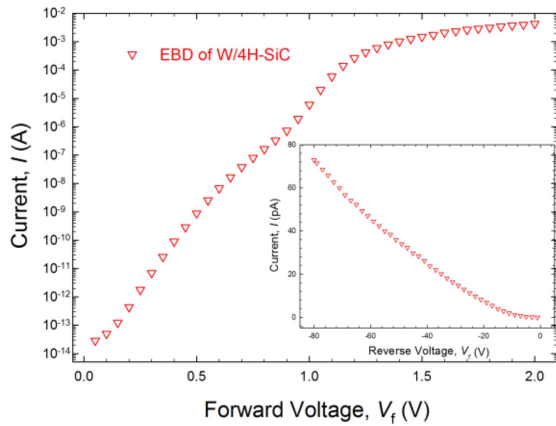

Fig. 1: The *I-V* characteristics of W Schottky contact to 4H-SiC deposited by EBD. The inset is the reverse *I-V* characteristics.

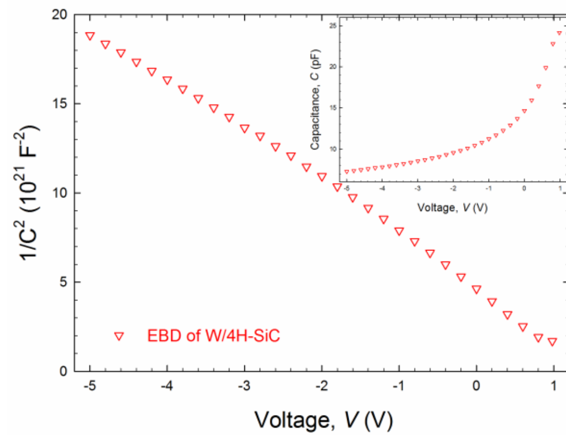

Fig. 2: $1/C^2$ as a function of voltage for W Schottky contact to 4H-SiC deposited by EBD. The inset is the capacitance as a function of voltage.

© University of Pretoria

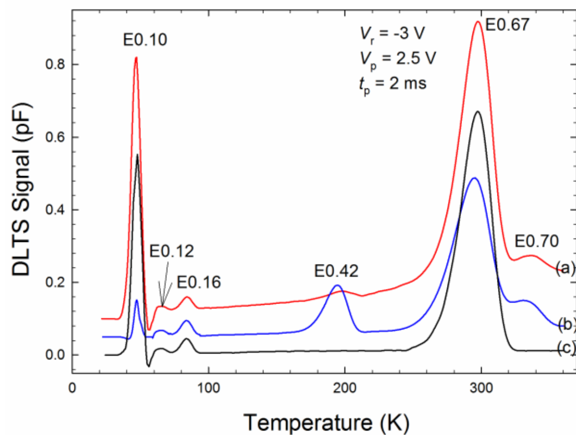

Fig. 3: Conventional DLTS spectra of (a) W/4H-SiC deposited by EBD, Ni/4H-SiC deposited by RE (b) after HEEI and (c) as-grown. The spectrum in the temperature range 56-360 K is scaled up by a factor of 8. The DLTS measurements were obtained at a quiescent reverse bias of −3.0 V, filling pulse of amplitude 0.5 V, width of 2.0 ms and at rate window of 10 s^{-1}.

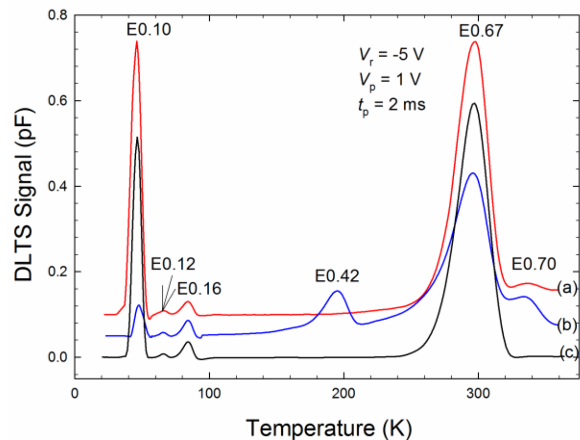

Fig. 4: Conventional DLTS spectra of (a) W/4H-SiC deposited by EBD, Ni/4H-SiC deposited by RE (b) after HEEI and (c) as-grown. The spectrum in the temperature range 56-360 K is scaled up by a factor of 8. The measurements were obtained at a quiescent reverse bias of −5.0 V, filling pulse of amplitude 4.0 V, width of 2.0 ms and at rate window of 10 s^{-1}.

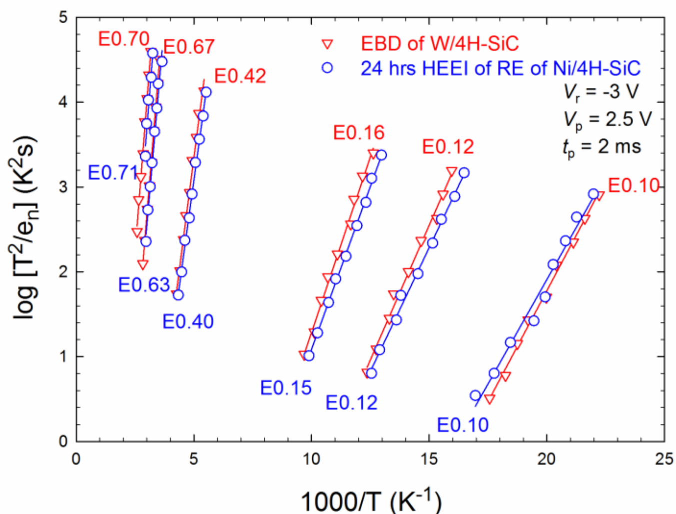

Fig. 5: Arrhenius plots of electrically active deep level defects in EBD of W/4H-SiC and HEEI of RE of Ni/4H-SiC SBDs devices. The measurements were obtained at a quiescent reverse bias of −3.0 V, filling pulse of amplitude 0.5 V, width of 2.0 ms and at multi-rate windows.

© University of Pretoria

PAPER VI: Electrical characterization of defects introduced in *n*-type N-doped 4H-SiC during electron beam exposure

Ezekiel Omotoso, Walter Ernst Meyer, Francois Danie Auret, Sergio Manuel Martins Coelho, and Phuti Ngako Mahloka Ngoepe

Solid State Phenomena, Trans Tech Papers 242 (2015): 427-433.
doi: 10.4028/www.scientific.net/SSP.242.427

© University of Pretoria

UNIVERSITEIT VAN PRETORIA
UNIVERSITY OF PRETORIA
YUNIBESITHI YA PRETORIA

Solid State Phenomena Vol. 242 (2016) pp 427-433
© (2016) Trans Tech Publications, Switzerland
doi:10.4028/www.scientific.net/SSP.242.427

Submitted: 2015-05-27
Accepted: 2015-05-28
Online: 2015-10-23

Electrical characterization of defects introduced in *n*-type N-doped 4H-SiC during electron beam exposure

Ezekiel Omotoso[1, 2, a *], Walter Ernst Meyer[1, b], Francois Danie Auret[1, c], Sergio Manuel Martins Coelho[1, d], and Phuti Ngako Mahloka Ngoepe[1, f]

[1] Department of Physics, University of Pretoria, Private Bag X20, Hatfield 0028, South Africa
[2] Departments of Physics, Obafemi Awolowo University, Ile-Ife, 220005, Nigeria
[a]ezekiel.omotoso@up.ac.za, [b]wmeyer@up.ac.za, [c]danie.auret@up.ac.za,
[d]Sergio.coelho@up.ac.za, [f]phuti.ngoepe@up.ac.za

Keywords: silicon carbide, defects, deep level transient spectroscopy, electron beam exposure,

Abstract. Deep level transient spectroscopy (DLTS) was used to characterize the defects introduced in *n*-type, N-doped, 4H-SiC while being exposed to electron beam evaporation conditions. This was done by heating a tungsten source using an electron beam current of 100 mA, which was not sufficient to evaporate tungsten. Two new defects were introduced during the exposure of 4H-SiC samples to electron beam deposition conditions (without metal deposition) after resistively evaporated nickel Schottky contacts. We established the identity of these defects by comparing their *signatures* to those of high energy particle irradiation induced defects of the same materials. The defect $E_{0.42}$ had acceptor-like behaviour and could be attributed to be a silicon or carbon vacancy. The $E_{0.71}$ had intrinsic nature and was linked to a carbon vacancy and/or carbon interstials.

Introduction

Metallization is a very important processing step in the microelectronics and photovoltaic industries. Electron beam deposition is one of the popular techniques in the fabrication of ohmic and Schottky barrier contacts at high controllable rate. Auret *et al* [1] and Coelho *et al* [2] have reported that metallization procedures, including electron beam deposition (EBD), induced defects at and close to the metal-semiconductor junction [3]. These defects influence the performance of the devices and alter the contacts' Schottky barrier heights [4].

The defects introduced by the electron beam when energetic particles interact with the semiconductor surface will lead to lattice damage depending on the energy and duration of the exposure. These defects may either be of benefit or detrimental to device performance.

Silicon carbide (SiC) has drawn the interest of many researchers due to its wide bandgap of 3.4 eV [5] and the excellent properties such as high thermal conductivity, high breakdown field and high saturated drift velocity [6]. These characteristics make SiC a very good semiconductor capable of outperforming silicon in electronic devices for high-power, high-frequency and high-temperature applications [7]. SiC is also a key material for next-generation photonics [8].

In this paper, we have investigated the effect of exposing nitrogen-doped, n-type 4H-SiC to electron beam conditions (without metal deposition) prior to metal deposition by resistive evaporation. The motivation is mainly to study the influence of electron beam exposure (EBE) on the 4H-SiC semiconductor and the signatures of the defects present after the deposition of nickel Schottky contacts. The defects emanated were compared with the defects in as-grown SiC and SiC after bombardment with alpha-particles from a ^{241}Am source and by high energy electrons from a ^{90}Sr source.

Experimental Procedure

We have used an *n*-type, N-doped 4H-SiC wafer, double polished with Si face epi-layer, resistivity of 0.02 Ω-cm and doping density of 7.1×10^{15} cm^{-2}. The 4H-SiC wafer was supplied by CREE Res. Inc. Prior to metallization, the samples were cut into smaller pieces with dimensions of

All rights reserved. No part of contents of this paper may be reproduced or transmitted in any form or by any means without the written permission of Trans Tech Publications, www.ttp.net. (ID: 137.215.6.53-23/10/15,19:29:57)

© University of Pretoria

UNIVERSITEIT VAN PRETORIA
UNIVERSITY OF PRETORIA
YUNIBESITHI YA PRETORIA

approximately 4 mm × 2 mm. The samples were degreased by boiling for 5 minutes each in trichloroethylene, acetone, methanol and followed by 1 minute rinse in de-ionized water. They were also etched in a 40% concentration of HF for 30 seconds in order to remove the native oxide layer on the samples, and then rinsed in de-ionized water, followed by blowing dry with nitrogen gas as reported earlier by Omotoso *et al* [9].

Directly after cleaning, the samples were mounted on a metal contact mask and inserted into the vacuum chamber that was pumped down to 10^{-5} mbar before thermal evaporation of Ni ohmic contacts onto the highly doped (1.0×10^{18} cm^{-3}) back surface of the samples. Ohmic contact was evaporated at a deposition rate of 0.9 Å s^{-1} for approximately 30 minutes to achieve the thickness of 3000 Å. The samples were annealed in a tube furnace under flowing argon gas at 950℃ for 10 minutes to form nickel silicides [10] in order to reduce the contact resistance, thus forming an ohmic contact.

The cleaning procedures were repeated after annealing of the ohmic contact but only for three minutes in an ultrasonic bath. The samples were also dried with nitrogen gas before the fabrication of nickel Schottky barrier diodes (SBDs). SBDs were fabricated in two stages: nickel Schottky contacts, 0.6 mm in diameter and of thickness 100 Å were first deposited by resistive evaporation technique before being quickly transferred into the electron beam deposition chamber for exposure to the electron beam. Electron beam exposure (EBE) of the samples was achieved by using a 10 kV source (MDC model e-Vap 10CVS) with samples placed 50 cm away from the metal crucible as earlier reported by Auret et al [1] and Coelho et al [2]. The samples were exposed to EBE conditions for 50 minutes from a heated tungsten source using a beam current of 100 mA and an acceleration voltage of 10 kV [2]. This current was not enough to evaporate tungsten, but would have been sufficient to evaporate most other metals. During the entire exposure, the vacuum in the deposition chamber was reduced to 10^{-4} mbar by leaking in forming gas H15 (N_2:H_2 of 85%:15% by volume) [2].

Hereafter, the samples were removed and returned quickly to the resistive deposition chamber. Additional Ni was deposited resulting in thickness of 1000 Å Schottky diodes and an area of 2.8×10^{-3} cm^2 were deposited at a rate of 0.2 Å s^{-1} and a vacuum of approximately 5×10^{-6} mbar by means of resistive evaporation, a process known to not introduce defects measurable by DLTS [2].

Subsequent to SBD fabrication, current-voltage (*I-V*) and capacitance-voltage (*C-V*) measurements were carried out to determine the quality of the diodes. The *I-V* and *C-V* measurements were carried out by an HP 4140 B pA meter/DC voltage source and an HP 4192A LF Impedance Analyzer, respectively. The defects introduced into the samples were thereafter characterised by conventional deep level transient spectroscopy (DLTS). The DLTS spectra were recorded over the temperature range 30 – 350 K, at a quiescent reverse bias of –5.0 V, filling pulse height of amplitude 6 V, filling pulse width of 2.0 ms and at different rate windows, in order to determine the defect signatures by means of Arrhenius plots.

In order to aid identification of the defects introduced by EBE, they were compared to the defects present in resistively deposited SBDs as-grown, irradiated by alpha-particles (with energy of approximately 5.4 MeV) from an ^{241}Am radio-nuclide and high energy electrons (above 200 keV). The alpha particle irradiation was done at a fluence rate of 7×10^{6} cm^{-2} s^{-1} for 2 hours to obtain a fluence of 5×10^{10} alpha-particles-cm^{-2}. The ^{90}Sr radionuclides used decay first to Y with the emission of an 0.5 MeVelectron of halflife of 28.5 years and then decay to Zr with the emission of a 2.3 MeV electron of halflife of 64.1 hours [11]. The ^{90}Sr radio-nuclide source had a fluence rate of 1×10^{9} electrons-cm^{-2} s^{-1} with energies above 200 keV. Here the sample was irradiated for 24 hours in order to obtain a fluence of 2×10^{10} electron-cm^{-2}.

Results and Discussion

Defects in as-grown 4H-SiC

The defects introduced during the EBE were compared with defects present in as-grown SiC, as well as defects introduced by alpha-particle and high energy electron irradiation. It has been reported in literature that RE does not introduced defect in measurable quantities [2]. Therefore, this

© University of Pretoria

UNIVERSITEIT VAN PRETORIA
UNIVERSITY OF PRETORIA
YUNIBESITHI YA PRETORIA

technique was employed to evaporate nickel on n-type 4H-SiC for both ohmic and Schottky contacts because of aforementioned advantage. The electrical characteristics of the Schottky contacts are summarised in Table 1. The DLTS spectrum of the control sample recorded at a rate window of 20 s^{-1} is shown in Fig. 1. The spectrum showed the presence of four defect levels, labelled $E_{0.10}$, $E_{0.12}$, $E_{0.16}$ and $E_{0.65}$, where "E" refers to an electron trap and the number at the subscript say 0.10, is the activation enthalpy of the defect below the conduction band. Both the activation enthalpy and the corresponding apparent capture cross section, referred to as the defect's *signature*, were determined from the Arrhenius plots, and are tabulated in Table 2.

Table 1 Comparison of electrical characteristics of Ni/4H-SiC Schottky barrier diodes for different processes.

Samples	n	I_s [A]	R_s [Ω]	V_{bi} [V]	N_D [cm^{-3}]	$\phi_{I\text{-}V}$ [eV]	$\phi_{C\text{-}V}$ [eV]
As-grown	1.04	15.5×10^{-18}	48	1.07	7.8×10^{15}	1.25	1.36
α-particle irradiation	1.07	2.6×10^{-18}	270	1.23	7.4×10^{15}	1.31	1.52
HEE irradiation	1.13	1.4×10^{-19}	60	1.32	6.8×10^{15}	1.38	1.60
EBE	1.26	6.6×10^{-17}	13	1.41	8.0×10^{15}	1.21	1.68

Table 2 Electronic properties of defects detected by DLTS in Ni/4H-SiC SBD after various processing steps.

Process	Defect label	E_T [eV]	σ_a [cm^2]	T_{20} [K]	Defect ID	Refs.
RE	$E_{0.10}$	$E_C - 0.10$	3×10^{-12}	45	N	[12]
	$E_{0.12}$	$E_C - 0.12$	1×10^{-15}	65	Ti	[13]
	$E_{0.16}$	$E_C - 0.16$	1×10^{-15}	85	Ti	[14]
	$E_{0.65}$	$E_C - 0.65$	4×10^{-15}	304	$V_{C/Si}$ (Z_1/Z_2)	[14, 15]
α-particle	$E_{0.10}$	$E_C - 0.10$	2×10^{-12}	44	N	[12]
	$E_{0.12}$	$E_C - 0.12$	1×10^{-15}	65	Ti	[13]
	$E_{0.16}$	$E_C - 0.16$	3×10^{-15}	85	Ti	[14]
	$E_{0.39}$	$E_C - 0.39$	2×10^{-15}	192	$V_{C/Si}$	[16]
	$E_{0.61}$	$E_C - 0.61$	5×10^{-15}	302	$V_{C/Si}$ (Z_1/Z_2)	[12, 17]
	$E_{0.70}$	$E_C - 0.70$	6×10^{-15}	333	$V_{C/Si}$ (Z_1/Z_2)	[14, 15]
HEE	$E_{0.10}$	$E_C - 0.10$	1×10^{-16}	44	N	[12]
	$E_{0.12}$	$E_C - 0.12$	4×10^{-12}	65	Ti	[13]
	$E_{0.16}$	$E_C - 0.16$	1×10^{-15}	84	Ti	[14]
	$E_{0.22}$	$E_C - 0.22$	2×10^{-17}	141	?	?
	$E_{0.40}$	$E_C - 0.40$	3×10^{-15}	199	$V_{C/Si}$	[16]
	$E_{0.65}$	$E_C - 0.65$	3×10^{-15}	300	$V_{C/Si}$ (Z_1/Z_2)	[14, 15]
	$E_{0.70}$	$E_C - 0.70$	3×10^{-15}	338	$V_{C/Si}$ (Z_1/Z_2)	[14, 15]
EBE	$E_{0.10}$	$E_C - 0.10$	1×10^{-11}	44	N	[12]
	$E_{0.12}$	$E_C - 0.12$	2×10^{-16}	64	Ti	[13]
	$E_{0.16}$	$E_C - 0.16$	2×10^{-15}	84	Ti	[14]
	$E_{0.42}$	$E_C - 0.42$	5×10^{-15}	201	$V_{C/Si}$	[16]
	$E_{0.66}$	$E_C - 0.66$	4×10^{-15}	302	$V_{C/Si}$ (Z_1/Z_2)	[14, 15]
	$E_{0.71}$	$E_C - 0.71$	1×10^{-15}	340	$V_{C/Si}$ (Z_1/Z_2)	[14, 15]

Alpha-particle irradiation

The electrical characteristics of the diode after irradiation are shown in Table 1. The diode was still of good quality after irradiation. The deep levels introduced by irradiation were also characterised by DLTS (see Fig. 1). Alpha-particle irradiated SBD introduced two defects ($E_{0.39}$ and $E_{0.62}$) with complicated broad peaks. The activation energies of the two defects are 0.39 and 0.62 eV, respectively. The attributes of the defects were tabulated in Table 2.

© University of Pretoria

UNIVERSITEIT VAN PRETORIA
UNIVERSITY OF PRETORIA
YUNIBESITHI YA PRETORIA

High energy electron (HEE) irradiation

The results obtained from the *I-V* and *C-V* measurements as shown in Table 1 confirmed the suitability of the SBDs for DLTS measurements. As already reported, high energy electron irradiation of 4H-SiC yields three new defects [9]. The peaks could be attributed to vacancies in both silicon and carbon sublattices deepening on the energy required to displace the relevant atom [18]. The broadness of the peaks may be as a result of superposition of several peaks that have closely spaced activation energies. Point defects are formed due to the low mass of the electron relative to the nucleus since the recoiling nucleus does not have enough kinetic energy to cause further displacements [11]. The attribute of the defects introduced by high energy electrons are also tabulated in Table 2.

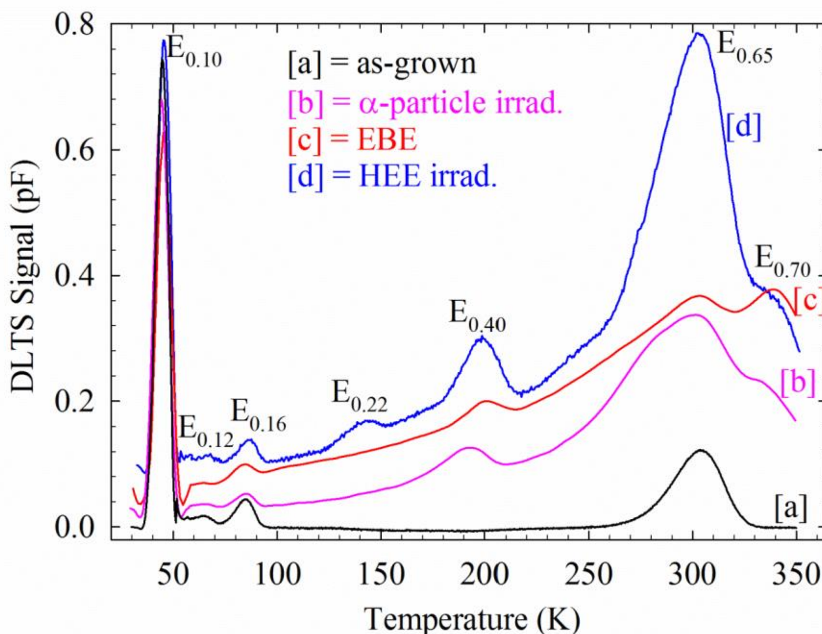

Fig. 1: DLTS spectra of Ni/4H-SiC for: [a] as-grown; [b] irradiated with α-particles; [c] exposed to electron beam condition without metal deposition (EBE); [d] irradiated with high energy electrons.

Electron beam exposure, without metal deposition

In most experimental setups in electron beam evaporators, the position of the sample and the sample holder during the pre-metallization heating and degassing of the metal may be varied. The sample may be rotated to face away from the crucible or shield the sample with a shutter during the experimental procedure. This procedure may not be applicable to larger commercial systems where metallization of large areas is required. In this section, we investigate the effect of exposing a 4H-SiC sample to electron beam deposition conditions, however, *without metal deposition*.

The electrical characteristics of the EBE exposed diode after deposition are shown in Table 1. It was noted that the carrier density as determined by *C-V* measurements was 8.0×10^{15} cm^{-3}.

In Fig. 2, we compare the spectra recorded using SBDs prepared by resistive evaporation of Ni (a), alpha-particle irradiated (b), high energy electron irradiated (c), and electron beam deposition conditions, *without metal deposition* (d). From the spectra, it was observed that the electron beam exposure introduced two defects which were similar to defects introduced by high energy particle irradiation but in lower concentration. We therefore conclude that exposure of samples to electron

© University of Pretoria

UNIVERSITEIT VAN PRETORIA
UNIVERSITY OF PRETORIA
YUNIBESITHI YA PRETORIA

beam *without metal deposition* could be another mechanism of introducing defects $E_{0.42}$ and $E_{0.71}$ without bombardment with high energy particle irradiation. The defect $E_{0.42}$ was reported earlier by Doyle *et al* [16], who reported that it has acceptor-like behaviour. A similar defect level has been attributed to the silicon vacancy [19], carbon vacancy, split interstitial or antisites after low energy electron irradiation [18]. The $E_{0.71}$ is commonly known as the Z_1Z_2 defect. Defect $E_{0.71}$ has intrinsic nature and is linked to a carbon vacancy, carbon interstials and complexes of carbon vacancies and interstials [16, 20, 21]

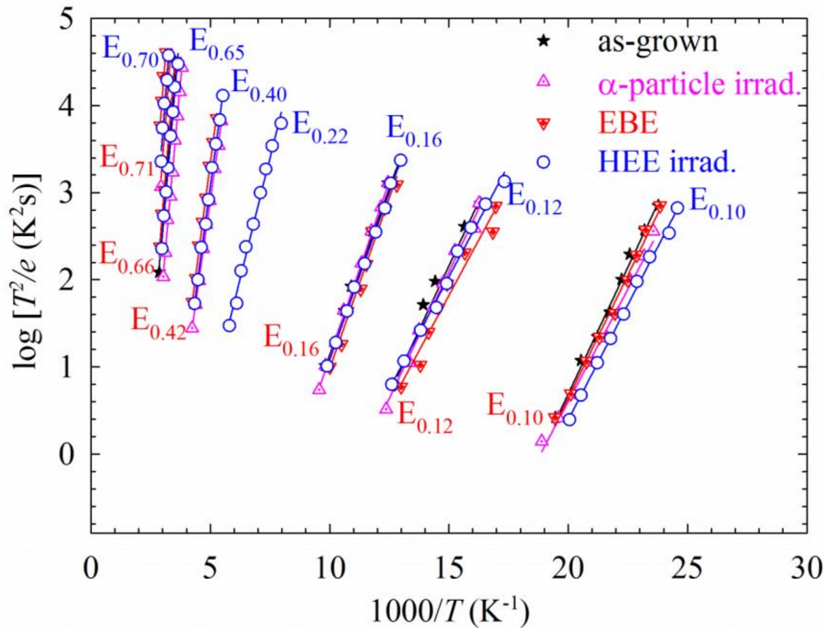

Fig. 2: Arrhenius plots of Ni/4H-SiC for: [a] as-grown ; [b] irradiated with α-particles; [c] exposed to electron beam condition without metal deposition (EBE); [d] irradiated with high energy electrons.

Conclusions

The current-voltage and the capacitance-voltage characteristics demonstrated that the Ni/4H-SiC SBDs prepared were suitable for the research. Deep level transient spectroscopy revealed the presence of four defects below the conduction band ($E_{0.10}$, $E_{0.12}$, $E_{0.16}$ and $E_{0.65}$) after resistive evaporation, which we conclude were in the as-grown material. We observed two additional defects, $E_{0.42}$ and $E_{0.71}$ after electron beam exposure, without metal deposition. The apparent capture cross sections of defects $E_{0.42}$ and $E_{0.71}$ were estimated from the intercept of the Arrhenius plot to be 5×10^{-15} cm^2 and 1×10^{-15} cm^2, respectively. The signatures of defects $E_{0.42}$ and $E_{0.71}$ are similar to defects induced as a result of high energy particles such as alpha-particle and high energy electron irradiation. The defect $E_{0.42}$ has acceptor-like behaviour and has also been attributed to the silicon or carbon vacancy. The defect $E_{0.71}$, known as Z_1Z_2, has intrinsic nature that is linked to a carbon vacancy, carbon interstials and complexes of carbon vacancies and interstials.

We therefore show that, although 10 keV electrons are not supposed to cause damage in SiC, EBE does cause damage near the sample surface, similar to that produced by high energy particles. It is therefore concluded that electron beam exposure is detrimental to device properties. Proper shielding as well as deposition of metal in the best possible vacuum should also be employed.

© University of Pretoria

UNIVERSITEIT VAN PRETORIA
UNIVERSITY OF PRETORIA
YUNIBESITHI YA PRETORIA

Acknowledgement

This work is based on the research supported in part by the National Research Foundation (NRF) of South African (Grant specific unique reference number (UID) 78838). The Grant holder acknowledges that opinions, findings and conclusions or recommendations expressed in this publication generated by the NRF supported are that of authors and that NRF accepts no liability whatsoever in this regard.

References

[1] F.D. Auret, S.M.M. Coelho, J.M. Nel, W.E. Meyer, Electrical characterization of defects introduced in n-Si during electron beam deposition of Pt, physica status solidi (a), 209 (2012) 1926-1933.
[2] S.M.M. Coelho, F.D. Auret, P.J. Janse van Rensburg, J.M. Nel, Electrical characterization of defects introduced in n-Ge during electron beam deposition or exposure, Journal of Applied Physics, 114 (2013) 1737081-1737088.
[3] F.D. Auret, P.M. Mooney, Deep levels introduced during electron-beam deposition of metals on n-type silicon, Journal of Applied Physics, 55 (1984) 988-993.
[4] G. Myburg, F. Auret, Influence of the electron beam evaporation rate of Pt and the semiconductor carrier density on the characteristics of Pt/n-GaAs Schottky contacts, Journal of applied physics, 71 (1992) 6172-6176.
[5] L.M. Tolbert, B. Ozpineci, S.K. Islam, M.S. Chinthavali, Wide bandgap semiconductors for utility applications, Power and Energy Systems, Proceedings, 1 (2003) 317-321.
[6] M. Siad, M. Abdesslam, A.C. Chami, Role of carbon in the formation of ohmic contact in Ni/4HSiC and Ni/Ti/4HSiC, Applied Surface Science, 258 (2012) 6819-6822.
[7] R. Madar, Materials science: Silicon carbide in contention, Nature, 430 (2004) 974-975.
[8] S. Yamada, B.-S. Song, T. Asano, S. Noda, Silicon carbide-based photonic crystal nanocavities for ultra-broadband operation from infrared to visible wavelengths, Applied Physics Letters, 99 (2011) 2011021-2011023.
[9] E. Omotoso, W.E. Meyer, F.D. Auret, A.T. Paradzah, M. Diale, S.M.M. Coelho, P.J. Janse van Rensburg, The influence of high energy electron irradiation on the Schottky barrier height and the Richardson constant of Ni/4H-SiC Schottky diodes, Materials Science in Semiconductor Processing, 39 (2015) 112-118.
[10] T. Marinova, A. Kakanakova-Georgieva, V. Krastev, R. Kakanakov, M. Neshev, L. Kassamakova, O. Noblanc, C. Arnodo, S. Cassette, C. Brylinski, B. Pecz, G. Radnoczi, G. Vincze, Nickel based ohmic contacts on SiC, Materials Science and Engineering: B, 46 (1997) 223-226.
[11] F. Auret, S. Goodman, G. Myburg, W. Meyer, Electrical characterization of defects introduced in n-GaAs by alpha and beta irradiation from radionuclides, Appl. Phys. A, 56 (1993) 547-553.
[12] T. Kimoto, A. Itoh, H. Matsunami, S. Sridhara, L. Clemen, R. Devaty, W. Choyke, T. Dalibor, C. Peppermüller, G. Pensl, Nitrogen donors and deep levels in high-quality 4H–SiC epilayers grown by chemical vapor deposition, Applied physics letters, 67 (1995) 2833-2835.
[13] A.A. Lebedev, Deep level centers in silicon carbide: A review, Semiconductors, 33 (1999) 107-130.
[14] T. Dalibor, G. Pensl, H. Matsunami, T. Kimoto, W.J. Choyke, A. Schöner, N. Nordell, Deep Defect Centers in Silicon Carbide Monitored with Deep Level Transient Spectroscopy, physica status solidi (a), 162 (1997) 199-225.
[15] I. Pintilie, L. Pintilie, K. Irmscher, B. Thomas, Formation of the Z1,2 deep-level defects in 4H-SiC epitaxial layers: Evidence for nitrogen participation, Applied Physics Letters, 81 (2002) 4841-4843.
[16] J. Doyle, M.K. Linnarsson, P. Pellegrino, N. Keskitalo, B. Svensson, A. Schoner, N. Nordell, J. Lindstrom, Electrically active point defects in n-type 4H–SiC, Journal of applied physics, 84 (1998) 1354-1357.

© University of Pretoria

UNIVERSITEIT VAN PRETORIA
UNIVERSITY OF PRETORIA
YUNIBESITHI YA PRETORIA

[17] G. Pensl, W.J. Choyke, Electrical and optical characterization of SiC, Physica B: Condensed Matter, 185 (1993) 264-283.
[18] L. Storasta, J.P. Bergman, E. Janzén, A. Henry, J. Lu, Deep levels created by low energy electron irradiation in 4H-SiC, Journal of Applied Physics, 96 (2004) 4909-4915.
[19] F. Nava, G. Bertuccio, A. Cavallini, E. Vittone, Silicon carbide and its use as a radiation detector material, Measurement Science and Technology, 19 (2008) 102001.
[20] C. Hemmingsson, N.T. Son, O. Kordina, J.P. Bergman, E. Janzén, J.L. Lindström, S. Savage, N. Nordell, Deep level defects in electron-irradiated 4H SiC epitaxial layers, Journal of Applied Physics, 81 (1997) 6155-6159.
[21] T.A.G. Eberlein, R. Jones, P.R. Briddon, Z_1/Z_2 Defects in 4H–SiC, Physical Review Letters, 90 (2003) 2255021-2255024.

© University of Pretoria

PAPER VII: Electrical characterization of 5.4 MeV alpha-particle irradiated 4H-SiC with low doping density

A. T. Paradzah, F. D. Auret, M. J. Legodi, E. Omotoso, and M. Diale

Nuclear Instruments and Methods in Physics Research Section B: Beam Interactions with Materials and Atoms 358 (2015): 112-116
doi:10.1016/j.nimb.2015.06.006

© University of Pretoria

UNIVERSITEIT VAN PRETORIA
UNIVERSITY OF PRETORIA
YUNIBESITHI YA PRETORIA

Nuclear Instruments and Methods in Physics Research B 358 (2015) 112–116

Contents lists available at ScienceDirect

Nuclear Instruments and Methods in Physics Research B

journal homepage: www.elsevier.com/locate/nimb

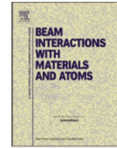

Electrical characterization of 5.4 MeV alpha-particle irradiated 4H-SiC with low doping density

A.T. Paradzah *, F.D. Auret, M.J. Legodi, E. Omotoso, M. Diale

Department of Physics, University of Pretoria, Pretoria 0002, South Africa

ARTICLE INFO

Article history:
Received 27 April 2015
Received in revised form 2 June 2015
Accepted 5 June 2015

Keywords:
n-Type 4H-SiC
Schottky diode
Deep level transient spectroscopy (DLTS)
Alpha particle irradiation
Defects

ABSTRACT

Nickel Schottky diodes were fabricated on 4H-SiC. The diodes had excellent current rectification with about ten orders of magnitude between −50 V and +2 V. The ideality factor was obtained as 1.05 which signifies the dominance of the thermionic emission process in charge transport across the barrier. Deep level transient spectroscopy revealed the presence of four deep level defects in the 30–350 K temperature range. The diodes were then irradiated with 5.4 MeV alpha particles up to fluence of 2.6×10^{10} cm^{-2}. Current–voltage and capacitance–voltage measurements revealed degraded diode characteristics after irradiation. DLTS revealed the presence of three more energy levels with activation enthalpies of 0.42 eV, 0.62 eV and 0.76 eV below the conduction band. These levels were however only realized after annealing the irradiated sample at 200 °C and they annealed out at 400 °C. The defect depth concentration was determined for some of the observed defects.

© 2015 Elsevier B.V. All rights reserved.

1. Introduction

Silicon Carbide (SiC) has excellent electronic and physical properties which include high electron drift velocity, high breakdown voltage, radiation hardness and high thermal conductivity [1]. These properties make SiC a suitable candidate for the fabrication of devices that can operate in harsh environments (exposed to radiation and/or at elevated temperatures).

Characteristics of electronic devices can be severely degraded by the presence of electrically active defects. The identification and control of as-grown and radiation induced defects is therefore important as the elimination or control of defect levels associated with these defects is required for effective device technology to progress [2]. While semiconductor materials have in-grown electronic defects, energetic particles such as electrons, protons, alpha particles, pions, neutrons and γ-ray photons can also cause bulk and/or surface damage in materials [3]. This damage leads to the formation of point defects and clusters resulting in the degradation of diode quality as they may lead to increased leakage current and decreased effective doping density [2].

It is therefore important to study and understand defects induced by radiation damage if a semiconductor is to be successfully used for fabrication of devices that can operate in harsh environments. Electron, proton and alpha particle irradiation has been performed on SiC to study the formation of defects and understand the hardness of the material. It has been observed from these studies that different types of irradiation induce the same types of defects in SiC but in different concentrations [4]. Alpha particle irradiation is however expected to cause more damage due to a superior mass compared to other forms of irradiation.

In this study, nickel Schottky contacts were fabricated on *n*-type 4H-SiC with a doping density of 3.7×10^{14} cm^{-3}. Deep level transient spectroscopy was performed to study the defects in the as-grown material and also to assess how alpha irradiation modifies these defects. Current–voltage (I–V) and capacitance–voltage (C–V) measurements were utilized to evaluate the effect of alpha irradiation on the quality of the diodes. Annealing studies were done to determine the thermal dynamics of both the as-grown and the radiation induced defects.

2. Experimental

4H-SiC with a low doping density of ~4×10^{14} cm^{-3} was used in this study. Sample degreasing was done by boiling in trichloroethylene (TCE), acetone and methanol for 5-min in each solution. This was followed by rinsing in de-ionized water before a 30-s dip in hydrofluoric acid (HF) to remove the native oxide layer. This was followed by rinsing in de-ionized water and a blow-dry using N_2 gas. A 300 nm thick nickel ohmic contact was resistively deposited onto the highly doped (1×10^{18} cm^{-3}) back side and annealed in flowing argon for 20 min at 950 °C. Cleaning was repeated as before except that, instead of boiling, 3 min rinsing in each of the

* Corresponding author.

http://dx.doi.org/10.1016/j.nimb.2015.06.006
0168-583X/© 2015 Elsevier B.V. All rights reserved.

© University of Pretoria

UNIVERSITEIT VAN PRETORIA
UNIVERSITY OF PRETORIA
YUNIBESITHI YA PRETORIA

three solvents were performed in an ultrasonic bath. Nickel Schottky contacts with a diameter of 0.6 mm and thicknesses of 100 nm were then resistively deposited onto the 3.7×10^{14} cm^{-3} doped side. Deep level transient spectroscopy (DLTS) measurements were carried out using a National Instruments Digital Acquisition (DAQ) based Laplace-DLTS system. Irradiation was done using a 5.4 MeV radioactive alpha source (Am-241) of dose rate 7.1×10^{6} cm^{-2} s^{-1} to fluences of up to 2.6×10^{10} cm^{-2}. The diodes were annealed after irradiation in steps of 100 °C in flowing argon gas up to 600 °C. TRIM simulation projected the alpha particles to peak at a depth of 24.8 μm below the nickel ohmic. Maximum vacancy concentration was also projected at a depth of 24.8 μm as 0.014 per Angstrom – Ion, translating to ~3.64×10^{18} vacancies.

3. Results and discussion

3.1. Current–voltage results

Forward I–V characteristics of the nickel Schottky contact before and after alpha irradiation to fluence of 2.6×10^{10} cm^{-2} (this fluence corresponds to 60 min of irradiation) are shown in Fig. 1. A linear current–voltage relationship was obtained before irradiation and the fitting was done using a thermionic emission model given by the relation [5,6]:

$$I_{S-M} = I_s[\exp(qV/nk_BT) - 1] \quad (1)$$

where I_{S-M} is the current flowing from the semiconductor into the metal, I_s is known as the saturation current, q is the electronic charge, V is the applied voltage, n is the ideality factor, k_B is the Boltzmann constant and T is the temperature at which the measurements were taken. The saturation current is given by the equation [5,6]:

$$I = AA^*T^2 \exp(-q\Phi_{b0}/nk_BT) \quad (2)$$

A is the effective Schottky diode area, A^* is the Richardson constant and Φ_{b0} is the zero bias Schottky barrier height.

The ideality factor is obtained from the gradient of the linear region of the I–V curves according to Eq. (1). Before irradiation, the ideality factor was obtained as 1.05, a close to unity value which shows that the thermionic emission model describes current flow across the metal–semiconductor interface sufficiently. After irradiation to fluence of 2.6×10^{10} cm^{-2}, the ideality factor increased to 1.35. The large ideality factor value obtained after irradiation implies that there are other current transport mechanisms in addition to the thermionic emission mechanism. The most probable additional current transport mechanism is generation–recombination current resulting from atomic displacements induced by alpha particle irradiation. This is also observed on the I–V curve obtained after irradiation, Fig. 1, which is non-linear especially at low voltages where the effect of thermionic emission is minimal. The Schottky barrier height was obtained from I–V measurements following Eq. (2). The Schottky barrier height was obtained as 1.21 eV before irradiation and an increase to 1.28 eV was observed after a total alpha-particle fluence of 2.6×10^{10} cm^{-2}. The increase in the SBH is very small and this allows for the continued normal operation of the Schottky diodes.

The reverse leakage current was measured to voltages of −50 V. Reverse leakage current curves obtained before irradiation and after a total irradiation fluence of 2.6×10^{10} cm^{-2} are presented in Fig. 2. Low leakage current values are observed showing good rectification quality of the SiC Schottky diodes. An increase in the leakage current is observed with increasing reverse bias. This is attributed to Schottky barrier lowering, a phenomena where the SBH is lowered as the electric field resulting from external biasing increases [7].

The reverse current obtained at −50 V increased from 9.0×10^{-12} A to 1.2×10^{-11} A after irradiation. The increase in the leakage current show the effect of irradiation where defects induced by irradiation are suggested to be responsible for the increase. However the diode rectification was retained after irradiation and this shows that SiC is a radiation hard semiconductor. The current measured at applied voltages of −50 V and +2 V changes by approximately ten orders of magnitude even after irradiation which shows good rectification of SiC.

3.2. Capacitance–voltage results

The effects of alpha-particle irradiation on the free carrier concentration and the SBH were evaluated using C–V measurements. The free carrier concentration N_D and the SBH Φ_{Bn} were respectively determined from the slope and the intercept of the graph of $1/C^2$ vs. V, Fig. 3. N_D was obtained according to the relation [7]:

$$\frac{d(1/C^2)}{dV} = \frac{2}{A^2 \epsilon_0 \epsilon_s q N_D} \quad (3)$$

where C is the depletion width capacitance and ϵ_s is the semiconductor permittivity, and ϵ_0 is the permittivity of free space. The SBH was obtained from [7]:

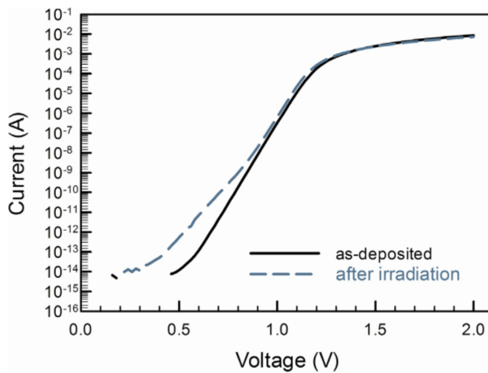

Fig. 1. Forward current–voltage curves obtained before and after 5.4 MeV alpha particle irradiation to fluence of 2.6×10^{10} cm^{-2}.

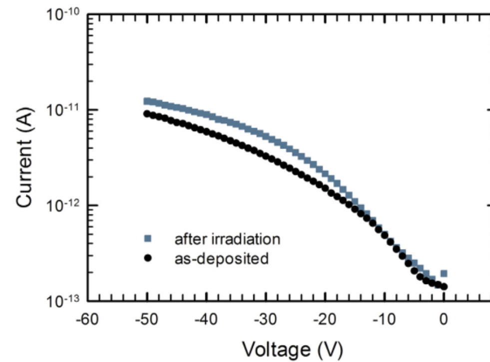

Fig. 2. Reverse leakage current curves measured up to −50 V before and after alpha particle irradiation to fluence of 2.6×10^{10} cm^{-2}.

© University of Pretoria

UNIVERSITEIT VAN PRETORIA
UNIVERSITY OF PRETORIA
YUNIBESITHI YA PRETORIA

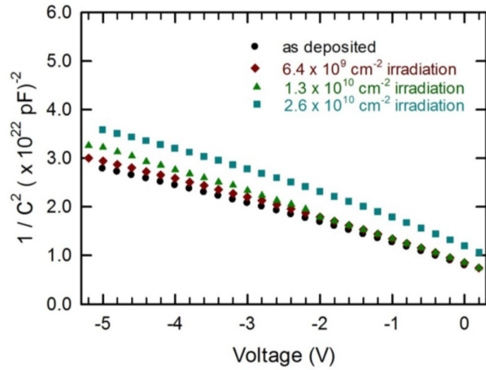

Fig. 3. $1/C^2$ graphs obtained before and after alpha particle irradiation at indicated fluences to $2.6 \times 10^{10}\,cm^{-2}$.

$$\Phi_{Bn} = V_{bi} + V_n + \frac{k_B T}{q} - \Delta\Phi \quad (4)$$

where $\Delta\Phi$ is the Schottky barrier lowering due to the image force effect, V_n is the depth of the Fermi level below the conduction band and is obtained from the relation:

$$V_n = \frac{k_B T}{q} \ln\left(\frac{N_c}{N_D}\right) \quad (5)$$

V_{bi} is the built in potential which is obtained as the voltage intercept of the linear C–V relationship, Fig. 3 and N_c is the effective density of states in the conduction band.

The SBH was obtained as 1.86 eV before irradiation and it increased to 2.02 eV after irradiation to fluence of $2.6 \times 10^{10}\,cm^{-2}$. The increase in the SBH can be seen from Fig. 3 where the voltage intercept of the $1/C^2$ vs. V curve increases after irradiation. There were no major changes in the curves at intermediate irradiation fluences. The SBH obtained through capacitance–voltage measurements is larger than that obtained from current–voltage measurements. This is due to the inhomogeneity of the metal–semiconductor interface where electrons crosses the junction via "small barrier regions" hence the smaller I–V measured SBH [8].

The free carrier concentration decreased from $4.9 \times 10^{14}\,cm^{-3}$ before irradiation to $2.9 \times 10^{14}\,cm^{-3}$ after irradiation to fluence of $2.6 \times 10^{10}\,cm^{-3}$. Non-linear curves of $1/C^2$ against voltage, shows that the free carrier concentration is not constant below the metal–semiconductor junction. This is also shown by the depth profiles, Fig. 4. The decrease in the free carrier concentration is an indication that defects were introduced by irradiation and the defects are of acceptor-like nature hence they trap the free carriers leading to the observed reduction. Some recovery in the free carrier concentration was observed after annealing the irradiated diodes at 200 °C and annealing to 600 °C did not lead to further recovery.

The reduction in the free carrier concentration with irradiation can be quantified by the free carrier removal rate. The free carrier removal rate is obtained from the slope of the graph of $\Delta(N_D - N_A)/\Phi$, Φ being the fluence and $\Delta(N_D - N_A)$ is the change in the free carrier concentration [9]. The free carrier removal rate was obtained after irradiating the diodes at three different fluences up to $2.6 \times 10^{10}\,cm^{-2}$ as $15 \times 101\,cm^{-1}$. This is a large value and is a result of the high energy (5.4 MeV) of the irradiating alpha particles. Alpha particles are also heavy particles compared to most particles used in irradiation studies hence more damage is realized leading to this large value.

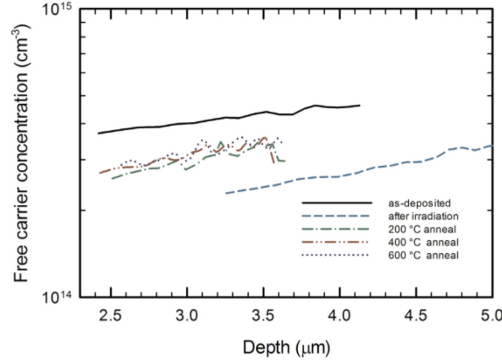

Fig. 4. Free carrier concentration depth profiles obtained before irradiation, after alpha particle irradiation to fluence of $2.6 \times 10^{10}\,cm^{-2}$ and at subsequent annealing temperatures.

Table 1
Diode characteristics before and after 5.4 MeV alpha irradiation to fluence of $2.6 \times 10^{10}\,cm^{-2}$.

	Ideality factor	Φ_{IV} (eV)	Φ_{CV} (eV)	Leakage current (A) at −50 V bias	Free carrier density (cm^{-3})
Before irradiation	1.05	1.21	1.86	9.0×10^{-12}	4.9×10^{14}
After irradiation	1.35	1.28	2.09	1.2×10^{-11}	2.9×10^{14}

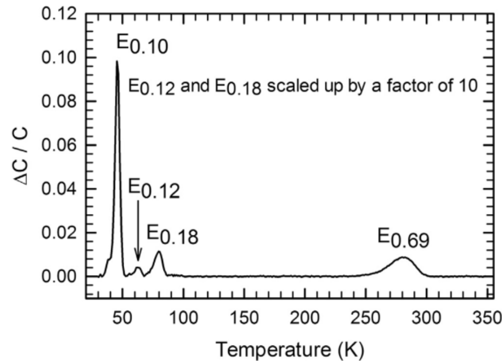

Fig. 5. DLTS spectra for the as deposited sample. Spectra obtained at constant reverse bias of −5 V, filling pulse of −1 V and rate window of $2.5\,s^{-1}$.

The Schottky barrier parameters obtained before irradiation and after $2.6 \times 10^{10}\,cm^{-2}$ alpha-particle irradiation are summarized in Table 1.

3.3. DLTS results

The DLTS spectra obtained from the as-deposited material, Fig. 5 shows the presence of four energy levels which have been labeled $E_{0.10}$, $E_{0.12}$, $E_{0.18}$ and $E_{0.69}$. These have activation energies of E_c − 0.10 eV, E_c − 0.12 eV, E_c − 0.18 eV and E_c − 0.69 eV respectively. The capture cross sections of the levels and respective attributions are presented in Table 2.

© University of Pretoria

UNIVERSITEIT VAN PRETORIA
UNIVERSITY OF PRETORIA
YUNIBESITHI YA PRETORIA

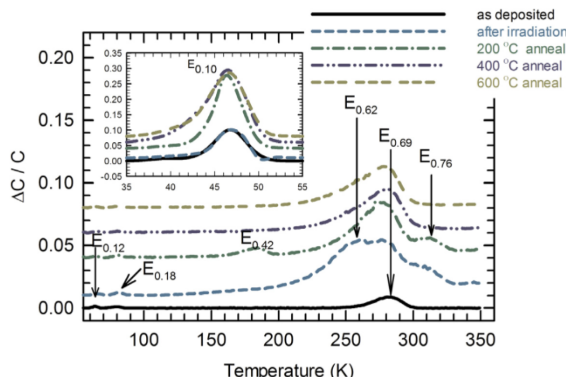

Fig. 6. DLTS spectra for the as deposited sample, after alpha particle irradiation to fluence of 2.6×10^{10} cm^{-2} and after successive annealing temperatures. Spectra obtained at constant reverse bias of −5 V, filling pulse of −1 V and rate window of 2.5 s^{-1}.

Table 2
As grown and defects observed by DLTS in 4H-SiC after 5.4 MeV irradiation and annealing.

Trap level	$E_c - E_t$ (eV)	σ_n (cm^2)	N_T before irradiation (cm^{-3})	N_T after irradiation (cm^{-3})	Attribution
$E_{0.10}$	0.10	7×10^{-14}	9.4×10^{13}	6.0×10^{13}	*N* impurity – [22]
$E_{0.12}$	0.12	1×10^{-14}	2.2×10^{11}	2.3×10^{11}	Ti impurity – [21]
$E_{0.18}$	0.18	1×10^{-14}	5.4×10^{11}	6.0×10^{13}	Ti impurity – [11,14]
$E_{0.42}$	0.42	1×10^{-15}	–	2.8×10^{13}	V_{Si} – [21]
$E_{0.69}$	0.69	2×10^{-14}	8.2×10^{12}	9.4×10^{13}	Z_1/Z_2 – [18]
$E_{0.62}$	0.62	–	–	–	–
$E_{0.76}$	0.76	1×10^{-14}	–	5.0×10^{13}	–

The defect $E_{0.10}$ has been attributed to nitrogen dopants occupying cubic sites [10,11]. When occupying a hexagonal site in 4H-SiC, this defect level is expected to have an activation energy of ~0.050 eV [12,13]. This level is the nitrogen donor responsible for the *n*-type doping in SiC.

The $E_{0.12}$ and $E_{0.18}$ levels are related to transitional metal titanium [11,14]. To within experimental error, Achtziger et al. [14] observed and attributed the $E_{0.12}$ defect level to titanium impurity. A defect level with energy E_c – 0.18 eV has also been reported and associated with a titanium impurity [11]. The $E_{0.12}$ and $E_{0.18}$ levels could both be a single defect occupying different geometrical positions in the material, where it is seen as $E_{0.12}$ when occupying a hexagonal site while it is seen as $E_{0.18}$ when occupying a cubic lattice site [14].

The $E_{0.69}$ level is a prominent defect that is found in 4H-SiC. While the defect level is widely agreed to be of intrinsic nature, there is no agreement on the exact structure of the defect. The possible structure of the defect has been attributed to a silicon vacancies, carbon vacancies, silicon and carbon antisite complexes [15–18]. The structure of the defect has essentially been linked to nearly all possible intrinsic defects that can be found in SiC. Low energy and high energy particle irradiation measurements have been performed to possibly link the defect structure of the defect to either carbon or silicon exclusively but this did not solve the puzzle [19,20].

Fig. 6 shows normalized DLTS spectra taken before irradiation, after irradiation and after annealing from 200 °C to 600 °C. After irradiation the $E_{0.69}$ level broadens and shows an increase in intensity. The broadening of the $E_{0.69}$ level after irradiation is possibly due to presence of more energy levels which may be contained within the level. The sample was then annealed to possibly separate these energy levels. After annealing at 200 °C, three defects

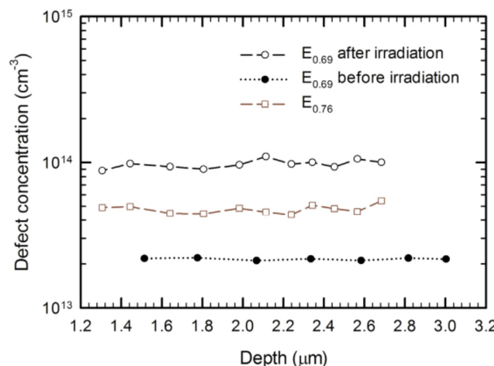

Fig. 7. Depth concentration profiles for defects $E_{0.69}$ (before and after irradiation) and $E_{0.76}$.

$E_{0.42}$, $E_{0.62}$ and $E_{0.76}$ with energies E_c – 0.42 eV, E_c – 0.62 eV and E_c – 0.76 eV were observed. The apparent capture cross sections of the observed defects were calculated from Arrhenius plots to be 1×10^{-15} cm^2, 2×10^{-14} cm^2 and 1×10^{-14} cm^2, respectively.

Defects $E_{0.42}$ and $E_{0.76}$ have been reported in previous studies [2,11]. Level $E_{0.42}$ is attributed to silicon vacancies while $E_{0.76}$ has not been assigned any particular structure [21]. Doyle et al. [2] observed the two defects after electron irradiation and isochronal annealing with the defects only being observed after annealing at 200 °C. Castaldini et al. [11], also observed the same defects after both electron and proton irradiation and suggests the defects are

© University of Pretoria

UNIVERSITEIT VAN PRETORIA
UNIVERSITY OF PRETORIA
YUNIBESITHI YA PRETORIA

intrinsic. These levels were annealed out at 400 °C in this study. The fact that defects $E_{0.42}$ and $E_{0.76}$ were observed after the same particle fluence and annealed out after the same heat treatment suggests that the defects might be closely related structurally.

The concentration of the $E_{0.69}$ level increases significantly after irradiation and remains relatively stable up to the 600 °C annealing temperature. The possibility that this level is linked to carbon vacancies and/or interstitials or carbon divacancies can therefore be easily comprehended in the light of this increase in concentration after irradiation. Previous studies done on this defect suggest it could be a defect complex composed of several energy levels [18,21]. Hemmingsson et al. [20] reported that the defect $E_{0.69}$, commonly referred to as the Z_1/Z_2 is composed of two closely spaced levels that have negative U behavior. It was also established in this study that after alpha particle irradiation to a fluence of $2.6 \times 10^{10}\,cm^{-2}$, a defect with an energy of $E_c - 0.62$ eV appears on the lower temperature side of $E_{0.69}$. This defect is however not stable and was annealed out at 200 °C.

Depth concentrations of defects $E_{0.69}$ and $E_{0.76}$ were determined from Laplace-DLTS measurements by varying the voltages pulses and are presented in Fig. 7. The depth concentration of defect $E_{0.69}$ was obtained before and after particle irradiation for comparison and an increase resulting from irradiation is clear. It is seen from the graph that the concentration of both defects is constant in the investigated depth range. This is in agreement with the prediction of SRIM simulations where the vacancy concentration is constant to a depth of ~24 μm.

Levels $E_{0.12}$ and $E_{0.18}$ were not noticeably affected by irradiation. The concentration of the level $E_{0.10}$ increased after annealing at 200 °C without showing further changes at higher annealing temperatures. While the $E_{0.10}$ level is almost definitely a nitrogen impurity, it is not clear what the source of the increase in concentration after irradiation is. The defect parameters for the observed defects are summarized in Table 2.

4. Conclusions

I–V, *C–V* and DLTS measurements were used to evaluate the effect of 5.4 MeV alpha-particle irradiation on nickel Schottky diodes fabricated on nitrogen doped 4H-SiC. After irradiation to fluence of $2.6 \times 10^{10}\,cm^{-2}$, the Schottky diodes retained rectification showing the radiation hardness of SiC. A large free carrier removal rate was obtained from *C–V* measurements indicating the presence of acceptor like defects as a result of irradiation. DLTS measurements revealed the presence of deep level defects before irradiation and three other deep level defects were observed after alpha-particle irradiation. The irradiation induced defects were all annealed out at temperatures below 600 °C.

Acknowledgement

The authors would like to acknowledge the National Research Foundation (NRF) of South Africa for financial support

References

[1] K. Danno, D. Nakamura, T. Kimoto, Appl. Phys. Lett. 90 (2007) 202109.
[2] J.P. Doyle, M.O. Aboelfotoh, B.G. Svensson, A. Schoner, N. Nordell, Diam. Relat. Mater. 6 (1997) 1388.
[3] F. Roccaforte, C. Bongiorno, F. La Via, V. Raineri, Appl. Phys. Lett. 85 (2004) 6152.
[4] A.A. Lebedev, A.I. Veinger, D.V. Davydov, V.V. Kozlovski, N.S. Savkina, A.M. Strel'chuk, J. Appl. Phys. 88 (2000) 6265.
[5] K.P. Schoen, J.M. Woodall, J.A. Cooper Jr., M.R. Melloch, Electron devices, IEEE Trans. Electron. Devices 45 (1998) 1595.
[6] S.K. Cheung, N.W. Cheung, Appl. Phys. Lett. 49 (1986) 85.
[7] S.M. Sze, K.K. Ng, Physics of Semiconductor Devices, John Wiley & Sons, New Jersey, 2007.
[8] F. Roccaforte, F. La Via, V. Raineri, R. Pierobon, E. Zanoni, J. Appl. Phys. 93 (2003) 9137.
[9] F.D. Auret, S.A. Goodman, M. Hayes, M.J. Legodi, H.A. van Laarhoven, D.C. Look, Appl. Phys. Lett. 79 (2001) 3074.
[10] T. Kimoto, A. Itoh, H. Matsunami, S. Sridhara, L.L. Clemen, R.P. Devaty, W.J. Choyke, T. Dalibor, C. Peppermuller, G. Pensl, Appl. Phys. Lett. 67 (1995) 2833.
[11] A. Castaldini, A. Cavallini, L. Rigutti, F. Nava, S. Ferrero, F. Giorgis, J. Appl. Phys. 98 (2005) 053706.
[12] A.O. Evwaraye, S.R. Smith, W.C. Mitchel, MRS Online Proc. Libr. 410 (1995) 57.
[13] C.Q. Chen, J. Zeman, F. Engelbrecht, C. Peppermüller, R. Helbig, Z.H. Chen, G. Martinez, J. Appl. Phys. 87 (2000) 3800.
[14] N. Achtziger, W. Witthuhn, Appl. Phys. Lett. 71 (1997) 110.
[15] T. Hiyoshi, T. Kimoto, Appl. Phys. Express 2 (2009) 091101.
[16] L. Storasta, J.P. Bergman, E. Janzén, A. Henry, J. Lu, J. Appl. Phys. 96 (2004) 4909.
[17] J. Zhang, L. Storasta, J.P. Bergman, N.T. Son, E. Janzén, J. Appl. Phys. 93 (2003) 4708.
[18] I. Pintilie, L. Pintilie, K. Irmscher, B. Thomas, Appl. Phys. Lett. 81 (2002) 4841.
[19] F.C. Beyer, C. Hemmingsson, H. Pedersen, A. Henry, J. Isoya, N. Morishita, T. Ohshima, E. Janzen, Phys. Scripta T141 (2010) 014006.
[20] C. Hemmingsson, N.T. Son, O. Kordina, J.P. Bergman, E. Janzen, J.L. Lindstrom, S. Savage, N. Nordell, J. Appl. Phys. 81 (1997) 6155.
[21] T.A.G. Eberlein, R. Jones, P.R. Briddon, Phys. Rev. Lett. 90 (2003) 225502.
[22] A. Castaldinia, A. Cavallinia, L. Polentaa, F. Navab, C. Canalic, C. Lanzierid, Appl. Surf. Sci. 187 (2002) 248.

© University of Pretoria

4.7 References

1. Zhao, J.H., K. Sheng, and R.C. Lebron-Velilla, *Silicon carbide schottky barrier diode.* International Journal of High Speed Electronics and Systems, 2005. **15**(04): p. 821-866.

2. Omotoso, E., et al., *Effects of 5.4 MeV alpha-particle irradiation on the electrical properties of nickel Schottky diodes on 4H–SiC.* Nuclear Instruments and Methods in Physics Research Section B: Beam Interactions with Materials and Atoms, 2015: p. 5.

3. Hökelek, E. and G.Y. Robinson, *Schottky contacts on chemically etched p- and n-type indium phosphide.* Applied Physics Letters, 1982. **40**(5): p. 426-428.

4. Crowell, C.R., *Richardson constant and tunneling effective mass for thermionic and thermionic-field emission in Schottky barrier diodes.* Solid-State Electronics, 1969. **12**(1): p. 55-59.

5. Crowell, C.R., *The physical significance of the T0 anomalies in Schottky barriers.* Solid-State Electronics, 1977. **20**(3): p. 171-175.

6. Kozlovski, V. and V. Abrosimova, *Radiation defect engineering.* International Journal of High Speed Electronics and Systems, 2005. **15**(01): p. 1-253.

7. Auret, F., et al., *Electrical characterization of argon ion sputter-induced defects in GaAs.* South African Journal Science, 1991. **87**(3): p. 127-129.

8. Auret, F.D., et al., *Electrical characterization of defects introduced in n-Si during electron beam deposition of Pt.* Physica Status Solidi (A), 2012. **209**(10): p. 1926-1933.

9. Auret, F.D., et al., *Electrical characterization of defects introduced during electron beam deposition of Pd Schottky contacts on n-type Ge.* Applied Physics Letters, 2006. **88**(24): p. 242110.

10. Coelho, S.M.M., et al., *IV and CV measurements of Schottky diodes deposited on Ge by electron beam and sputter deposition.* Physica Status Solidi (C) Current Topics in Solid State Physics, 2008. **5**(2): p. 626-629.

11. Coelho, S.M.M., et al., *Electrical characterization of defects introduced in n-Ge during electron beam deposition or exposure.* Journal of Applied Physics, 2013. **114**(17): p. 1737081-1737088.

12. Saxena, V. and R. Prakash, *Effect of steric hinderance on junction properties of poly (3-alkylthiophene)s based schottky diodes.* Polymer Bulletin, 2000. **45**(3): p. 267-274.

13. Son, N.T., et al., *Negative-U System of Carbon Vacancy in 4H-SiC.* Physical Review Letters, 2012. **109**(18): p. 187603.

© University of Pretoria

14. Tung, R.T., *Recent advances in Schottky barrier concepts.* Materials Science and Engineering: R: Reports, 2001. **35**(1): p. 1-138.

© University of Pretoria

Chapter 5

Conclusions

Electrical characterization of process- and irradiation-induced defects in *n*-type 4H-SiC has been successfully achieved using the current-voltage, capacitance-voltage and deep-level transient spectroscopy techniques. Conclusions specific to each of the experimental results have been presented in the Papers 1 to 7 or at the end of each section in Chapter 4.

The qualities of the as-grown Ni/4H-SiC devices fabricated resistively were tested using *I-V* and *C-V* measurements. The devices were of good quality with ideality factor close to unity (1.04), the barrier height of 1.25 eV and reverse current of 10^{-14} A. The samples were also successfully characterized by deep-level transient spectroscopy which revealed the presence of four electrically active levels in the as-grown material with energies of approximately 0.10, 0.12, 0.16 and 0.65 eV below the conduction band minimum.

The diodes fabricated by resistive evaporation were intentionally irradiated with alpha-particle and high-energy electron irradiation at various fluences, and characterized by means of *I-V* and *C-V* measurements. The electrical properties of the samples deviated slightly based on the type of irradiation and fluence received. However, the diodes retained their good quality (ideality factor less than 2) much better compared to devices manufactured on conventional semiconductors (such as Si, Ge and GaAs). The electrically active defects present after irradiation were characterized by means of DLTS and high-resolution Laplace DLTS. The high-energy electron irradiation introduced three new defects with energies E_C – 0.22, E_C – 0.40 and E_C – 0.71 eV that were not observed in the as-grown material and also caused an increase in concentration of defects with energies E_C – 0.10 and E_C – 0.65 eV present in as-grown SBDs. Two extra electrically active defects with energies E_C – 0.39 and E_C – 0.62 eV were present after bombardment with alpha-particles. The alpha-particle irradiation also caused a significant increase in the concentration of the defects with energies E_C – 0.10 and E_C – 0.65 eV and also a slight change in their energies. Laplace DLTS was successfully used to

© University of Pretoria

split defect with energy E_C – 0.42 eV observed by conventional DLTS into E_C – 0.39 and E_C – 0.42 eV which were assumed to be due to the same defect. Also, the E_C – 0.65 and E_C – 0.70 with closely spaced emission rates were split by Laplace DLTS to three defects with energies E_C – 0.65, E_C – 0.70 and E_C – 0.76 eV. The defects with energies E_C – 0.39 and E_C – 0.40 eV were assigned to silicon or carbon vacancy which shows acceptor-like behaviour. While the defects with energy levels E_C – 0.65, E_C – 0.70 and E_C – 0.76 eV were assigned to the carbon vacancy, an intrinsic defect. The structures of defects with energy levels E_C – 0.22 and E_C – 0.76 eV have not yet been confirmed.

Electron-beam deposition (EBD) introduced two additional defects with energies E_C – 0.42 and E_C – ~0.70 eV during the process of depositing high melting point metal (W) on 4H-SiC substrate. The defects were characterized by DLTS and it was observed that the defects were close to the metal-semiconductor junction. Also, electron-beam exposure of the substrate with a thin metal layer to electron beam conditions without metal deposition induced two electrically-active defects similar to EBD. These electrically-active defects with energies, E_C – 0.42 and E_C – ~0.70 eV, may be caused by the product of elastic collisions between 10 keV electrons and residual vacuum gases which were ionized around the filament and accelerated by the electric field towards the substrate. The assignments of these defects were determined by comparing their signatures with the defects introduced by high-energy particle irradiation, showing that EBD and EBE also introduce the E_C – 0.42 and E_C – ~0.70 eV (Z_1/Z_2) defects related to the carbon vacancy in 4H-SiC SBDs.

The low-temperature *I-V* characteristics of 4H-SiC SBDs displayed strong temperature dependence. Thermionic emission was the predominant current transport mechanism at high temperatures (i.e. close to room temperature) while other forms of current transport mechanisms (such as generation-recombination) became dominant at lower temperatures. The Schottky barrier heights decreased and ideality factor increased with decreasing temperature. The decrease in barrier height in *I-V* measurements has been attributed to barrier inhomogeneities at the metal–4H-SiC interface. In contrast, unreasonably large barrier heights calculated from *C-V* characteristics at lower temperatures. This was attributed to the carrier freeze out that modified the electric field, thereby affecting the junction capacitance and the value of the built-in voltage as determined from the intercept on the voltage axis. Also, irradiation by high-energy

© University of Pretoria

particles did influence the modified Richardson constant but had no effect on the mean barrier height of the devices.

The main conclusion that can be drawn from this study is that silicon carbide has properties that make it very promising to provide solutions to frequent damage of devices used in aerospace, manufacturing industries, defence and radiation harsh environments.

5.1 Further research

- Characterization of defects introduced by the following:
  - ✓ proton and deuterium irradiation at different fluences
  - ✓ high energy and thermal neutron irradiation at different fluences
  - ✓ sputter damage of 4H-SiC at different energies
  - ✓ inductive coupling plasma etching of 4H-SiC
  - ✓ in situ low temperature irradiation and DLTS measurements to be carried out in the in-situ irradiation facility.
- Identification of defects' structure by photoluminescence, electron-paramagnetic resonance, positron annihilation, etc.
- Annealing kinetics of defects in as-grown 4H-SiC.
- Critical study of defects assigned to nitrogen impurities.
- Temperature dependent *I-V* and *C-V* measurements at high temperatures.

© University of Pretoria

Appendix A

List of publications and conferences attended

This appendix contains list of all publications and other research outputs published, accepted in peer review journal or in manuscript form to be submitted for publication.

A.1 List of Publications

I. **E. Omotoso**, W. E. Meyer, F. D. Auret, A. T. Paradzah, M. Diale, S. M. M. Coelho, PJ Janse van Rensburg, and P. N. M. Ngoepe. Effects of 5.4 MeV alpha-particle irradiation on the electrical properties of nickel Schottky diodes on 4H-SiC. *Nuclear Instruments and Methods in Physics Research Section B: Beam Interactions with Materials and Atoms* 365A (2015): 264-268. doi:10.1016/j.nimb.2015.07.019.

II. **E. Omotoso**, W. E. Meyer, F. D. Auret, A. T. Paradzah, M. Diale, S. M. M. Coelho, and P. J Janse van Rensburg. The influence of high energy electron irradiation on the Schottky barrier height and the Richardson constant of Ni/4H-SiC Schottky diodes. *Materials Science in Semiconductor Processing* 39 (2015): 112-118. doi:10.1016/j.mssp.2015.04.031.

III. **E. Omotoso**, W. E. Meyer, F. D. Auret, M. Diale, and P. N. M. Ngoepe. Response of Ni/4H-SiC Schottky barrier diodes to alpha-particle irradiation at different fluences. *Physica B: Condensed Matter* 480 (2015): 196-200. doi:10.1016/j.physb.2015.08.014.

IV. **Ezekiel Omotoso**, Walter. E. Meyer, F. Danie. Auret, Alexander. T. Paradzah, and Matshisa J. Legodi. Electrical characterization of deep levels created by bombarding nitrogen-doped 4H-SiC with alpha-particle irradiation. *Nuclear Instruments and Methods in Physics Research Section B: Beam Interactions with Materials and Atoms* (2015): doi:10.1016/j.nimb.2015.09.084.

V. **Ezekiel Omotoso**, Walter Ernst Meyer, Francois Danie Auret, and Sergio Manuel Martins Coelho. Electrical characterization of defects introduced during electron beam deposition of W Schottky barrier diodes on *n*-type 4H-SiC. *Manuscript*.

© University of Pretoria

VI. **Ezekiel Omotoso**, Walter Ernst Meyer, Francois Danie Auret, Sergio Manuel Martins Coelho, and Phuti Ngako Mahloka Ngoepe. Electrical characterization of defects introduced in *n*-type N-doped 4H-SiC during electron beam exposure. *Solid State Phenomena, Trans Tech Papers* 242 (2015): 427-433. doi: 10.4028/www.scientific.net/SSP.242.427.

VII. A. T. Paradzah, F. D. Auret, M. J. Legodi, **E. Omotoso**, and M. Diale. Electrical characterization of 5.4 MeV alpha-particle irradiated 4H-SiC with low doping density. *Nuclear Instruments and Methods in Physics Research Section B: Beam Interactions with Materials and Atoms* 358 (2015): 112-116. doi:10.1016/j.nimb.2015.06.006.

VIII. **E. Omotoso**, W. E. Meyer, F. D. Auret, and M. Diale. Effect of room temperature annealing on Ni/4H-SiC Schottky barrier diodes after alpha-particle irradiation at high fluence. *Submitted for proceeding South African Institute of Physics 2015*.

A.2 List of national and international conferences

I. **E. Omotoso**, W. E. Meyer, F. D. Auret, S. M. M. Coelho, and P. N. M. Ngoepe "Characterization of temperature dependence of the electron capture cross section of E-center in Sb-doped germanium", The 59th Annual Conference of the South Africa Institute of Physics hosted by the University of Johannesburg, 7th – 11th July, 2014. ***Poster presentation***.

II. P. N. M. Ngoepe, W. E. Meyer, F. D. Auret, **E. Omotoso**, S. M. M. Coelho, and M. Diale "A DLTS investigation of the annealing behaviour of the E-center in alpha-particle irradiated Ge", The 59th Annual Conference of the South Africa Institute of Physics hosted by the University of Johannesburg, 7th – 11th July, 2014. ***Poster presentation.***

III. **E. Omotoso**, W. E. Meyer, F. D. Auret, A. T. Paradzah, J. P. Janse Van Rensburg, S. M. M. Coelho, P. N. M. Ngoepe, and M. Diale "Effect of 5.4 MeV alpha-particles irradiation on electrical properties of nickel Schottky diodes on 4H-SiC", The 19th International Conference on Ion Beam Modification of Materials (IBMM 2014) held in Leuven, Belgium, 14th – 19th September, 2014. ***Poster presentation***.

IV. **E. Omotoso**, W. E. Meyer, F. D. Auret, M. Diale S. M. M. Coelho, and P. N. M. Ngoepe "Response of Ni/4H-SiC Schottky barrier diodes to alpha-particle

© University of Pretoria

irradiation at different fluences", The 6th South African Conference on Photonics Materials (SACPM 2015) held in Mabula Game Lodge, South Africa, 4th – 8th May, 2015. ***Oral presentation***.

V. P. N. M. Ngoepe, W. E. Meyer, M. Diale, F. D. Auret, **E. Omotoso**, H. C. Swart, M. M. Duvenhage, and E. Coetsee "Chemical and electrical characteristics of annealed Ni/Au and Ni/IR/Au contacts on AlGaN", The 6th South African Conference on Photonics Materials (SACPM 2015) held in Mabula Game Lodge, South Africa, 4th – 8th May, 2015. ***Poster presentation***.

VI. **E. Omotoso**, M. Schmidt, W. E. Meyer, J. P. Janse Van Rensburg, and F. D. Auret "Low-temperature alpha-particle irradiation of Pd 4H-SiC Schottky barrier diodes", The 6th South African Conference on Photonics Materials (SACPM 2015) held in Mabula Game Lodge, South Africa, 4th – 8th May, 2015. ***Poster presentation***.

VII. **E. Omotoso**, W. E. Meyer, F. D. Auret, and M. Diale "Electrical characterization of deep level created by bombarding nitrogen-doped 4H-SiC with alpha-particle irradiation", The 22nd International Conference on Ion Beam Analysis held in Opatija, Croatia, 14th – 19th June, 2015. ***Poster presentation***.

VIII. **E. Omotoso**, W. E. Meyer, F. D. Auret, and M. Diale "Effect of temperature annealing on 4H-SiC Schottky barrier diodes after alpha-particle irradiation at high fluences", The 60th Annual Conference of the South Africa Institute of Physics hosted by the Nelson Mandela Metropolitan University, 29th June – 3rd July, 2015. ***Poster presentation***.

IX. M. Diale, M. J. Legodi, **E. Omotoso**, and F. D. Auret "Electrical characterization of MeV alpha-particle irradiated Ni/4H-SiC diodes and their recovery by annealing treatment", The 60th Annual Conference of the South Africa Institute of Physics hosted by the University of Johannesburg, 29th June – 3rd July, 2015. ***Oral presentation***.

X. **E. Omotoso**, W. E. Meyer, F. D. Auret, S. M. M. Coelho, M. Diale, and P. N. M. Ngoepe "Electrical characterization of defects introduced during electron beam deposition of W Schottky contacts on n-type 4H-SiC", The 28th International Conference on Defects in Semiconductors held in Aalto University, Espoo, Finland, 27th – 31st July, 2015. ***Poster presentation***.

© University of Pretoria

XI. P. N. M. Ngoepe, W. E. Meyer, M. Diale, F. D. Auret, S. M. M. Coelho, and **E. Omotoso** "DLTS characterization of defects in GaN introduced by electron beam exposure", The 28th International Conference on Defects in Semiconductors held in Aalto University, Espoo, Finland, 27th – 31st July, 2015. ***Poster presentation***.

XII. **E. Omotoso**, W. E. Meyer, F. D. Auret, S. M. M. Coelho, M. Diale, P. N. M. Ngoepe "Electrical characterization of defects introduced in n-type N-doped 4H-SiC during electron beam exposure", Gettering and Defect Engineering in Semiconductor Technology (GADEST) XVI, Bad Staffelstein, Germany, 20th – 25th September, 2015. ***Poster presentation***.

© University of Pretoria

Appendix B

Deep level defects analyzed in 4H-SiC

The Table B.1 show the summary of deep level defects observed and characterized by deep-level transient spectroscopy (DLTS) and high-resolution Laplace DLTS in 4H-SiC during this study after various processing and irradiation techniques.

© University of Pretoria

Table B.1: Deep level defects observed and characterized in 4H-SiC during this study.

Process	Defect label	E_T (eV)	σ_a (cm^2)	Defect ID
Resistive evaporation	$E_{0.10}$	$E_C - 0.10$	3×10^{-12}	N
	$E_{0.12}$	$E_C - 0.12$	1×10^{-15}	Ti
	$E_{0.16}$	$E_C - 0.16$	1×10^{-15}	Ti
	$E_{0.65}$	$E_C - 0.65$	4×10^{-15}	V_C (Z_1/Z_2)
Alpha-particle irradiation	$E_{0.10}$	$E_C - 0.10$	2×10^{-12}	N
	$E_{0.12}$	$E_C - 0.12$	1×10^{-15}	Ti
	$E_{0.16}$	$E_C - 0.16$	3×10^{-15}	Ti
	$E_{0.39}$	$E_C - 0.39$	2×10^{-15}	$V_{C/Si}$
	$E_{0.61}$	$E_C - 0.61$	5×10^{-15}	V_C (Z_1/Z_2)
	$E_{0.70}$	$E_C - 0.70$	6×10^{-15}	V_C (Z_1/Z_2)
High-energy electron irradiation	$E_{0.10}$	$E_C - 0.10$	1×10^{-16}	N
	$E_{0.12}$	$E_C - 0.12$	4×10^{-12}	Ti
	$E_{0.16}$	$E_C - 0.16$	1×10^{-15}	Ti
	$E_{0.22}$	$E_C - 0.22$	2×10^{-17}	?
	$E_{0.40}$	$E_C - 0.40$	3×10^{-15}	$V_{C/Si}$
	$E_{0.65}$	$E_C - 0.65$	3×10^{-15}	V_C (Z_1/Z_2)
	$E_{0.70}$	$E_C - 0.70$	3×10^{-15}	V_C (Z_1/Z_2)
Electron-beam exposure	$E_{0.10}$	$E_C - 0.10$	1×10^{-11}	N
	$E_{0.12}$	$E_C - 0.12$	2×10^{-16}	Ti
	$E_{0.16}$	$E_C - 0.16$	2×10^{-15}	Ti
	$E_{0.42}$	$E_C - 0.42$	5×10^{-15}	$V_{C/Si}$
	$E_{0.66}$	$E_C - 0.66$	4×10^{-15}	V_C (Z_1/Z_2)
	$E_{0.71}$	$E_C - 0.71$	1×10^{-15}	V_C (Z_1/Z_2)
Electron-beam deposition	$E_{0.10}$	$E_C - 0.10$	1×10^{-13}	N
	$E_{0.12}$	$E_C - 0.12$	3×10^{-15}	Ti
	$E_{0.16}$	$E_C - 0.16$	3×10^{-15}	Ti
	$E_{0.42}$	$E_C - 0.42$	6×10^{-15}	$V_{C/Si}$
	$E_{0.67}$	$E_C - 0.67$	1×10^{-14}	V_C (Z_1/Z_2)
	$E_{0.70}$	$E_C - 0.70$	1×10^{-15}	V_C (Z_1/Z_2)

© University of Pretoria

IBMM 2014 in Belgium

Effects of 5.4 MeV Alpha-particle Irradiation on the Electrical Properties of Nickel Schottky Diodes on 4H-SiC

E. Omotoso [a, b, *], W.E. Meyer [a], F.D. Auret [a], A.T. Paradzah [a], M. Diale [a], S.M.M. Coelho [a], P.J. Janse van Rensburg [a], P.N.M. Ngoepe [a]

[a] Department of Physics, University of Pretoria, Pretoria 0002, South Africa

[b] Department of Physics, Obafemi Awolowo University, Ile-Ife 220005, Nigeria

ezekiel.omotoso@up.ac.za

Introduction

- SiC is a semiconductor with a wide band-gap of 3.26 eV [1].
- SiC is radiation hard, i.e. not easily degraded by alpha and electron irradiation.
- SiC is suitable for devices used at high temperature and harsh radiation fields [2].
- The theoretical effective Richardson constant for n-type 4H-SiC is 146 $Acm^{-2}K^{-2}$ [3].
- Irradiation is used to introduce defects in semiconductors in order to investigate the defects' properties by means of DLTS on Schottky diodes.
- Effects of radiation and temperature on semiconductors are technologically important for radiation to sensing applications as well as manufacturing processes and high temperature and high power applications [2].
- In this work, the effect of alpha-particle irradiation on nickel Schottky diodes on 4H-SiC was investigated.

Experimental Procedure

- Nitrogen doped n-type 4H-SiC sample was used.
- Degrease: trichloroethylene; acetone; methanol (boiled for 5 mins each).
- Rinse: De-ionized water for 1 min.
- Etch: 40% HF for 30 seconds.
- Rinse: De-ionized water, followed by blow-dry with N_2 gas.
- Ohmic contacts: 3000 Å Ni by resistive evaporation, annealed 950°C in Ar for 10 mins.
- Schottky diodes: 1000 Å Ni by resistive evaporation.
- Irradiation: 8.5 × 10^8 alpha-particles-cm^{-2} from an Am^{241} source.
- Electrical characterization: *I-V* and *C-V*, Conventional DLTS measurements before and after irradiation.

Results and Discussion

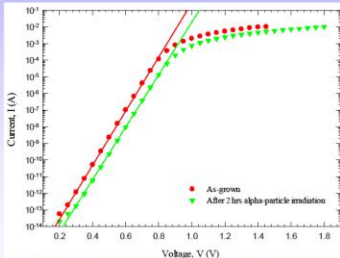

Fig. 1. Forward I-V characteristics of Ni/4H-SiC Schottky diodes before and after irradiation measured at 300 K.

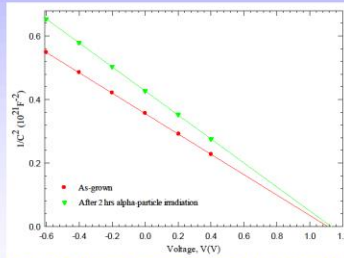

Fig. 2. $1/C^2$ as a function of voltage characteristics of Ni/4H-SiC before and after 5.4 MeV alpha-particles irradiation at 300 K.

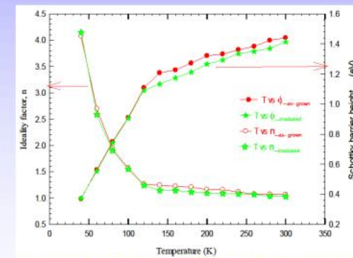

Fig. 3. Ideality factors and I-V SBH as function of temperature before and after irradiation, measured at temperatures 40-300 K.

⇒ Figs. 1 and 2 show the effect of 5.4 MeV alpha-particles irradiation on n-type 4H-SiC at 300 K.
⇒ The electrical properties of the SBD of Ni/4H-SiC are tabulated in Table 1.
⇒ The results from *I-V* and *C-V* show that the SBD are suitable for DLTS measurements.
⇒ Fig. 3 shows gradual change in *n* and SBH before and after irradiation from temperature >120 K
⇒ There is deviation from thermionic emission theory at temperature <120 K

Table 1. Comparison of some electrical parameters of Ni/4H-SiC before and after alpha-particle irradiation estimated from I-V and C-V characteristics at 300 K.

Sample	n	I_s (A)	R_s (Ω)	V_{bi} (V)	N_d (cm^{-3})	ϕ_{I-V} (eV)	ϕ_{C-V} (eV)
As-grown	1.04	16 × 10^{-18}	48	1.07	5.5 × 10^{15}	1.25	1.36
Irradiated	1.07	2.6 × 10^{-18}	270	1.23	5.2 × 10^{15}	1.31	1.52

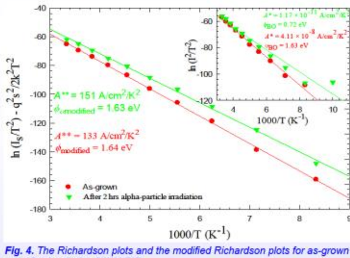

Fig. 4. The Richardson plots and the modified Richardson plots for as-grown and after irradiation Ni/4H-SiC.

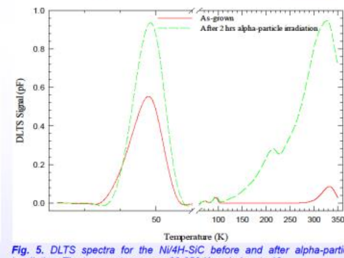

Fig. 5. DLTS spectra for the Ni/4H-SiC before and after alpha-particles irradiation. The temperature range 60-350 K scaled up to 10

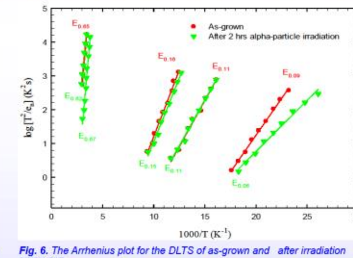

Fig. 6. The Arrhenius plot for the DLTS of as-grown and after irradiation Ni/4H-SiC.

⇒ The values of the Richardson constants, *A* in the insert of Fig. 4 are extremely small compared to the theoretical value of 146 $Acm^{-2}K^{-2}$ [3].
⇒ It indicates that the active area is smaller than the device area.
⇒ The deviation of *A* may be as a result of effect of barrier inhomogeneity at MS interface [4].
⇒ The Gaussian distribution model of barrier height was used to correct the deviation.
⇒ The modified Richardson constant, A^{**} before and after irradiation (Fig. 4) were determined to be 133 and 151 $Acm^{-2}K^{-2}$, respectively. They are in good agreement with literature [3].

⇒ In Figs. 5 and 6, the conditions used for DLTS are V_r = -5.0 V, V_p = 1.0 V, t_p = 1.0 ms and RW = 200 s^{-1}.
⇒ Four defects with levels labelled as $E_{0.09}$, $E_{0.11}$, $E_{0.16}$ and $E_{0.65}$ present in as-grown sample.
⇒ After 5.4 MeV alpha-particles irradiation, five defects with levels $E_{0.06}$, $E_{0.11}$, $E_{0.15}$, $E_{0.62}$ and $E_{0.67}$.
⇒ The formation of new defect causes changes in electrical properties of SBD.

$$\phi_{I-V} = \frac{kT}{q}\ln\left(\frac{AA^{*}T^2}{I_s}\right) \quad (1) \qquad n = \frac{q}{kT}\left(\frac{dV}{d(\ln I)}\right) \quad (2)$$

$$\phi_{C-V} = V_{bi} + \frac{kT}{q}\ln\frac{N_c}{N_d} \quad (3) \qquad \ln\left(\frac{I_s}{T^2}\right) - \left(\frac{q^2\sigma^2}{2k^2T^2}\right) = \ln(AA^{**}) - \frac{q\Phi_{Bm}}{kT} \quad (4)$$

Conclusions

- The Ni/4H-SiC contacts have successfully been fabricated by resistive evaporation technique.
- The effects of 5.4 MeV alpha-particle irradiation on SBD have been investigated by *I-V*, *C-V* and DLTS.
- From *I-V* measurements at 300 K we found *n*, SBH and R_s increase with irradiation but I_s decreases with irradiation.
- The electrical behaviour of the SBD deviated from thermionic emission theory below 120 K.
- The modified Richardson constants before and after irradiation are 133 and 151 $Acm^{-2}K^{-2}$, respectively by using Gaussian distribution method.
- The electrical properties of SBDs show little response to 5.4 MeV alpha-particle irradiation with removal rate of 5.9 × 10^3 cm^{-1} which corroborate its uses in radiation harsh environments.

Acknowledgement

The authors acknowledge the financial support of the South Africa National Research Foundation.

References

1. L.M. Tolbert, B. Ozpinecie, S.K. Islam, M.S. Chinthavali, *Proc. Int. Conf. Power and Energy Systems*, **1**, 317 (2003).
2. A. Akbay, H. Korkut, K. Ejderha, T. Korku, A. Turut, *J. Radioanal. Nucl. Chem.* **289**, 145 (2011).
3. V. Kazukauskas, J.-V.Vaitkus, *Opto-Electron. Rev.*, **12**, 377 (2004).
4. F. Roccaforte, F.La Via, A. Baeri, V. Raineri, L. Calcagno, F. Mangano, *J. Appl. Phys.*, **96**,4313 (2004).
5. İ. Dökme, Ş. Altindal, M.M. Bülbül, *Appl. Surf. Sci.*, **252**, 7749 (2006).

UNIVERSITEIT VAN PRETORIA
UNIVERSITY OF PRETORIA
YUNIBESITHI YA PRETORIA
Denkleiers • Leading Minds • Dikgopolo tša Dihlalefi

Department of Physics www.up.ac.za

© University of Pretoria

IBA 2015 in Croatia

Electrical characterization of deep levels created by bombarding nitrogen-doped 4H-SiC with alpha-particles

*Ezekiel Omotoso [a, b, *], Walter E. Meyer [a], F. Danie Auret [a] and Alexander T. Paradzah [a]*

[a] Department of Physics, University of Pretoria, Pretoria 0002, South Africa

[b] Department of Physics, Obafemi Awolowo University, Ile-Ife 220005, Nigeria

ezekiel.omotoso@up.ac.za

Introduction

Silicon Carbide

- Semiconductor (SC) with a wide bandgap of 3.26 eV [1].
- Suitable for electronic devices capable of operating at:
  - high temperature, high power and high frequency [2],
  - harsh radiation environment e.g. space, accelerator facilities, nuclear power plant [3].
- Superior to Si in number of applications.

Deep level defects

- Acts as carrier traps in SC, could be advantageous or detrimental to device [4].
- Formation of defects
  - during the growth, fabrication of electronic devices, operation during the radiation harsh environment, and particle irradiation.

Experimental

Sample preparation

- Nitrogen doped n-type 4H-SiC sample of doping density 7.1 × 10^{15} cm^{-3} was used.
- Degrease: trichloroethylene, acetone, methanol (boiled for 5 min in each).
- Rinse: De-ionized water for 1 min.
- Etch: 40% HF for 30 seconds.
- Rinse: De-ionized water, followed by blow-dry with N_2 gas.
- Ohmic contacts: 3000 Å Ni by resistive evaporation, annealed 950 ℃ in Ar for 10 min.
- Schottky diodes: NiAu (20% Au) 1000 Å thickness by resistive evaporation.
- Irradiation: 4.1 × 10^{11} and 8.9 x 10^{11} alpha-particles-cm^{-2} from an Am^{241} source.
- Annealing: annealed in argon ambient at 300 ℃ for 20 minutes

Contact quality evaluation and defect studies

- Current-voltage (*I-V*) and Capacitance-voltage (*C-V*) measurements.
- Deep Level Transient Spectroscopy (DLTS) and Laplace-DLTS measurements.

Results and Discussion

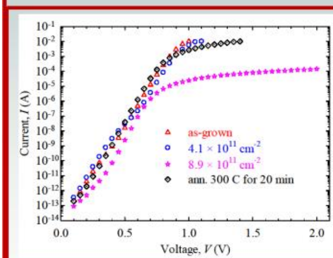

Fig. 1. Forward logarithmic I-V characteristics of 4H-SiC SBD in process (i), (ii), (iii) and (iv).

Table 1. Schottky diode parameters obtained in as-grown (i), irradiated with 5.4 MeV at fluence 4.1 × 10^{11} (ii), 8.9 × 10^{11} (iii), and after annealing at 300 ℃ for 20 minutes

Condition	n	I_s (A)	R_s (Ω)	V_{bi}	N_D (cm^{-3})	ϕ_{I-V} (eV)	ϕ_{C-V} (eV)
(i)	1.12	2.1 × 10^{-14}	12	0.93	7.0 × 10^{15}	1.06	1.21
(ii)	1.20	1.1 × 10^{-14}	15	2.38	4.6 × 10^{15}	1.08	2.68
(iii)	1.77	6.9 × 10^{-15}	13000	18.3	2.9 × 10^{15}	1.09	18.6
(iv)	1.15	1.9 × 10^{-15}	48	2.96	4.4 × 10^{15}	1.13	3.25

- Thermionic emission dominated in (i) up to approx. 0.9 V at 300 K (Fig 1).
- Generation-recombination dominated in (ii), (iii) and (iv) below 0.7 V
- Series resistance is dominant in (iii), and reduced after annealing in (iv).
- Increase in *n* attributed to deviation from thermionic emission.
- The fluence and annealing dependency of *n*, ϕ_{I-V} and I_s may be connected to the movement of Fermi level pinning at the surface of SiC.
- After irradiation carrier density decreases and V_{bi} increases, recovers partially after annealing.
- The 8.9 × 10^{11} cm^{-2} irradiated sample is almost compensated, due to series resistance capacitance measurement may be unreliable.

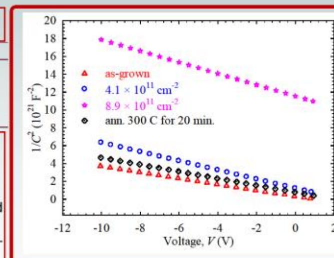

Fig. 2. $1/C^2$ as a function of voltage for 4H-SiC SBD in process (i), (ii), (iii) and (iv).

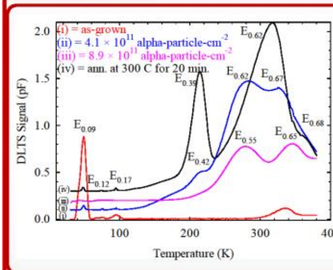

Fig. 3. Conventional DLTS spectra of 4H-SiC showing the present of the defects after process (i), (ii), (iii) and (iv) obtained at V_r = –5 V, V_p = 1 V, t_p = 1 ms and Rw = 20 s^{-1}.

Table 2. Electronic properties of defects detected in 4H-SiC by DLTS at conditions (i), (ii), (iii) and (iv) and Laplace-DLTS after process (iv).

Process	Defect label	E_a [eV]	σ_a [cm^2]	Defect ID
(i)	$E_{0.09}$	E_C – 0.09	8 × 10^{-15}	N
	$E_{0.11}$	E_C – 0.11	2 × 10^{-16}	Ti
	$E_{0.16}$	E_C – 0.16	1 × 10^{-15}	Ti
	$E_{0.65}$	E_C – 0.65	4 × 10^{-15}	$V_{C/Si}$ (Z_1/Z_2)
(ii)	$E_{0.10}$	E_C – 0.10	8 × 10^{-14}	N
	$E_{0.12}$	E_C – 0.12	2 × 10^{-15}	Ti
	$E_{0.16}$	E_C – 0.17	9 × 10^{-15}	Ti
	$E_{0.39}$	E_C – 0.39	2 × 10^{-16}	$V_{C/Si}$
	$E_{0.62}$	E_C – 0.62	2 × 10^{-14}	$V_{C/Si}$ (Z_1/Z_2)
	$E_{0.67}$	E_C – 0.67	4 × 10^{-15}	$V_{C/Si}$ (Z_1/Z_2)
(iii)	$E_{0.55}$	E_C – 0.55	2 × 10^{-15}	$V_{C/Si}$ (Z_1/Z_2) ?
	$E_{0.65}$	E_C – 0.65	3 × 10^{-15}	$V_{C/Si}$ (Z_1/Z_2)
	$E_{0.70}$	E_C – 0.70	1 × 10^{-15}	$V_{C/Si}$ (Z_1/Z_2)
(iv)	$E_{0.08}$	E_C – 0.08	9 × 10^{-15}	N
	$E_{0.12}$	E_C – 0.12	5 × 10^{-16}	Ti
	$E_{0.17}$	E_C – 0.17	7 × 10^{-15}	Ti
	$E_{0.42}$	E_C – 0.42	6 × 10^{-15}	$V_{C/Si}$
	$E_{0.67}$	E_C – 0.67	1 × 10^{-14}	$V_{C/Si}$ (Z_1/Z_2)
	$E_{0.74}$	E_C – 0.74	6 × 10^{-15}	$V_{C/Si}$ (Z_1/Z_2)
L-DLTS	$E_{0.39}$	E_C – 0.39	5 × 10^{-15}	$V_{C/Si}$
	$E_{0.42}$	E_C – 0.42	5 × 10^{-15}	$V_{C/Si}$
	$E_{0.65}$	E_C – 0.65	8 × 10^{-15}	$V_{C/Si}$ (Z_1/Z_2)
	$E_{0.70}$	E_C – 0.70	4 × 10^{-14}	$V_{C/Si}$ (Z_1/Z_2)
	$E_{0.76}$	E_C – 0.76	1 × 10^{-14}	$V_{C/Si}$ (Z_1/Z_2)

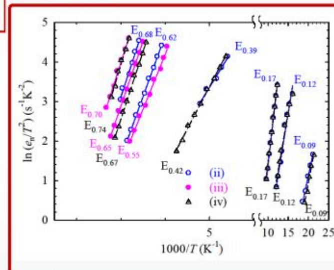

Fig. 4: Arrhenius plots of deep level defects in 4H-SiC SBD for process (ii), (iii) and (iv), obtained from conventional DLTS.

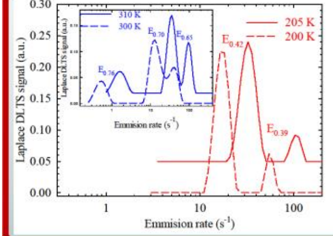

Fig. 5. Laplace-DLTS spectra recorded at a V_r = –5 V, V_p = 1 V for temperatures 200, 205, 300 and 310 K.

- In (i) four defects (Table 2) observed in the as-grown SiC samples (Fig. 3).
- In (ii) two new defects ($E_{0.39}$ and $E_{0.62}$) observed, amplitude of shallow defect $E_{0.09}$ reduced to 12%, peak of $E_{0.62}$ and $E_{0.67}$ broad, indicating the presence of more than two levels whose energies are closely spaced.
- In (iii) shallow defects disappeared as a result of intense damage that lowers the position of the Fermi level in the bandgap, below shallow defect levels, therefore the defect levels were never filled by DLTS filling pulse.
- In (iv) shallow defects re-appeared after annealing.
- Laplace-DLTS in Fig. 5 indicates the presence of two close defects $E_{0.39}$ and $E_{0.42}$, the two defects had acceptor-like behaviour and could be attributed to silicon or carbon vacancy.
- Insert of Fig. 5 shows the three close emission rate that were split by Laplace-DLTS, $E_{0.65}$, $E_{0.70}$ and $E_{0.76}$ defects are known as Z_1/Z_2, had intrinsic nature [5].

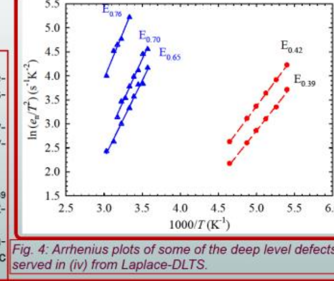

Fig. 4: Arrhenius plots of some of the deep level defects observed in (iv) from Laplace-DLTS.

Conclusions

- I-V and C-V characteristics demonstrated the suitability of 4H-SiC SBDs for the study.
- Four defects observed in as-grown material, the amplitude of $E_{0.09}$ reduced to 12% after conditions (ii).
- Shallow defects disappeared after condition (iii), and re-appeared after condition (iv).
- Laplace-DLTS was used to separate defects that overlapped in convectional DLTS spectra.
- According to literature $E_{0.39}$ and $E_{0.42}$ had acceptor-like behaviour, and $E_{0.65}$, $E_{0.70}$ and $E_{0.76}$ defects has intrinsic nature linked to carbon vacancy and/or carbon interstials.

References

1. 1. L.M. Tolbert *et al*, *Proc. Int. Conf. Power and Energy Systems*, **1**, 317 (2003).
2. A. Akbay *et al*, J. radioanal. Nucl ch, 289 (2011) 145-148
3. L. Kin Kiong *et al*, Nuclear Science, IEEE Transactions on, 50 (2003) 194-200
4. Ž. Pastuović *et al*, Nucl. Instrum. Meth. B. 348 (2015) 233-239.
5. T.A.G. Eberlein *et al*, Phys. Rev. Lett., 90 (2003) 2255021-2255024.

UNIVERSITEIT VAN PRETORIA
UNIVERSITY OF PRETORIA
YUNIBESITHI YA PRETORIA

Department of Physics www.up.ac.za

© University of Pretoria

SAIP 2015 in South Africa

Effect of room temperature annealing on Ni/4H-SiC Schottky barrier diodes after alpha-particle irradiation at high fluence

E. Omotoso [a, b,*], *W. E. Meyer* [a], *F. D. Auret* [a] *and M. Diale* [a]

[a] *Department of Physics, University of Pretoria, Pretoria 0002, South Africa*

[b] *Department of Physics, Obafemi Awolowo University, Ile-Ife 220005, Nigeria*

ezekiel.omotoso@up.ac.za

Introduction

Silicon Carbide

- Wide bandgap semiconductor (3.26 eV) [1].
- Suitable for electronic devices capable of operating at:
  - high temperature, high power and high frequency [2];
  - harsh radiation environment e.g. space, accelerator facility, nuclear power plant [3].
- Key material for the next-generation photonics.

Metal-semiconductor Schottky barrier diodes

- Widely used where high switching speed is required.
- Ideal rectifiers in PV systems and high-efficiency power supplies.
- Performance of devices can be quantified in term of n, SBH, I_s and N_d.
- Useful for characterising semiconductor material.

Experimental Procedure

Sample preparation

- Nitrogen-doped *n*-type 4H-SiC sample of doping density 1.9×10^{16} cm^{-3} was used.
- Degrease: trichloroethylene, acetone, methanol (boiled for 5 min in each).
- Rinse: De-ionized water for 1 min.
- Etch: 40% HF for 30 seconds.
- Rinse: De-ionized water, followed by blow-dry with N_2 gas.
- Ohmic and Schottky contacts: resistive evaporation.
- Irradiation: α-particle irradiation at 9.2×10^{11} cm^{-2} fluence from an Am^{241} source.

Contact quality evaluation and defect studies

- Current-voltage (*I-V*) and Capacitance-voltage (*C-V*) measurements.
- Deep level transient spectroscopy measurements.
- Sample left at room temperature after high fluence irradiation for 1 week.

Results and Discussion

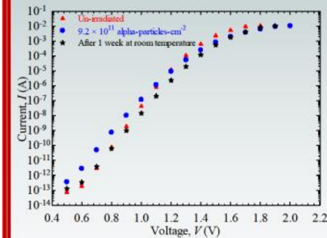

Fig. 1: Forward logarithmic I-V characteristics of a 4H-SiC SBD before irradiation, after a fluence of 9.2 × 10^{11} cm^{-2} from an Am^{241} radionuclide source, and after 1 week at RT.

Table 1: Summary of important parameters of a Ni/4H-SiC SBD before irradiation, after fluence of 9.2 × 10^{11} cm^{-2} from an ^{241}Am radionuclide source, and after 1 week at RT, calculated from I-V and C-V characteristics.

Sample	*n*	$\phi_{I\text{-}V}$ (eV)	$\phi_{C\text{-}V}$ (eV)	I_s (10^{-21}A)	N_d (10^{16}cm^{-3})	C (pF) at –5 V
Un-irradiated	1.20	1.47	2.44	2	1.6	34.9
9.2×10^{11} cm^{-2}	1.85	1.34	3.66	520	1.1	25.6
After 1 wk @ RT	1.45	1.40	3.83	36	1.2	27.5

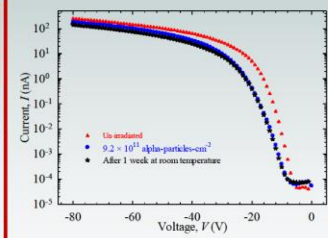

Fig. 2: Reverse logarithmic I-V characteristics of a 4H-SiC SBD before irradiation, after a fluence of 9.2 × 10^{11} cm^{-2} from an ^{241}Am radionuclide source, and after 1 week at RT.

- Thermionic emission dominated in all the three plots up to approx. 1.2 V Fig 1.
- Ideality factor increases after the bombardment and decreases after 1 week at room temperature.
- Increase in *n* attributed to deviation from thermionic emission.
- Series resistance also increases after irradiation as shown in Fig. 1.
- After irradiation free carrier concentration decreases, and increases slightly after 1 week at room temperature as shown in Fig. 4.

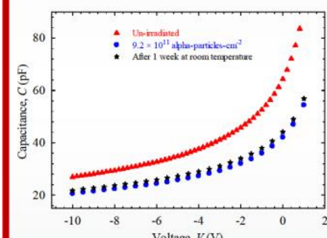

Fig. 3: The C-V characteristics of a 4H-SiC SBD before irradiation, after a fluence of 9.2 × 10^{11} cm^{-2} from an Am^{241} radionuclide source, and after 1 week at RT.

Table 2: Electronic properties of defects detected in 4H-SiC by DLTS before and after alpha-particle irradiation at high fluence.

Defect	E_T (eV)	σ_a (cm^2)	T_{peak} (K)	Attribution
$E_{0.09}$	E_c–0.09	8×10^{-15}	51	N impurity
$E_{0.11}$	E_c–0.11	2×10^{-16}	74	Ti impurity
$E_{0.16}$	E_c–0.16	1×10^{-15}	94	Ti impurity
$E_{0.39}$	E_c–0.39	2×10^{-15}	217	V_{Si}
$E_{0.62}$	E_c–0.62	1×10^{-13}	301	Z_1/Z_2
$E_{0.65}$	E_c–0.65	4×10^{-15}	332	Z_1/Z_2 (C/Si vacancy)

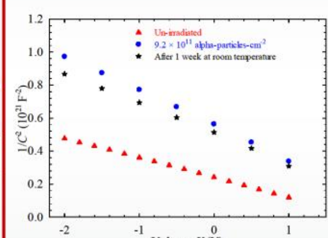

Fig. 4: Plots of 1/C^2 as a function of voltage of a 4H-SiC SBD before irradiation, after a fluence of 9.2 × 10^{11} cm^{-2} from an ^{241}Am radionuclide source, and after 1 week at RT.

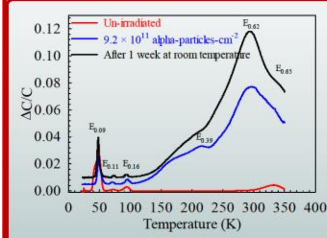

Fig. 5: DLTS spectra of a 4H-SiC SBD before irradiation, after a fluence of 9.2 × 10^{11} cm^{-2} from an ^{241}Am radionuclide source, and after 1 week at RT.

- Four defects observed in the as-grown SiC samples (Fig. 5).
- Two defects ($E_{0.39}$ and $E_{0.62}$) introduced after irradiation .
- The signatures and attributes of the defects present before and after irradiation are tabulated in Table 2.
- The $E_{0.65}$ appeared at low rate windows after irradiation.
- The $E_{0.65}$ defects are known as Z_1/Z_2, believed to be intrinsic [4].
- After irradiation, peak height of shallow defect $E_{0.09}$ reduced, probably due to Fermi-level lowering.
- The deep level defect $E_{0.39}$ disappeared or annealed out after 1 week at room temperature.
- The deep level defect, $E_{0.39}$ is not stable at RT.
- The broadness of $E_{0.62}$ and $E_{0.65}$ revealed the presence of more than one defect.

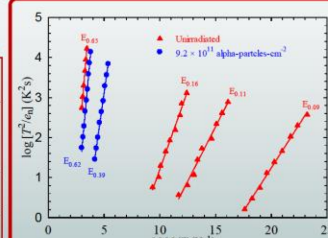

Fig. 6: Arrhenius plots of deep level defects of a 4H-SiC SBD before irradiation and after a fluence of 9.2 × 10^{11} cm^{-2} from an ^{241}Am radionuclide source.

Conclusions

- *I-V* and *C-V* characteristics demonstrated the suitability of 4H-SiC SBDs for the study.
- Four deep level defects observed in as-grown material, the amplitude of $E_{0.09}$ reduced after bombardment with 9.2×10^{11} cm^{-2} fluence from alpha-particle.
- Two deep level defects introduced after irradiation.
- According to literature $E_{0.39}$ had acceptor-like behaviour, and $E_{0.65}$ defect had intrinsic nature linked to carbon vacancy and/or carbon interstials.

References

1. L.M. Tolbert *et al*, *Proc. Int. Conf. Power and Energy Systems*, **1**, 317 (2003).
2. A. Akbay *et al*, J. radioanal. Nucl ch, 289 (2011) 145-148
3. L. Kin Kiong *et al*, Nuclear Science, IEEE Transactions on, 50 (2003) 194-200
4. T.A.G. Eberlein *et al*, Phys. Rev. Lett., 90 (2003) 2255021-2255024.

UNIVERSITEIT VAN PRETORIA
UNIVERSITY OF PRETORIA
YUNIBESITHI YA PRETORIA

Department of Physics www.up.ac.za

© University of Pretoria

ICDS 2015 in Finland

Electrical characterization of defects introduced during electron beam deposition of W Schottky contacts on n-type 4H-SiC

E. Omotoso [a, b, *], W. E. Meyer [a], F. D. Auret [a], S. M. M. Coelho [a], P. N. M. Ngoepe [a] and M. Diale[a]

[a] Department of Physics, University of Pretoria, Pretoria 0002, South Africa

[b] Department of Physics, Obafemi Awolowo University, Ile-Ife 220005, Nigeria

ezekiel.omotoso@up.ac.za; wmeyer@up.ac.za

Introduction

Silicon Carbide

- Semiconductor (SC) with a wide bandgap of 3.26 eV [1].
- Suitable for electronic devices capable of operating at:
  - high temperature, high power and high frequency [2],
  - harsh radiation environment e.g. space, accelerator facilities, nuclear power plants [3].
- Superior to Si in a number of applications.

Deep level defects

- Act as carrier traps in SC, could be advantageous or detrimental to device.
- Formation of deep level defects
  - during growth and fabrication of electronic devices; operation under radiation harsh environment; and particle irradiation.

Aim and objective

- To study the electronic properties of defects introduced in *n*-type 4H-SiC during the electron beam deposition (EBD) of W Schottky contacts.

Experimental Procedure

Sample preparation

- Nitrogen-doped *n*-type 4H-SiC sample with doping density 3.7×10^{14} cm^{-3} was used.
- Degrease: trichloroethylene, acetone, methanol (boiled for 5 min in each).
- Rinse: De-ionized water for 1 min.
- Etch: 40% HF for 30 seconds.
- Rinse: De-ionized water, followed by blow-dry with N_2 gas.
- Ohmic contacts: 300nm Ni by resistive evaporation, annealed at 950 ℃ in Ar for 10 min.
- Schottky diodes: Tungsten of 40 nm thickness was evaporated by a 240 mA, 1 kV electron beam.
- Control: Irradiation with 8.6×10^{14} electrons-cm^{-2} from an ^{90}Sr source.

Contact quality evaluation and defect studies

- Current-voltage (*I-V*) measurements.
- Capacitance-voltage (*C-V*) measurements.
- Deep Level Transient Spectroscopy (DLTS).

Results and Discussion

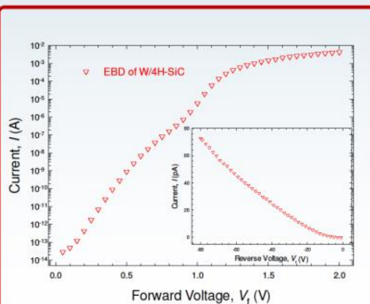

Fig. 1. I-V characteristics of W Schottky contact to 4H-SiC deposited by EBD. The inset is the reverse I-V characteristics.

- Thermionic emission dominated above approximately 0.55 V at 300 K (Fig. 1).
- Generation-recombination dominated from below 0.55 V.
- Series resistance is dominant at higher voltage.
- High value of ideality factor, *n*, attributed to deviation from thermionic emission.
- *I-V* measurements demonstrated that EBD resulted in degradation of Schottky contact (resulted in degraded *I-V* characteristics).
- From the inset (Fig. 1), the reverse current increased with voltage, but remained below 100 pA.
- From Fig. 2, the N_d estimated greater than the doping density of material. This indicated the presence of deep level defects.

Table 1. Schottky diode parameters obtained from I-V and C-V W/n-4H-SiC SBD deposited by electron beam

n	I_s (A)	R_s (Ω)	V_{bi}	N_d (cm^{-3})	ϕ_{I-V} (eV)	ϕ_{C-V} (eV)
2.50	6.2×10^{-13}	158	1.82	5.8×10^{14}	0.98	1.82

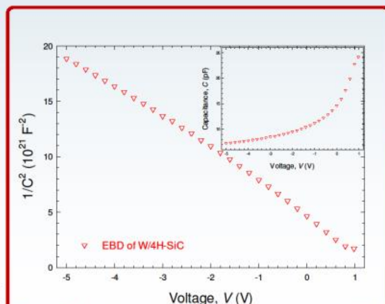

Fig. 2. $1/C^2$ as a function of voltage for W Schottky contact to 4H-SiC deposited by EBD. Inset is the capacitance as a function of voltage.

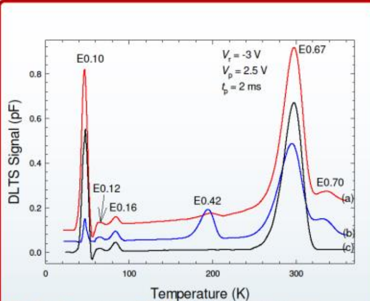

Fig. 3. Conventional DLTS spectra of (a) W/4H-SiC deposited by EBD, Ni/4H-SiC by RE (b) after HEEI and (c) as-grown. (The region 56 – 360 K is scaled up by a factor of 8.)

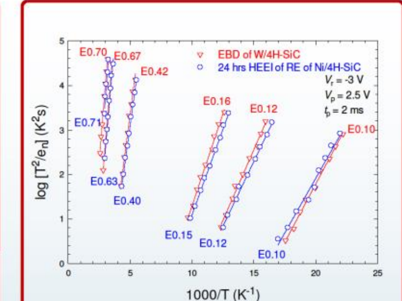

Fig. 4: Arrhenius plots of deep level defects in EBD of W/4H-SiC and HEEI of RE of Ni/4H-SiC SBD devices.

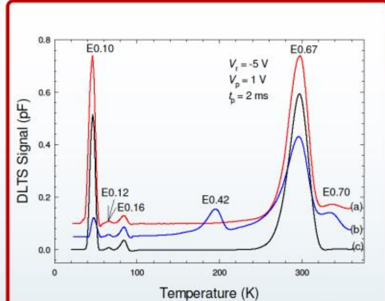

Fig. 5. Conventional DLTS spectra of (a), (b) and (c) (see Fig. 3)measured under different bias conditions, deeper into the semiconductor. (56 – 360 K scaled up by a factor of 8).

- Four defects present in control Fig. 3 (spectrum (c)).
- After EBD, six defects observed with the conditions in Fig. 3.
- Two defects (E0.42 & E0.70) introduced by metallisation.
- E0.42 defects introduced was close to the W/n-4H-SiC junction
- These defects influence the device performance and alter barrier height (BH) of the contacts [4].

Table 2. Signatures of defects introduced into the devices by EBD and high energy electron irradiation (HEEI).

Process	Defect label	E_a [eV]	σ_a [$\times 10^{-15} cm^2$]	Defect ID
EBD/HEEI	E0.10	$E_C - 0.10$	100/30	N
	E0.12	$E_C - 0.12$	3/0.8	Ti
	E0.16/0.15	$E_C - 0.16/0.15$	3/1	Ti
	E0.42/0.40	$E_C - 0.42/0.40$	6/3	$V_{C/Si}$
	E0.67/0.63	$E_C - 0.67/0.63$	10/3	$V_{C/Si}$ (Z_1/Z_2) [5]
	E0.70/0.71	$E_C - 0.70/0.71$	1/3	$V_{C/Si}$ (Z_1/Z_2) [5]

- Defects, E0.42 & E0.70 introduced have electronic properties similar to defects introduced by HEEI [6].
- E0.42 was not observed in Fig. 5, which shows that the defect is very closed to the surface.
- EBD defects are introduced by heavy metal or gas ions, the defects may be vacancy cluster and complex with impurities.

Conclusions

- *I-V* and *C-V* characteristics demonstrated the suitability of W/4H-SiC SBDs for the DLTS study.
- EBD introduced two defects at and close to metal-semiconductor junction (W/*n*-4H-SiC junction).
- Study revealed that the two defects introduced during EBD have same electronic properties as defects in HEEI.
- According to literature E0.42 has acceptor-like behaviour, and E0.67 and E0.70 defects are of intrinsic nature linked to carbon vacancies and/or carbon interstitials.

References

1. L.M. Tolbert *et al*, *Proc. Int. Conf. Power and Energy Systems*, **1**, 317(2003).
2. A. Akbay *et al*, *J. radioanal. Nucl Ch*, 289 145-148 (2011).
3. L. Kin Kiong *et al*, *Nuclear Science*, IEEE Transactions on, 50 194-200 (2003).
4. F. D. Auret *et al*, *J Appl Phys*, 55(6), 1581 (1984).
5. T.A.G. Eberlein *et al*, Phys. Rev. Lett., 90, 2255021-2255024 (2003).
6. E. Omotoso *et al*, *Mat Sci Semicon Proc*, 39, 112-118 (2015).

UNIVERSITEIT VAN PRETORIA
UNIVERSITY OF PRETORIA
YUNIBESITHI YA PRETORIA
Denkleiers • Leading Minds • Dikgopolo tša Dihlalefi

Department of Physics www.up.ac.za

© University of Pretoria

GADEST 2015 in Germany

Electrical characterization of defects introduced in *n*-type N-doped 4H-SiC during electron beam exposure

*Ezekiel Omotoso [a, b, *], Walter E. Meyer [a], Francois D. Auret [a], Sergio M. M. Coelho [a] and Phuti N. M. Ngoepe [a]*
[a] Department of Physics, University of Pretoria, Pretoria 0002, South Africa
[b] Department of Physics, Obafemi Awolowo University, Ile-Ife 220005, Nigeria
ezekiel.omotoso@up.ac.za; walter.meyer@up.ac.za

Introduction

Silicon Carbide

- Semiconductor with a wide bandgap of 3.26 eV [1].
- Suitable for electronic devices capable of operating at:
  - high temperature, high power and high frequency [2],
  - harsh radiation environment e.g. space, accelerator facilities, nuclear power plants [3].
- Superior to Si in a number of applications.

Deep level defects

- Act as carrier traps, could be advantageous or detrimental to device.
- Formation of deep level defects:
  during growth and fabrication of electronic devices; operation under radiation harsh environment; and particle irradiation.

Aim and objective

- To investigate the effect of exposing *n*-type 4H-SiC to e-beam conditions (without metal deposition).
- To study the electronic properties of defects introduced in *n*-type 4H-SiC during the electron beam exposure (EBE) and compare the signatures with as-grown SiC, and after bombardment with α-particles and HEE from an ^{241}Am and a ^{90}Sr sources, respectively.

Experimental Procedure

Sample preparation

- Nitrogen-doped *n*-type 4H-SiC sample with doping density 7.1×10^{15} cm^{-3} was used.
- Degrease: trichloroethylene, acetone, methanol (boiled for 5 min in each).
- Rinse: De-ionized water for 1 min.
- Etch: 40% HF for 30 seconds to remove native oxide layer on the samples.
- Rinse: De-ionized water, followed by blow-dry with N_2 gas.
- Ohmic contacts: 300 nm Ni by resistive evap., annealed at 950 ℃ in Ar for 10 min.
- Cleaning procedures repeated after annealing, but only for 3 min. in ultrasonic bath
- Schottky barrier diodes: Fabrication of SBDs were in 2 stages:
  - 1st stage: Ni Schottky contacts of 10 nm were thermally evaporated, followed by exposure to e-beam condition without evaporating W for 50 min.
  - 2nd stage: Additional Ni Schottky contacts of 90 nm were thermally evaporated.
- Comparison: Irradiation with electrons (^{90}Sr) and α-particles (^{241}Am).

Contact quality evaluation and defect studies

- Current-voltage (*I-V*) & capacitance-voltage (*C-V*) measurements.
- Deep Level Transient Spectroscopy (DLTS).

Results and Discussion

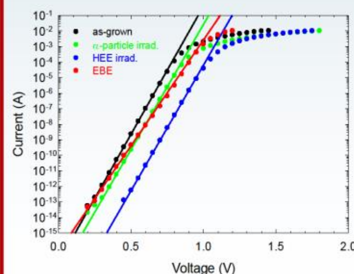

Fig. 1. I-V characteristics of Ni/4H-SiC Schottky contacts for as-grown, α-particle and HEE irradiated and e-beam exposure (EBE).

- Thermionic emission dominated (Fig. 1 and Table 1.)
- Series resistance of α-particle irradiated contact increased, while that of EBE contact decreased significantly.
- High value of ideality factor *n*, in EBE SBD attributed to slight deviation from thermionic emission, probably due to interface states.
- *I-V and C-V* measurements demonstrated that e-beam exposure (without metal deposition) resulted in degradation of Schottky contacts.

Table 1. SBDs parameters obtained from I-V and C-V of Ni/4H-SiC Schottky contacts for as-grown, α-particle and HEE irradiated, and EBE.

Samples	n	I_s [$\times 10^{-18}$A]	R_s [Ω]	N_D [$\times 10^{15}$cm^{-3}]	ϕ_{I-V} [eV]	ϕ_{C-V} [eV]
As-grown	1.04	16	48	7.2	1.24	1.26
α-particle irrad.	1.07	3	70	6.7	1.29	1.36
HEE irrad.	1.13	0.1	60	7.3	1.38	1.60
EBE	1.26	66	13	7.7	1.21	1.38

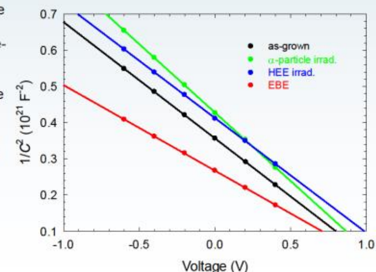

Fig. 2. 1/C² as a function of voltage for Ni/4H-SiC Schottky contacts for as-grown, α-particle and HEE irradiated and e-beam exposure.

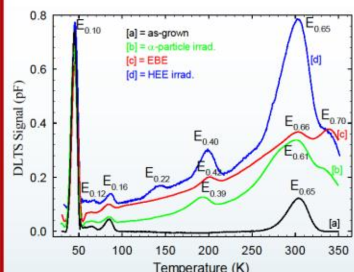

Fig. 3. Conventional DLTS spectra of Ni/4H-SiC for as-grown, α-particle and HEE irradiated and e-beam exposure.

- Four defects present in as-grown (Fig. 3) [4].
- α-particle introduced two defects ($E_{0.39}$ & $E_{0.70}$) [4].
- HEE irradiation introduced three defects ($E_{0.22}$, $E_{0.40}$ & $E_{0.70}$), with the identity of $E_{0.22}$ not yet clear [5].
- EBE induced $E_{0.42}$ & $E_{0.71}$ defects in Ni/4H-SiC SBD, which have similar attributes to defects introduced by high energy particles, but in lower concentration.

Table 2. Signatures of deep level defects present in Ni/4H-SiC for as-grown, α-particle and HEE irradiated and EBE.

Process	Defect label	E_T [eV]	σ_a [cm^2]	Defect ID
As-grown	$E_{0.10}$	$E_C - 0.10$	3×10^{-12}	N
	$E_{0.12}$	$E_C - 0.12$	1×10^{-15}	Ti
	$E_{0.16}$	$E_C - 0.16$	1×10^{-15}	Ti
	$E_{0.65}$	$E_C - 0.65$	4×10^{-15}	V_C (Z_1/Z_2)
α-particle	$E_{0.10}$	$E_C - 0.10$	2×10^{-12}	N
	$E_{0.12}$	$E_C - 0.12$	1×10^{-15}	Ti
	$E_{0.16}$	$E_C - 0.16$	3×10^{-15}	Ti
	$E_{0.39}$	$E_C - 0.39$	2×10^{-15}	$V_{C/Si}$
	$E_{0.61}$	$E_C - 0.61$	5×10^{-15}	V_C (Z_1/Z_2)
	$E_{0.70}$	$E_C - 0.70$	6×10^{-15}	V_C (Z_1/Z_2)
HEE	$E_{0.10}$	$E_C - 0.10$	1×10^{-16}	N
	$E_{0.12}$	$E_C - 0.12$	4×10^{-12}	Ti
	$E_{0.16}$	$E_C - 0.16$	1×10^{-15}	Ti
	$E_{0.22}$	$E_C - 0.22$	2×10^{-17}	?
	$E_{0.40}$	$E_C - 0.40$	3×10^{-15}	$V_{C/Si}$
	$E_{0.65}$	$E_C - 0.65$	3×10^{-15}	V_C (Z_1/Z_2)
	$E_{0.70}$	$E_C - 0.70$	3×10^{-15}	V_C (Z_1/Z_2)
EBE	$E_{0.10}$	$E_C - 0.10$	1×10^{-11}	N
	$E_{0.12}$	$E_C - 0.12$	2×10^{-16}	Ti
	$E_{0.16}$	$E_C - 0.16$	2×10^{-15}	Ti
	$E_{0.42}$	$E_C - 0.42$	5×10^{-15}	$V_{C/Si}$
	$E_{0.66}$	$E_C - 0.66$	4×10^{-15}	V_C (Z_1/Z_2)
	$E_{0.71}$	$E_C - 0.71$	1×10^{-15}	V_C (Z_1/Z_2)

Fig. 4: Arrhenius plots of deep level defects in of Ni/4H-SiC for as-grown, α-particle and HEE irradiated and e-beam exposure.

- The exposure of samples to electron-beam (without metal deposition) could be another mechanism of introducing defects $E_{0.42}$ & $E_{0.71}$ without high energy particle irradiation.
- Doyle *et al* reported earlier that $E_{0.42}$ has acceptor-like behaviour [6]. Some attributed the defect to $V_{C/Si}$ or anti-sites.
- $E_{0.71}$ is commonly known as Z_1/Z_2 defect. It has intrinsic nature linked to carbon vacancy [7].

Conclusions

- EBE introduced two defects, $E_{0.42}$ and $E_{0.71}$, related to $V_{C/Si}$ and V_C (Z_1/Z_2), respectively.
- According to literature $E_{0.42}$ has acceptor-like behaviour.
- EBE did not introduce the $E_{0.22}$, introduced by HEE irradiation.
- The study revealed that the two defects introduced during the exposure have same electronic properties as defects induced as a result of high energy particles (α-particle and HEE irradiation).

References

1. L.M. Tolbert *et al*, *Proc. Int. Conf. Power and Energy Systems* **1** 317(2003).
2. A. Akbay *et al*, *J. Radioanal. Nucl. Ch.* **289** 145-148 (2011).
3. L. Kin Kiong *et al*, IEEE Trans. *Nucl. Sci.* **50** 194-200 (2003).
4. E. Omotoso *et al*, Nucl. Instr. Meth. B (2015) (in press).
5. E. Omotoso *et al*, *Mat Sci. Semicon. Proc.* **39** 112-118 (2015).
6. Doyle et al, *J. App. Phys.* **84** 1354-1357 (1998).
7. Son et al, *Phys. Rev. Lett.* **109** 187603 (2012).

UNIVERSITEIT VAN PRETORIA
UNIVERSITY OF PRETORIA
YUNIBESITHI YA PRETORIA
Denkleiers • Leading Minds • Dikgopolo tša Dihlalefi

Department of Physics www.up.ac.za

© University of Pretoria